ESTIMATION OF AIRCRAFT STATES AND WIND EXPOSURE IN AERIAL REFUELING

by

JE HYEON LEE

Presented to the Faculty of the Graduate School of
The University of Texas at Arlington in Partial Fulfillment
of the Requirements
for the Degree of

DOCTOR OF PHILOSOPHY

THE UNIVERSITY OF TEXAS AT ARLINGTON
December 2011

To my wife Moon Gyu Lee, my sons Yoon Sang and Yoon Seo

whom I love and who love me.

ACKNOWLEDGEMENTS

I thank the United States and the University of Texas at Arlington (UTA) for giving me the chance to study in America, which is the leading country in the area of the aerospace engineering in the world. I could finish my Ph.D. program in Aerospace Engineering due to the financial support of UTA through STEM (Science, Technology, Engineering, and Mathematics) scholarship, GTA (Graduate Teaching Assistantship), and Dean's scholarship.

I thank my supervisor, Dr. Atilla Dogan, who has given me the guidance to reach the solution whenever I face a difficult situation in my research. His knowledge and guidance are invaluable to me. Due to his wide and deep range of knowledge in flight dynamics, simulation, control and estimation, I could obtain Ph.D. degree with the title of "Estimation of Aircraft States and Wind Exposure in Aerial Refueling", which is a very challenging problem.

I thank Dr. David Hullender, who has given me advice with respect to my research. Due to his advice, I could deeply understand the measurement part in the Kalman filter. Also, I thank Dr. Don Wilson, Dr. Frank Lu and Dr. Saibun Tjuatja, who helped me as my final defense committee members. Due to their advice, I could complete my Ph.D. study.

Finally, I thank my family who have supported me in so many ways.

November 21, 2011

ABSTRACT

ESTIMATION OF AIRCRAFT STATES AND WIND
EXPOSURE IN AERIAL REFUELING

JE HYEON LEE, Ph.D.

The University of Texas at Arlington, 2011

Supervising Professor: Atilla Dogan

When a tanker and receiver aircraft fly in tight formation in an aerial refueling operation, they are exposed to various sources of wind with varying magnitude and direction. The tanker and the receiver aircraft experience prevailing wind and turbulence. The receiver aircraft is also subject to an additional wind field induced by the wake of the tanker. The receiver aircraft is required to fly in a precise trajectory relative to the tanker. Especially, the receiver aircraft should stay at a position with small tolerances for the fuel transfer operation while the tanker aircraft flies straight level and makes constant altitude turns. To improve the trajectory tracking and the station keeping performance of the receiver under measurement noise, the estimation of the receiver states and some of the tanker states are needed in the trajectory-tracking controller. This research has shown that the estimation of the wind exposure should be known for a successful implementation of an estimator for the states of the aircraft. A Square-Root Unscented Kalman Filter is developed for each aircraft based on their nonlinear equations of motion augmented with equations representing the effect of the wind on the aircraft dynamics. The estimation algorithms are evaluated in an

integrated simulation environment that includes full 6-DOF nonlinear equations of motion of each aircraft, the controllers for each aircraft, models for prevailing wind, turbulence and vortex-induced wind as well as the aerodynamic interference on the receiver dynamics. A parameter study is used to evaluate the performance of the estimation algorithm under either white measurement noise or colored measurement noise.

TABLE OF CONTENTS

LIST OF ILLUSTRATIONS

LIST OF TABLES

CHAPTER 1

INTRODUCTION

Aircraft flying in the atmosphere are influenced by the motion of air. When a tanker and receiver aircraft fly in tight formation in an aerial refueling operation, they are exposed to various sources of wind with varying magnitude and direction. The tanker and the receiver aircraft experience prevailing wind and turbulence. The receiver aircraft is also subject to an additional wind field induced by the wake of the tanker. The receiver aircraft is required to fly in a precise trajectory relative to the tanker. Especially, the receiver aircraft should stay at a position with small tolerances for the fuel transfer operation while the tanker aircraft flies straight level and makes constant altitude turns in the presence of wind. Currently, aerial refueling of receiver aircraft has to be performed by the pilot, which is one of the most demanding piloting tasks. Relying on some visual cues, the receiver aircraft pilot has to fly the aircraft to the refueling contact position and keep it there within a small space relative to the tanker. There are current efforts underway for developing control technologies to automate the refueling operation for the receiver aircraft. These efforts are to reduce the pilot workload and also equip unmanned aerial vehicles with aerial refueling capability. Estimation of the aircraft states and wind components the aircraft experience is a crucial enabler for this objective.

To do the automated aerial refueling successfully, the relative position should be controlled with small tolerance. The relative position controlled designed by linear quadratic regulator method requires full state feedback. If the full states are provided by the poor sensors, the performance of the precise relative position controller will be

degraded or more seriously the relative position control may fail due to the large noise levels of the sensors. Due to the large measurement noise level and the unmeasured variable information such as a wind velocity, the relative position of the receiver aircraft is hard to be controlled. To eliminate the sources causing failure in automated aerial refueling, this work adapts a Kalman filter, and uses estimated state feedback control.

1.1 Literature Review

Among aerospace applications that require wind information is the problems of precise position determination. Air traffic control automation is such an application [1, 2]. Many aircraft may need to circle over the airport waiting to land while others are taking off or landing. In adverse weather conditions such as heavy rain, deep fog, or wind gust, it is challenging for aircraft to land safely. To prevent a possible collision or conflict between aircraft, air traffic control automation could be used. The air traffic control automation is to keep a safe physical separation between aircraft, a key requirement for which is to calculate current position of the aircraft precisely. To estimate the precise position of the aircraft, wind should be taken into account. Path planning or trajectory prediction for guidance of unmanned aerial vehicle (UAV) is another application for wind estimation [2, 3, 4, 5, 6]. A small UAV can be significantly influenced by wind in determining its position. Aircraft velocity relative to the air is not the same as the inertial velocity in the presence of wind. Hence, the path planning or trajectory prediction requires wind information. Another application that requires wind information is aerial refueling (AR) [7, 8, 9]. An AR operation involves a tanker aircraft and a receiver aircraft. While the tanker flies in a specific pattern, the receiver aircraft follows the tanker aircraft in close proximity. To determine the relative position of the receiver aircraft, wind velocity should be known, as relative

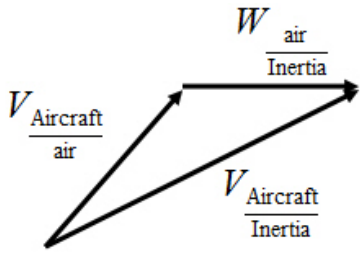

Figure 1.1. Velocity Triangle Vector.

position determination is sensitive to wind. Formation flight is another application for the wind estimation. Formation flight involves a leader aircraft and follower or wing-man aircraft. Formation flight is used to minimize drag and maximize flying range through vortex effect generated from a leader [10, 11, 12]. The upwash generated by vortex of the leader reduces drag. To maintain the maximum drag reduction, the follower stays in a relative position from the leader with tight position tolerance. The additional wind field induced by the trailing vortices of the lead aircraft information affects lift and drag of the follower as well as the relative position. The vortex effect could be expressed by vortex induced wind on the follower aircraft [7, 9, 13]. Hence, wind information is required to keep the relative position within the tight position tolerance. A common aspect of these applications is to determine precise position in the presence of wind.

There are ground-based wind measurement methods with various limitations such as low measurement rate, the constant wind velocity assumption and distance between the aircraft and ground stations where the wind is measured. Some of these limitations can be overcome by onboard wind estimation. Wind estimation techniques can be divided into three categories, (i) Graphical method using velocity triangle vector, (ii) Constant wind model using nonlinear Kalman filter and (iii) Time-varying wind model without Kalman filter. The most common technique is to use velocity

triangle vector shown in Fig. 1.1 [1, 3, 5, 14, 15, 16]. The velocity triangle vector is the relation among (i) the ground speed of an aircraft from a radar track or GPS, (ii) airspeed of an aircraft from a pitot tube, and (iii) wind velocity relative to the inertial frame. Reference [1] directly uses velocity triangle vector to extract wind velocity. In Ref. [1], an aircraft has a constant turning airspeed with known airspeed data and

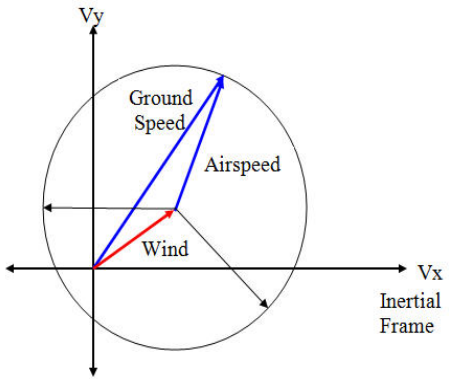

Figure 1.2. Velocity Plot.

inertial velocity vector is measured by radar track. The airspeed of an aircraft and its inertial velocity vector are known. Wind is assumed to be constant. As shown in Fig. 1.2, the known airspeed vector is placed at the center of the velocity plot because the magnitude of the airspeed is constant. The constant wind vector is calculated by subtracting the airspeed vector from the ground speed vector [1]. This approach relies on measurement update without wind model. Thus, noisy wind information will be obtained. Additionally, the method focuses on extracting the local wind information based on the circular flight pattern and a radar track. The second group [4, 14] uses measurements update and constant wind model in nonlinear Kalman filter. The available measurements are the ground speed from a radar track or a GPS and airspeed from a pitot tube. The second group uses a constant wind model, which

does not reflect abrupt change of wind velocity like wind gust. The constant wind model approximation is the main limitation of this approach. The third group uses measurements update, nonlinear equations of motion (EoM), nonlinear wind model, and time delayed moving average filter (MAF) to estimate wind velocity [17]. The available measurements are ground velocity of the aircraft from GPS in addition to the conventional auto-pilot sensors. The other variables are obtained from a numerical calculation of EoM. The third group is limited to the case of a low speed aircraft such as a small UAV because the error in the wind linearly increases with airspeed [17]. This linearly increasing error can be reduced through Kalman filter. Without the Kalman filter, the convergence of the wind estimation is not guaranteed. To overcome these issues, first wind model should be constructed by a time-varying model. Second, Kalman filter algorithm should be used to reduce the noise level and guarantee the convergence of the wind estimation. Hence, estimation by Kalman filter is the main approach used in this research for wind estimation along with state estimation.

In this problem, state estimation and noise rejection require the employment of nonlinear Kalman filter. The translational dynamics and translational kinematics of an aircraft have wind terms multiplied by the states. This means that the components of the wind vector would be part of the system matrix of the Linear Kalman Filter (LKF) at the nominal condition. The wind components vary with time. This implies that the system matrix of the LKF would become a time dependent matrix, which is inconsistent with the general LKF requirement of constant system matrices. Thus, the nonlinear Kalnam filter is required. The most widely used nonlinear estimator is the Extended Kalman Filter (EKF). The filter has the accuracy of the first order approximation of the Taylor series expansion at the nominal condition. However, due to the first order Taylor series approximation, the EKF could have a divergence problem [18, 19]. The second order extended Kalman Filter (SOEKF) has the second

order approximation in Taylor series expansion. Even though it is a second order approximation, the SOEKF is less accurate than the Unscented Kalman Filter (UKF) [18]. The Particle Filter (PF), known as the sequential Monte Carlo method (SMC), is a nonlinear estimator dealing with a non-Gaussian distribution [20, 21]. The number of the particles is proportional to the estimation accuracy, which yields to high computational burden. Even though the computational burden could be reduced by Rao-Blackwellization, the PF has more computational burden than that of a EKF. Further, the accuracy of PF may rapidly degrade if the number of the estimation variables is greater than three [22]. On the other hand, recently proposed Unscented Kalman Filter (UKF) overcomes the drawbacks of EKF, SOEKF, and PF. The UKF is easier to implement and has the second order approximation effect at the Taylor series expansion under the Gaussian white noise assumption [23, 24, 25, 26]. The UKF may have a computational problem called singularity during the square root calculation of a symmetric covariance matrix of the state. The singularity problem is overcome by the Square Root Unscented Kalman Filter (SR-UKF) [27, 28, 29, 30]. The SR-UKF directly propagates the square root instead of the symmetric covariance matrix at each step. Therefore, the SR-UKF is used in this research to estimate the aircraft states and the wind velocity.

1.2 Original Contributions

This research work has made the following original contributions:

◦ A new method is developed for the estimation of time-varying wind vector onboard an aircraft flying at high speed based on onboard sensor measurement.

◦ A wind model is obtained as a set of nonlinear differential equations by rearranging the nonlinear translational equations of motion that includes the wind effect through explicit terms with wind components and their derivatives.

◦ The nonlinear model used in the system update of the estimator is augmented with the wind model. This makes the wind components parts of the system state vector. The estimator with the augmented system model can estimate the wind components as well as the aircraft states.

◦ The Square-Root Unscented Kalman Filter (SR-UKF) framework is used for the estimator. A potential singularity problem in the implementation of this estimator is avoided by tuning the covariance matrix of the process noise.

◦ The SR-UKF developed in this research is implemented with both white measurement noise and colored measurement noise cases. The measurement model is modified to handle colored measurement noise. Through a parameter study, it is shown that the performance of the estimator degrades as the measurement error noise becomes more colored in the sense that the correlation time constant increases.

◦ The state and wind estimations are performed in both tanker and the receiver aircraft flying in an aerial refueling operation. The equations of motion of the receiver are written relative to the tanker aircraft's body frame, a non-inertial reference frame. As a result, the equations of motion of the receiver aircraft requires some of the states of the tanker aircraft. Thus, in turn, causes the system update of the receiver estimator to require the measurement or estimation of the tanker states. In the implementation of the receiver estimation in a simulation environment, the tanker state estimates are transmitted to the receiver aircraft for its estimator's system update.

◦ When the receiver aircraft flies in the wake of the tanker, it is exposed to a non-uniform wind field induced by the trailing vortices of the tanker. Thus, the total wind experienced by the receiver aircraft is due to prevailing wind, turbulence and the vortex induced wind while the wind the tanker aircraft is exposed to is due to only prevailing wind and turbulence. The SR-UKF estimator implemented on the receiver

can successfully estimate the total wind exposure. By comparing wind estimation of the tanker with that of the receiver, the vortex induced wind the receiver is exposed to can easily be identified.

- The trajectory tracking controller flies the receiver aircraft relative to the tanker aircraft, which flies straight level and turns at constant altitude with constant speed. The estimated states are successfully used in the feedback control when the measurement error noise is white. The feedback controller was also successful when the correlation time constant of the colored noise is small.

1.3 Organization of the Dissertation

This dissertation is organized as follows. Chapter 2 introduces modeling of aircraft dynamics, measurement and wind. Tanker and receiver equations of motion, tanker and receiver controller, models of wind sources (prevailing wind, turbulence, wake vortex induced wind, total reference wind), and measurement noise models for white and colored noise are discussed in Chapter 2. Chapter 3 reviews linear and nonlinear Kalman filter (linear Kalman filter, extended Kalman filter, unscented Kalman filter, and square-root unscented Kalman filter) and colored measurement in Kalman filter. As estimation parts, Chapter 4 introduces estimation of aircraft states and wind exposure at tanker aircraft, Chapter 5 introduces state and wind estimation without aerodynamic model, and Chapter 6 introduces relative position control of receiver aircraft through estimated state feedback. Chapter 7 presents and discusses the simulation results and parameter studies. Chapter 8 gives the conclusion.

CHAPTER 2

MODELING OF AIRCRAFT DYNAMICS, MEASUREMENT AND WIND

This chapter gives the details of the simulation environment used for the implementation and evaluation of the estimation and control of aircraft flying in formation for aerial refueling. In an aerial refueling operation, while the tanker aircraft flies through a trajectory with straight level legs and constant altitude turns, the receiver aircraft is required to fly relative to the tanker aircraft. The motion of the receiver aircraft includes station keeping at observation, pre-contact, and contact position as well as transitioning between these positions as depicted in Fig. 2.1. As an environ-

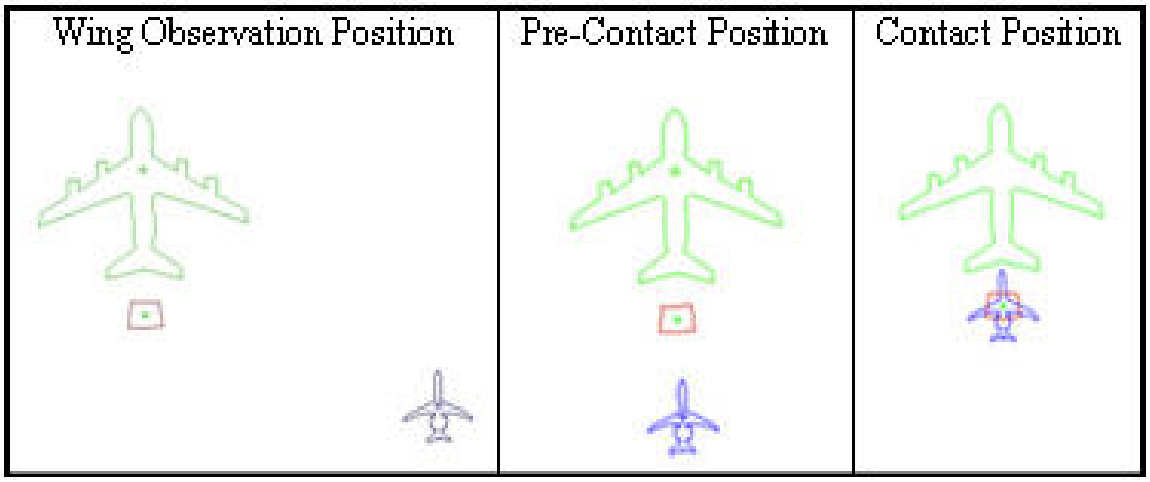

Figure 2.1. Three Aerial Refueling Positions.

mental factor adversely affecting aerial refueling operation, both aircraft are exposed to the prevailing wind and turbulence. The receiver aircraft is additionally exposed to the wake vortex induced wind because of the wake of the tanker aircraft. The three

wind sources, prevailing wind, turbulence, and wake vortex induced wind constitutes the total wind disturbing the precise position control. Measurement noise could be another source of disturbance for the position tracking control of the receiver relative to the tanker. The integrated simulation environment includes the models of all the aspects of the problem: (i) the nonlinear equations of motion for the tanker aircraft and the receiver aircraft, (ii) controllers for flying the tanker through a trajectory relative to the inertial frame and the receiver relative to the tanker, (iii) all sources of wind the aircraft are exposed to, and (iv) measurement error noise for each aircraft. The following sections describes all these components separately.

2.1 Tanker Equations of Motion

The aircraft model here represents a KC-135 tanker aircraft flying through a trajectory with straight level and turning segments in an aerial refueling operation. The equations of motion of the tanker aircraft including the dynamics effect of wind exposure are given in Ref. [7, 31] and repeated herein as reference. The translational dynamics is

$$\begin{aligned}\begin{bmatrix}\dot{V}_T\\ \dot{\beta}_T\\ \dot{\alpha}_T\end{bmatrix} &= \varepsilon_{\mathbf{T}}^{-\mathbf{1}}\mathbf{S}(\omega_{B_T})(\mathbf{R}_{\mathbf{B_T W_T}}V_{w_T}) - \varepsilon_{\mathbf{T}}^{-\mathbf{1}}\mathbf{R}_{\mathbf{B_T I}}\dot{W}_{I_T}\\ &+ \frac{1}{m_T}\varepsilon_{\mathbf{T}}^{-\mathbf{1}}(\mathbf{R}_{\mathbf{B_T I}}M_T + \mathbf{R}_{\mathbf{B_T W_T}}A_T + P_T)\end{aligned} \tag{2.1}$$

$$\varepsilon_{\mathbf{T}}^{-\mathbf{1}} = \begin{bmatrix}\cos\alpha_T\cos\beta_T & \sin\beta_T & \cos\beta_T\sin\alpha_T\\ -\frac{1}{V_T}\cos\alpha_T\sin\beta_T & \frac{1}{V_T}\cos\beta_T & -\frac{1}{V_T}\sin\alpha_T\sin\beta_T\\ -\frac{1}{V_T}\sec\beta_T\sin\alpha_T & 0 & \frac{1}{V_T}\cos\alpha_T\sec\beta_T\end{bmatrix},\ V_{w_T} = \begin{bmatrix}V_T\\ 0\\ 0\end{bmatrix} \tag{2.2}$$

$$M_T = \begin{bmatrix} 0 \\ 0 \\ m_{_T} g \end{bmatrix} A_T = \begin{bmatrix} -D_T \\ -S_T \\ -L_T \end{bmatrix} P_T = \begin{bmatrix} T_x \\ T_y \\ T_z \end{bmatrix} = \begin{bmatrix} T_{_T} \cos \delta_T \\ 0 \\ -T_{_T} \sin \delta_T \end{bmatrix} \tag{2.3}$$

$$\mathbf{S}(\omega_{B_T}) = \begin{bmatrix} 0 & r_{_T} & -q_{_T} \\ -r_{_T} & 0 & p_{_T} \\ q_{_T} & -p_{_T} & 0 \end{bmatrix} \tag{2.4}$$

where ($V_{_T}$, $\beta_{_T}$, $\alpha_{_T}$) are airspeed, side slip angle, and angle of attack, $m_{_T}$ is the mass of the tanker aircraft, ω_{B_T} is the representation of the angular velocity vector with components ($p_{_T}$, $q_{_T}$, $r_{_T}$), M_T is the gravitational force representation in the inertial frame, A_T is the aerodynamic force representation in the wind frame, P_T is the propulsion force representation in the tanker body frame, W_{I_T} is the wind representation expressed in the inertial frame, $\mathbf{R_{B_T W_T}}$ is the rotational matrix from the tanker's wind frame to the tanker's body frame, and $\mathbf{R_{B_T I}}$ is the rotational matrix from the inertial frame to the tanker's body frame.

The aerodynamic forces are given by

$$D_T = \frac{1}{2}\rho V_{_T}^2 S_{_T} C_{D_T} \tag{2.5a}$$

$$S_T = \frac{1}{2}\rho V_{_T}^2 S_{_T} C_{S_T} \tag{2.5b}$$

$$L_T = \frac{1}{2}\rho V_{_T}^2 S_{_T} C_{L_T} \tag{2.5c}$$

where $S_{_T}$ is the reference area of the tanker aircraft and ρ is the air density. The aerodynamic coefficients are

$$C_{D_T} = C_{D_0} + C_{D_{\alpha^2}}\alpha_{_T}^2 \tag{2.6a}$$

$$C_{S_T} = C_{S_0} + C_{S_\beta}\beta_{_T} + C_{S_{\delta_r}}\delta_{r_{_T}} \tag{2.6b}$$

$$C_{L_T} = C_{L_0} + C_{L_\alpha}\alpha_{_T} + C_{L_{\alpha^2}}(\alpha_{_T} - \alpha_{ref})^2 + C_{L_q}\frac{c_{_T}}{2V_{_T}}q_{rel} + C_{L_{\delta_e}}\delta_{e_T} \tag{2.6c}$$

where the angular velocity term (q_{rel}) is relative to the surrounding air, $\delta_{r_{_T}}$ and δ_{e_T} are the rudder and elevator deflections, respectively. The relative angular velocity is calculated from the angular velocity relative to the inertial frame and the angular velocity of the air relative to the inertial frame as

$$\begin{aligned} p_{_{rel}} &= p_{_T} - p_{_{eff}} \\ q_{_{rel}} &= q_{_T} - q_{_{eff}} \\ r_{_{rel}} &= r_{_T} - r_{_{eff}} \end{aligned} \tag{2.7}$$

where (p_{rel}, q_{rel}, r_{rel}) are the angular velocity components relative to the surrounding air, ($p_{_T}$, $q_{_T}$, $r_{_T}$) are the angular velocity relative to the inertial frame, ($p_{_{eff}}, q_{_{eff}}, r_{_{eff}}$) are the rotational wind relative to the inertial frame. The details of the calculation of the rotational wind components can be seen in Ref. [32, 33].

The rotational dynamics is

$$\dot{\omega}_{_{B_T}} = \underline{\underline{\mathbf{I}}}_{\mathbf{T}}^{-\mathbf{1}}\left[M_{B_T} + \mathbf{S}(\omega_{_{B_T}})\underline{\underline{\mathrm{I}}}_{T}\omega_{_{B_T}}\right] \tag{2.8}$$

where $\underline{\underline{\mathbf{I}}}_{\mathbf{T}}$ is the moment of inertia matrix of the tanker aircraft, and M_{B_T} is the applied moment on the tanker aircraft in the tanker body frame. The moments are given by

$$\begin{aligned}
\mathcal{L}_T &= \frac{1}{2}\rho V_T^2 S_a b_T C_{\mathcal{L}_T} \\
\mathcal{M}_T &= \frac{1}{2}\rho V_T^2 S_a c_T C_{\mathcal{M}_T} + \triangle_{z_T} T_T \\
\mathcal{N}_T &= \frac{1}{2}\rho V_T^2 S_a b_T C_{\mathcal{N}_T}
\end{aligned} \tag{2.9}$$

where b_T is the wingspan of the tanker aircraft, c_T is the chord length of the tanker aircraft, $\triangle_{z_T}$ is the moment arms of the thrust in the tanker's body frame, and T_T is the thrust generated by engine. The moment coefficients are expressed by

$$\begin{aligned}
C_{\mathcal{L}_T} &= C_{\mathcal{L}_0} + C_{\mathcal{L}_{\delta_a}}\delta_{a_T} + C_{\mathcal{L}_{\delta_r}}\delta_{r_T} + C_{\mathcal{L}_\beta}\beta_T + C_{\mathcal{L}_p}\frac{b_T}{2V_T}p_{rel} + C_{\mathcal{L}_r}\frac{b_T}{2V_T}r_{rel} \\
C_{\mathcal{M}_T} &= C_{\mathcal{M}_\alpha}\alpha_T + C_{\mathcal{M}_{\delta_e}}\delta_{e_T} + C_{\mathcal{M}_q}\frac{c_T}{2V_T}q_{rel} \\
C_{\mathcal{N}_T} &= C_{\mathcal{N}_0} + C_{\mathcal{N}_{\delta_a}}\delta_{a_T} + C_{\mathcal{N}_{\delta_r}}\delta_{r_T} + C_{\mathcal{N}_\beta}\beta_T + C_{\mathcal{N}_p}\frac{b_T}{2V_T}p_{rel} + C_{\mathcal{N}_r}\frac{b_T}{2V_T}r_{rel}
\end{aligned} \tag{2.10}$$

where δ_{a_T} is the aileron deflection.

The rotational kinematics is

$$\begin{aligned}
\dot{\psi}_T &= (q_T \sin\phi_T + r_T \cos\phi_T)\sec\theta_T \\
\dot{\theta}_T &= (q_T \cos\phi_T - r_T \sin\phi_T) \\
\dot{\phi}_T &= p_T + (q_T \sin\phi_T + r_T \cos\phi_T)\tan\theta_T
\end{aligned} \tag{2.11}$$

where $(\psi_T, \theta_T, \phi_T)$ are the Euler angles relative to the inertial frame.

The translational kinematics is

$$\dot{r}_{B_T} = \mathbf{R}^{\mathbf{T}}_{\mathbf{B_T I}}\mathbf{R}_{\mathbf{B_T W_T}}V_{w_T} + W_{I_T} \tag{2.12}$$

where $\dot{r}_{B_T}$ is the velocity of the tanker aircraft relative to the inertia frame. The integration of the velocity is the position vector.

The tanker aircraft model is represented in a compact form as

$$\dot{\mathrm{x}}_T = f(\mathrm{x}_\mathrm{T}, u, W_{I_T}, \dot{W}_{I_T}), \quad \mathrm{x}_T \in \Re^{12} \tag{2.13}$$

The state vector is given by

$$\mathrm{x}_T = [V_T, \beta_T, \alpha_T, p_T, q_T, r_T, \psi_T, \theta_T, \phi_T, x_T, y_T, z_T]^T \tag{2.14}$$

The control input is defined by

$$u = [\delta_{a_T}, \delta_{e_T}, \delta_{r_T}, T_T]^T \tag{2.15}$$

where (δ_{a_T}, δ_{e_T}, δ_{r_T}) are aileron, elevator, and rudder deflection respectively, and T_T is the thrust.

2.2 Receiver Equations of Motion

In aerial refueling simulations conducted in this research, a model representing Learjet 25 receiver aircraft as a surrogate receiver is used. In an aerial operation, the receiver aircraft should fly and be controlled relative to the tanker aircraft. Thus, the equations of motion are written in terms of the position and orientation of the receiver relative to the body frame of the tanker.

The matrix form of the translational dynamics is [7, 31]

$$\begin{bmatrix} \dot{V} \\ \dot{\beta} \\ \dot{\alpha} \end{bmatrix} = \varepsilon_{\mathbf{R}}^{-\mathbf{1}} \left[\mathbf{S}(\omega_{B_R B_T}) + \mathbf{R}_{\mathbf{B_R B_T}} \mathbf{S}(\omega_{B_T}) \mathbf{R}_{\mathbf{B_R B_T}}^{\mathbf{T}} \right] (\mathbf{R}_{\mathbf{B_R W_R}} V_w + W_{B_R}) - \varepsilon_{\mathbf{R}}^{-\mathbf{1}} \dot{W}_{B_R} + \frac{1}{m_R} \varepsilon_{\mathbf{R}}^{-\mathbf{1}} (\mathbf{R}_{\mathbf{B_R B_T}} \mathbf{R}_{\mathbf{B_T I}} M_R + \mathbf{R}_{\mathbf{B_R W_R}} A_R + P_R) \tag{2.16}$$

where

$$\varepsilon_{\mathbf{R}}^{-\mathbf{1}} = \begin{bmatrix} \cos\alpha\cos\beta & \sin\beta & \cos\beta\sin\alpha \\ -\frac{1}{V}\cos\alpha\sin\beta & \frac{1}{V}\cos\beta & -\frac{1}{V}\sin\alpha\sin\beta \\ -\frac{1}{V}\sec\beta\sin\alpha & 0 & \frac{1}{V}\cos\alpha\sec\beta \end{bmatrix} \tag{2.17}$$

where (V, β α) are velocity relative to the wind frame, side slip angle, and angle of attack, $\omega_{B_R B_T}$ is the relative angular velocity in the component form, V_w is the component of the velocity relative to the wind frame, m_R is the mass of the receiver aircraft, W_{B_R} is the representation of the wind expressed in the receiver body frame and thus $\dot{W}_{B_R}$ is the wind derivative relative to the receiver body frame expressed in the receiver body frame. Further, $\mathbf{R}_{\mathbf{B_R B_T}}$ is the rotational matrix from the tanker's body frame to the receiver's body frame and $\mathbf{R}_{\mathbf{B_R W_R}}$ is the rotational matrix from the receiver's wind frame to the receiver's body frame.

The external force is the sum of the gravitational force M_R expressed in the inertia frame, the aerodynamics force A_R expressed in the receiver body frame, and

the propulsive force P_R expressed in the receiver body frame. The matrix forms of the external forces are give by

$$M_R = \begin{bmatrix} 0 \\ 0 \\ m_{_R} g \end{bmatrix} A_R = \begin{bmatrix} -D \\ -S \\ -L \end{bmatrix} P_R = \begin{bmatrix} T_x \\ T_y \\ T_z \end{bmatrix} \tag{2.18}$$

where g is the gravity, (D, S, L) are drag, side force, and lift, (T_x, T_y, T_z) are the thrust in x-y-z directions of the receiver body frame.

The aerodynamic forces are given by

$$D = \frac{1}{2}\rho V^2 S_{_R} C_D \tag{2.19a}$$

$$S = \frac{1}{2}\rho V^2 S_{_R} C_S \tag{2.19b}$$

$$L = \frac{1}{2}\rho V^2 S_{_R} C_L \tag{2.19c}$$

where $S_{_R}$ is the reference area of the receiver aircraft. The aerodynamic force coefficients are

$$C_D = C_{D_0} + C_{D_\alpha}\alpha + C_{D_{\alpha 2}}\alpha^2 + C_{D_{\delta_e}}\delta_e + C_{D_{\delta_e 2}}\delta_e^2 + C_{D_{\delta_s}}\delta_s + C_{D_{\delta_s 2}}\delta_s^2 \tag{2.20a}$$

$$C_S = C_{S_0} + C_{S_\beta}\beta + C_{S_{\delta_a}}\delta_a + C_{S_{\delta_r}}\delta_r \tag{2.20b}$$

$$C_L = C_{L_0} + C_{L_\alpha}\alpha + C_{L_\alpha 2}(\alpha - \alpha_{ref})^2 + C_{L_q}\frac{c}{2V_{_R}}q_{rel} + C_{L_{\delta_e}}\delta_e + C_{L_{\delta_s}}\delta_s \tag{2.20c}$$

where q_{rel} is the pitch component of the angular velocity of the aircraft relative to the surrounding air in the body frame. The other two components are q_{rel} and r_{rel}.

All together, the representation of the angular velocity of the receiver relative to the surrounding air in the body frame is

$$\omega_{rel} = \begin{bmatrix} p_{rel} \\ q_{rel} \\ r_{rel} \end{bmatrix} \tag{2.21}$$

which can be written in terms of the angular velocity of the receiver relative to the tanker, angular velocity of the receiver relative to the inertial frame and the angular velocity of the surrounding air relative to the inertial frame, i.e., rotational wind, as

$$\omega_{rel} = \omega_{_{B_R B_T}} + \mathbf{R_{B_R B_T}} \omega_{_{B_T}} - \begin{bmatrix} p_{_{eff}} \\ q_{_{eff}} \\ r_{_{eff}} \end{bmatrix} \tag{2.22}$$

where $(p_{_{eff}}, q_{_{eff}}, r_{_{eff}})$ are the rotational wind relative to the inertial frame, expressed in the body frame of the receiver. The details of the rotational wind calculation can be found in Refs. [32, 33]

The matrix form of the rotational dynamics is [7, 31]

$$\begin{aligned} \dot{\omega}_{_{B_R B_T}} &= \underline{\underline{\mathrm{I}}}_R^{-1} M_{B_R} + \underline{\underline{\mathrm{I}}}_R^{-1} \mathbf{S}(\omega_{_{B_R B_T}} + \mathbf{R_{B_R B_T}} \omega_{_{B_T}}) \underline{\underline{\mathrm{I}}}_R (\omega_{_{B_R B_T}} + \mathbf{R_{B_R B_T}} \omega_{_{B_T}}) \\ &- \mathbf{S}(\omega_{_{B_R B_T}}) \mathbf{R_{B_R B_T}} \omega_{_{B_T}} - \mathbf{R_{B_R B_T}} \dot{\omega}_{_{B_T}} \end{aligned} \tag{2.23}$$

where $\underline{\underline{I}}_R$ is the inertia matrix of the receiver aircraft, and M_{B_R} is the moment of the receiver aircraft at the receiver body frame as

$$M_{B_R} = \begin{bmatrix} \mathcal{L} \\ \mathcal{M} \\ \mathcal{N} \end{bmatrix} \tag{2.24}$$

where ($\mathcal{L}$, $\mathcal{M}$, $\mathcal{N}$) are roll moment, pitch moment, and yaw moment. The moments are given by

$$\begin{aligned} \mathcal{L} &= \frac{1}{2}\rho V^2 S_{_R} b C_{\mathcal{L}} - \triangle_z T_y + \triangle_y T_z \\ \mathcal{M} &= \frac{1}{2}\rho V^2 S_{_R} c C_{\mathcal{M}} + \triangle_z T_x + \triangle_x T_z \\ \mathcal{N} &= \frac{1}{2}\rho V^2 S_{_R} b C_{\mathcal{N}} - \triangle_y T_x - \triangle_x T_y \end{aligned} \tag{2.25}$$

where b is the wingspan, c is the chord length of the receiver aircraft, ($\triangle_x$, $\triangle_y$, $\triangle_z$) are the moment arms of the thrust in the body frame of the receiver and (T_x, T_y, T_z) are thrust relative to the receiver body frame. The moment coefficients are

$$\begin{aligned} C_{\mathcal{L}} &= C_{L_0} + C_{L_{\delta_a}}\delta_a + C_{L_{\delta_r}}\delta_r + C_{L_\beta}\beta + C_{L_p}\frac{b}{2V}p_{rel} + C_{L_{r_{rel}}}\frac{b}{2V}r_{rel} \\ C_{\mathcal{M}} &= C_{M_0} + C_{M_\alpha}\alpha + C_{M_{\delta_e}}\delta_e + C_{M_q}\frac{c}{2V}q_{rel} + C_{M_{\delta_s}}\delta_s \\ C_{\mathcal{N}} &= C_{N_0} + C_{N_{\delta_a}}\delta_a + C_{N_{\delta_r}}\delta_r + C_{N_\beta}\beta + C_{N_p}\frac{b}{2V}p_{rel} + C_{N_{r_{rel}}}\frac{b}{2V}r_{rel} \end{aligned} \tag{2.26}$$

where (δ_a,δ_e,δ_r,δ_s) are the deflections for the aileron, elevator, rudder and stabilizer, respectively.

Rotational kinematics is [7, 31]

$$\begin{aligned}\dot{\psi} &= (q\sin\phi + r\cos\phi)\sec\theta \\ \dot{\theta} &= (q\cos\phi - r\sin\phi) \\ \dot{\phi} &= p + (q\sin\phi + r\cos\phi)\tan\theta\end{aligned} \tag{2.27}$$

where the orientation (ψ, θ, ϕ), and the angular velocity *(p,q,r)* are relative to the tanker expressed in the receiver body frame.

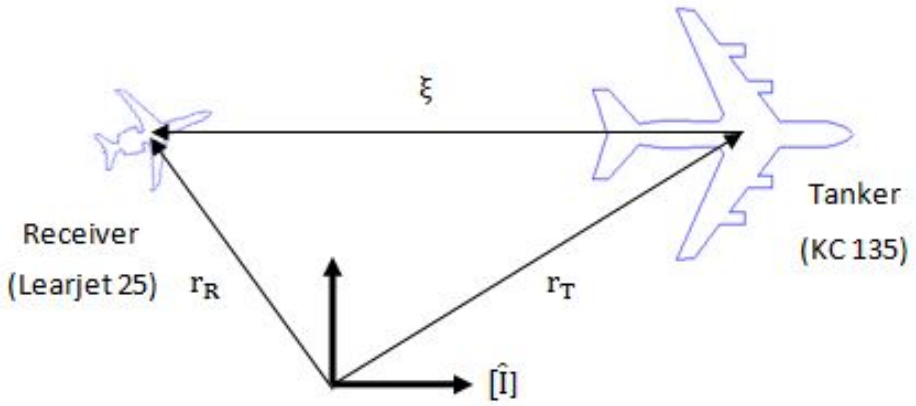

Figure 2.2. Relative Position Vector of the Receiver Aircraft.

As depicted in Fig. 2.2, the position vector of the receiver relative to the inertia frame is the sum of the position vector of the tanker relative to the inertia frame and the relative position vector of the receiver with respect to the tanker.

$$[\hat{\underline{I}}]^T r_R = [\hat{\underline{I}}]^T r_T + [\hat{\underline{I}}]^T \mathbf{R}^{\mathbf{T}}_{\mathbf{B_T I}} \xi \tag{2.28}$$

where r_R is the representation of the position of the receiver relative to the inertia frame expressed in the inertia frame, r_T is the representation of the position of the tanker relative to the inertia frame expressed in the inertia frame, and ξ is the repre-

sentation of the receiver position relative to the tanker expressed in the tanker body frame. The matrix form of the relative translational kinematics is [7, 31].

$$\dot{\xi} = \mathbf{R}^{\mathbf{T}}_{\mathbf{B_R B_T}} \mathbf{R}_{\mathbf{B_R W_R}} V_w + \mathbf{R}^{\mathbf{T}}_{\mathbf{B_R B_T}} W_{B_R} - \mathbf{R}_{\mathbf{B_T I}} \dot{r}_T + \mathbf{S}(\omega_{\mathbf{B_T}})\xi \tag{2.29}$$

where ξ is written in component form as

$$\xi = \begin{bmatrix} \xi_1 \\ \xi_2 \\ \xi_3 \end{bmatrix} \tag{2.30}$$

The receiver aircraft model is represented in a compact form as

$$\dot{\mathrm{x}}_{\mathrm{R}} = f(\mathrm{x}_R, \mathrm{x}_{\mathrm{T}}, u, W_{B_R}, \dot{W}_{B_R}) \tag{2.31}$$

The state vector is given by

$$\mathrm{x}_R = [V, \beta, \alpha, p, q, r, \psi, \theta, \phi, \xi_1, \xi_2, \xi_3]^T \tag{2.32}$$

The control input is defined by

$$u_R = [\delta_a, \delta_e, \delta_r, \delta_s, T, \delta_y, \delta_z]^T \tag{2.33}$$

where (δ_a, δ_e, δ_r, δ_s) are aileron deflection angle, elevator deflection angle, rudder deflection angle, and stabilizer deflection angle, T is the thrust, (δ_y, δ_z) are engine nozzle deflections for an aircraft capable of thrust vectoring control. The thrust vectoring is not used in this work.

2.3 Tanker Controller

In an aerial refueling operation, the tanker aircraft is flown by a pilot through a pre-specified trajectory, consisting of straight level and turn segments, at a constant altitude and with a constant airspeed. In the simulation, this is achieved by a feedback controller. The controller is designed in Ref. [31] based on a commanded constant airspeed, a commanded constant altitude and a commanded time-varying yaw-rate. This section gives a brief overview of the controller as a reference.

Table 2.1. Six Nominal Conditions

Nominal Condition	Yaw Rate	Airspeed
1	$\dot{\psi}_1$	V_1
2	$\dot{\psi}_1$	V_2
3	$\dot{\psi}_2$	V_1
4	$\dot{\psi}_2$	V_3
5	$\dot{\psi}_3$	V_1
6	$\dot{\psi}_3$	V_2

The control law developed using an LQR-based approach relies on gain scheduling to cover the whole range of flight conditions that the tanker aircraft flies in an aerial refueling operation. The gain scheduling uses commanded airspeed and commanded yaw rate as scheduling variables. The six nominal conditions defined based on the scheduling variables are listed in Table 2.1. For each nominal condition, the nonlinear equations of motion are linearized and an LQR-controller is designed based on the linear model of each nominal condition. The linear model for each nominal condition is

$$\Delta\dot{\mathrm{x}}_T = \mathbf{A}\Delta\mathrm{x}_T + \mathbf{B}\Delta u \tag{2.34}$$

where $\Delta \mathrm{x}_T$ is the linearized system state vector of the tanker aircraft, and Δu is the linearized control input. The linearized control input vector is defined by

$$\Delta u = [\Delta\delta_{a_T}\ \Delta\delta_{e_T}\ \Delta\delta_{r_T}\ \Delta_{T_T}]^T \tag{2.35}$$

For improving steady-state performance of tracking the commanded signals, three integral control terms are added to the LQR-controllers. For this, three error signals are defined between the commanded outputs and actual outputs as

$$\dot{e} = \Delta \mathrm{y}_T - \Delta \mathrm{y}_c \tag{2.36}$$

where

$$e = \begin{bmatrix} \Delta V - \Delta V_c \\ \Delta z - \Delta z_c \\ \Delta\dot{\psi} - \Delta\dot{\psi}_c \end{bmatrix} \tag{2.37}$$

where Δ indicates deviation from the nominal condition, and the subscript c indicates the commanded signal. The augmented equation, for each nominal condition, obtained by combining both Eq. (2.34) and Eq. (2.36) is

$$\begin{bmatrix} \Delta\dot{\mathrm{x}}_T \\ \dot{e} \end{bmatrix} = \begin{bmatrix} \mathbf{A} & 0 \\ \mathbf{C} & 0 \end{bmatrix} \begin{bmatrix} \Delta \mathrm{x}_T \\ e \end{bmatrix} + \begin{bmatrix} \mathbf{B} \\ 0 \end{bmatrix} \Delta u + \begin{bmatrix} 0 \\ -\Delta \mathrm{y}_c \end{bmatrix} \tag{2.38}$$

The state feedback control law for Eq. (2.38), with the gains calculated by the LQR procedure, is

$$\begin{aligned} \Delta u_i &= -\mathrm{K_i} \cdot \Delta \mathrm{x}_{T_i} - \mathrm{K_{e,i}} \cdot e \\ u_i &= u_{0,i} + \Delta u_i \\ \Delta \mathrm{x}_{T_i} &= \mathrm{x}_T - \mathrm{x}_{T_{0,i}} \end{aligned} \tag{2.39}$$

where $i \in \{1, 2, 3, 4, 5, 6\}$ corresponding to the six nominal conditions of Table 2.1, and $[\mathrm{K_i}\ \mathrm{K_{e,i}}]$ is the augmented state feedback gain matrix obtained by minimizing the cost function in LQR design technique.

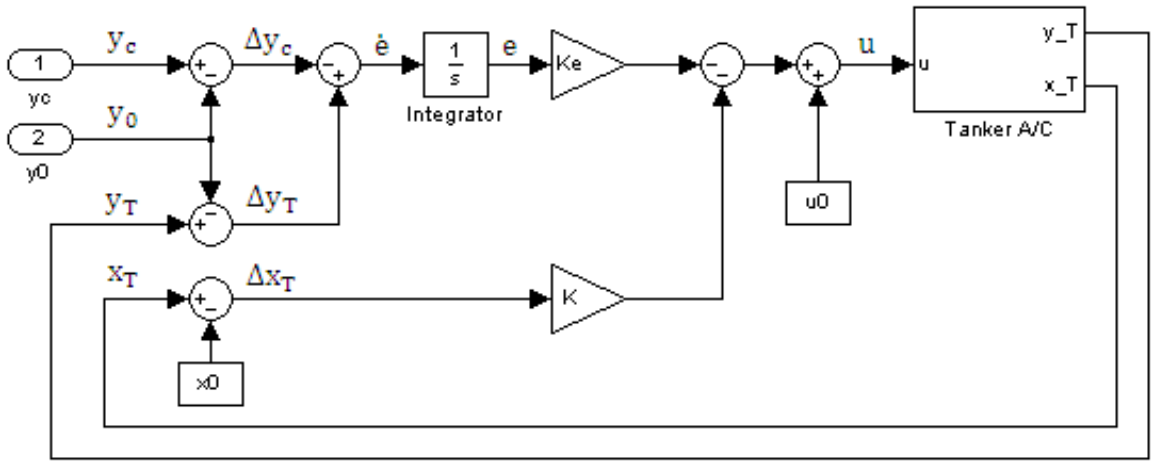

Figure 2.3. LQR-based Controller for Tanker Aircraft.

For the implementation of the gain scheduling controller, a Lagrange interpolation is used between the six linear controllers designed for each nominal condition. Thus, the gain scheduling control law is

$$
\begin{aligned}
u = & \frac{(\dot{\psi}_c - \dot{\psi}_2)(\dot{\psi}_c - \dot{\psi}_3)(V_c - V_2)}{(\dot{\psi}_1 - \dot{\psi}_2)(\dot{\psi}_1 - \dot{\psi}_3)(V_1 - V_2)}\, u_1 + \frac{(\dot{\psi}_c - \dot{\psi}_1)(\dot{\psi}_c - \dot{\psi}_3)(V_c - V_2)}{(\dot{\psi}_2 - \dot{\psi}_1)(\dot{\psi}_2 - \dot{\psi}_3)(V_1 - V_2)}\, u_3 \\
& + \frac{(\dot{\psi}_c - \dot{\psi}_1)(\dot{\psi}_c - \dot{\psi}_2)(V_c - V_2)}{(\dot{\psi}_3 - \dot{\psi}_1)(\dot{\psi}_3 - \dot{\psi}_2)(V_1 - V_2)}\, u_5 + \frac{(\dot{\psi}_c - \dot{\psi}_2)(\dot{\psi}_c - \dot{\psi}_3)(V_c - V_1)}{(\dot{\psi}_1 - \dot{\psi}_2)(\dot{\psi}_1 - \dot{\psi}_3)(V_2 - V_1)}\, u_2 \\
& + \frac{(\dot{\psi}_c - \dot{\psi}_1)(\dot{\psi}_c - \dot{\psi}_3)(V_c - V_1)}{(\dot{\psi}_2 - \dot{\psi}_1)(\dot{\psi}_2 - \dot{\psi}_3)(V_2 - V_1)}\, u_4 + \frac{(\dot{\psi}_c - \dot{\psi}_1)(\dot{\psi}_c - \dot{\psi}_2)(V_c - V_1)}{(\dot{\psi}_3 - \dot{\psi}_1)(\dot{\psi}_3 - \dot{\psi}_2)(V_2 - V_1)}\, u_6
\end{aligned}
\tag{2.40}
$$

Figure 2.3 shows the implementation of the LQR-controller in the nonlinear simulation environment.

2.4 Receiver Controller

In an aerial refueling operation, the receiver aircraft's position should be controlled relative to the tanker while the tanker aircraft flies through its pre-specified trajectory. Thus, the receiver controller is designed to track the commanded position of the receiver relative to the tanker. For the design of the receiver controller, the same method summarized above for the tanker aircraft is used. Namely, a state-feedback and integral control method is used and the gain scheduling approach is used to cover the whole flight range of the aircraft in an aerial refueling operation. The gain scheduling uses the tanker's commanded airspeed and yaw rate as scheduling variables and has the six set of gains computed by the LQR technique at each of the six nominal conditions, defined in Table 2.1. As with the tanker's controller, the details of the receiver controller design can be found in Refs. [7, 31]

The linearized model of the receiver equations of motion for each nominal condition is

$$\Delta\dot{\mathrm{x}}_R = \mathbf{A}\Delta\mathrm{x}_R + \mathbf{B}\Delta u \tag{2.41}$$

where $\Delta\mathrm{x}_R$ is the linearized system state vector of the receiver aircraft, and Δu is the linearized control input vector, defined as

$$\Delta u = [\Delta\delta_a \ \Delta\delta_e \ \Delta\delta_r \ \Delta T \ \Delta\delta_y \ \Delta\delta_z]^T \tag{2.42}$$

where T is a thrust, $(\delta_y,\ \delta_z)$ are engine nozzle deflections for an aircraft capable of thrust vectoring control and $(\delta_a,\ \delta_e,\ \delta_r)$ are the aileron, elevator and rudder deflections, respectively. In this work, the engine nozzle deflections are zeros as the aircraft simulated does not have thrust vectoring capability.

For the integral control of the relative position, the error states are defined as

$$\dot{e} = \Delta\mathrm{y}_{_R} - \Delta\mathrm{y}_c \tag{2.43}$$

where

$$e = \begin{bmatrix} \Delta\xi_1 - \Delta\xi_{1,c} \\ \Delta\xi_2 - \Delta\xi_{2,c} \\ \Delta\xi_3 - \Delta\xi_{3,c} \end{bmatrix} \tag{2.44}$$

where Δ indicates deviation from the nominal condition, and the subscript c indicates the commanded signal. The augmented equation, for each nominal condition, obtained by combining both Eq. (2.41) and Eq. (2.43) is

$$\begin{bmatrix} \Delta\dot{\mathrm{x}}_R \\ \dot{e} \end{bmatrix} = \begin{bmatrix} \mathbf{A} & 0 \\ \mathbf{C} & 0 \end{bmatrix} \begin{bmatrix} \Delta\mathrm{x}_R \\ e \end{bmatrix} + \begin{bmatrix} \mathbf{B} \\ 0 \end{bmatrix} \Delta u + \begin{bmatrix} 0 \\ -\Delta\mathrm{y}_c \end{bmatrix} \tag{2.45}$$

The state feedback control law for Eq. (2.45), with the gains calculated by the LQR procedure, is

$$\begin{aligned} \Delta u_i &= -\mathrm{K_i} \cdot \Delta \mathrm{x}_{R_i} - \mathrm{K_{e,i}} \cdot e \\ u_i &= u_{0,i} + \Delta u_i \\ \Delta \mathrm{x}_{R_i} &= \mathrm{x}_R - \mathrm{x}_{R_{0,i}} \end{aligned} \tag{2.46}$$

where $i \in \{1, 2, 3, 4, 5, 6\}$ corresponding to the six nominal conditions of Table 2.1, and $[\mathrm{K_i}\ \mathrm{K_{e,i}}]$ is the augmented state feedback gain matrix obtained by minimizing the cost function in LQR design technique.

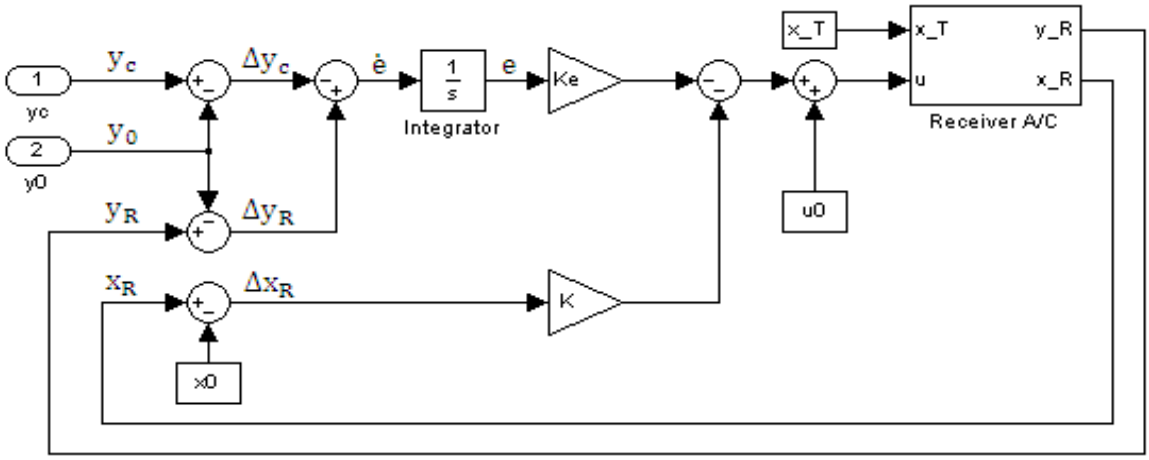

Figure 2.4. LQR-based Controller for Receiver Aircraft.

For the implementation of the gain scheduling controller, a Lagrange interpolation is used between the six linear controllers designed for each nominal condition. Thus, the gain scheduling control law is

$$\begin{aligned} u = & \frac{(\dot{\psi}_c - \dot{\psi}_2)(\dot{\psi}_c - \dot{\psi}_3)(V_c - V_2)}{(\dot{\psi}_1 - \dot{\psi}_2)(\dot{\psi}_1 - \dot{\psi}_3)(V_1 - V_2)} \, u_1 + \frac{(\dot{\psi}_c - \dot{\psi}_1)(\dot{\psi}_c - \dot{\psi}_3)(V_c - V_2)}{(\dot{\psi}_2 - \dot{\psi}_1)(\dot{\psi}_2 - \dot{\psi}_3)(V_1 - V_2)} \, u_3 \\ & + \frac{(\dot{\psi}_c - \dot{\psi}_1)(\dot{\psi}_c - \dot{\psi}_2)(V_c - V_2)}{(\dot{\psi}_3 - \dot{\psi}_1)(\dot{\psi}_3 - \dot{\psi}_2)(V_1 - V_2)} \, u_5 + \frac{(\dot{\psi}_c - \dot{\psi}_2)(\dot{\psi}_c - \dot{\psi}_3)(V_c - V_1)}{(\dot{\psi}_1 - \dot{\psi}_2)(\dot{\psi}_1 - \dot{\psi}_3)(V_2 - V_1)} \, u_2 \\ & + \frac{(\dot{\psi}_c - \dot{\psi}_1)(\dot{\psi}_c - \dot{\psi}_3)(V_c - V_1)}{(\dot{\psi}_2 - \dot{\psi}_1)(\dot{\psi}_2 - \dot{\psi}_3)(V_2 - V_1)} \, u_4 + \frac{(\dot{\psi}_c - \dot{\psi}_1)(\dot{\psi}_c - \dot{\psi}_2)(V_c - V_1)}{(\dot{\psi}_3 - \dot{\psi}_1)(\dot{\psi}_3 - \dot{\psi}_2)(V_2 - V_1)} \, u_6 \end{aligned} \tag{2.47}$$

Figure 2.4 shows the implementation of the LQR-controller in the nonlinear simulation environment.

2.5 Models of Wind Sources

The tanker aircraft, while flying through the commanded trajectory, and the receiver aircraft, while flying relative to the tanker, are exposed to the prevailing wind and turbulence. The receiver aircraft is also subject to an additional wind field induced by the wake of the tanker aircraft, which is called the wake vortex induced wind. The vortex induced wind field is highly nonuniform and thus its magnitude and direction vary depending on the position relative to the tanker. For example, when the receiver is at the observation position, the receiver is outside the wake of the tanker, and the magnitude of the vortex induced wind is zero. Thus, the receiver is exposed to the superposition of the prevailing wind and the turbulence. when the receiver is at the contact position, it is subject to the superposition of the prevailing wind, vortex induced wind and the turbulence.

2.5.1 Prevailing Wind

The prevailing wind (W_{pre}) relative to the inertial frame is obtained by two different methods. One is based on a set of flight data. The second method is based on a probabilistic method, which is referred to, in this paper, as Exponentially Correlated Wind Model (ECWM).

2.5.1.1 Flight Data Based Model

The prevailing wind is extracted from a test flight data including a KF-135R as the tanker aircraft and a Learjet 25 as the surrogate receiver aircraft. The test flight was conducted over Lake Ontario, north of Rochester, NY, on September 22, 2004 as part of the AFRL Automated Aerial Refueling (AAR) program. During the flight over Lake Ontario, the flight data measured onboard the tanker and the receiver aircraft were recorded. In a prior work, Lewis calculated the total wind based on the flight data and the velocity triangle vector [7]. The equation form of the velocity triangle vector is

$$W_I = \dot{r}_{B_T} - \mathbf{R^T_{B_TI}} \mathbf{R_{B_TW_T}} [V_T \;\; 0 \;\; 0]^T \tag{2.48}$$

where W_I is the representation of the wind vector in the inertial frame, $\dot{r}_{B_T}$ is the representation of the tanker aircraft's inertial velocity in the inertial frame, $\mathbf{R_{B_TI}}$ is the rotational matrix from the inertial frame to the tanker body frame, $\mathbf{R_{B_TW_T}}$ is the rotational matrix from the tanker aircraft's wind frame to the body frame, and V_T is the tanker aircraft's airspeed.

The total wind relative to inertial frame is calculated by Eq. (2.48), based on the GPS reading ($\dot{r}_{B_T}$), IMU or magnetometer readings ($\mathbf{R_{B_TI}}$), and airdata sensor readings (V_T and $\mathbf{R_{B_TW_T}}$). After the turbulence effect is removed by the mean calculation, the mean value of Eq. (2.48) is considered to be the prevailing wind.

The mean value is calculated using a non-causal moving-window averaging filter [7]. This reference prevailing wind used in this research is entered into the simulation as exogenous input and thus independent of the states of the aircraft during simulation.

2.5.1.2 Exponentially correlated Wind Model (ECWM)

The prevailing wind is generated based on an exponentially correlated stochastic model, called ECWM (Exponentially Correlated Wind Model). The ECWM is proposed to provide randomly generated wind profile. The concept of the ECWM is obtained from the Dryden turbulence model, that is, a random process is generated by filtering a white noise through a linear system representation by a transfer function with a large correlation time constant. The components of the prevailing wind are computed by

$$\begin{aligned} \dot{W}_{pre,X} &= -\, b_{\mathrm{w}}\, W_{pre,X} + \sqrt{a_{\mathrm{w}} \cdot b_{\mathrm{w}}}\, \eta_x \\ \dot{W}_{pre,Y} &= -\, b_{\mathrm{w}}\, W_{pre,Y} + \sqrt{a_{\mathrm{w}} \cdot b_{\mathrm{w}}}\, \eta_y \\ \dot{W}_{pre,Z} &= 0 \end{aligned} \tag{2.49}$$

where a_{w} is the coefficient to show the extent of the mean square value of the prevailing wind, b_{w} is the inverse time constant to show the extent of the correlation of the prevailing wind, and (η_x, η_y) are the zero-mean Gaussian white noises with one-sided power spectrum density of one. The two constants a_{w} and b_{w} are

$$\begin{aligned} a_{\mathrm{w}} &= 2(E[W_{pre}]^2 + \sigma_{\mathrm{w}}^2) \\ b_{\mathrm{w}} &= 1/\tau_{\mathrm{w}} \end{aligned} \tag{2.50}$$

where τ_{w} is the correlation time constant that controls the degree of the correlation of the wind.

Wind can be expressed by a magnitude and direction. The initial value of the magnitude, $W_{pre,0}$, is determined by a Gaussian distribution with the specific mean and variance of the wind and the initial condition of the direction, $\psi_{\mathrm{w},0}$, is computed by a uniform distribution within the range from 0 to 2π. The initial conditions of the components of the wind in inertial frame, transformed from a magnitude-direction coordinate, are

$$\begin{aligned} W_{pre,X_0} =& |W_{pre,0}| \cdot \cos\psi_{\mathrm{w},0} \\ W_{pre,Y_0} =& |W_{pre,0}| \cdot \sin\psi_{\mathrm{w},0} \\ W_{pre,Z_0} =& 0 \end{aligned} \tag{2.51}$$

2.5.2 Turbulence

The Dryden model is used to model the turbulence as a random process [34]. The Dryden model is expressed by first order differential equations. The input is the zero mean Gaussian white noise with unity power spectrum. The differential equations of the Dryden model are

$$\begin{bmatrix} \dot{x}_{w1} \\ \dot{x}_{w2} \\ \dot{x}_{w3} \\ \dot{x}_{w4} \\ \dot{x}_{w5} \end{bmatrix} = \begin{bmatrix} -\frac{V}{L_u} & 0 & 0 & 0 & 0 \\ 0 & 0 & 1 & 0 & 0 \\ 0 & -\frac{V}{L_v} & -2\frac{V}{L_v} & 0 & 0 \\ 0 & 0 & 0 & 0 & 1 \\ 0 & 0 & 0 & -\frac{V}{L_w} & -2\frac{V}{L_w} \end{bmatrix} \begin{bmatrix} x_{w1} \\ x_{w2} \\ x_{w3} \\ x_{w4} \\ x_{w5} \end{bmatrix} + \begin{bmatrix} \sqrt{\frac{2V\sigma_u^2}{\pi L_u}} & 0 & 0 \\ 0 & 0 & 0 \\ 0 & 1 & 0 \\ 0 & 0 & 0 \\ 0 & 0 & 1 \end{bmatrix} \begin{bmatrix} \eta_1 \\ \eta_2 \\ \eta_3 \end{bmatrix} \tag{2.52}$$

where (x_{w1}, x_{w2}, x_{w3}, x_{w4}, x_{w5}) are states of the Dryden model, V is the airspeed of the aircraft, and (η_1, η_2, η_3) are the zero mean Gaussian white noise with unity power spectrum.

The components of wind due to turbulence is expressed in the body frame as

$$W_{tur} = \begin{bmatrix} 1 & 0 & 0 & 0 & 0 \\ 0 & \frac{\sigma_v}{\sqrt{\pi}}\left(\frac{V}{L_v}\right)^{1.5} & \sigma_v\sqrt{\frac{3V}{\pi L_v}} & 0 & 0 \\ 0 & 0 & 0 & \frac{\sigma_w}{\sqrt{\pi}}\left(\frac{V}{L_w}\right)^{1.5} & \sigma_w\sqrt{\frac{3V}{\pi L_w}} \end{bmatrix} \begin{bmatrix} x_{w1} \\ x_{w2} \\ x_{w3} \\ x_{w4} \\ x_{w5} \end{bmatrix} \tag{2.53}$$

where σ_u, σ_v, and σ_w are turbulence intensity set to 0.39 m/s (1.3 ft/s) at an altitude of 7010 m (22,998 ft), and L_u, L_v, and L_w are set to 533.4 m, which represents light turbulence, as marked in Fig 2.5, which is reproduced from [34]. The values of L and σ are recommended in MIL-F-8785C [34]. Figure 2.6 shows the components of the reference turbulence relative to the inertial frame.

2.5.3 Wake Vortex Induced Wind

Since the vortex induced wind field acting on the receiver aircraft is highly nonuniform, standard aerodynamic force and moment equations, based on airspeed, angle of attack and sideslip angle, cannot be used directly. A method, called NWEMT (Nonuniform Wind Effect Modeling Technique), enables the use of standard dynamic equations of motion and aerodynamic build-up equations with wind effect terms included [7, 32]. The NWEMT approximates the nonuniform wind field the aircraft is exposed to by uniform translational and rotational wind components. The effective translational and rotational wind components are directly integrated into the equations of motion through the wind terms in the translational dynamics and kinematics equations as well as through the angular velocity of the surrounding air components in the aerodynamic force and moment expressions.

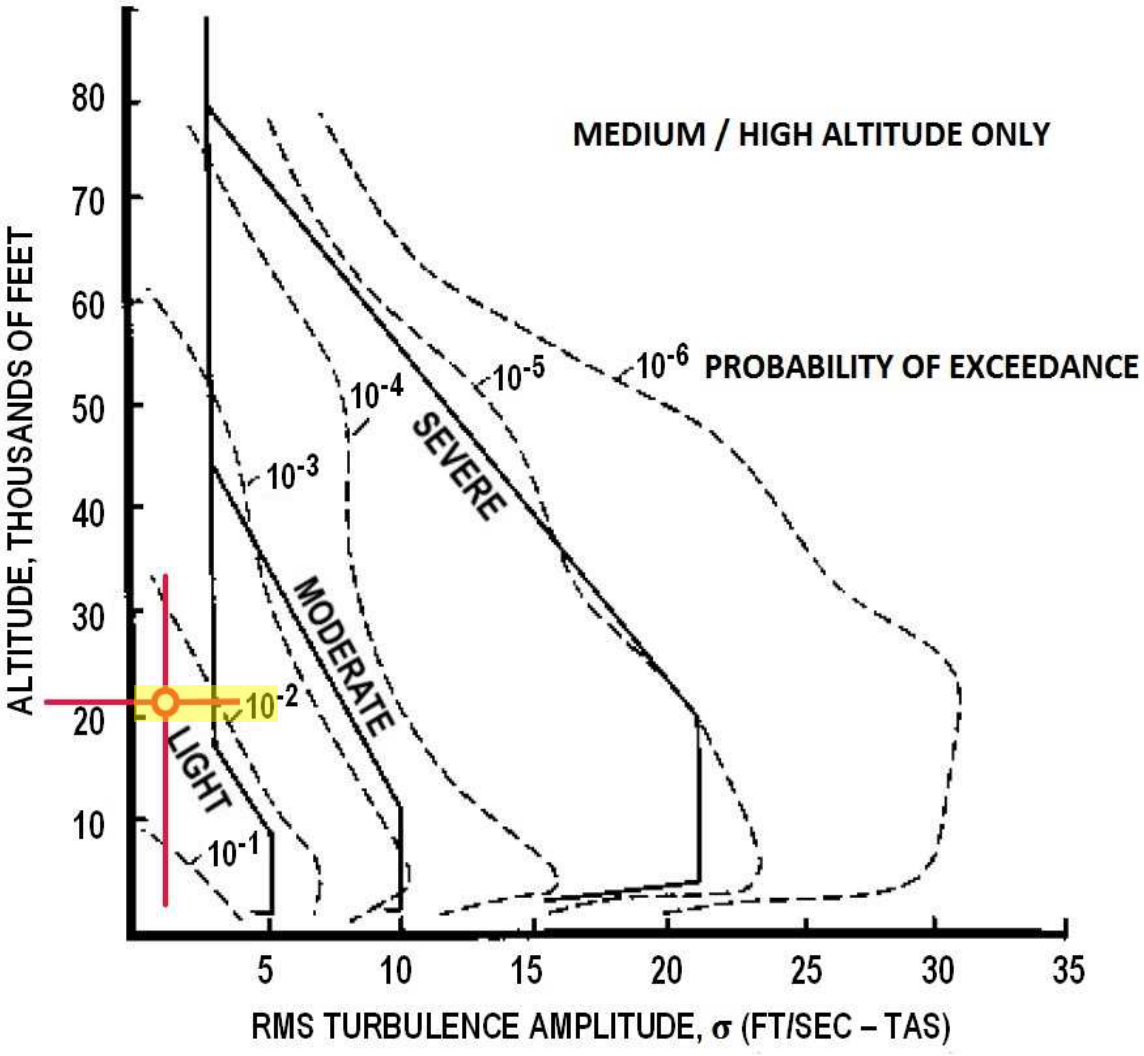

Figure 2.5. Turbulence Intensity.

2.5.4 Total Reference Wind for Tanker and Receiver

The total wind the tanker aircraft is exposed to is the superposition of the prevailing wind and the turbulence. On the other hand, the receiver is exposed to the total wind that is the superposition of the prevailing wind, vortex-induced wind and the turbulence. Fig. 2.7 shows the components of the total wind, based on the flight data based prevailing wind and the Dryden based turbulence. Fig. 2.8 shows an example of the total wind, based on the ECWM and the Dryden turbulence. Fig. 2.9

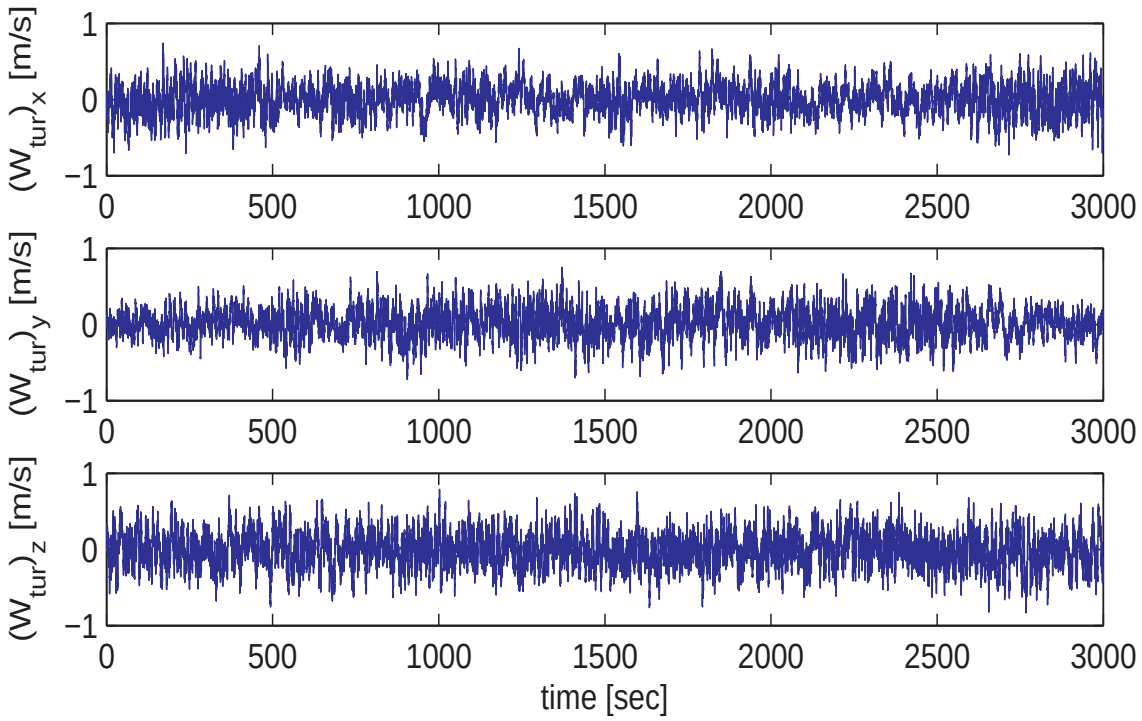

Figure 2.6. Turbulence Generated by Dryden Model.

shows the components of the total wind based on the fight data based prevailing wind, the Dryden based turbulence, and wake vortex induced wind acting on the receiver aircraft.

2.6 Sensors and Measurement Noise Models

Both aircraft are assumed to be equipped with conventional autopilot sensors, an airdata sensor, and inertial measurement unit (IMU), a magnetometer, and GPS. The airdata sensor measures airspeed, side slip angle, and angle of attack. IMU measures acceleration, angular acceleration, and attitude. The magnetometer measures the orientation. GPS measures absolute velocity and position. Measurement equation is

$$\widetilde{\mathrm{y}}_k = \mathbf{C}\ \mathrm{x}_k + \mathrm{v}_k \tag{2.54}$$

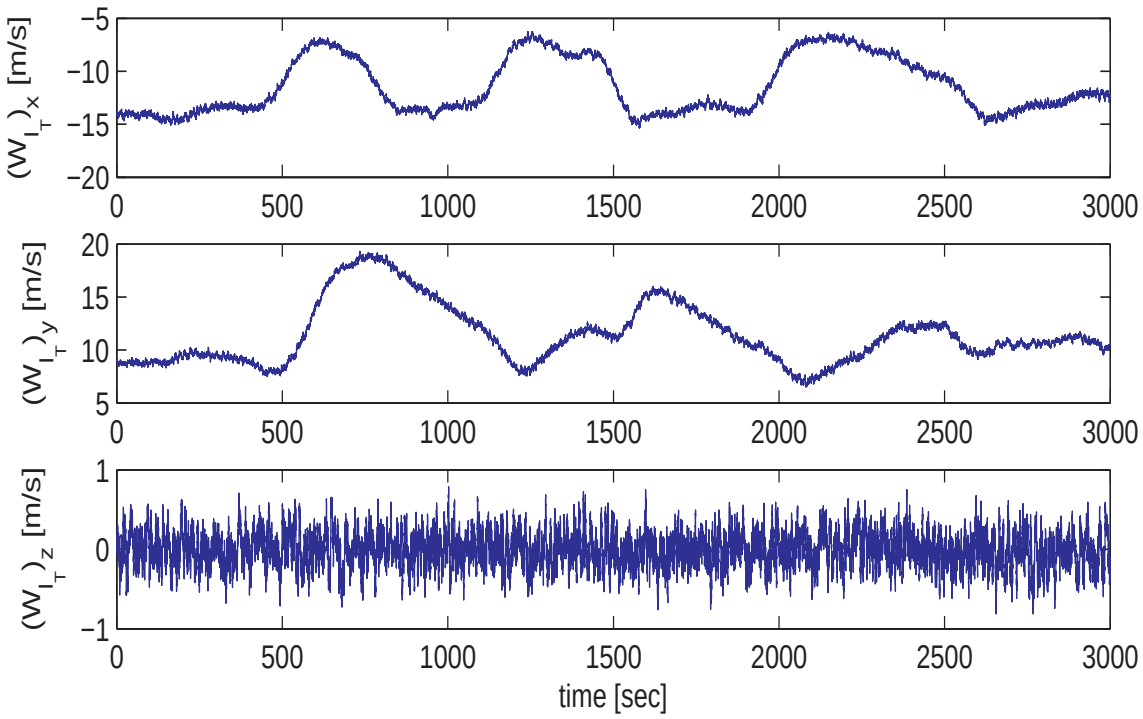

Figure 2.7. Wind Profile Based on Flight Data Based Prevailing Wind and Dryden Turbulence.

where $x_k \in \Re^{12}$ is the state vector, $v_k \in \Re^{12}$ is the measurement noise and $\mathbf{C}$ is the distribution matrix. This work assumes that the full states are measured by the aforementioned sensors. The measurement noise can be modeled as zero-mean Gaussian white-noise, or zero-mean colored noise. The standard deviations of the measurement noises for each sensor with the white noise or the colored noise are shown in Table 2.2. The noise characteristics are obtained from a test flight data given in Ref. [7]. Even if the noise variance listed in Table 2.2 are the smaller ones used in this research, they are still larger relative to a commercial sensor LN-251 made by Northrop Grumman [35].

For the performance evaluation of the estimators developed in this research in a worst case in terms of inaccurate measurement noise, the second noise characteristics

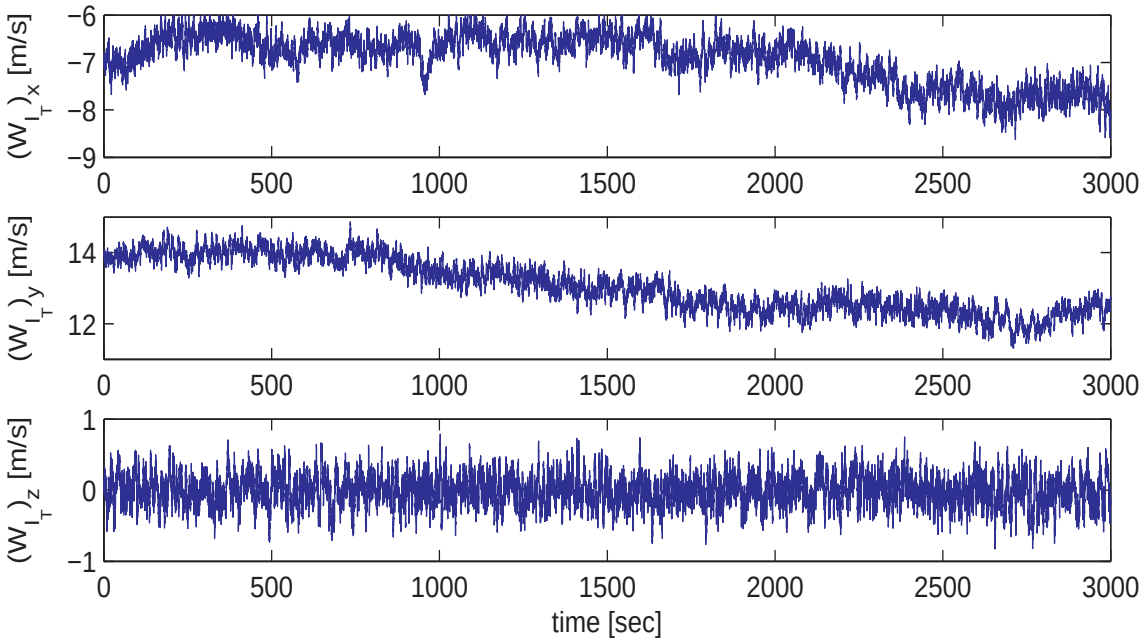

Figure 2.8. Wind Profile Based on ECWM Prevailing Wind and Dryden Turbulence.

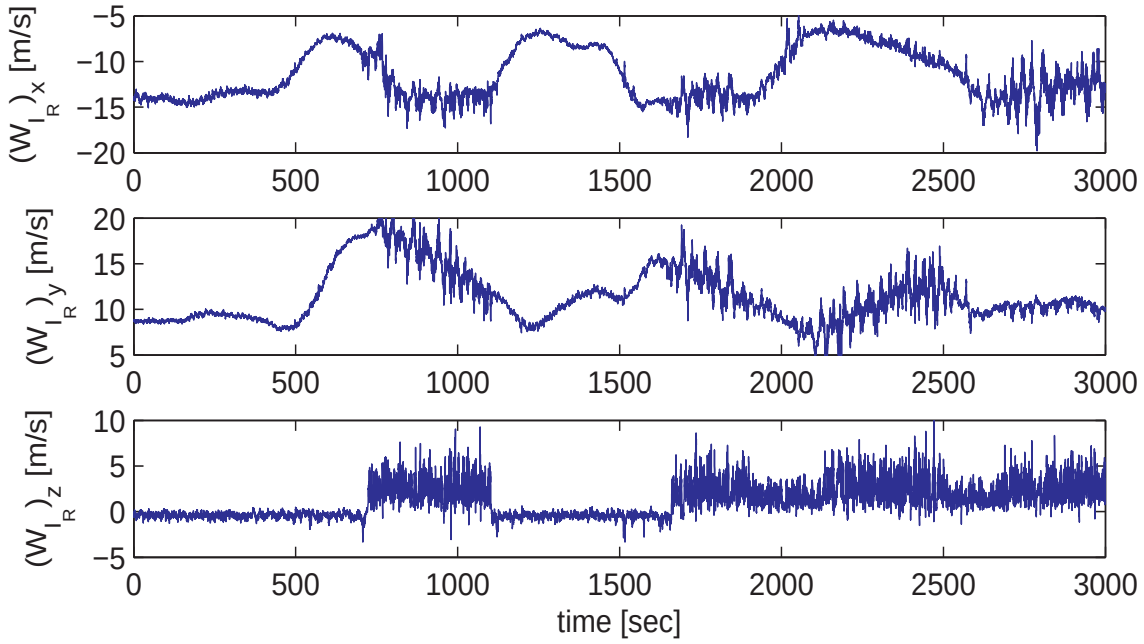

Figure 2.9. Wind Profile Based on Flight Data Based Prevailing Wind, Dryden Turbulence and Wake Vortex Induced Wind at Receiver Aircraft.

Table 2.2. Measurement Characteristics for Both Aircraft

	V_T *or* V [m/s]	β_T or β [rad]	α_T or α [rad]	p_T *or* p [rad/s]	q_T *or* q [rad/s]	r_T *or* r [rad/s]
σ	0.2	0.0035	0.0044	0.0131	0.0131	0.0131
Max. Nom.*	190	0	0.1005	0.0041	0.0478	0.0406
Percent Err [%]	0.32					
	ψ_T or ψ [rad]	θ_T or θ [rad]	ϕ_T or ϕ [rad]	x_T or ξ_1 [m]	y_T or ξ_2 [m]	z_T or ξ_3 [m]
σ	0.0044	0.0044	0.0044	3	3	3
Max. Nom.*		0.0652	0.8659			7010
Percent Err [%]			1.52			0.13

*Max. Nom. is the maximum of the nominal values.

are set to be ten times larger than those of Table 2.2 except for the velocity and the position vectors. The velocity and position vector are twenty times and two times larger than those of Table 2.2, respectively. The second noise characteristics are listed on Table 2.3 This is to obtain the sensor characteristics such that the

Table 2.3. Second Measurement Characteristics for Both Aircraft

	V_T *or* V [m/s]	β_T or β [rad]	α_T or α [rad]	p_T *or* p [rad/s]	q_T *or* q [rad/s]	r_T *or* r [rad/s]
σ	6	0.035	0.044	0.131	0.131	0.131
Max. Nom.*	190	0	0.1005	0.0041	0.0478	0.0406
Percent Err [%]	9.47					
	ψ_T or ψ [rad]	θ_T or θ [rad]	ϕ_T or ϕ [rad]	x_T or ξ_1 [m]	y_T or ξ_2 [m]	z_T or ξ_3 [m]
σ	0.044	0.044	0.044	6	6	6
Max. Nom.*		0.0652	0.8659			7010
Percent Err [%]			15.24			0.26

*Max. Nom. is the maximum of the nominal values.

standard deviations of the second measurement noises are calculated by the percent error of the nominal value within the three standard deviation bound. For instance,

the nominal speed of the aircraft is 190 m/s. 9.47 percent error of the airspeed is 18 m/s. Thus, the standard deviation is 6 m/s.

2.6.1 White Noise Model

The measurement noise can be modeled as zero-mean Gaussian white-noise, which is a widely used measurement noise model [21, 36, 37, 38]. The measurement noise is directly added to the actual value of the corresponding states of the aircraft.

2.6.2 Colored Noise Model

Colored measurement noise can be treated as exponentially correlated random variables [38]. In this work, the only source of the colorness of the measurement noise is assumed to be the correlation with time. Colored measurement noise model developed by a first order differential equation is

$$\dot{\mathrm{v}}_i = -b_{\mathrm{v}}\ \mathrm{v}_i + \sqrt{a_{v_i} \cdot b_v}\ w_{\mathrm{v}} \tag{2.55}$$

where a_{v_i} is the coefficient to show the degree of the mean square value of the measurement noise, i is the index for each measurement, w_{v} is zero-mean Gaussian white noise with variance Q and b_{v} is the inverse correlation time constant to show the extent of the correlation of the measurement. As the correlation time constant (τ_{v}) decreases, the noise becomes more like white measurement noise. In contrast, as the correlation time constant increases, the correlation error starts to behave like a bias error.

The auto-correlation of Eq. (2.55) is

$$R_{\mathrm{v}_i\mathrm{v}_i}(\tau) = \frac{a_{\mathrm{v}_i}}{2}\ e^{-b_{\mathrm{v}}|\tau|} \tag{2.56}$$

where τ is the time interval parameter. When τ is zero, the auto-correlation becomes

$$R_{\mathrm{v}_i\mathrm{v}_i}(0) = \frac{a_{\mathrm{v}_i}}{2} \tag{2.57}$$

where $R_{\mathrm{v}_i\mathrm{v}_i}(0)$ is the mean square value of the measurement noise, which is the variance if the mean value of the measurement noise is zero. The two constant a_{v_i} and b_{v} are

$$a_{\mathrm{v}_i} = 2\ E[\mathrm{v}_i^2] \tag{2.58}$$

$$b_{\mathrm{v}} = \frac{1}{\tau_{\mathrm{v}}} \tag{2.59}$$

The zero-mean Gaussian white noise, w_{v} in Eq. (2.55) is the input to the first order differential equation. To generate the correlated measurement noises with the variances listed Table 2.2 or Table 2.3, the variance of w_{v} should be calculated from the discrete form of Eq. (2.55) such as

$$\mathrm{v}_{i,k+1} = e^{-b_{\mathrm{v}}T}\mathrm{v}_{i,k} + (1 - e^{-b_{\mathrm{v}}T})\sqrt{\frac{a_{\mathrm{v}_i}}{b_{\mathrm{v}}}}w_{\mathrm{v},k} \tag{2.60}$$

At the steady state, $\mathrm{v}_{i,k+1}$ equals $\mathrm{v}_{i,k}$. Thus, the variance of w_{v} is

$$\Phi_i = \frac{1 - (e^{-b_{\mathrm{v}}\ T})^2}{(1 - e^{-b_{\mathrm{v}}\ T})^2}\frac{b_{\mathrm{v}}}{a_{\mathrm{v}_i}}\ \mathrm{var}(\mathrm{v}_i) \tag{2.61}$$

where $\mathrm{var}(\mathrm{v}_i)$ is the square value of the standard deviation given in Table 2.2 or Table 2.3. In the matrix form, the the colored noise equation is

$$\dot{\mathrm{v}} = \mathbf{A}_{\mathrm{v}}\mathrm{v} + \mathbf{G}_{\mathrm{v}}W_{\mathrm{v}} \tag{2.62}$$

where $\mathbf{A}_{\mathrm{v}} = diag(-b_{\mathrm{v}}, \cdots, -b_{\mathrm{v}}) \in \Re^{m\times m}$ and $\mathbf{G_v} = diag(\sqrt{a_{\mathrm{v}_1} b_{\mathrm{v}}}, \cdots, \sqrt{a_{\mathrm{v}_m} b_{\mathrm{v}}}) \in \Re^{m\times m}$, W_{v} is a zero-mean Gaussian white noise. The discrete form of W_{v} is $W_{\mathrm{v,k}}$, whose covariance is $\mathbf{\Phi} = diag(\Phi_1, \cdots, \Phi_m)$. Note that *diag* means diagonalization.

CHAPTER 3

OVERVIEW OF KALMAN FILTERING APPROACHES

Kalman Filter (KF) is an optimal estimator, whose main purpose is to estimate a state vector of a system and to reject a noise vector from a measurement vector. There are different versions of KF depending on whether the system and measurement equations are linear or nonlinear. If the system and measurement equations are linear, a linear KF is used. If the system and/or measurement equations are nonlinear, nonlinear estimators such as an Extended Kalman Filter (EKF), an Unscented Kalman Filter (UKF), and Square-Root Unscented Kalman Filter (SR-UKF) should be used. This chapter presents a brief overview of these four kinds of the Kalman filtering approaches: Linear KF, EKF, UKF, and SR-UKF. This discussion is limited to continuous system and discrete measurement, while there are other combination of the system and measurement models.

3.1 Linear Kalman Filter

The linear Kalman Filter (LKF) is used when the system equation and the measurement equation are linear. The continuous linear system and discrete measurement equations are given as

$$\begin{aligned} \dot{x} &= \mathbf{A}\ x + \mathbf{B}\ u + \mathbf{G}\ w \\ \widetilde{y}_k &= \mathbf{H}\ x_k + v_k \end{aligned} \tag{3.1}$$

where $x \in \Re^n$ is the state vector, $u \in \Re^p$ is the control input vector, $w \in \Re^q$ is the process noise vector characterized by Gaussian white noise with zero mean and

variance of $\mathbf{Q} \in \Re^{q \times q}$, $v_k \in \Re^m$ is the measurement noise characterized by Gaussian white noise with zero mean and covariance of $\mathbf{R_k} \in \Re^{m \times m}$, and $\widetilde{y}_k \in \Re^m$ is a discrete measurement vector. The subscript k indicates discrete time.

The general implementation of a KF consists of two steps: Measurement Update and System Update. The discrete measurement update of the KF is [25, 26, 39]

$$\mathbf{K_k} = \mathbf{P_k}^{-}\mathbf{H}^T \left[\mathbf{H}\mathbf{P_k}^{-}\mathbf{H}^T + \mathbf{R_k}\right]^{-1} \tag{3.2a}$$

$$\mathbf{P_k}^{+} = \left[\mathbf{I} - \mathbf{K_k}\mathbf{H}\right]\mathbf{P_k}^{-} \tag{3.2b}$$

$$\hat{x}_k^{+} = \hat{x}_k^{-} + \mathbf{K_k}\left[\widetilde{y}_k - \mathbf{H}\hat{x}_k^{-}\right] \tag{3.2c}$$

where $\mathbf{K_k} \in \Re^{n \times m}$ is the Kalman gain for the linear estimator, $\mathbf{P_k}^{-} \in \Re^{n \times n}$ is a priori state covariance estimate, $\mathbf{P_k}^{+} \in \Re^{n \times n}$ is a posteriori state covariance estimate, $\hat{x}_k^{-} \in \Re^n$ is a priori state estimate and $\hat{x}_k^{+} \in \Re^n$ is a posteriori state estimate. Note that $\mathbf{I}$ indicates an identity matrix and the superscript $(\cdot)^T$ indicates transpose. The initial condition for $\mathbf{P_k}^{-}$ is generally selected to include large numbers in the form of a diagonal matrix. The initial condition for $\hat{x}_k^{-}$ is selected based on a reasonable guess.

The continuous system update of KF is [25, 26, 39]

$$\dot{\hat{x}} = \mathbf{A}\hat{x} + \mathbf{B}u \tag{3.3a}$$

$$\dot{\mathbf{P}} = \mathbf{A}\mathbf{P} + \mathbf{P}\mathbf{A}^T + \mathbf{G}\mathbf{Q}\mathbf{G}^T \tag{3.3b}$$

where $\hat{x}$ is the estimated state vector before the measurement update and $\mathbf{P}$ is the state covariance matrix before the measurement update. The continuous system update is done by numerical integration using Runge-Kutta method. The system

update rate is set to the simulation update rate (T), which is determined by rule of thumb as

$$T \leq \frac{1}{10\ |\lambda_{max}|} \tag{3.4}$$

where λ_{max} is a maximum real eigenvalue of the system matrix ($\mathbf{A}$). The measurement update rate is set to be the same as the system update rate.

The limitation of the linear KF is that the system matrix $\mathbf{A}$ and measurement matrix $\mathbf{H}$ must be constant. If the system matrix $\mathbf{A}$ and/or the measurement matrix $\mathbf{H}$ are time-varying, nonlinear estimators such as EKF, UKF, or SR-UKF should be considered.

3.2 Extended Kalman Filter

Extended Kalman Filter (EKF) has the same structure as the linear KF except for the linearization of the system and measurement functions around the current estimate. The linearization is conducted by a first order approximation of the Taylor series expansion [25, 26, 39]. Consider the nonlinear system and measurement equation as

$$\begin{aligned} \dot{x} &= f(x, u, t) + \mathbf{G}\ w \\ \widetilde{y}_k &= h(x_k) + v_k \end{aligned} \tag{3.5}$$

where $x \in \Re^n$ is the state vector, $u \in \Re^p$ is the control input vector, $w \in \Re^q$ is the process noise vector characterized by Gaussian white noise with zero mean and variance of $\mathbf{Q} \in \Re^{q \times q}$, $v_k \in \Re^m$ is the measurement noise characterized by Gaussian white noise with zero mean and covariance of $\mathbf{R_k} \in \Re^{m \times m}$, and $\widetilde{y}_k \in \Re^m$ is a discrete measurement vector.

The discrete measurement update of EKF is [25, 26, 39]

$$\mathbf{K_k} = \mathbf{P_k}^{-}\mathbf{H_k}^{T}\left[\mathbf{H}\mathbf{P_k}^{-}\mathbf{H_k}^{T} + \mathbf{R_k}\right]^{-1} \tag{3.6a}$$

$$\mathbf{P_k}^{+} = \left[\mathbf{I} - \mathbf{K_k}\mathbf{H_k}\right]\mathbf{P_k}^{-} \tag{3.6b}$$

$$\hat{x}_k^{+} = \hat{x}_k^{-} + \mathbf{K_k}\left[\widetilde{y}_k - \mathbf{H_k}\hat{x}_k^{-}\right] \tag{3.6c}$$

$$\mathbf{H_k} = \left.\frac{\partial h}{\partial x}\right|_{\hat{x}_k^{-}} \tag{3.6d}$$

where $\mathbf{K_k} \in \Re^{n\times m}$ is the Kalman gain, $\mathbf{P_k}^{-} \in \Re^{n\times n}$ is a priori state covariance estimate, $\mathbf{P_k}^{+} \in \Re^{n\times n}$ is a posteriori state covariance estimate, $\hat{x}_k^{-} \in \Re^{n}$ is a priori state estimate and $\hat{x}_k^{+} \in \Re^{n}$ is a posteriori state estimate. The initial condition for $\mathbf{P_k}^{-}$ is generally selected to have large numbers in the form of a diagonal matrix. The initial condition for $\hat{x}_k^{-}$ is selected based on a reasonable guess.

The continuous system update of KF is [25, 26, 39]

$$\dot{\hat{x}} = f(\hat{x}, u, t) \tag{3.7a}$$

$$\dot{\mathbf{P}} = \mathbf{A}\mathbf{P} + \mathbf{P}\mathbf{A}^{T} + \mathbf{G}\mathbf{Q}\mathbf{G}^{T} \tag{3.7b}$$

$$\mathbf{A} = \left.\frac{\partial f}{\partial x}\right|_{\hat{x}=\hat{x}_k^{+}} \tag{3.7c}$$

where $\hat{x}$ is the estimated state vector before the measurement update and $\mathbf{P}$ is the state covariance matrix before the measurement update. In this approach, since the system and measurement update rate are set to the same rate, the nominal values of the system update is obtained from the result of the measurement update and the nominal values of the measurement update is obtained from the result of the system update. If the system and measurement equations are highly nonlinear, the linearized equations for the system and measurement cannot adequately represent the nonlinear

motion by the first order approximation. Due to this limitation of EKF, UKF has become a widely used nonlinear estimator as an alternative [25, 26].

3.3 Unscented Kalman Filter

The Unscented Kalman Filter (UKF) deals with nonlinear equations through a forth order approximation effect in the Tayor series expansion [24]. Another advantage of the UKF is that the mean and covariance are propagated directly by the nonlinear system and measurement equations without the linearization process [24, 25, 26, 39]. Due to these advantages, UKF has become a widely used nonlinear estimator as an alternative to EKF.

Consider the system equation and measurement equation, respectively, as

$$\dot{x} = f(x, u, t) + w \tag{3.8a}$$

$$\widetilde{y}_k = h(x_k) + v_k \tag{3.8b}$$

where $x \in \Re^n$ is the state vector, $u \in \Re^p$ is the control input vector, $w \in \Re^q$ is the process noise vector characterized by Gaussian white noise with zero mean and variance of $\mathbf{Q} \in \Re^{q \times q}$, $v_k \in \Re^m$ is the measurement noise characterized by Gaussian white noise with zero mean and covariance of $\mathbf{R_k} \in \Re^{m \times m}$, and $\widetilde{y}_k \in \Re^m$ is a discrete measurement vector.

In a linear KF or EKF, process noises are not used in the system update and measurement noises are not used in the measurement update because they are assumed to be zero by mean calculation. In contrast, in UKF, the process noises are used in the system update and measurement noises are used in the measurement update through sigma points, which are the points around the prior mean for the states, process noises and measurement noises. The sigma points are divided into two groups.

The sigma points for the states are the first group, whose values are around the prior mean states, the sigma points for the noises are the other group, whose values are around zero. The degree of scattering for the sigma points is based on the covariances of $\mathbf{P}$, $\mathbf{Q}$ and $\mathbf{R}$. Thus, an augmented state vector is defined as the concatenation of the vectors of the states, process noise and measurement noise, the sigma points are determined by augmented state vector and the augmented state covariance matrix. The augmented state and state covariance matrix are respectively [25, 26]

$$\hat{x}^a_{k-1} = [\hat{x}_{k-1}\ 0\ 0]^T, \quad \hat{x}^a_{k-1} \in \Re^L \tag{3.9a}$$

$$\mathbf{P}^a_{x_{k-1}} = diag(P^+_{x_{k-1}}, Q, R_k), \quad \mathbf{P}^a_{x_{k-1}} \in \Re^{L\times L} \tag{3.9b}$$

where $\mathbf{P}^+_{x_{k-1}}$ is a posteriori state covariance estimate, $L = n + q + m$ and $diag$ means diagonalization. The initial condition for $\mathbf{P}^+_{x_{k-1}}$ is generally selected to consist of large numbers in the form of a diagonal matrix. The initial condition for $\hat{x}_{k-1}$ is selected based on a reasonable guess. The sigma points are generated by [22, 23, 24, 25, 26]

$$\chi_{k-1} = \begin{bmatrix} \chi^x_{k-1} \\ \chi^w_{k-1} \\ \chi^v_{k-1} \end{bmatrix} = \begin{bmatrix} \hat{x}^a_{k-1} & \hat{x}^a_{k-1} + \gamma\sqrt{\mathbf{P}^a_{x_{k-1}}} & \hat{x}^a_{k-1} - \gamma\sqrt{\mathbf{P}^a_{x_{k-1}}} \end{bmatrix} \tag{3.10}$$

where $\chi_{k-1} \in \Re^{n\times(2L+1)}$ is sigma points, $\gamma = \sqrt{L+\lambda}$, $\lambda = \alpha^2(L+\kappa) - L$, constant α specifies the spread of the sigma points around the prior mean and normally ranges from 1×10^{-4} to 1 [25]. The scaling factor κ is the tuning parameter for the higher order approximation. For the case of the Gaussian distribution, $\kappa = 3 - L$ minimizes the mean square error up to the fourth order [24]. χ^x_{k-1} is the sigma points for the

state, χ^w_{k-1} is the sigma points for the process noise, and χ^v_{k-1} is the sigma points for the measurement noise. The system update process is [22, 23, 24, 25, 26]

$$\chi^x_{k|k-1} = f(\chi^x_{k-1}, u_{k-1}, \chi^w_{k-1}) \tag{3.11a}$$

$$\hat{x}^-_k = \sum_{i=0}^{2L} w^m_i \chi^x_{i,k|k-1} \tag{3.11b}$$

$$\mathbf{P}^-_{x_k} = \sum_{i=0}^{2L} w^c_i \left(\chi^x_{i,k|k-1} - \hat{x}^-_k\right)\left(\chi^x_{i,k|k-1} - \hat{x}^-_k\right)^T \tag{3.11c}$$

where

$$w^m_0 = \frac{\lambda}{L+\lambda} \tag{3.12a}$$

$$w^c_0 = \frac{\lambda}{L+\lambda} + (1 - \alpha^2 + \beta) \tag{3.12b}$$

$$w^m_i = w^c_i = \frac{1}{2(L+\lambda)} \tag{3.12c}$$

and (w^m_0, w^c_i) are weighting factors for the mean calculation, (w^c_0, w^c_i) are weighting factors for the state covariance calculation. β is the secondary scaling factor. For Gaussian distribution, $\beta = 2$ is optimal [29]. $\hat{y}^-_k$ is the estimated output before the measurement update and $P^-_{x_k}$ is a priori state covariance estimate. Eq. (3.11a) propagates the current state vector to the next state vector using each column vector of the sigma points through the nonlinear system equations of Eq. (3.14a). Eq. (3.11b) calculates the mean value through the updated sigma points for the state, which is called a priori state estimate. Eq. (3.11c) calculates a priori state covariance estimate.

The measurement update process is [22, 23, 24, 25, 26]

$$\mathbf{Y}_{k|k-1} = h\left(\chi^x_{k|k-1}\right) + \chi^v_{k-1} \tag{3.13a}$$

$$\hat{y}^-_k = \sum_{i=0}^{2L} w^m_i \mathbf{Y}_{i,k|k-1} \tag{3.13b}$$

$$\mathbf{P}_{y_k} = \sum_{i=0}^{2L} w^c_i \left(\mathbf{Y}_{i,k|k-1} - \hat{y}^-_k\right)\left(\mathbf{Y}_{i,k|k-1} - \hat{y}^-_k\right)^T \tag{3.13c}$$

$$\mathbf{P}_{x_k y_k} = \sum_{i=0}^{2L} w^c_i (\chi^x_{i,k|k-1} - \hat{x}^-_k)(\mathbf{Y}_{i,k|k-1} - \hat{y}^-_k)^T \tag{3.13d}$$

$$\mathbf{K_k} = \mathbf{P}_{x_k y_k} (\mathbf{P}_{y_k})^{-1} \tag{3.13e}$$

$$\hat{x}^+_k = \hat{x}^-_k + \mathbf{K_k}(\widetilde{y}_k - \hat{y}^-_k) \tag{3.13f}$$

$$\mathbf{P}^+_{x_k} = \mathbf{P}^-_{x_k} - \mathbf{K_k}\mathbf{P}_{y_k}\mathbf{K_k}^T \tag{3.13g}$$

where Eq. (3.13a) and Eq. (3.13b) compute the estimated output by mean calculation. $\mathbf{P}^+_{x_k}$ is a posteriori state covariance estimate, $\mathbf{P}_{y_k}$ is the measurement covariance estimate, $\mathbf{P}_{x_k y_k}$ is the cross covariance estimate, $\mathbf{K_k}$ is the Kalman gain, and $\hat{x}^+_k$ is a posteriori state estimate. Eq. (3.13c) calculates the measurement covariance estimate, Eq. (3.13d) calculates cross covariance of the state and the measurement, Eq. (3.13e) calculates Kalman gain, Eq. (3.13f) propagates a priori state estimate to a posteriori state estimate by multiplying the Kalman gain and the residual of the measurement. Eq. (3.13g) propagates a priori state covariance matrix to a posteriori state covariance matrix. To generate the sigma points of Eq. (3.10), a square root of the augmented state covariance, $\sqrt{\mathbf{P}^a_{x_{k-1}}}$, is calculated at every time step, which can potentially lead to a computational singularity. To avoid the computational singularity problem, Square-Root Unscented Kalman Filter (SR-UKF) is proposed [27].

3.4 Square-Root Unscented Kalman Filter

SR-UKF propagates the square root of the covariance matrix of the state instead of the covariance matrix itself [27]. By the propagation of the square root itself, the square root calculation causing a computational singularity is avoided. Since the SR-UKF has the same advantages as the UKF, SR-UKF also is preferred for nonlinear problems over the EKF. Consider the system equation and measurement equation, respectively, as

$$\dot{x} = f(x, u, t) + w \tag{3.14a}$$

$$\widetilde{y}_k = h(x_k) + v_k \tag{3.14b}$$

where $x \in \Re^n$ is the state vector, $u \in \Re^p$ is the control input vector, $w \in \Re^q$ is the process noise vector characterized by Gaussian white noise with zero mean and variance of $\mathbf{Q} \in \Re^{q \times q}$, $v_k \in \Re^m$ is the measurement noise characterized by Gaussian white noise with zero mean and covariance of $\mathbf{R_k} \in \Re^{m \times m}$, and $\widetilde{y}_k \in \Re^m$ is a discrete measurement vector.

The SR-UKF has same structure as the UKF except for the augmented state covariance propagation. Instead of the augmented state covariance propagation at the UKF, square root propagation of the augmented state covariance is used at the SR-UKF. The square root of the augmented state covariance become [27, 28]

$$\mathbf{S}^a_{x_{k-1}} = diag(\mathbf{S}_{x_{k-1}}, \sqrt{\mathbf{Q}}, \sqrt{\mathbf{R}}), \quad \mathbf{S}^a_{x_{k-1}} \in \Re^{L \times L} \tag{3.15}$$

where $\mathbf{S}_{x_{k-1}} = chol(\mathbf{P}_{k-1})^T$, *chol* means Cholesky factorization that produces a lower triangular matrix $\mathbf{S}_{x_{k-1}}$, satisfying the relation $\mathbf{S}_{x_{k-1}} \cdot \mathbf{S}^T_{x_{k-1}} = \mathbf{P}_{k-1}$.

The sigma points are also changed to [27, 28]

$$\chi_{k-1} = \begin{bmatrix} \chi^{\mathrm{x}}_{k-1} \\ \chi^{w}_{k-1} \\ \chi^{v}_{k-1} \end{bmatrix} = [\hat{x}^a_{k-1} \quad \hat{x}^a_{k-1} + \gamma \mathbf{S}^a_{x_{k-1}} \quad \hat{x}^a_{k-1} - \gamma \mathbf{S}^a_{x_{k-1}}], \quad \chi_{k-1} \in \Re^{n \times (2L+1)} \tag{3.16}$$

where $\gamma = \sqrt{L + \lambda}$, $\lambda = \alpha^2(L + \kappa) - L$, constant α specifies the spread of the sigma points around the prior mean, the scaling factor κ is the tuning parameter for the higher order approximation, χ^x_{k-1} is the sigma points for the state, χ^w_{k-1} is the sigma points for the process noise, and χ^v_{k-1} is the sigma points for the measurement noise.

For the system update of the SR-UKF, Eq. (3.11c) at the UKF is modified to [27, 28]

$$[\mathbf{Q}^-_k, \mathbf{S}^T_{x_k}] = QR\left(\sqrt{w^c_1}(\chi^x_{1:2L,k|k-1} - \hat{x}^-_k)^T\right) \tag{3.17a}$$

$$\mathbf{S}_{x_k} = \left[\mathbf{S}^T_{x_k}(1:n, 1:n)\right]^T \tag{3.17b}$$

$$\mathbf{S}^T_{x_k} = cholupdate\left(\mathbf{S}^T_{x_k}, \sqrt{w^c_0}(\chi^x_{0,k|k-1} - \hat{x}^-_k), ' + '\right) \tag{3.17c}$$

where QR is called the QR decomposition. Note that $chol(\mathbf{P})^T$ returns the Cholesky factorization of $\mathbf{P}$, which is a lower triangular matrix $\mathbf{S}$, $cholupdate(\mathbf{S}^T, x, ' + ')$ returns the upper triangular Cholesky factor of $\mathbf{P} + x \cdot x^T$ and $cholupdate(\mathbf{S}^T, x, ' - ')$ returns the upper triangular Cholesky factor of $\mathbf{P} - x \cdot x^T$.

The measurement update of the SR-UKF is [27, 28]

$$\mathbf{Y}_{k|k-1} = h(\chi^x_{k|k-1}) + \chi^v_{k-1} \tag{3.18a}$$

$$\hat{y}^-_k = \sum_{i=0}^{2L} w^m_i \mathbf{Y}_{i,k|k-1} \tag{3.18b}$$

$$\left[\mathbf{Q}_{y_k}, \mathbf{S}^T_{y_k}\right] = QR\left(\sqrt{w^c_1}(\mathbf{Y}_{1:2L,k|k-1} - \hat{y}^-_k)^T\right) \tag{3.18c}$$

$$\mathbf{S}_{y_k} = \left[\mathbf{S}^T_{y_k}(1:m, 1:m)\right]^T \tag{3.18d}$$

$$\mathbf{S}^T_{y_k} = cholupdate\left(\mathbf{S}^T_{y_k}, \sqrt{w^c_0}(\mathbf{Y}_{0,k|k-1} - \hat{y}^-_k), ' + '\right) \tag{3.18e}$$

$$\mathbf{P}_{x_k y_k} = \sum_{i=0}^{2L} w^c_i (\chi^{\mathrm{x}}_{i,k|k-1} - \hat{x}^-_k)(\mathbf{Y}_{i,k|k-1} - \hat{y}^-_k)^T \tag{3.18f}$$

$$\mathbf{K_k} = (\mathbf{P}_{x_k y_k}/\mathbf{S}^T_{y_k})/\mathbf{S}_{y_k} = \mathbf{P}_{x_k y_k}(\mathbf{S}_{y_k}\mathbf{S}^T_{y_k})^{-1} \tag{3.18g}$$

$$\hat{x}^+_k = \hat{x}^-_k + \mathbf{K_k}(\widetilde{y}_k - \hat{y}^-_k) \tag{3.18h}$$

$$\mathbf{U} = \mathbf{K_k}\mathbf{S}_{y_k} \tag{3.18i}$$

$$\mathbf{S}^T_{x_{a,k}} = cholupdate(\mathbf{S}^T_{x_k}, \mathbf{U}, ' - ') \tag{3.18j}$$

$$\mathbf{S}^+_{x_k} = (\mathbf{S}^T_{x_k})^T \tag{3.18k}$$

where Eq. (3.18a) and Eq. (3.18b) compute the estimated output by mean calculation. $\mathbf{S}^+_{\mathrm{x}_k}$ and $\mathbf{S}_{y_k}$ are lower triangle matrices for the square root of a posteriori state covariance estimate and for the square root of the measurement covariance, respectively. $\mathbf{P}_{\mathrm{x}_k y_k}$ is the cross covariance estimate, $\mathbf{K_k}$ is the Kalman gain, and $\hat{x}^+_k$ is a posteriori state estimate. Eqs. (3.18c) to (3.18e) calculate the square root of the measurement covariance matrix, Eq. (3.18f) calculates cross covariance of the state and the measurement, Eq. (3.18g) calculates Kalman gain, Eq. (3.18h) propagates a priori state estimate to a posteriori state estimate by multiplying the Kalman gain

and the residual of the measurement. Eq. (3.18i) to Eq. (3.18k) propagate the square root of a priori state covariance matrix to that of a posteriori state covariance matrix.

3.5 Colored Measurement in Kalman Filter

In the real world, measurement error is are most likely to colored noises rather than the white noise, which is introduced as a theoretical construction to provide mathematical simplicity in derivation of a measurement model. This chapter deals with the characteristics of the colored measurement noise (CMN) and introduces a method to deal with measurements characterized by CMN in Kalman Filter (KF).

The characteristics of CMN can be explained by the non-constant PSD, while PSD of the white measurement noise (WMN) is constant. The constant PSD of WMN explains that all of the measurement noises are totally independent, which is uncorrelated with time. In contrast, CMN is correlated with time. The extent of the correlation of CMN is linear to the correlation time constant (τ_{v}). As the correlation time constant increases, the extent of the correlation increases, and the exponentially correlated error behaving like a bias error increases. Fig. 3.1 shows that as the correlation time constant (τ_{v}) increase, the colored measurement noise signal behaves like a bias error. Due to the exponentially correlated error, a general KF based on white measurements should be modified to handle a timely correlated colored measurements. The degree of the correlation is calculated by

$$\text{Degree of Correlation } [\%] = e^{-\tau/\tau_{\mathrm{v}}} \times 100 \tag{3.19}$$

For instance, if τ_{v} is 20 seconds and τ, a time interval parameter, is 10 seconds, the degree of the correlation is 60.7 %.

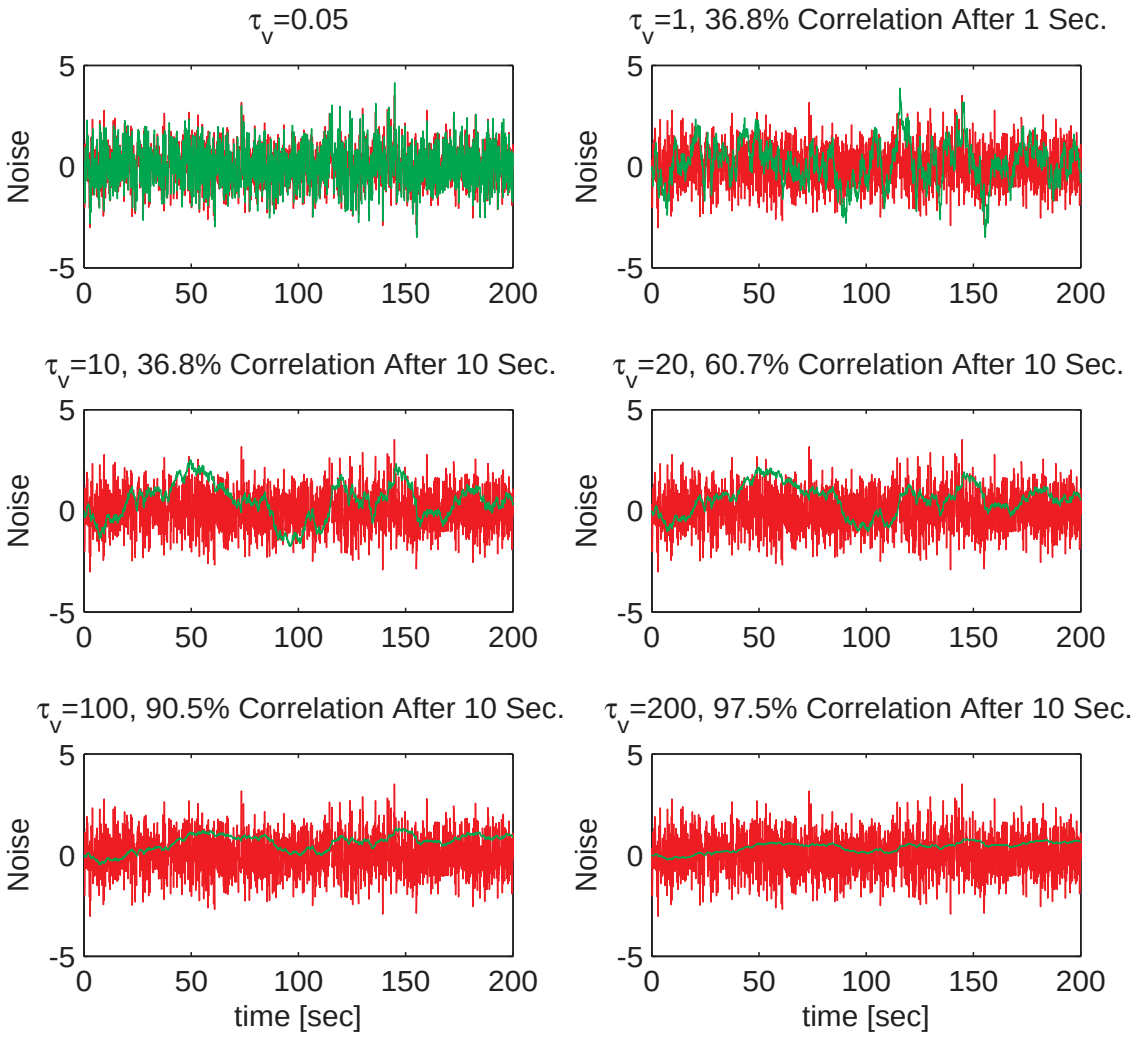

Figure 3.1. Exponentially Correlated Error Behaving Like a Bias Error.

There are two approaches to dealing with colored measurements in KF. The first method augments colored measurement noise equations into equations of motion of the system [25]. By augmentation, the states of the system and the corresponding colored measurement noises are obtained by integrating the augmented system equation in KF. The sum of the state vector and the corresponding CMN vector becomes an estimate of the colored measurements. The estimate of the colored measurements will be compared with the colored measurements to minimize the estimation error. The disadvantage of this method is that their is no measurement covariance matrix ($\mathbf{R}$) in estimation, which acts as a weighting factor to increase accuracy of the estimation. Without the measurement covariance or without knowing the accurate measurement covariance of $\mathbf{R}$, it is hard to obtain accurate estimate.

The main idea of the second approach to dealing with colored measurement in KF is to remove the colored noise from the colored measurement [25, 26, 39]. Generally, this approach is developed and used for linear system update and measurement update in Kalman structure while aircraft system equations in this research are nonlinear. The limitation of nonlinearity could be overcome by modifying the measurement quality. In defining the new measurement equation, two constraints should be considered: (i) CMN could be removed and (ii) the newly defined measurement should be measurable. Consider the continuous system, discrete colored measurement equation and continuous noise equation, respectively, as

$$\dot{x} = \mathbf{A}x + \mathbf{B}u + \mathbf{G}w \tag{3.20a}$$

$$\widetilde{y}_k = \mathbf{C}x_k + v_k \tag{3.20b}$$

$$\dot{v} = \mathbf{A_v}v + \mathbf{G_v}W_v \tag{3.20c}$$

where $x \in \Re^n$ is the state vector, $u \in \Re^p$ is the control input vector, $w \in \Re^q$ is the zero-mean Gaussian white noise vector with variance of $\mathbf{Q} \in \Re^{q \times q}$, $v_k \in \Re^m$ is the colored noise vector, and $W_v \in \Re^m$ is the zero-mean Gaussian white noise with variance of $\mathbf{\Phi}$ calculated by Eq. (2.61). Note that $\mathbf{A}$, $\mathbf{B}$, $\mathbf{G}$, $\mathbf{C}$, $\mathbf{A_v}$ and $\mathbf{G}_{\mathrm{v}}$ are constant. Equation (3.20a) and (3.20c) can be discretized by Euler method, respectively, as

$$\frac{x_k - x_{k-1}}{T} = \mathbf{A}x_k + \mathbf{B}u_k + \mathbf{G}w_k \tag{3.21a}$$

$$\frac{v_k - v_{k-1}}{T} = \mathbf{A_v}v_k + \mathbf{G}_{\mathrm{v}}W_{v,k} \tag{3.21b}$$

where T is a update rate. In this research, the update rate for the continuous equation is same as that of the discrete equation. Equation (3.21a) and (3.21b) are used to define the new measurement to remove colored noise.

The newly defined measurement model in discrete is

$$\widetilde{y}_{N,k} = \frac{\widetilde{y}_k - \widetilde{y}_{k-1}}{T} - \mathbf{A}_{\mathrm{v}}\widetilde{y}_k - \mathbf{CB}u_k \tag{3.22a}$$

$$= \frac{\mathbf{C}(x_k - x_{k-1})}{T} + \frac{v_k - v_{k-1}}{T} - \mathbf{A}_{\mathrm{v}}(\mathbf{C}x_k + v_k) - \mathbf{CB}u_k \tag{3.22b}$$

$$= \mathbf{C}(\mathbf{A}x_k + \mathbf{B}u_k + \mathbf{G}w_k) + (\mathbf{A}_{\mathrm{v}}v_k + \mathbf{G}_{\mathrm{v}}W_{v,k}) - \mathbf{A}_{\mathrm{v}}(\mathbf{C}x_k + v_k) - \mathbf{CB}u_k \tag{3.22c}$$

$$= \mathbf{C_N}x_k + v_{N,k} \tag{3.22d}$$

where $\mathbf{C_N} = \mathbf{CA} - \mathbf{A}_{\mathrm{v}}\mathbf{C}$, $v_{N,k} = \mathbf{CG}w_k + \mathbf{G}_{\mathrm{v}}W_{v,k}$. The new measurement noise $v_{N,k}$ is characterized by zero-mean Gaussian white noise with covariance $\mathbf{R_{N,k}}$ satisfying a white noise assumption of a general KF, which is calculated by

$$\mathbf{R_{N,k}} = E[v_{N,k}v_{N,k}^T] \tag{3.23a}$$

$$= \mathbf{CGQG}^T\mathbf{C}^T + \mathbf{G}_{\mathrm{v}}\mathbf{\Phi}{\mathbf{G}_{\mathrm{v}}}^T \tag{3.23b}$$

In this case, $v_{N,k}$ is correlated with w_k. The degree of correlation between $v_{N,k}$ and w_k is calculated by

$$E[w_k v_{N,k}^T] = \mathbf{M} \tag{3.24a}$$

$$\mathbf{M} = \mathbf{Q}\mathbf{G}^T\mathbf{C}^T \tag{3.24b}$$

KF is generally derived under the condition that the process noise vector is not correlated with the measurement noise vector. To remove the correlation between the process noise vector and the measurement noise vector, the system equation is modified. In this research, since the update rate of the continuous equation is same as that of the discrete equation, $\widetilde{y}_N = \widetilde{y}_{N,k}$, $x = x_k$, $v_N = v_{N,k}$ and $\mathbf{R_N} = \mathbf{R_{N,k}}$ are satisfied.

$$\dot{x} = \mathbf{A}x + \mathbf{B}u + \mathbf{G}w + \mathbf{GMR_N}^{-1}(\widetilde{y}_N - \mathbf{C_N}x - v_N) \tag{3.25a}$$

$$= \mathbf{A_N}x + u_N + w_N \tag{3.25b}$$

where

$$\mathbf{A_N} = \mathbf{A} - \mathbf{GMR_N}^{-1}\mathbf{C_N} \tag{3.26a}$$

$$u_N = \mathbf{B}u + \mathbf{GMR_N}^{-1}\widetilde{y}_N \tag{3.26b}$$

$$w_N = \mathbf{G}w - \mathbf{GMR_N}^{-1}v_N \tag{3.26c}$$

where $w_{_N}$ is a new process noise characterized by zero-mean Gaussian white noise with variance $\mathbf{Q_N}$. The variance of the new process noise is

$$\mathbf{Q_N} = E[w_{_N} w_{_N}^T] \tag{3.27a}$$

$$= \mathbf{GQG}^T - \mathbf{GMR_N}^{-1}\mathbf{M}^T\mathbf{G}^T \tag{3.27b}$$

Therefore, the newly defined continuous system and discrete measure equations satisfying conditions of general KF are

$$\dot{x} = \mathbf{A_N} x + u_{_N} + w_{_N} \tag{3.28a}$$

$$\widetilde{y}_{N,k} = \mathbf{C_N} x_k + v_{_{N,k}} \tag{3.28b}$$

The un-correlation between the new process noise ($w_{_N}$) and the newly defined measurement noise ($v_{_N}$) can be proved by

$$E[w_{_N} v_{_N}^T] = E[(\mathbf{G}w - \mathbf{GMR_N}^{-1} v_{_N}) v_{_N}^T] \tag{3.29a}$$

$$= \mathbf{G}E[w v_{_N}] - \mathbf{GMR_N}^{-1} E[v_{_N} v_{_N}] = 0 \tag{3.29b}$$

CHAPTER 4

ESTIMATION OF AIRCRAFT STATES AND WIND EXPOSURE AT TANKER AIRCRAFT

This chapter presents the method used for the estimation of the aircraft states and the wind components in tanker aircraft. The nonlinear estimator developed in this chapter is based on SR-UKF. Simulation experiments have shown that the convergence of the estimation of aircraft states is not possible without including the wind information in the equation of motion (EOM) of the aircraft. Thus, to avoid the issue of divergence in the state estimation, the equations of motion are augmented with a dynamic wind model for the system update of the estimator. With this approach, the convergence of the estimator guarantees the estimation of the aircraft states as well as the wind components.

4.1 Wind Modeling for Estimation

The wind model for the tanker aircraft is obtained by rearranging Eq. (2.1) in terms of wind as

$$\dot{W}_{I_T} = \mathbf{R}^{\mathbf{T}}_{\mathbf{B_T I}} \left\{ \mathbf{S}(\omega_{B_T})\mathbf{R}_{\mathbf{B_T W_T}} V_{w_T} + \frac{1}{m_{_T}}(\mathbf{R}_{\mathbf{B_T I}} M_T + \mathbf{R}_{\mathbf{B_T W_T}} A_T + P_T) - \varepsilon_{\mathbf{T}} \begin{bmatrix} \dot{V}_{_T} \\ \dot{\beta}_{_T} \\ \dot{\alpha}_{_T} \end{bmatrix} \right\} \tag{4.1}$$

where the wind derivative ($\dot{W}_{I_T}$) is relative to the inertial frame and

$$\varepsilon_{\mathbf{T}} = \begin{bmatrix} \cos\beta_T \cos\alpha_T & -V_T \sin\beta_T \cos\alpha_T & -V_T \cos\beta_T \sin\alpha_T \\ \sin\beta_T & V_T \cos\beta_T & 0 \\ \cos\beta_T \sin\alpha_T & -V_T \sin\beta_T \sin\alpha_T & V_T \cos\beta_T \cos\alpha_T \end{bmatrix} \tag{4.2}$$

There is no direct measurement of the rate of change of the airdata ($\dot{V}_T$, $\dot{\beta}_T$, $\dot{\alpha}_T$). Hence, the rate of change of the airdata are replaced by the numerical calculation of the translational dynamics in Eq. (2.1). The aerodynamics force (A_T) is obtained by using the same aerodynamic model as in the translational equations of motion. The knowledge of the aerodynamic model is a very strong assumption and will be addressed by using the acceleration measurement instead in the next chapter.

4.2 Augmentation of the State-Space Model for System Update

The system equations are augmented by combining the wind model in Eq. (4.1) with the equations of motion in Eq. (2.13). As stated earlier, this is to have the convergence of the estimator and to estimate the wind components along with the aircraft states.

Augmented with the wind components, the augmented state vector is

$$\hat{\mathrm{x}}_a = [\hat{\mathrm{x}}_T, \hat{W}_{I_T}]^T, \quad \hat{\mathrm{x}}_a \in \Re^{15} \tag{4.3}$$

The augmented system is written in compact form as

$$\dot{\hat{\mathrm{x}}}_a = f(\hat{\mathrm{x}}_a, u, \hat{W}_{I_T}, \dot{\hat{W}}_{I_T}) + \eta \tag{4.4}$$

where $u \in \Re^4$ is the control input, $\hat{W}_{I_T} \in \Re^3$ is the estimated wind relative to the inertial frame, $\dot{\hat{W}}_{I_T} \in \Re^3$ is the estimated derivative of wind relative to the inertial frame, and $\eta \in \Re^{15}$ is the process noise for the system update of the estimation, which is a vector of Gaussian white noises with zero-mean and covariance $\mathbf{Q_a}$.

Without the covariance matrix $\mathbf{Q_a}$, the augmented system may cause a singularity because two different forms of the same matrix equations from Eqs. (2.1) and (4.1), are used in the augmented system equations. Singularity causes when the state error covariance matrix (P) in KF is non-positive definite. Another problem is due to the turbulence acting on the aircraft as part of the wind exposure. While the total reference turbulence generated by Dryden model acts as a colored process noise, the wind model used in the system update does not include noise. To represent the colorness of turbulence, three process noises could be added at the end of the components of wind model in Eq. (4.1). The process noises would be taken into account in system update (state and state error covariance propagation) of SR-UKF by a covariance matrix of the process noises, which is called $\mathbf{Q_0}$ in this research. In general, the specific values of $\mathbf{Q_0}$ are unknown and it is difficult to estimate the augmented states by tuning the three diagonal quantities of $\mathbf{Q_0}$ matrix. The process covariance matrix, $\mathbf{Q_0}$, plays the role of the control parameters to achieve successful estimation in the system update of KF. Through experience or trial and error, as the dimension of the process covariance matrix increases, KF may better estimate the augmented full states as well as the avoidance of singularity. The dimension of the process covariance matrix ($\mathbf{Q_a}$), used in this work, is chosen to be equal to the number of the states of the augmented system. By tuning the covariance matrix of the process noise ($\mathbf{Q_a}$), the singularity and turbulence problems are solved in the augmented system update of SR-UKF.

A procedure, called loop transfer recovery (LTR), is developed [25, 40] for tuning the covariance matrix of the process noise. The LTR is used to obtain a reasonably large stability margins of a LQR controller that uses the KF estimated states as feedback signals. A scalar tuning parameter is defined for tuning the covariance matrix such that

$$\mathbf{Q} = \mathbf{Q_1} + q^2\mathbf{B}\mathbf{B}^T \tag{4.5}$$

where q is a positive tuning parameter, B is the matrix for the control input in a linear system, and $\mathbf{Q_1}$ is the initial covariance matrix. As shown in the LTR application, tuning a covariance matrix is general. This research also uses a tuning approach to increase the estimation accuracy and to avoid singularity problem due to the improperly selected covariance matrix. The tuning procedure in this work is conducted by experience or trial and error.

Fig. 4.1 shows a depiction of the augmented system for the estimator of the tanker aircraft. Note in Fig. 4.1 that the derivative of wind relative to the inertial frame, $\frac{\mathrm{d}}{\mathrm{dt}}(\hat{W}_{I_T})$, is provided to system update of the estimation from the previous numerical calculation data, through a unit delay operation, z^{-1}, because there is no measurement of the derivative of wind relative to the inertial frame.

4.3 Calculated Measurement of Wind (CMW)

For the Kalman filter implementation for correction, measurement update must be conducted. However, there is no direct measurement of the wind for the measurement update. Instead of the direct measurement of the wind, the calculated measurement of wind (CMW) is used to increase the accuracy of the wind estimate. The

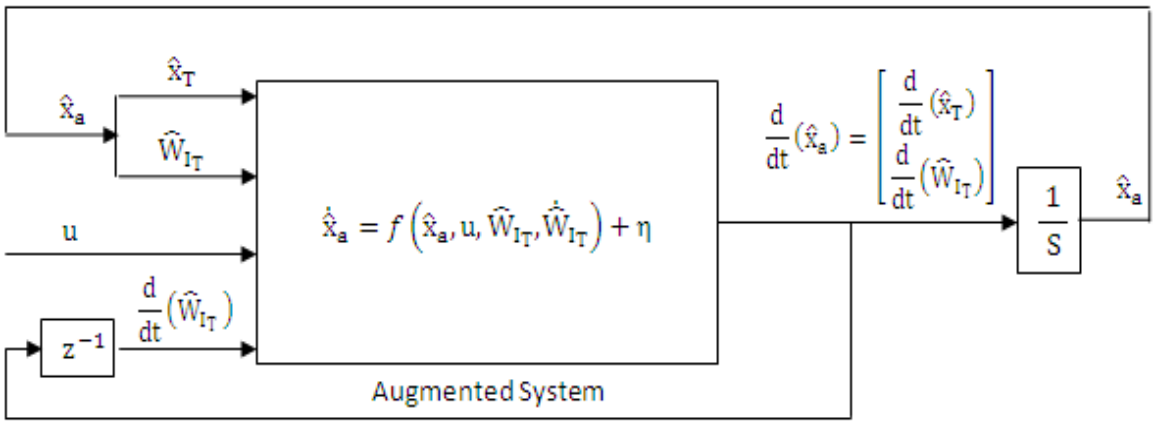

Figure 4.1. Augmented State Update in SR-UKF.

CMW for the tanker aircraft is obtained by rearranging Eq. (2.12) with respect to the wind as

$$W_{I_T} = \widetilde{\dot{r}}_{B_T} - \widetilde{\mathbf{R}}^{\mathbf{T}}_{\mathbf{B_T I}} \widetilde{\mathbf{R}}_{\mathbf{B_T W_T}} \widetilde{V}_{w_T} \tag{4.6}$$

where $\widetilde{\cdot}$ means measurement data of $(\cdot)$. However, the CMW for the measurement update of SR-UKF may have a large level of noise. To reduce the noise level of CMW, a filter with a moving average window (MAW) is used

$$W_{I_T}(k) = \frac{1}{2n+1} \sum_{i=k-2n}^{k} W_{I_T}(i), \quad W_{I_T} \in \Re^3 \tag{4.7}$$

where $2n+1$ is the window size.

The CMW is used for minimizing the error of the wind estimation based on the Kalman structure if measurement noise is white. If the measurement noise is colored, The CMW is not used in the measurement update of the KF because a newly defined measurement, which is general approach to deal with a colored measurement in KF,

can not be measured. Thus, the augmented measurement equation for the tanker aircraft in the condition of the white measurement noise is

$$\begin{aligned} \widetilde{\mathrm{y}}_{a,T,k} &= \begin{bmatrix} \mathrm{x}_{T,k} \\ W_{I_{T,k}} \end{bmatrix} + \mathrm{v}_{a,T,k}, \quad \widetilde{\mathrm{y}}_{a,T,k} \in \Re^{15} \\ \mathrm{v}_{a,T,k} &= \begin{bmatrix} \mathrm{v}_{T,k} \\ 0 \end{bmatrix} \end{aligned} \tag{4.8}$$

where $W_{I_{T,k}} \in \Re^3$ is the CMW, $\mathrm{v}_{a,T,k} \in \Re^{15}$ is the augmented measurement noise, and $\mathrm{v}_{T,k} \in \Re^{12}$ is the measurement noise for the state of the tanker aircraft. Note that the measurement covariance of the Kalman filter used as a weighting factor among the measurements has the same dimension as the measurement vector. In this work, the measurement covariances of the Kalman filter for the components of CMW is set by calculating variances of the CMW, which are calculated by Eq. (4.6) and (4.7) after measurement noises are added at the corresponding states while the tanker aircraft uses a true state vector as a feedback state vector. The specific variances of the CMW is calculated by the history of the CMW. The pre-calculated variances of the CMW are used in the measurement update of the KF.

4.4 Colored Measurement in Wind Estimation

The newly defined measurement equation in this chapter is slightly different from that in Section 3.5, Eq. (3.22a), because the system equation for the aircraft is not the same as the system equation for estimation due to the wind model. While the aircraft is disturbed by independent wind profile with turbulence, the augmented system equation in estimation relies on the wind model that calculates wind based on the estimated states. Thus, the process noise vectors for the aircraft and the system

equation for estimation are not the same. Additionally, the system equations for the aircraft and the estimation are nonlinear while the system equation in Section 3.5, Eq. (3.20a), are linear. As discussed in Section 3.5, a new measurement equation should be defined considering two constraints: (i) colored noise is removed and (ii) new defined vector is measurable. The continuous tanker aircraft equation reproduced by Eq. 2.13, discrete colored measurement equation and continuous noise equation, respectively, are

$$\dot{\mathrm{x}}_{_T} = f(\mathrm{x}_{_T}, u, W_{I_T}, \dot{W}_{I_T}) \tag{4.9a}$$

$$\widetilde{\mathrm{y}}_{_{T,k}} = \mathbf{C}\mathrm{x}_{_{T,k}} + \mathrm{v}_{_k} \tag{4.9b}$$

where $\mathrm{x}_{_T} \in \Re^{12}$ is the tanker state vector, $u \in \Re^4$ is the control input vector. $W_{I_T} \in \Re^3$ is wind velocity relative to the inertial frame, $\dot{W}_{I_T} \in \Re^3$ is the wind acceleration relative to the inertial frame, $\mathrm{y}_{_{T,k}} \in \Re^{12}$ is the colored measurement vector, $\mathrm{v}_{_k} \in \Re^{12}$ is the colored noise vector. The colored noise is generated by

$$\dot{\mathrm{v}} = \mathbf{A}_{\mathrm{v}}\mathrm{v} + \mathbf{G}_{\mathrm{v}}W_{\mathrm{v}} \tag{4.10}$$

where $W_{\mathrm{v}} \in \Re^{12}$ is the zero-mean Gaussian white noise with variance of $\mathbf{\Phi_T} \in \Re^{12\times12}$ calculated by Eq. (2.61). Note that $\mathbf{C} \in \Re^{12\times12}$, $\mathbf{A}_{\mathrm{v}} \in \Re^{12\times12}$ and $\mathbf{G}_{\mathrm{v}} \in \Re^{12\times12}$ are constant. Equation (4.9a) and (4.10) can be discretized by Euler method, respectively, as

$$\frac{\mathrm{x}_{_{T,k}} - \mathrm{x}_{_{T,k-1}}}{T} = f_k(\mathrm{x}_{_T}, u, W_{I_T}, \dot{W}_{I_T}) \tag{4.11a}$$

$$\frac{\mathrm{v}_{_k} - \mathrm{v}_{_{k-1}}}{T} = \mathbf{A}_{\mathrm{v}}\mathrm{v}_{_k} + \mathbf{G}_{\mathrm{v}}W_{\mathrm{v},k} \tag{4.11b}$$

where T is a update rate. In this research, the update rate for the continuous equation is same as that of the discrete equation. Equation (4.11a) and (4.11b) are used to define the new measurement to remove colored noise.

The new measurement equation for the tanker aircraft is characterized by the white measurement that is an assumption of a general KF, which is

$$\begin{aligned}
\widetilde{\mathrm{y}}_{T,N,k} &= \frac{\widetilde{\mathrm{y}}_{T,k} - \widetilde{\mathrm{y}}_{T,k-1}}{T} - \mathbf{A}_{\mathrm{v}}\widetilde{\mathrm{y}}_{T,k} && \text{(4.12a)}\\
&= \left[\frac{\mathbf{C}(\mathrm{x}_{T,k} - \mathrm{x}_{T,k-1})}{T} + \frac{\mathrm{v}_k - \mathrm{v}_{k-1}}{T}\right] - \mathbf{A}_{\mathrm{v}}(\mathbf{C}\mathrm{x}_{T,k} + \mathrm{v}_k) && \text{(4.12b)}\\
&= \left[\mathbf{C}f_k(\mathrm{x}_T, u, W_{I_T}, \dot{W}_{I_T}) + (\mathbf{A}_{\mathrm{v}}\mathrm{v}_k + \mathbf{G}_{\mathrm{v}}W_{\mathrm{v},k})\right] - \mathbf{A}_{\mathrm{v}}(\mathbf{C}\mathrm{x}_{T,k} + \mathrm{v}_k) && \text{(4.12c)}\\
&= h_k(\mathrm{x}_T, u, W_{I_T}, \dot{W}_{I_T}, b_{\mathrm{v}}) + \mathrm{v}_{T,N,k} && \text{(4.12d)}
\end{aligned}$$

where

$$\begin{aligned}
h_k(\mathrm{x}_T, u, W_{I_T}, \dot{W}_{I_T}, b_{\mathrm{v}}) &= (-\mathbf{A}_{\mathrm{v}}\ \mathbf{C})\mathrm{x}_{T,k} + \mathbf{C}\ f_k(\mathrm{x}_T, u, W_{I_T}, \dot{W}_{I_T})\\
\mathrm{v}_{T,N,k} &= \mathbf{G}_{\mathrm{v}}\ W_{\mathrm{v},k}
\end{aligned} \qquad (4.13)$$

where $\mathrm{v}_{T,N,k} \in \Re^{12\times 12}$ is a zero-mean Gaussian white noise with variance of $\mathbf{G}_{\mathrm{v}}\mathbf{\Phi}_{\mathbf{T}}\mathbf{G}_{\mathrm{v}}^T \in \Re^{12\times 12}$. Hence, the quality of Eq. (4.12a) could be measurable, and Eq. (4.12d) shows that the measurement noise is the zero-mean Gaussian white noise, which satisfies a white noise assumption of a general KF.

In summary, the augmented system equations for estimation are

$$\dot{\hat{\mathrm{x}}}_{a,T} = f(\hat{\mathrm{x}}_a, u, \hat{W}_{I_T}, \dot{\hat{W}}_{I_T}) + \eta_T \qquad (4.14)$$

where $\eta_{_T} \in Re^{15}$ are the white noise for a tanker aircraft. The measurement equations are

$$\widetilde{\mathrm{y}}_{_{T,N,k}} = h_k(\mathrm{x}_{_T}, u, W_{I_T}, \dot{W}_{I_T}, b_{\mathrm{v}}) + \mathrm{v}_{_{T,N,k}} \tag{4.15}$$

where $\mathrm{v}_{_{T,N,k}} \in \Re^{12}$ is the white noise vector. Note that τ_{v} to determine the extent of correlation in the colored noise is set to 20 second, which means 60.7 percent correlation after 10 seconds. If the variance of the measurement noise or the correlation time constant changes, the process noise covariance matrix should be tuned to obtain accurate estimate.

4.5 Application of SR-UKF

Because the system equation in Eq. (4.4) is nonlinear, a linear KF does not yield satisfactory performance due to the time-varying system matrix. Even through EKF is a nonlinear estimator, EKF using the linearization process by a first order approximation leads to divergent in estimation because the system equation is highly nonlinear and the aircraft operation covers various trim flights and accelerated flight. The family of UKF may be one solution to deal with the property of highly nonlinear. SR-UKF among the family is selected to avoid computational singularity, which is a potential problem in UKF implementation. This chapter uses continuous-discrete SR-UKF with the sample rate of 0.05 second for both system and measurement updates. By the application of the SR-UKF based on the system equation of Eq. (4.4) and the measurement equation of Eq. (4.8), the state and wind could be estimated. Since the magnitude of the eigenvalue of the stable system matrix with the largest real part is 1.1525, the sample rate is selected to be 0.05 second based on Eq. (3.4).

CHAPTER 5

STATE AND WIND ESTIMATION WITHOUT AERODYNAMIC MODEL

The previous chapter shows that, using SR-UKF with the system model augmented with the wind model, aircraft states and wind components can be estimated on a single aircraft. However, the approach relies on a strong assumption that the exact aerodynamic force and moment models are known for the system update of the estimator. This chapter will introduce a new method to estimate aircraft states and wind without the knowledge of the aerodynamic force and moment models. In the evaluation of the estimation, introduced in this chapter, in the simulation environment, the estimated state values are not used for the feedback controller. Instead, actual state variables are fedback to the controller. This practice is justified by the fact that the tanker airplane is flown by its pilot while the receiver should be flown by its flight control system in an automated aerial refueling operation. Thus, there is no need for feeding back the state variables in the tanker aircraft. Further, the measurement errors are Gaussian white noise processes.

5.1 Modeling of System Update for Estimation

The main part of system update of KF consists of the EOM of an aircraft, which includes aerodynamic force expressions in the translational dynamics and moment expressions in the rotational dynamics. Since it is not practical to assume the knowledge of the aerodynamic force and moment expressions for the system update of the estimation, the aerodynamic forces and moments should be replaced in the estimation algorithm by an alternative method.

The translational dynamics for the estimation is obtained from Eq. (2.1) after replacing the external force term by acceleration measurement relative to the inertial frame expressed in the tanker body frame. Thus, the translational dynamics equations become

$$\begin{bmatrix} \dot{\hat{V}}_T \\ \dot{\hat{\beta}}_T \\ \dot{\hat{\alpha}}_T \end{bmatrix} = \hat{\varepsilon}_{\mathbf{T}}^{-\mathbf{1}}\mathbf{S}(\hat{\omega}_{B_T})(\hat{\mathbf{R}}_{\mathbf{B_T W_T}}\hat{V}_{w_T}) - \hat{\varepsilon}_{\mathbf{T}}^{-\mathbf{1}}\hat{\mathbf{R}}_{\mathbf{B_T I}}\dot{\hat{W}}_{I_T} + \hat{\varepsilon}_{\mathbf{T}}^{-\mathbf{1}}\ \widetilde{a}_{B_T} \tag{5.1}$$

where $\widetilde{a}_{B_T}$ is the measurements of the components of an acceleration relative to the inertial frame expressed in the tanker body frame, and $\dot{\hat{W}}_{I_T}$ is obtained through a unit-delay operator, z^{-1}, because their is no direct measurement of wind derivative.

Similarly, aerodynamic moment terms in Eq. (2.8) can not be calculated without the moment expressions of the tanker aircraft. Since there is no direct measurement of the angular acceleration, the rotational dynamics is replaced by the difference of the angular velocity measurements in time, which yields

$$\dot{\hat{\omega}}_{B_T} = \frac{\widetilde{\omega}_{B_T}(t) - \widetilde{\omega}_{B_T}(t-T)}{dt} \tag{5.2}$$

where $\widetilde{\omega}_{B_T}$ is the measurement of angular velocity relative to the inertial frame expressed in the tanker body frame, and T is the sample period.

The rotational kinematics and translational kinematics are directly used from Eqs. (2.11) and (2.12), respectively, without modifications.

In compact form, the model of the tanker aircraft in estimation without the aerodynamic force and moment expressions becomes

$$\dot{\hat{\mathrm{x}}}_T = f(\hat{\mathrm{x}}_T, \dot{\hat{W}}_{I_T}, \widetilde{a}_{B_T}, \widetilde{\omega}_{B_T}), \quad \hat{\mathrm{x}}_T \in \Re^{12} \tag{5.3}$$

Note that, in this approach, control variables (δ_{a_T},δ_{e_T},δ_{r_T},T) are not required in the estimation.

5.2 Modeling of Wind

The modeling of wind for estimation is obtained by rearranging Eq. (5.1) with respect to the derivative of wind, which yields

$$\dot{\hat{W}}_{I_T} = \hat{\mathbf{R}}^{\mathbf{T}}_{\mathbf{B_T I}} \left\{ \mathbf{S}(\hat{\omega}_{B_T}) \hat{\mathbf{R}}_{\mathbf{B_T W_T}} \hat{V}_{w_T} + \widetilde{a}_{B_T} - \hat{\varepsilon}_{\mathbf{T}} \begin{bmatrix} \dot{\hat{V}}_T \\ \dot{\hat{\beta}}_T \\ \dot{\hat{\alpha}}_T \end{bmatrix} \right\} \tag{5.4}$$

where $\widetilde{a}_{B_T}$ is obtained from the acceleration measurements and the rate of change of the airdata ($\dot{\hat{V}}_T$, $\dot{\hat{\beta}}_T$, $\dot{\hat{\alpha}}_T$) is replaced by the numerical calculation of the translational dynamics, Eq. (5.1). In compact form, the model of wind used in estimation is

$$\dot{\hat{W}}_{I_T} = f(\hat{\mathrm{x}}_T, \dot{\hat{\mathrm{x}}}_T, \widetilde{a}_{B_T}), \quad \hat{W}_{I_T} \in \Re^3 \tag{5.5}$$

5.3 Augmentation for System Update of SR-UKF

The augmented state vector is defined as

$$\hat{\mathrm{x}}_a = [\hat{\mathrm{x}}_T, \hat{W}_{I_T}]^T, \quad \hat{\mathrm{x}}_a \in \Re^{15} \tag{5.6}$$

The augmented system can be written in compact form by combining Eq. (5.3) with Eq. (5.5) as

$$\dot{\hat{\mathrm{x}}}_a = f(\hat{\mathrm{x}}_a, \dot{\hat{W}}_{I_T}, \widetilde{a}_{B_T}, \widetilde{\omega}_{B_T}) + \eta \tag{5.7}$$

where $\eta \in \Re^{15}$ is the process noise with variance of $\mathbf{Q_a} \in \Re^{15\times15}$, which is used to avoid occurrence of the singularity problem due to employing two different versions of the same equation and also represent the effect of the turbulence as a process noise, as previously discussed in Section 4.2

Figure 5.1 shows the block diagram representation of the system update model along with the input-output notation of the augmented system. As depicted in the figure, the derivative of wind ($\dot{\hat{W}}_{I_T}$) uses time delay (z^{-1}), acceleration relative to the body tanker frame ($\widetilde{a}_{B_T}$) is obtained from the measurement directly, and the angular acceleration relative to the inertial frame expressed in the body tanker frame is obtained from the time difference of the angular velocity measurements. The augmented system does not require control variables since the aerodynamic models, which would require control variables, are not used in this implementation.

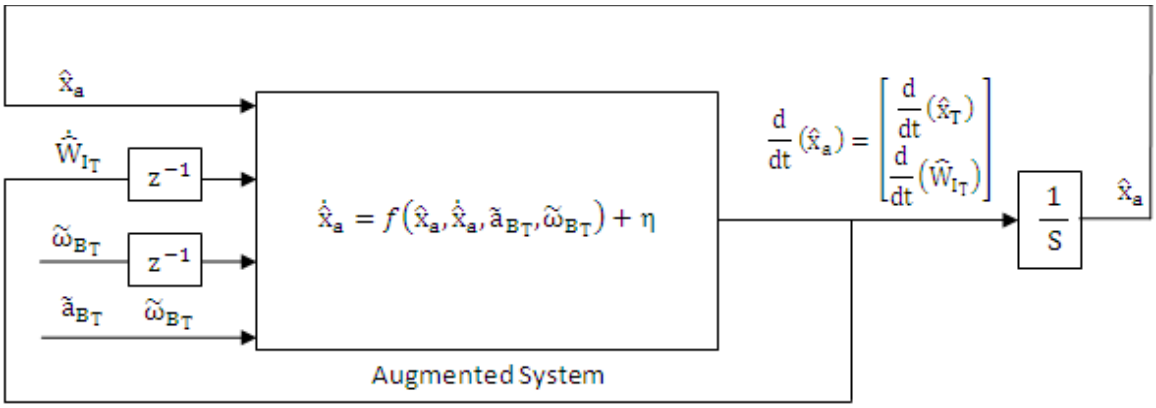

Figure 5.1. Augmented State Update without Aerodynamic Model.

5.4 Application of SR-UKF

Because the system equation in Eq. (5.7) is nonlinear, a linear KF does not yield satisfactory performance due to the time-varying system matrix. Even through

EKF is a nonlinear estimator, EKF using the linearization process by a first order approximation leads to divergent in estimation because the system equation is highly nonlinear and the aircraft operation covers various trim flights and accelerated flight. The family of UKF may be one solution to deal with the property of highly nonlinear. SR-UKF among the family is selected to avoid computational singularity, which is a potential problem in UKF implementation. This chapter uses continuous-discrete SR-UKF with the sample rate of 0.05 second for both system and measurement updates. By the application of the SR-UKF based on the system equation of Eq. (5.7) and the measurement equation of Eq. (4.8), the state and wind could be estimated without aerodynamic information. Since the magnitude of the eigenvalue of the stable system matrix with the largest real part is 1.1525, the sample rate is selected to be 0.05 second based on Eq. (3.4).

CHAPTER 6

RELATIVE POSITION CONTROL OF RECEIVER AIRCRAFT

In a boom-receptable aerial refueling operation, the receiver aircraft is controlled relative to the tanker aircraft. Specifically, the receiver aircraft should be kept at the refueling position with target limits for the boom operator in the tanker aircraft to establish the boom-receptacle connection and maintain it for fuel transfer. For an automated aerial refueling operation, the receiver aircraft is flown by a flight control system. In this research, the receiver aircraft is controlled by a MIMO-LQR based state feedback controller, which is introduced in Section 2.4. Since the receiver is controlled relative to the tanker, the receiver's feedback controller uses the receiver states and some of the tanker states. The tanker SR-UKF-based estimator, introduced in Chapter 3, estimates the tanker states, which are transmitted to the receiver for the controller. Further, this chapter introduces the estimator designed for the estimation of the receiver states as well as the wind components the receiver aircraft is exposed to. The design of the receiver estimation, the same method, introduced in Chapter 3 for the tanker aircraft, is used with some modifications. Recall that this method assumes the availability of the aerodynamic force and moment expressions.

6.1 Modeling of Wind for Estimation

A wind model can be obtained by rearranging Eq. (2.16) in terms of the wind derivative. Note that Eq. (2.16) has W_{B_R}, which is the representation (components) of the wind in the body-frame of the receiver. As a result, the integration of $\dot{W}_{B_R}$ does not yield the wind components. On the other hand, the integration of the derivative

of the wind components in the inertial frame results in the wind components. Thus, Eq. (2.16) should be written in terms of W_{I_R}, the components of the wind in the inertial frame. The relation between the components of the wind in body-frame and inertial frame is

$$W_{B_R} = \mathbf{R_{B_RI}} W_{I_R} \tag{6.1}$$

where $\mathbf{R_{B_RI}}$ is the rotation matrix from the inertial frame to the body frame of the receiver. The time derivative of this equation yields

$$\dot{W}_{B_R} = \dot{\mathbf{R}}_{\mathbf{B_RI}} W_{I_R} + \mathbf{R_{B_RI}} \dot{W}_{I_R} \tag{6.2}$$

where, from the Poisson's form of the rotational kinematics

$$\dot{\mathbf{R}}_{\mathbf{B_RI}} = \mathbf{S}(\omega_{B_R}) \mathbf{R_{B_RI}} \tag{6.3}$$

Eqs. (6.1), (6.2) and (6.3) yield

$$\dot{W}_{B_R} = \mathbf{S}(\omega_{B_R}) W_{B_R} + \mathbf{R_{B_RI}} \dot{W}_{I_R} \tag{6.4}$$

where the direct integration of $\dot{W}_{I_R}$ yields W_{I_R}, the components of wind in the inertial frame.

Substituting $\dot{W}_{B_R}$ from Eq. (6.4) in Eq. (2.16) leads to a new form of the translational dynamics for estimation as

$$\begin{bmatrix} \dot{\hat{V}} \\ \dot{\hat{\beta}} \\ \dot{\hat{\alpha}} \end{bmatrix} = \hat{\varepsilon}_{\mathbf{R}}^{-\mathbf{1}} \left[\mathbf{S}(\hat{\omega}_{_{B_R B_T}}) + \hat{\mathbf{R}}_{\mathbf{B_R B_T}} \mathbf{S}(\hat{\omega}_{_{B_T}}) \hat{\mathbf{R}}_{\mathbf{B_R B_T}}^{\mathbf{T}} \right] (\hat{\mathbf{R}}_{\mathbf{B_R W_R}} \hat{V}_w)$$

$$- \hat{\varepsilon}_{\mathbf{R}}^{-\mathbf{1}} \hat{\mathbf{R}}_{\mathbf{B_R I}} \dot{\hat{W}}_{I_R} + \frac{1}{m_{_R}} \hat{\varepsilon}_{\mathbf{R}}^{-\mathbf{1}} (\hat{\mathbf{R}}_{\mathbf{B_R B_T}} \hat{\mathbf{R}}_{\mathbf{B_T I}} M_R + \hat{\mathbf{R}}_{\mathbf{B_R W_R}} \hat{A}_R + P_R) \qquad (6.5)$$

which is rearranged with respect to the wind to obtain the wind derivative model relative to the inertial frame as

$$\dot{\hat{W}}_{I_R} = \hat{\mathbf{R}}_{\mathbf{B_R I}}^{\mathbf{T}} \left\{ \left[\mathbf{S}(\hat{\omega}_{B_R B_T}) + \hat{\mathbf{R}}_{\mathbf{B_R B_T}} \mathbf{S}(\hat{\omega}_{B_T}) \hat{\mathbf{R}}_{\mathbf{B_R B_T}}^{\mathbf{T}} \right] \left(\hat{\mathbf{R}}_{\mathbf{B_R W_R}} \hat{V}_w \right) \right\}$$

$$+ \hat{\mathbf{R}}_{\mathbf{B_R I}}^{\mathbf{T}} \left\{ \frac{1}{m_R} \left(\hat{\mathbf{R}}_{\mathbf{B_R B_T}} \hat{\mathbf{R}}_{\mathbf{B_T I}} M_R + \hat{\mathbf{R}}_{\mathbf{B_R W_R}} \hat{A}_R + P_R \right) - \hat{\varepsilon}_{\mathbf{R}} \begin{bmatrix} \dot{\hat{V}} \\ \dot{\hat{\beta}} \\ \dot{\hat{\alpha}} \end{bmatrix} \right\} \qquad (6.6)$$

where

$$\varepsilon_{\mathbf{R}} = \begin{bmatrix} \cos\beta\cos\alpha & -V\sin\beta\cos\alpha & -V\cos\beta\sin\alpha \\ \sin\beta & V\cos\beta & 0 \\ \cos\beta\sin\alpha & -V\sin\beta\sin\alpha & V\cos\beta\cos\alpha \end{bmatrix} \qquad (6.7)$$

where M_R, P_R, and aerodynamic expressions are assumed to be known, and the rate of change of the airdata (V, β, α) are replaced by the numerical calculation of the translational dynamics, Eq. (6.5).

6.2 Augmentation for System Update of Kalman Filter

The augmented system for the receiver aircraft is obtained by combining Eq. (2.31) and Eq. (6.6) after replacing $\dot{W}_{B_R}$ in Eq. (2.31) with Eq. (6.4). The state vector for the augmented system is

$$\hat{\mathrm{x}}_{a,R} = [\hat{\mathrm{x}}_R, \hat{W}_{I_R}]^T \tag{6.8}$$

In summary, the translational dynamics for estimation is Eq. (6.5). The rotational dynamics and rotational kinematics for estimation are the same as Eq. (2.23) and Eq. (2.27), respectively. The wind components in the receiver body frame in translational kinematics of Eq. (2.29) is transformed to components in the inertial frame by using Eq. (6.1) for the estimation, which is

$$\begin{aligned} \mathbf{R}^{\mathbf{T}}_{\mathbf{B_R B_T}} W_{B_R} &= \mathbf{R}^{\mathbf{T}}_{\mathbf{B_R B_T}} \left(\mathbf{R}_{\mathbf{B_R I}} W_{I_R}\right) \\ &= \mathbf{R}_{\mathbf{B_T I}} W_{I_R} \end{aligned} \tag{6.9}$$

where

$$\mathbf{R}^{\mathbf{T}}_{\mathbf{B_R B_T}} \mathbf{R}_{\mathbf{B_R I}} = \mathbf{R}_{\mathbf{B_T I}} \tag{6.10}$$

Eq. (2.29) and Eq. (6.9) yield the alternative translational kinematics as

$$\dot{\xi} = \mathbf{R}^{\mathbf{T}}_{\mathbf{B_R B_T}} \mathbf{R}_{\mathbf{B_R W_R}} V_w + \mathbf{R}_{\mathbf{B_T I}} W_{I_R} - \mathbf{R}_{\mathbf{B_T I}} \dot{r}_T + \mathbf{S}(\omega_{\mathbf{B_T}}) \xi \tag{6.11}$$

Thus, the translational kinematics, to be used in estimation, becomes

$$\dot{\hat{\xi}} = \hat{\mathbf{R}}^{\mathbf{T}}_{\mathbf{B_R B_T}} \hat{\mathbf{R}}_{\mathbf{B_R W_R}} \hat{V}_w + \hat{\mathbf{R}}_{\mathbf{B_T I}} \hat{W}_{I_R} - \hat{\mathbf{R}}_{\mathbf{B_T I}} \dot{\hat{r}}_T + \mathbf{S}(\hat{\omega}_{\mathbf{B_T}}) \hat{\xi} \tag{6.12}$$

In compact form, the augmented system is

$$\dot{\hat{\mathrm{x}}}_{a,R} = f(\hat{\mathrm{x}}_{a,R}, \hat{\mathrm{x}}_T, \dot{\hat{\mathrm{x}}}_T, u_R, \hat{W}_{I_R}, \dot{\hat{W}}_{I_R}) + \eta_R \tag{6.13}$$

where $\eta_R \in \Re^{15}$ is the zero-mean Gaussian white noise with variance $\mathbf{Q_R} \in \Re^{15\times 15}$, which is used in the system update of the KF, $u_R \in \Re^7$ is the control input, and $\hat{W}_{I_R} \in \Re^3$ is the estimated wind components in the inertial frame.

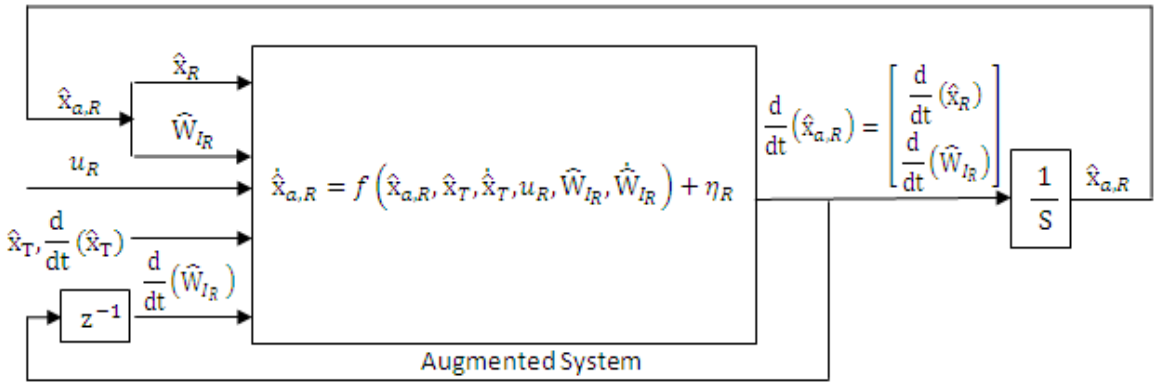

Figure 6.1. Augmented State Update in SR-UKF of Receiver Aircraft.

Fig. 6.1 shows a depiction of the augmented system in the KF system update for the receiver aircraft. The derivative of the wind relative to the inertial frame, $\frac{\mathrm{d}}{\mathrm{dt}}(\hat{W}_{I_R})$, is provided to the estimation system update from the previous numerical calculation, through a unit delay operation, z^{-1}, because there is no measurement of the derivative of wind relative to the inertial frame.

6.3 Calculated Measurement of Wind (CMW)

In Kalman filter implementation, measurement update must be provided for correction. However, there is no direct measurement of wind velocity for the measurement update. Instead of direct measurement, the calculated measurement of wind

(CMW) could be used to increase the accuracy of the estimation. An equation for calculating the CMW for the receiver aircraft is obtained by rearranging Eq. (6.11) with respect to the wind as

$$W_{I_R} = \widetilde{\mathbf{R}}^{\mathbf{T}}_{\mathbf{B_T I}}\widetilde{\dot{\xi}} - \widetilde{\mathbf{R}}^{\mathbf{T}}_{\mathbf{B_T I}}\widetilde{\mathbf{R}}^{\mathbf{T}}_{\mathbf{B_R B_T}}\widetilde{\mathbf{R}}_{\mathbf{B_R W_R}}\widetilde{V}_{w_R} + \widetilde{\dot{r}}_T - \widetilde{\mathbf{R}}^{\mathbf{T}}_{\mathbf{B_T I}}\widetilde{\mathbf{S}}(\omega_{B_T})\widetilde{\xi} \tag{6.14}$$

where $\widetilde{(\cdot)}$ means measurement data of $(\cdot)$. W_{I_R} calculated by Eq. (6.14) may have large noise level. To reduce the large noise level, the filter with a moving average window (MAW) that are introduced in Eq. (4.7) is used.

The CMW is used to minimize wind estimation error based on the Kalman structure. Thus, the augmented measurement equation for the receiver aircraft is

$$\begin{aligned} \widetilde{\mathrm{y}}_{a,R,k} &= \begin{bmatrix} \mathrm{x}_{R,k} \\ W_{I_{R,k}} \end{bmatrix} + \mathrm{v}_{a,R,k}, \quad \widetilde{\mathrm{y}}_{a,R,k} \in \Re^{15} \\ \mathrm{v}_{a,R,k} &= \begin{bmatrix} \mathrm{v}_{R,k} \\ 0 \end{bmatrix} \end{aligned} \tag{6.15}$$

where $W_{I_{R,k}} \in \Re^3$ is the CMW, $\mathrm{v}_{a,R,k} \in \Re^{15}$ is the augmented measurement noise, and $\mathrm{v}_{R,k} \in \Re^{12}$ is the measurement noise for the states of the receiver aircraft.

6.4 Colored Measurement in Wind Estimation

The newly defined measurement equation in this chapter is slightly different from that in Section 3.5, Eq. (3.22a), because the system equation for the aircraft is not the same as the system equation for estimation due to the wind model. While the aircraft is disturbed by independent wind profile with turbulence, the augmented system equation in estimation relies on the wind model that calculates wind based on

the estimated states. Thus, the process noise vectors for the aircraft and the system equation for estimation are not the same. Additionally, the system equations for the aircraft and the estimation are nonlinear while the system equation in Section 3.5, Eq. (3.20a), are linear. As discussed in Section 3.5, a new measurement equation should be defined considering two constraints: (i) colored noise is removed and (ii) new defined vector is measurable.

The continuous receiver aircraft equation reproduced by Eq. 2.31, discrete colored measurement equation and continuous noise equation, respectively, are

$$\dot{\mathrm{x}}_{R} = f(\mathrm{x}_{R}, \mathrm{x}_{T}, u, W_{B_R}, \dot{W}_{B_R}), \quad \mathrm{x}_{R} \in \Re^{12} \tag{6.16a}$$

$$\widetilde{\mathrm{y}}_{R,k} = \mathbf{C}\mathrm{x}_{R,k} + \mathrm{v}_{k}, \quad \widetilde{\mathrm{y}}_{R,k} \in \Re^{12} \tag{6.16b}$$

$$\dot{\mathrm{v}} = \mathbf{A}_{\mathrm{v}}\mathrm{v} + \mathbf{G}_{\mathrm{v}}W_{\mathrm{v}} \tag{6.16c}$$

where $\mathrm{x}_{R} \in \Re^{12}$ is the tanker state vector, $u \in \Re^{7}$ is the control input vector, $W_{B_R} \in \Re^{3}$ is wind velocity relative to the inertial frame expressed in the receiver body frame, $\dot{W}_{B_R} \in \Re^{3}$ is the wind acceleration written in the receiver body frame, $\mathrm{y}_{R,k} \in \Re^{12}$ is the colored measurement vector, $\mathrm{v}_{k} \in \Re^{12}$ is the colored noise vector and $W_{\mathrm{v}} \in \Re^{12}$ is the zero-mean Gaussian white noise with variance of $\mathbf{\Phi_R} \in \Re^{12\times12}$ calculated by Eq. (2.61). Note that $\mathbf{C} \in \Re^{12\times12}$, $\mathbf{A}_{\mathrm{v}} \in \Re^{12\times12}$ and $\mathbf{G}_{\mathrm{v}} \in \Re^{12\times12}$ are constant. Equation (6.16a) and (6.16c) can be discretized by Euler method, respectively, as

$$\frac{\mathrm{x}_{R,k} - \mathrm{x}_{R,k-1}}{T} = f_k(\mathrm{x}_{R}, \mathrm{x}_{T}, u, W_{B_R}, \dot{W}_{B_R}) \tag{6.17a}$$

$$\frac{\mathrm{v}_{k} - \mathrm{v}_{k-1}}{T} = \mathbf{A}_{\mathrm{v}}\mathrm{v}_{k} + \mathbf{G}_{\mathrm{v}}W_{\mathrm{v},k} \tag{6.17b}$$

The new measurement equation for the receiver aircraft is characterized by the white measurement that is an assumption of a general KF, which is

$$\widetilde{\mathrm{y}}_{R,N,k} = \frac{\widetilde{\mathrm{y}}_{R,k} - \widetilde{\mathrm{y}}_{R,k-1}}{T} - \mathbf{A}_{\mathrm{v}}\widetilde{\mathrm{y}}_{R,k} \tag{6.18a}$$

$$= \left[\frac{\mathbf{C}(\mathrm{x}_{R,k} - \mathrm{x}_{R,k-1})}{T} + \frac{\mathrm{v}_k - \mathrm{v}_{k-1}}{T}\right] - \mathbf{A}_{\mathrm{v}}(\mathbf{C}\mathrm{x}_{R,k} + \mathrm{v}_k) \tag{6.18b}$$

$$= \left[\mathbf{C}f_k(\mathrm{x}_R, \mathrm{x}_T, u, W_{B_R}, \dot{W}_{B_R}) + (\mathbf{A}_{\mathrm{v}}\mathrm{v}_k + \mathbf{G}_{\mathrm{v}}W_{\mathrm{v},k})\right] - \mathbf{A}_{\mathrm{v}}(\mathbf{C}\mathrm{x}_{R,k} + \mathrm{v}_k) \tag{6.18c}$$

$$= h_k(\mathrm{x}_R, \mathrm{x}_T, u, W_{B_R}, \dot{W}_{B_R}, b_{\mathrm{v}}) + \mathrm{v}_{R,N,k} \tag{6.18d}$$

where

$$\begin{aligned} h_k(\mathrm{x}_R, \mathrm{x}_T, u, W_{B_R}, \dot{W}_{B_R}, b_{\mathrm{v}}) &= (-\mathbf{A}_{\mathrm{v}}\ \mathbf{C})\mathrm{x}_{R,k} + \mathbf{C}\ f_k(\mathrm{x}_R, \mathrm{x}_T, u, W_{B_R}, \dot{W}_{B_R}) \\ \mathrm{v}_{R,N,k} &= \mathbf{G}_{\mathrm{v}}\ W_{\mathrm{v},k} \end{aligned} \tag{6.19}$$

where $\mathrm{v}_{R,N,k} \in \Re^{12\times 12}$ is a zero-mean Gaussian white noise with variance of $\mathbf{G}_{\mathrm{v}}\mathbf{\Phi}_{\mathbf{R}}{\mathbf{G}_{\mathrm{v}}}^T \in \Re^{12\times 12}$. Hence, the quality of Eq. (6.18a) could be measurable, and Eq. (6.18d) shows that the measurement noise is zero-mean Gaussian white noise, which satisfies the white noise assumption of a general KF.

In summary, the augmented system equations for estimation are

$$\dot{\hat{\mathrm{x}}}_{a,T} = f(\hat{\mathrm{x}}_a, u, \hat{W}_{I_T}, \dot{\hat{W}}_{I_T}) + \eta_T \tag{6.20}$$

$$\dot{\hat{\mathrm{x}}}_{a,R} = f(\hat{\mathrm{x}}_{a,R}, \hat{\mathrm{x}}_T, \dot{\hat{\mathrm{x}}}_T, u_R, \hat{W}_{I_R}, \dot{\hat{W}}_{I_R}) + \eta_R \tag{6.21}$$

where $\eta_T \in \Re^{15}$ and $\eta_R \in \Re^{15}$ are the white noise for a tanker and receiver aircraft respectively. The measurement equations are

$$\widetilde{\mathrm{y}}_{T,N,k} = h_k(\mathrm{x}_T, u, W_{I_T}, \dot{W}_{I_T}, b_{\mathrm{v}}) + \mathrm{v}_{T,N,k} \tag{6.22}$$

$$\widetilde{\mathrm{y}}_{R,N,k} = h_k(\mathrm{x}_R, \mathrm{x}_T, u, W_{B_R}, \dot{W}_{B_R}, b_\mathrm{v}) + \mathrm{v}_{R,N,k} \tag{6.23}$$

where $\mathrm{v}_{T,N,k} \in \Re^{12}$ and $\mathrm{v}_{R,N,k} \in \Re^{12}$ are white noise vectors. Note that τ_v quantifying the extent of correlation in the colored noise is set to 1 second, which means 36.8 percent correlation after 1 second. If the variance of the measurement noise or the correlation time constant changes, the process noise covariance matrix should be tuned to obtain accurate estimate.

6.5 Application of SR-UKF

Because the system equation in Eq. (6.13) is nonlinear, a linear KF does not yield satisfactory performance due to the time-varying system matrix. Even through EKF is a nonlinear estimator, EKF using the linearization process by a first order approximation leads to divergent in estimation because the system equation is highly nonlinear and the aircraft operation covers various trim flights and accelerated flight. The family of UKF may be one solution to deal with the property of highly nonlinear. SR-UKF among the family is selected to avoid computational singularity, which is a potential problem in UKF implementation. This chapter uses continuous-discrete SR-UKF with the sample rate of 0.05 second for both system and measurement updates. By the application of the SR-UKF based on the system equation of Eq. (6.13) and the measurement equation of Eq. (6.15), the state and wind for the receiver aircraft could be estimated. Since the magnitude of the eigenvalue of the stable system matrix with the largest real part is 1.1525, the sample rate is selected to be 0.05 second based on Eq. (3.4).

6.6 Linear Quadratic Gaussian (LQG) Controller

The LQR-based trajectory tracking controller for the receiver aircraft is presented in Section 2.4. The linear quadratic Gaussian (LQG) controller, implemented in this chapter, is the LQR-based controller with feedback signals are the state estimates, instead of measurement signals. This controller can potentially improve closed-loop performance by replacing the large noisy measurements with the estimated states. The LQG structure is shown in Fig. 6.2.

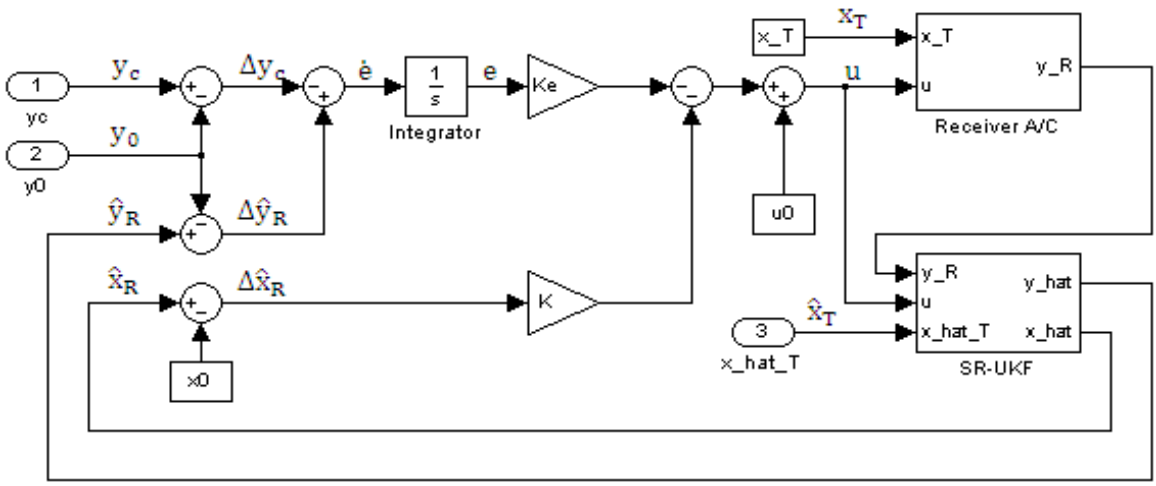

Figure 6.2. LQG Controller for Receiver Aircraft.

CHAPTER 7

RESULT OF SIMULATION AND PARAMETER STUDY

7.1 Estimation of Aircraft States and Wind Exposure at Tanker Aircraft

The SR-UKF estimation algorithm developed for the tanker aircraft are implemented in an integrated simulation environment. In the simulation, the controller of the tanker is commanded to fly the aircraft through the trajectory shown in Fig. 7.1 with the nominal airspeed of 190 m/s. Table 7.1 describes the four cases simulated in terms of the turbulence model, the prevailing wind generation, and the variation of the measurement noise. The purpose is to investigate the performance of the estimation algorithm in various simulated wind conditions and with sensors of various levels of measurement noise. For the controller of the tanker, the actual states are used in the feedback control.

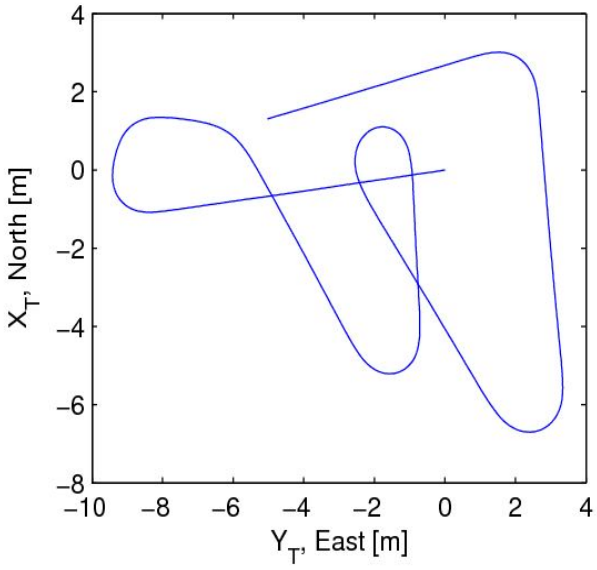

Figure 7.1. Trajectory of Tanker.

Table 7.1. Four Case Studies

	W_{tur}	W_{pre}	*Measurement Noise*	*Feedback Signal*
Case I	Dryden	Flight Data	Small Level	Actual
Case II	Dryden	ECWM	Small Level	Actual
Case III	Dryden	ECWM	Large Level	Actual
Case IV	Dryden	Flight Data	Large Level	Actual

7.1.1 Case I: Test Flight Wind and Small Measurement Noise

The tanker aircraft is exposed to the time-varying prevailing wind profile representing the condition of the test flight as described in Section 2.5.1.1. The measurement noise is modeled as Gaussian white noise with the characteristics listed in Table 2.2. The turbulence superimposed on the prevailing wind is obtained from the Dryden model, described in Section 2.5.2.

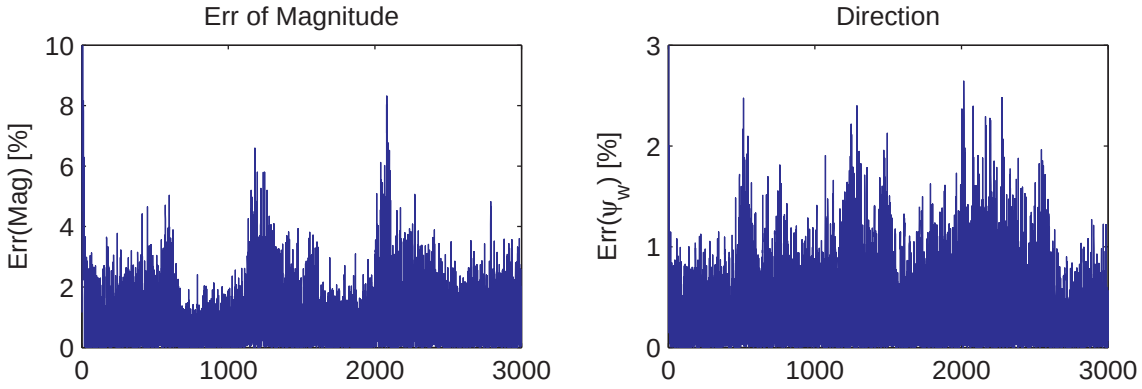

Figure 7.2. Percent Errors of Wind Estimate (Case I).

The estimated wind velocity vector is expressed in terms of its magnitude and direction and shown in Fig. 7.2. The magnitude error is usually less than 5% and the direction error in general remains less 3%. Even at the worst case when the

tanker aircraft turns, the magnitude and direction errors do not exceed 10% and 3%, respectively.

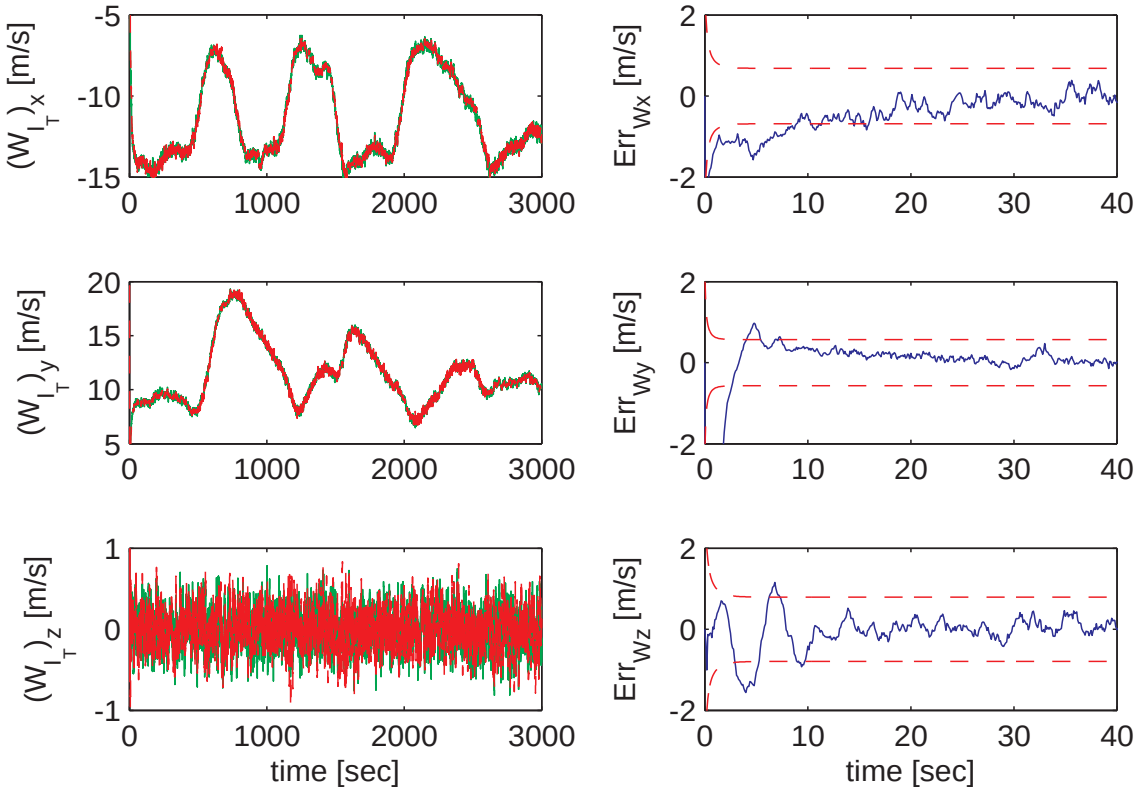

Figure 7.3. Comparison Between Reference and Estimated Wind (Case I).

The plots on the left hand side of Fig. 7.3 show the components of the reference wind and the estimated wind throughout the whole simulation. The figures clearly show that the estimation is successful in capturing very well the time variation of the wind. On the right hand side of Fig. 7.3, the estimation errors, in the component form, are shown in the first 40 seconds and compared with the 3σ bounds. The x- & y-component errors converge to the respective 3σ bounds in 20 seconds while the z-component error converges in 10 seconds.

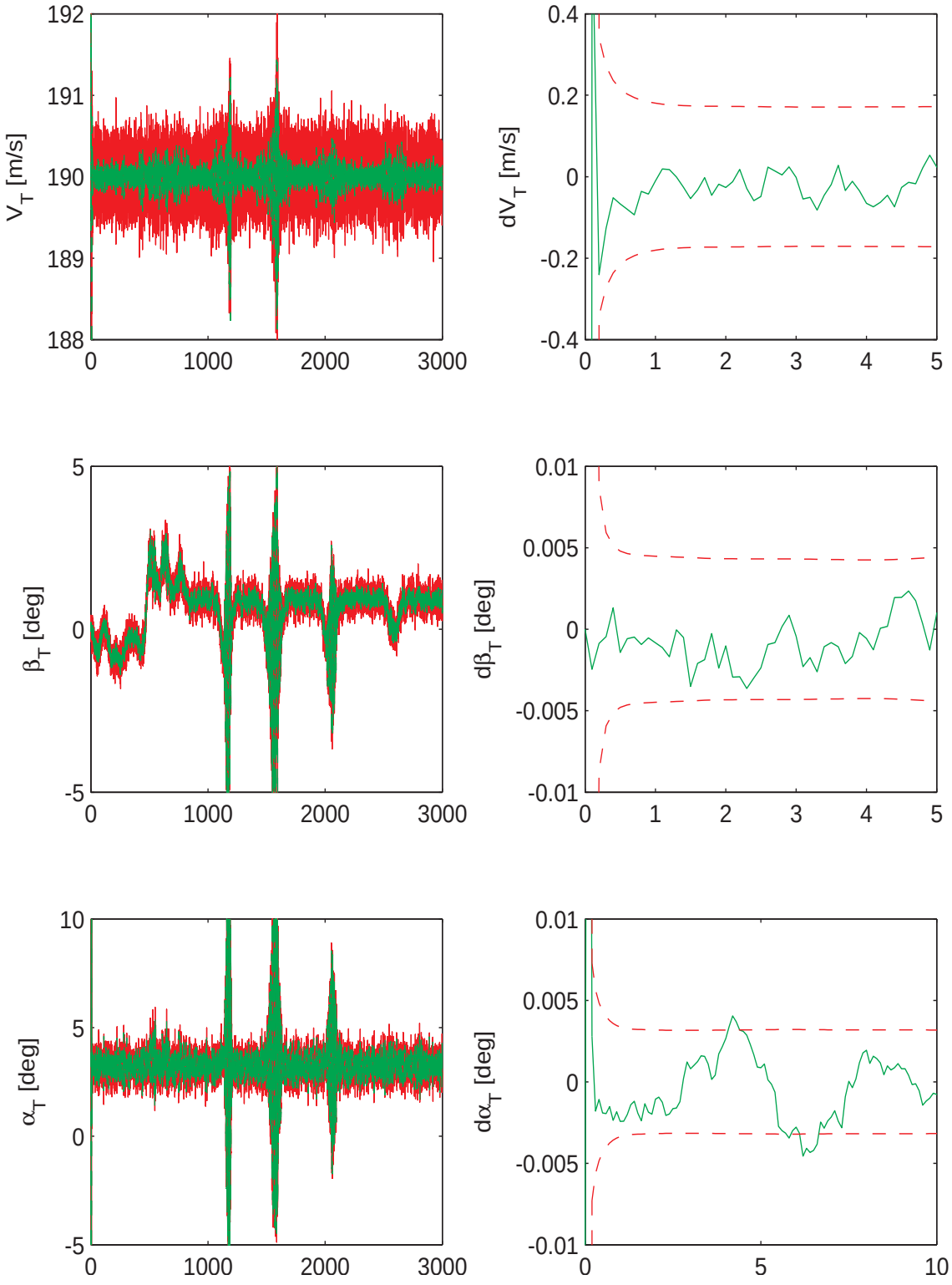

Figure 7.4. Measured and Estimated Airspeed, Sideslip Angle and Angle of Attack.

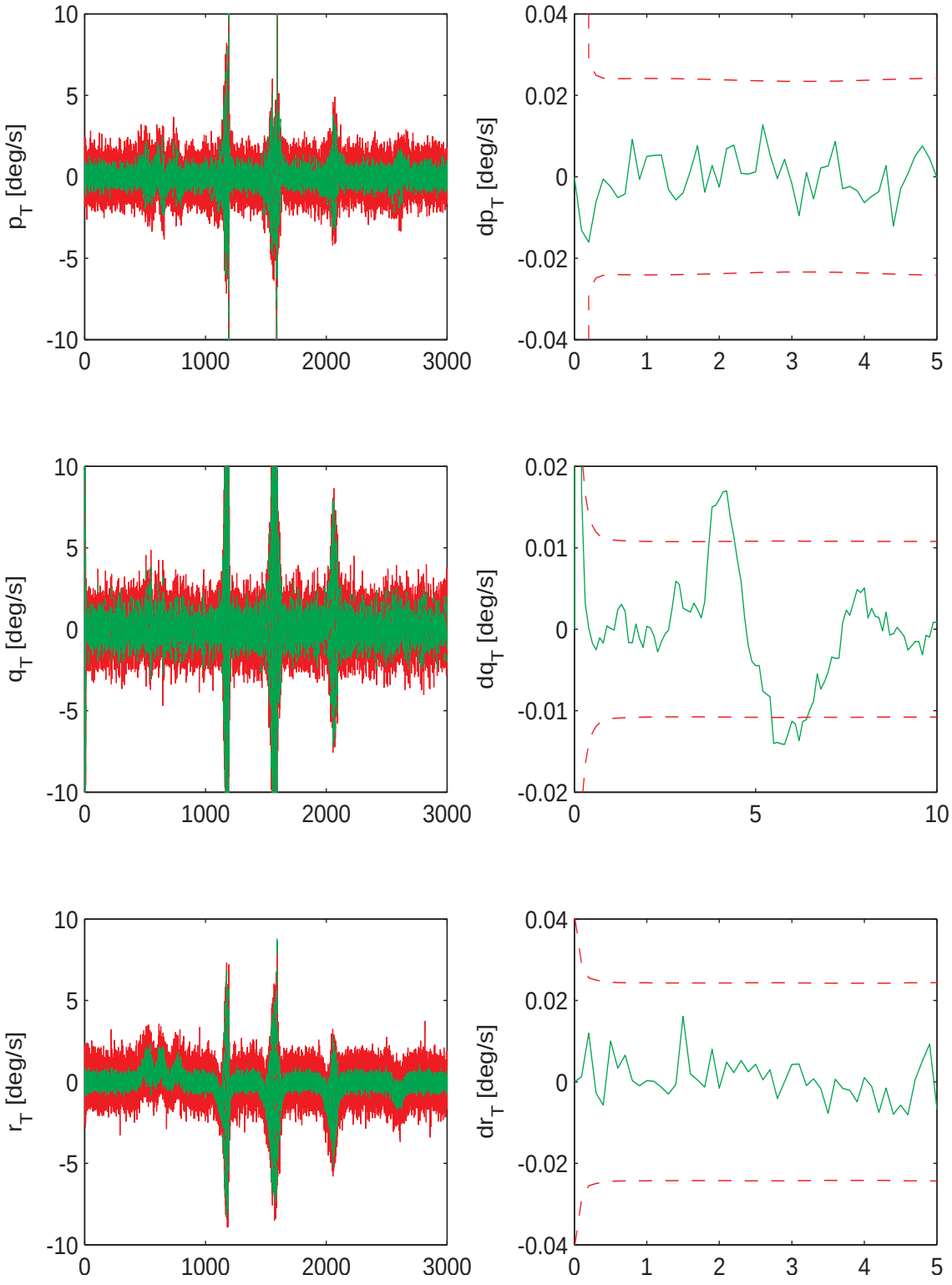

Figure 7.5. Measured and Estimated Angular Velocity Components.

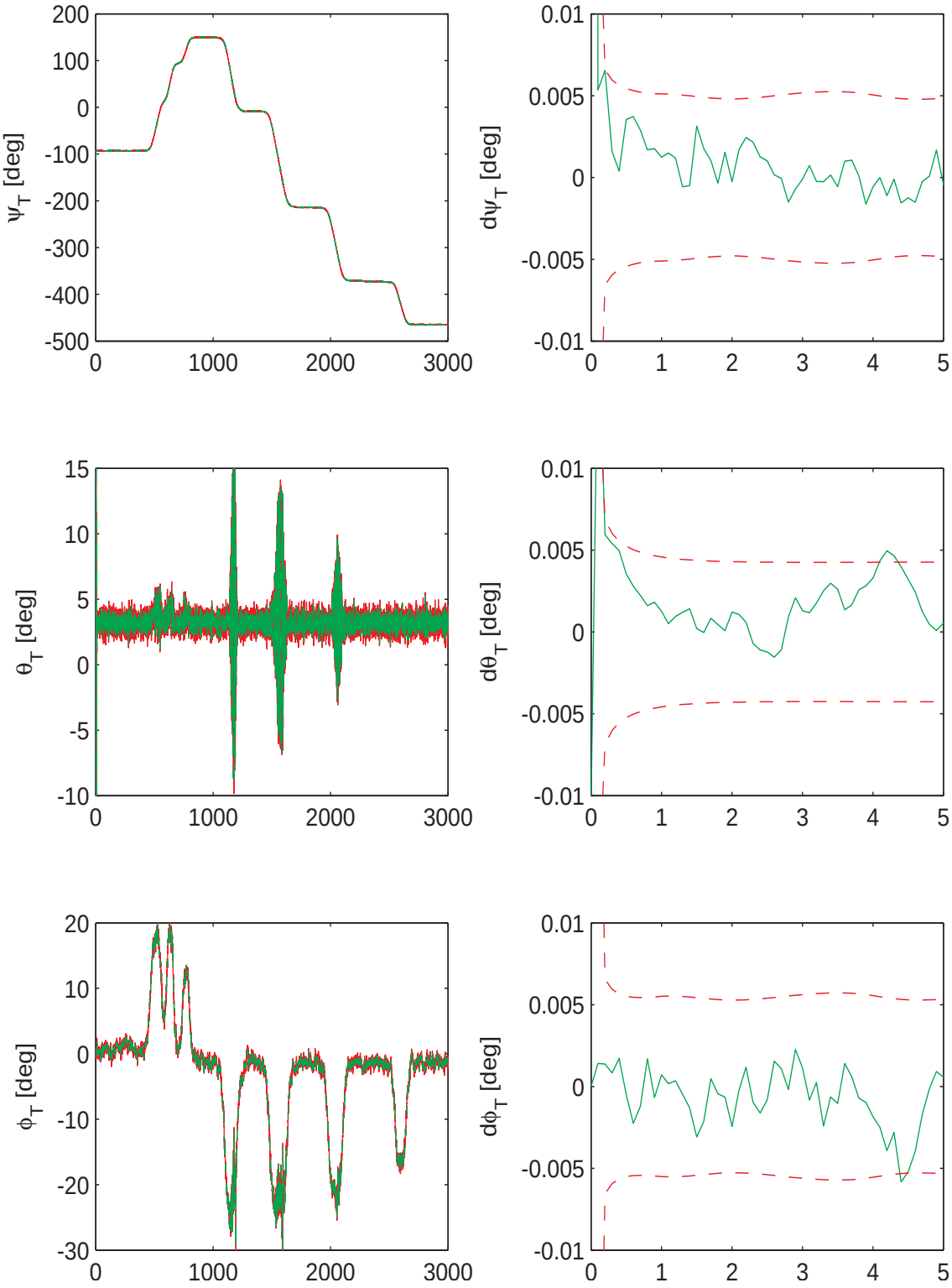

Figure 7.6. Measured and Estimated Euler Angles.

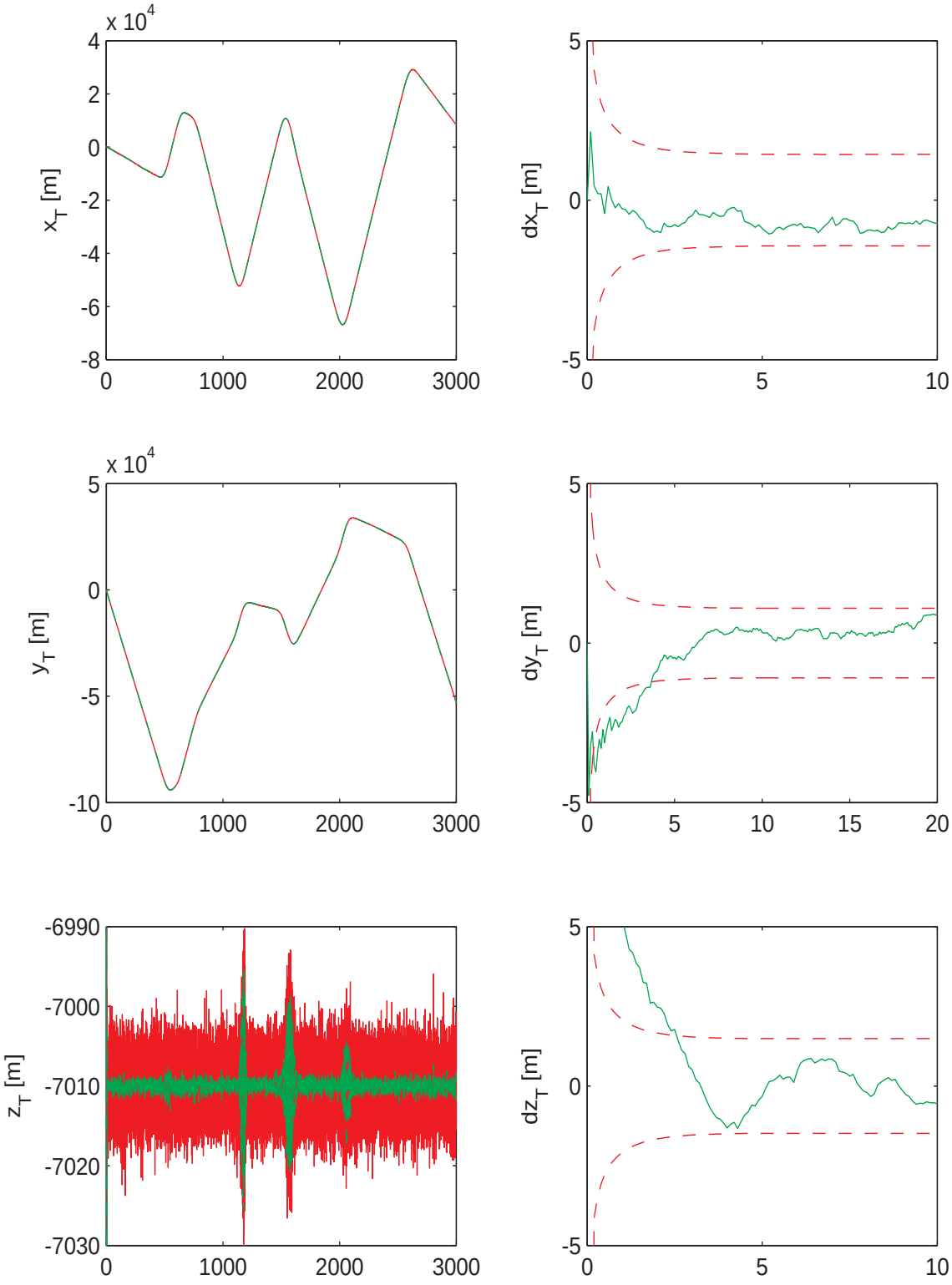

Figure 7.7. Measured and Estimated Position Components.

Figures 7.4 to 7.7 show the comparison of the estimated aircraft states with the measured states. All the states are successfully estimated while the tanker aircraft goes through various straight-level and turning segments of the commanded trajectory while exposed to the time varying prevailing wind and turbulence. Further, the noise levels in all the estimated states are reduced as compared to the respective measured states.

7.1.2 Case II: ECWM Prevailing Wind and Small Measurement Noise

In this case, the prevailing wind is generated by ECWM. The variation of this wind profile is less than that in Case I. Every other aspect of this simulation is the same as in Case I. The estimated wind vector is expressed in terms of its magnitude and direction. The percentage errors of the estimated wind in terms of magnitude and direction are shown in Fig. 7.8. The magnitude error is usually less than 4% and the direction error in general remains less 2%. The plots on the left hand side of Fig. 7.9 show the components of the reference wind and the estimated wind throughout the whole simulation. The figures clearly show that the estimation is successful in capturing very well the time variation of the wind. On the right hand side of Fig. 7.9, the estimation errors, in the component form, are shown in the first 40 seconds and compared with the 3σ bounds. The x- & y-component errors converge to the respective 3σ bounds in 20 seconds while the z-component error converges in 10 seconds. Figures 7.10 to 7.13 show the measured and estimated aircraft states throughout the whole simulation. This simulation case studies the performance of the estimation algorithm under a different wind profile and shows no change in the performance while the aircraft is exposed to a different prevailing wind profile.

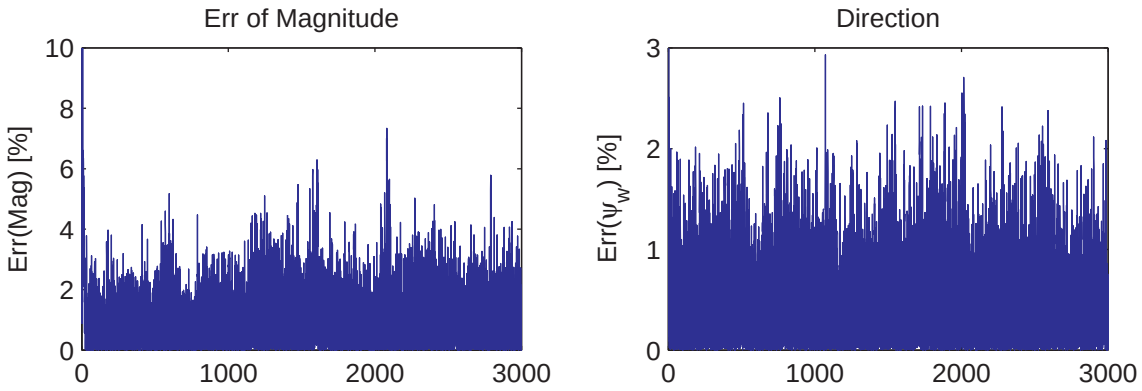

Figure 7.8. Percent Errors of Wind Estimate (Case II).

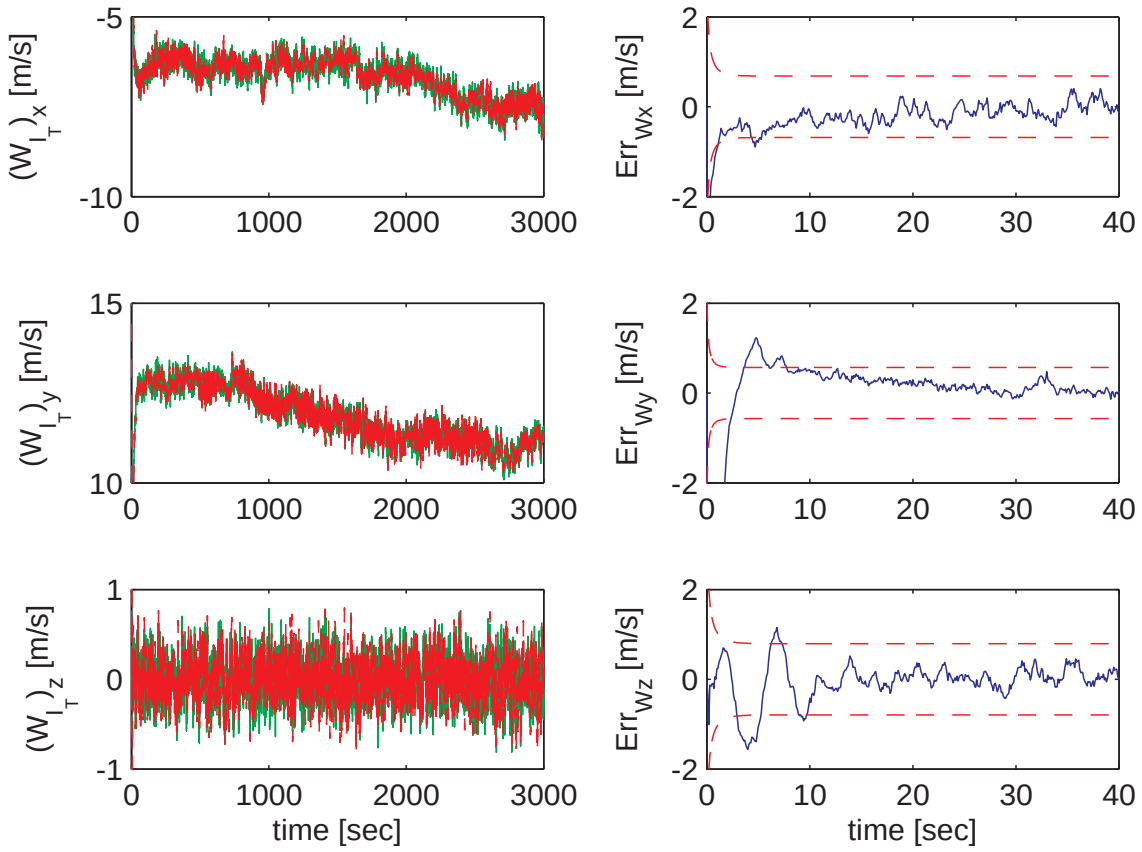

Figure 7.9. Comparison Between Reference and Estimated Wind (Case II).

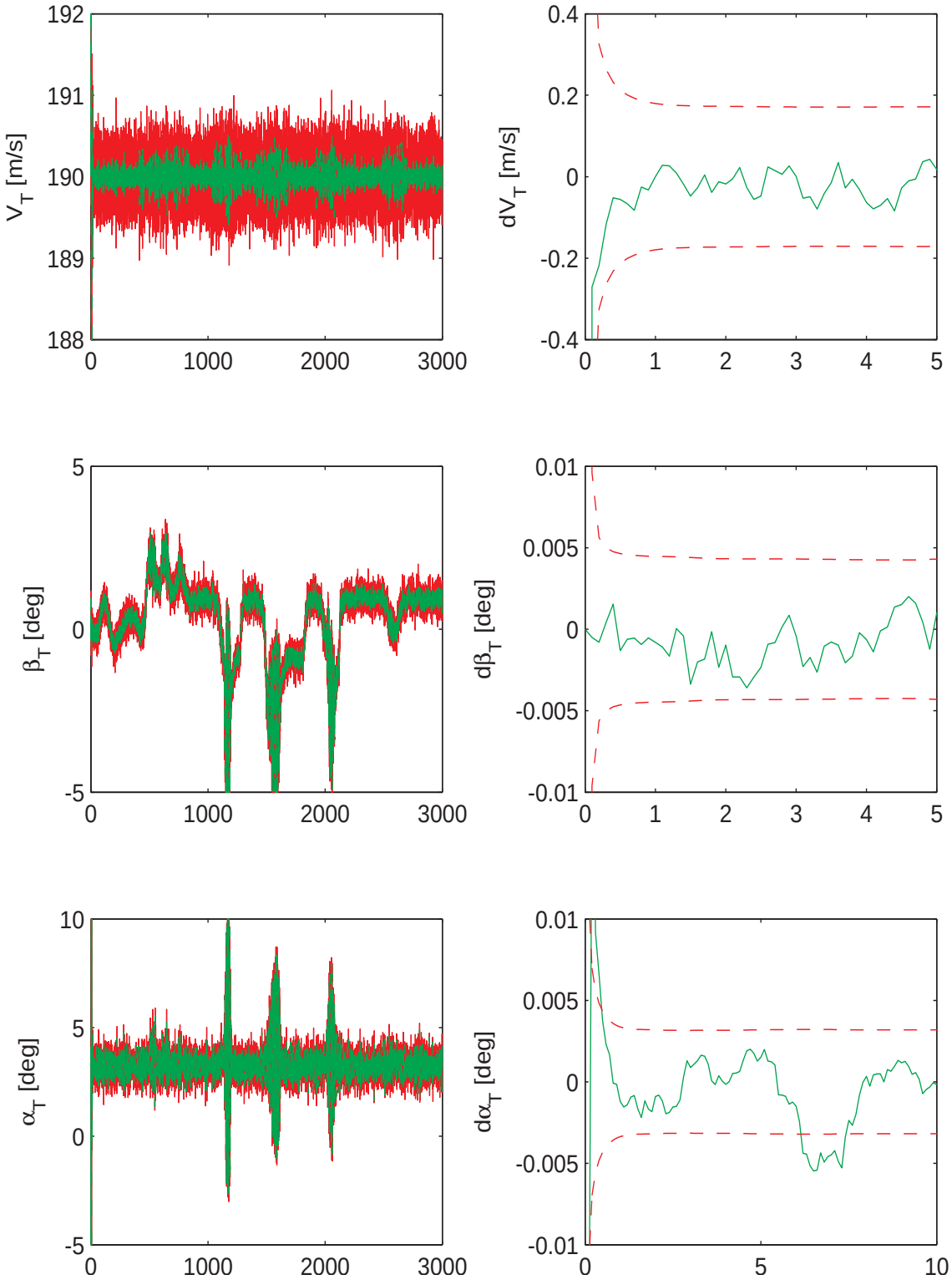

Figure 7.10. Measured and Estimated Airspeed, Sideslip Angle and Angle of Attack.

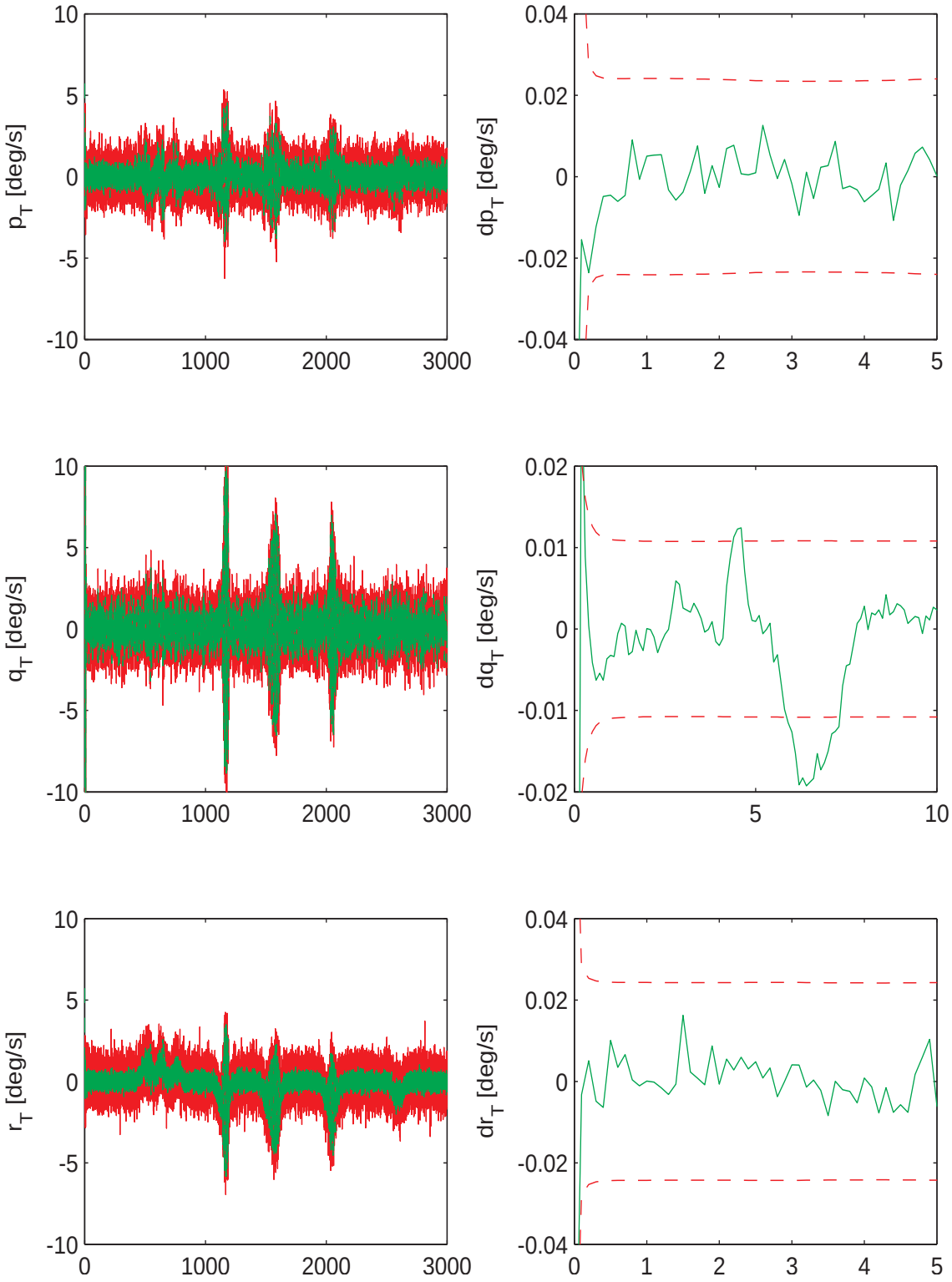

Figure 7.11. Measured and Estimated Angular Velocity Components.

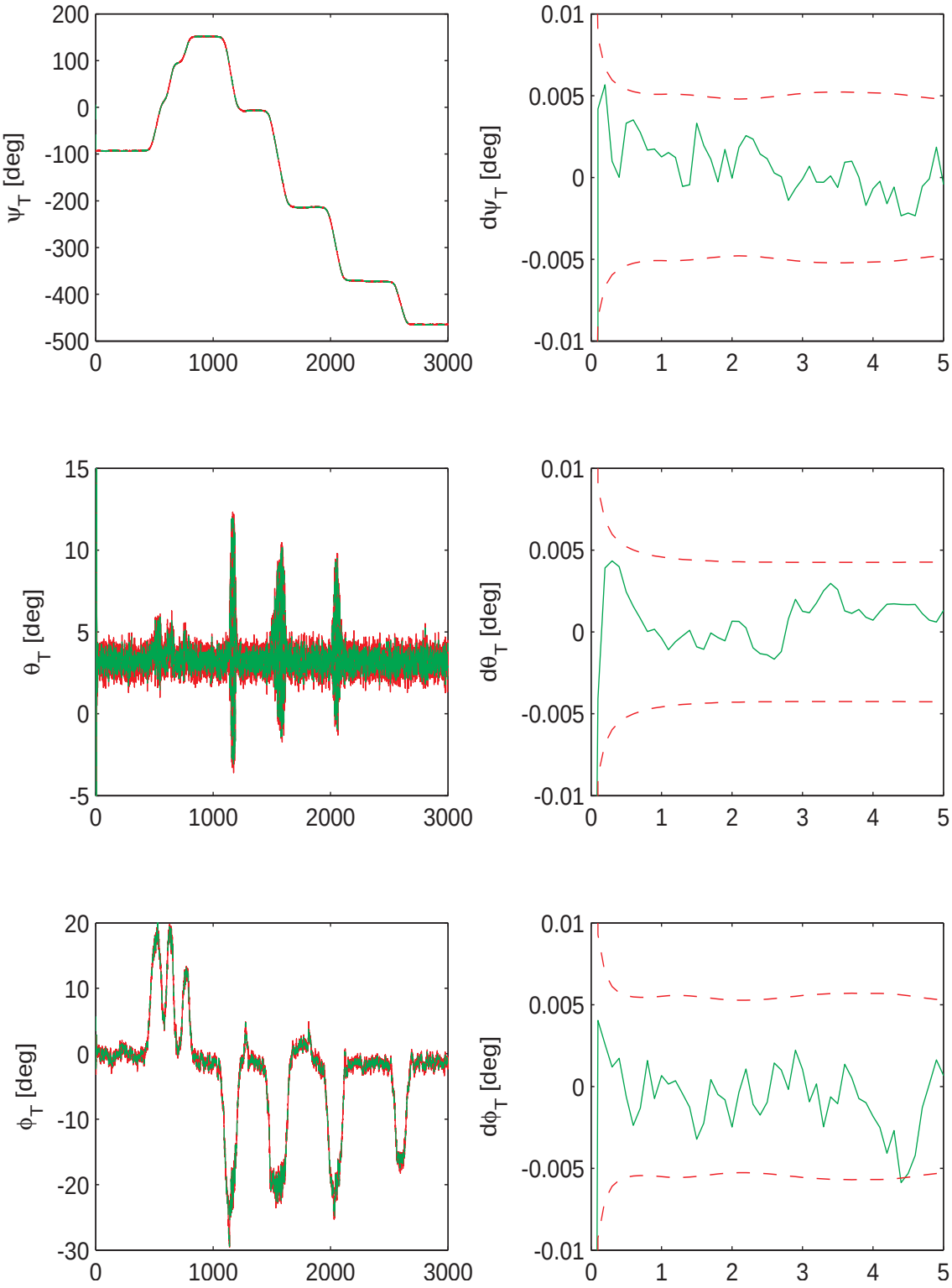

Figure 7.12. Measured and Estimated Euler Angles.

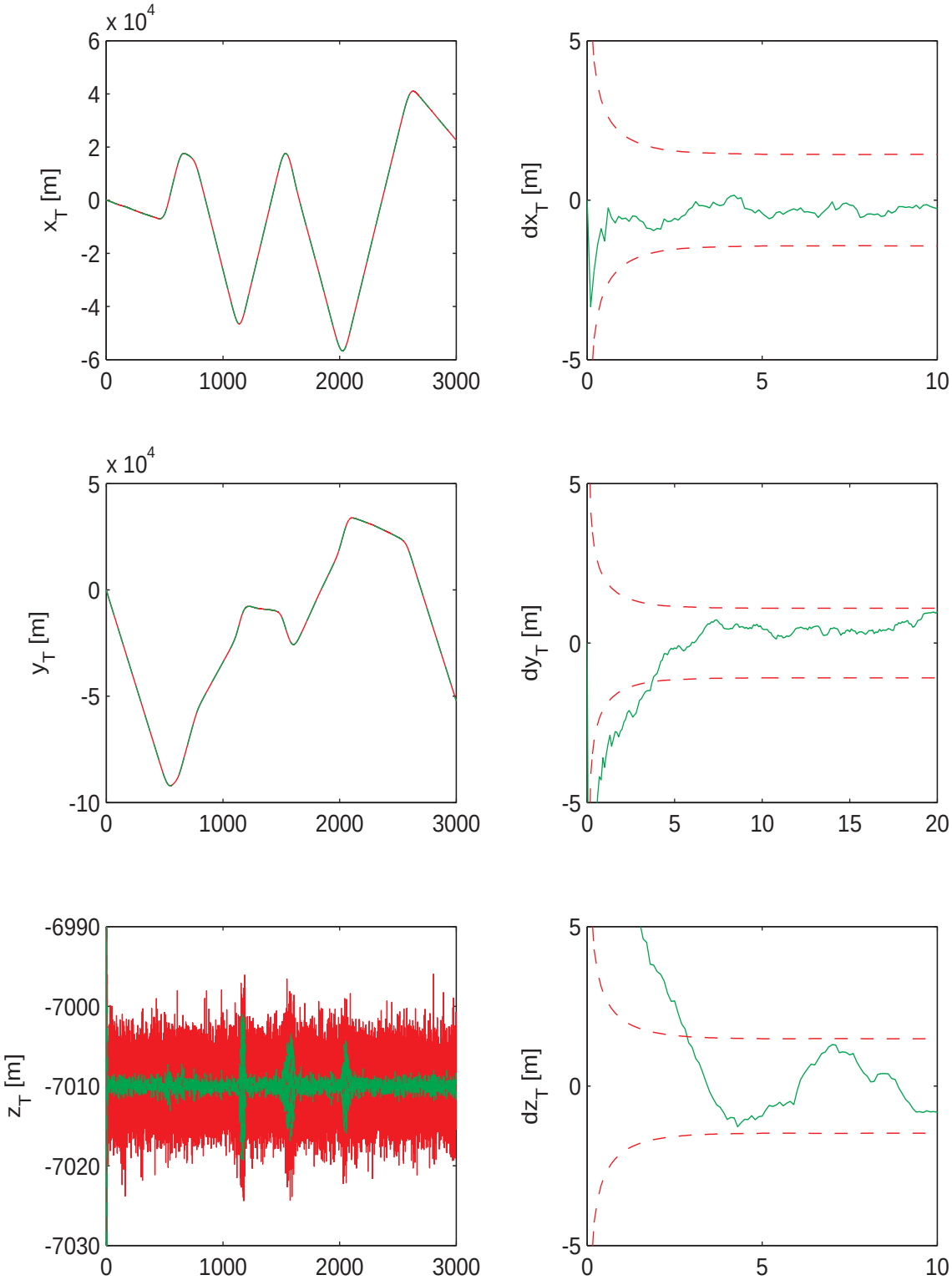

Figure 7.13. Measured and Estimated Position Components.

7.1.3 Case III: ECWM Prevailing Wind and Large Measurement Noise

Case III focuses on the sensitivity of the proposed estimation method against increased level of measurement noise, whose characteristics are given in Table 2.3. The estimated wind vector is expressed in terms of its magnitude and direction. The

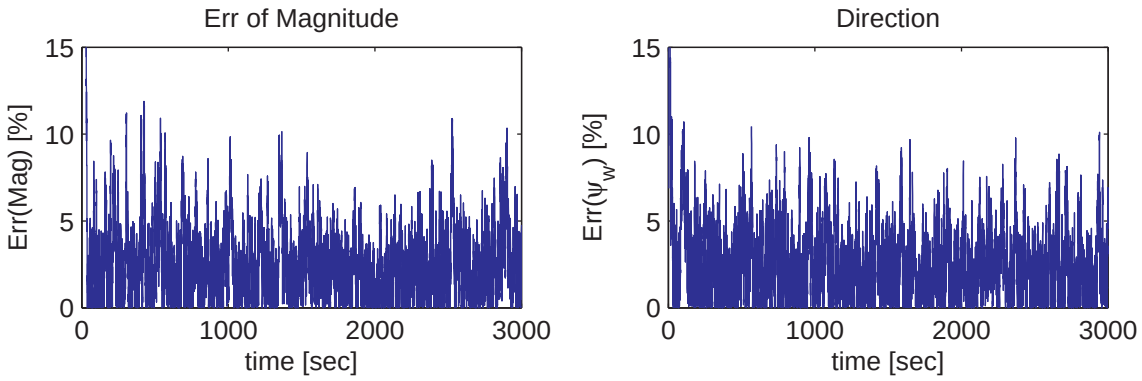

Figure 7.14. Percent Errors of Wind Estimate (Case III).

percentage errors of the estimated wind in terms of magnitude and direction are shown in Fig. 7.14. The magnitude error is usually less than 5% and the direction error in general remains less 5%. Even at the worst case when the tanker aircraft turns, the magnitude and direction errors do not exceed 12% and 10%, respectively.

The plots on the left hand side of Fig. 7.15 show the components of the reference wind and the estimated wind throughout the whole simulation. The figures clearly show that the estimation is successful in capturing very well the time variation of the wind. On the right hand side of Fig. 7.15, the estimation errors, in the component form, are shown in the first 200 seconds and compared with the 3σ bounds. The y-component error converges to the 3σ bound in 40 seconds while the x- & z-component errors converge almost immediately.

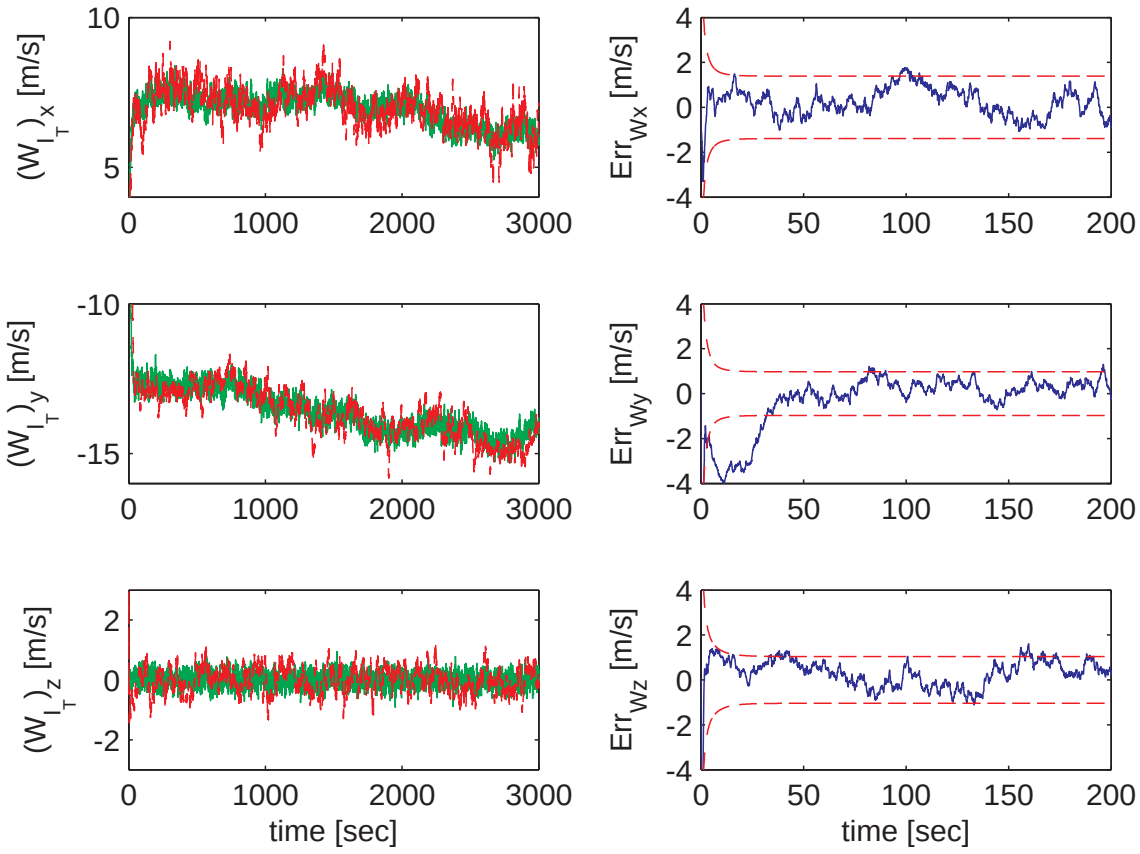

Figure 7.15. Comparison Between Reference and Estimated Wind (Case III).

Figures 7.16 to 7.19 show the comparison of the estimated aircraft states with the measured states in the case of very noisy measurement error. All the states are successfully estimated while the tanker aircraft goes through various straight-level and turning segments of the commanded trajectory while under the influence of the time varying prevailing wind generated from ECWM and turbulence. Further, the noise levels in all the estimated states are reduced as compared to the respective measured states with very high level of noise.

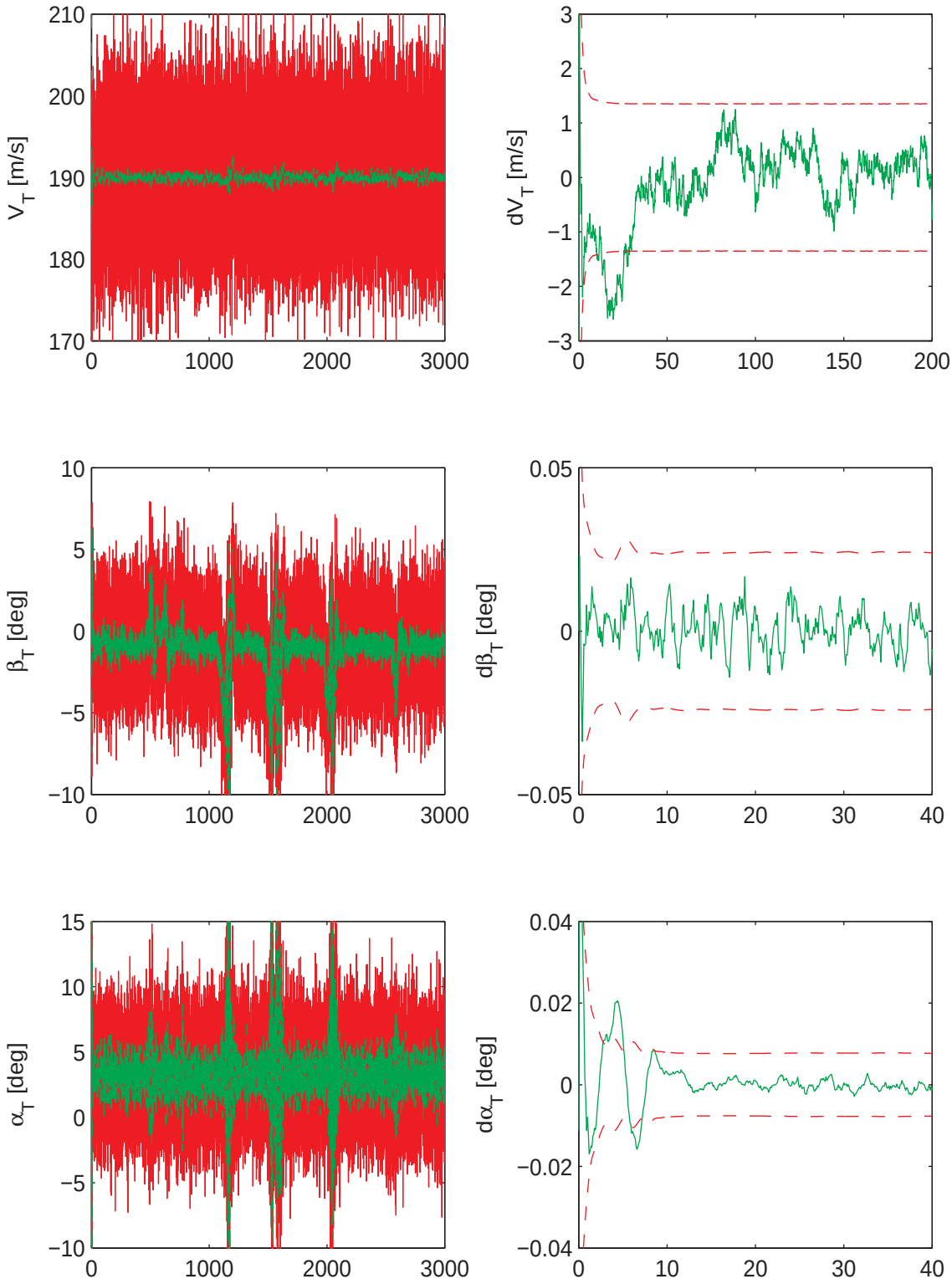

Figure 7.16. Measured and Estimated Airspeed, Sideslip Angle and Angle of Attack.

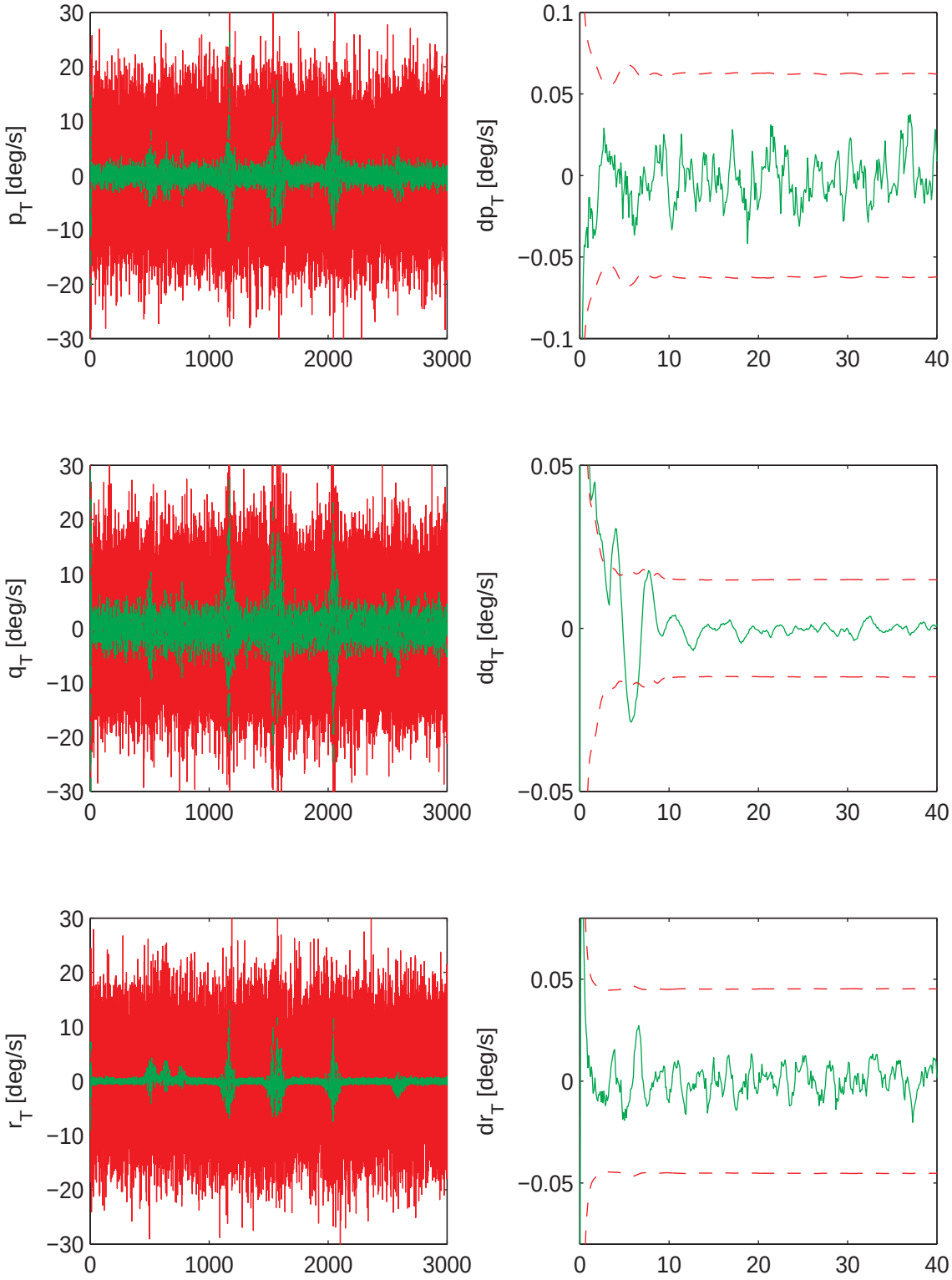

Figure 7.17. Measured and Estimated Angular Velocity Components.

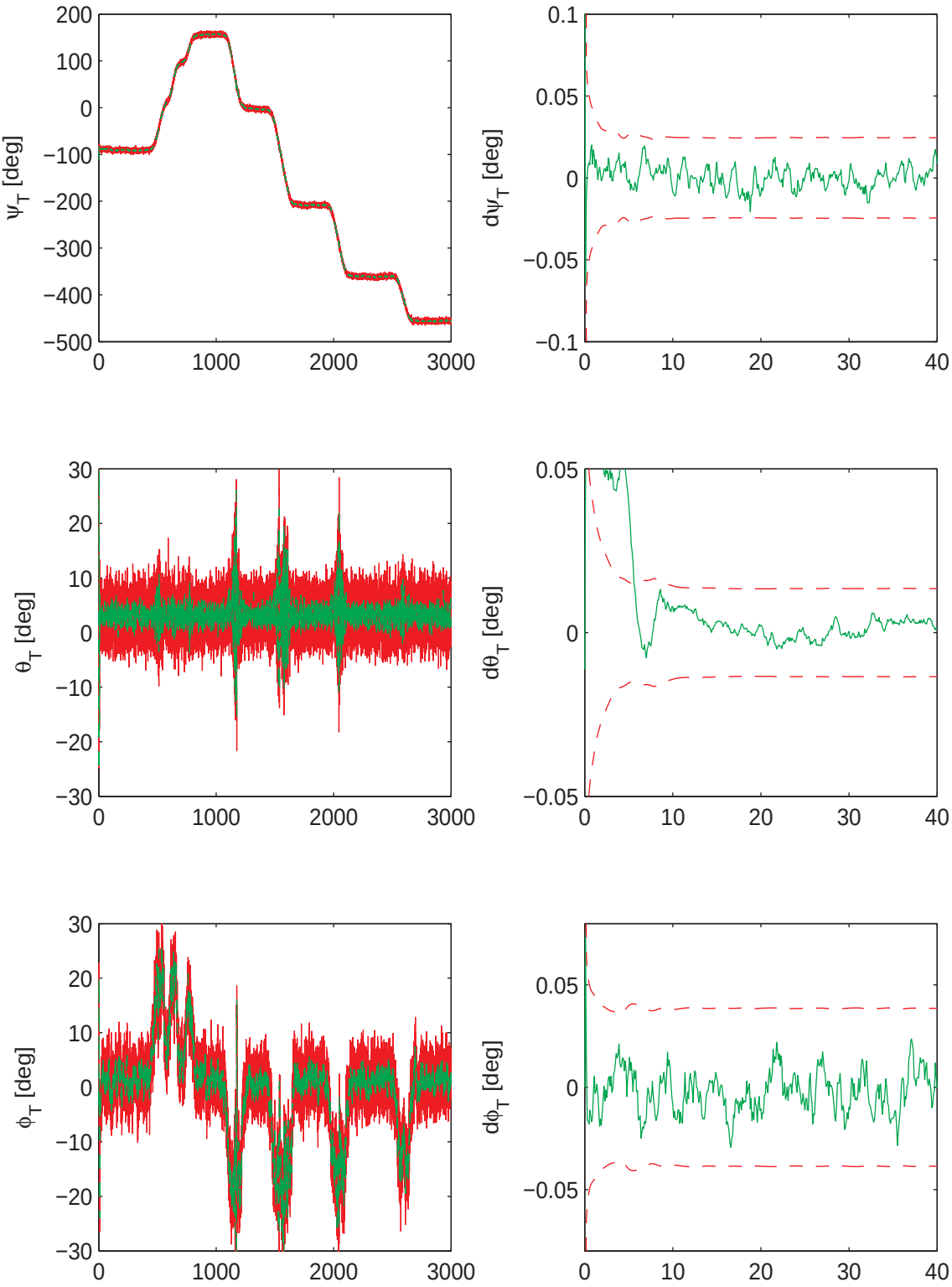

Figure 7.18. Measured and Estimated Euler Angles.

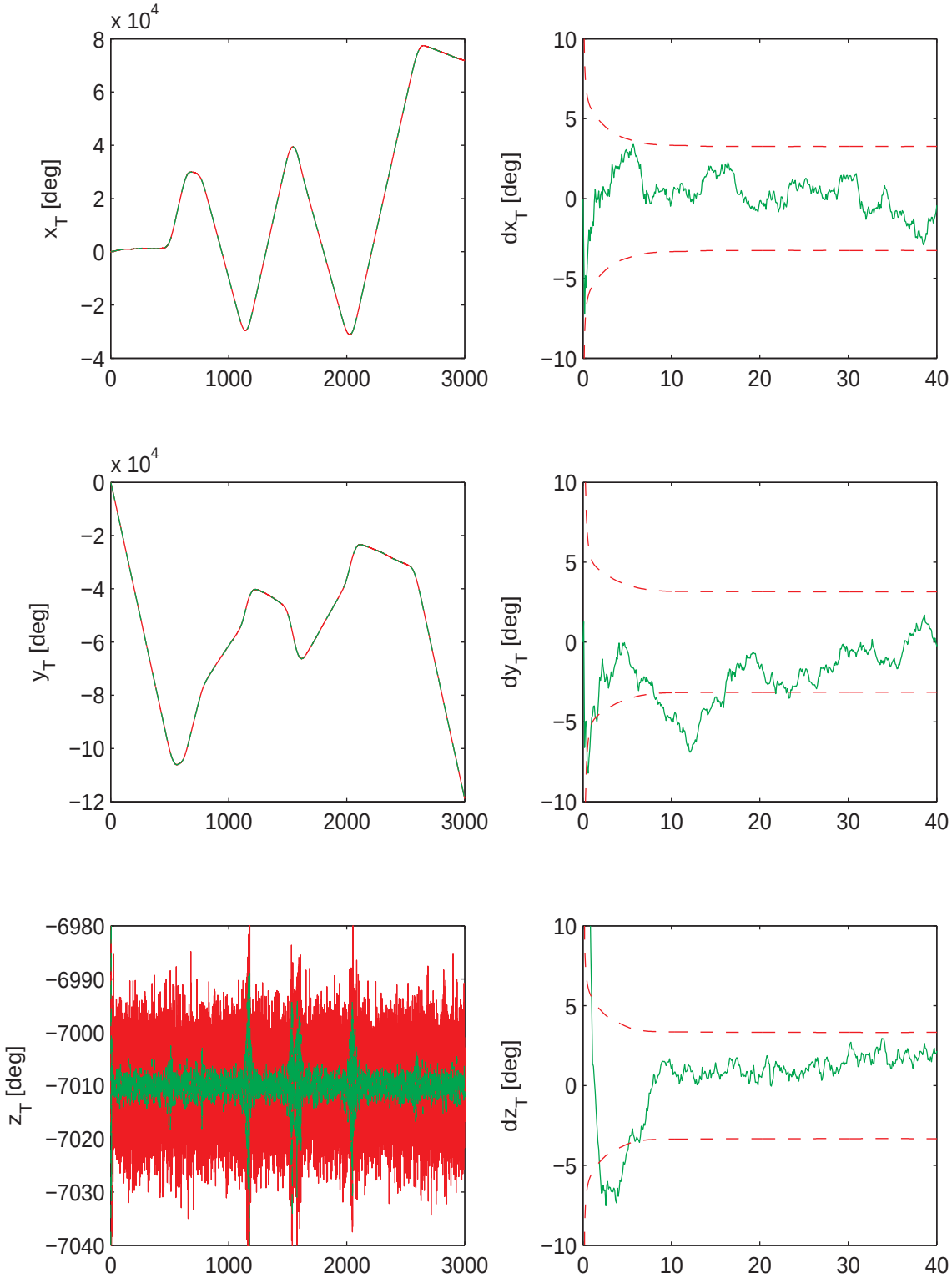

Figure 7.19. Measured and Estimated Position Components.

7.2 Tanker State and Wind Estimation Without Aerodynamic Model

This section investigates the performance of the estimation when aerodynamic force and moment models are not available in system update of the estimation. Instead, the estimation relies on measurements of translational acceleration and the difference of angular velocity measurements as an approximation for angular acceleration. For the controller of the tanker, the actual states are used in the feedback control.

7.2.1 Case III: ECWM Prevailing Wind and Large Measurement Noise

In this case, the prevailing wind is generated by the ECWM, presented in Section 2.5.1.2 and the turbulence is generated by the Dryden model described in Section 2.5.2. In this simulation case, measurement has a large level of noise, as described in Table 2.3.

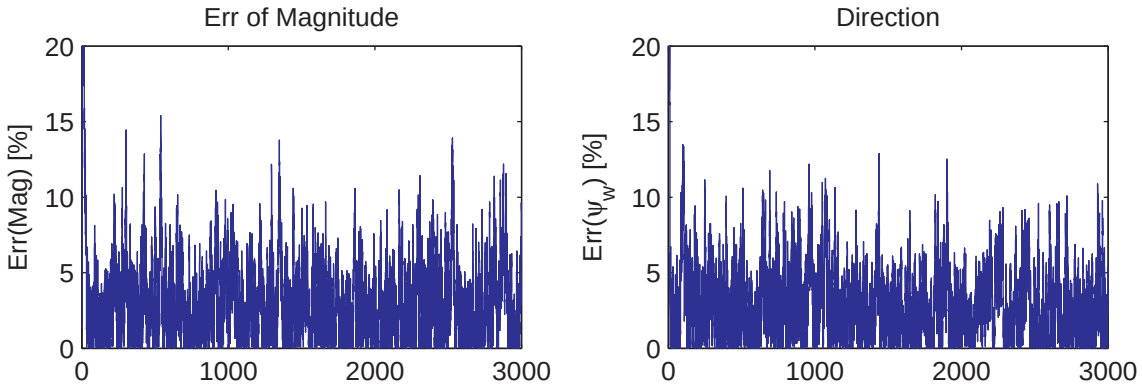

Figure 7.20. Percent Errors of Wind Estimate (Case III).

Figure 7.20 shows the percent estimation error in the wind vector in terms of its magnitude and direction. The magnitude error is usually less than 10% and the direction error in general remains less than 10%. The plots on the left hand

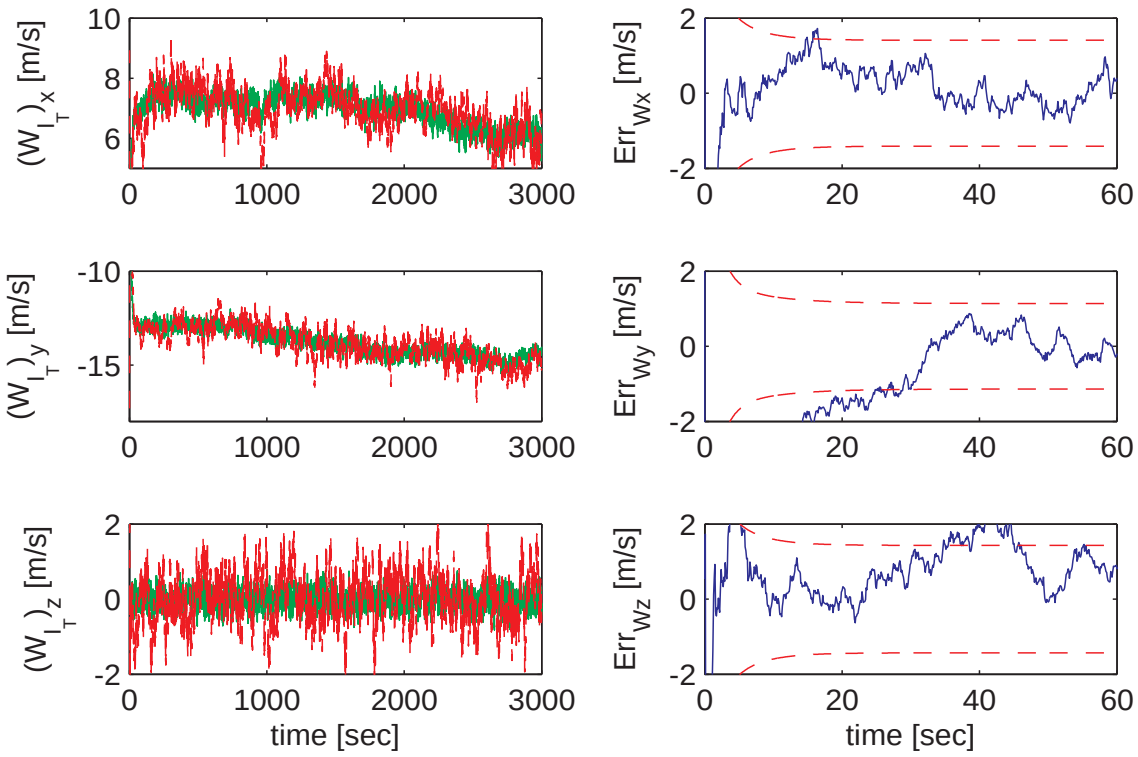

Figure 7.21. Comparison Between Reference and Estimated Wind (Case III).

side of Fig. 7.21 show the components of the reference wind and the estimated wind throughout the whole simulation. The figures show that the estimation is successful in capturing the time variation of the wind generated from ECWM. On the right hand side of Fig. 7.21, the estimation errors, in the component form, are shown in the first 60 seconds and compared with the 3σ bounds. The x- & y-component errors converge to the respective 3σ bounds in 20 seconds and 40 seconds while the z-component error converges almost immediately.

Figures 7.22 to 7.25 show the comparison of the estimated aircraft states with the measured states. All the states are successfully estimated while the tanker aircraft goes through various straight-level and turning segments of the commanded trajectory in the presence of time varying prevailing wind and turbulence.

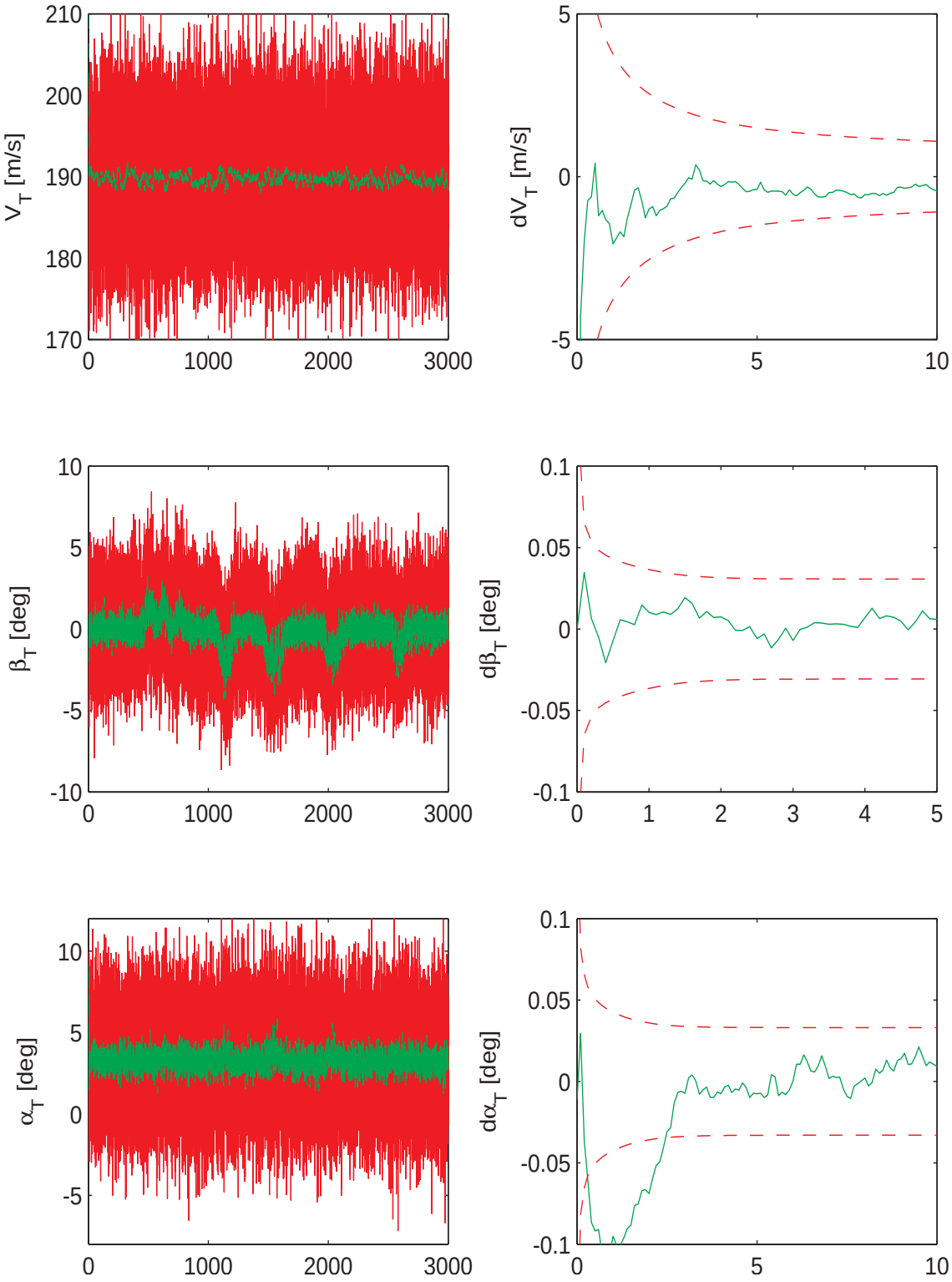

Figure 7.22. Measured and Estimated Airspeed, Sideslip Angle and Angle of Attack.

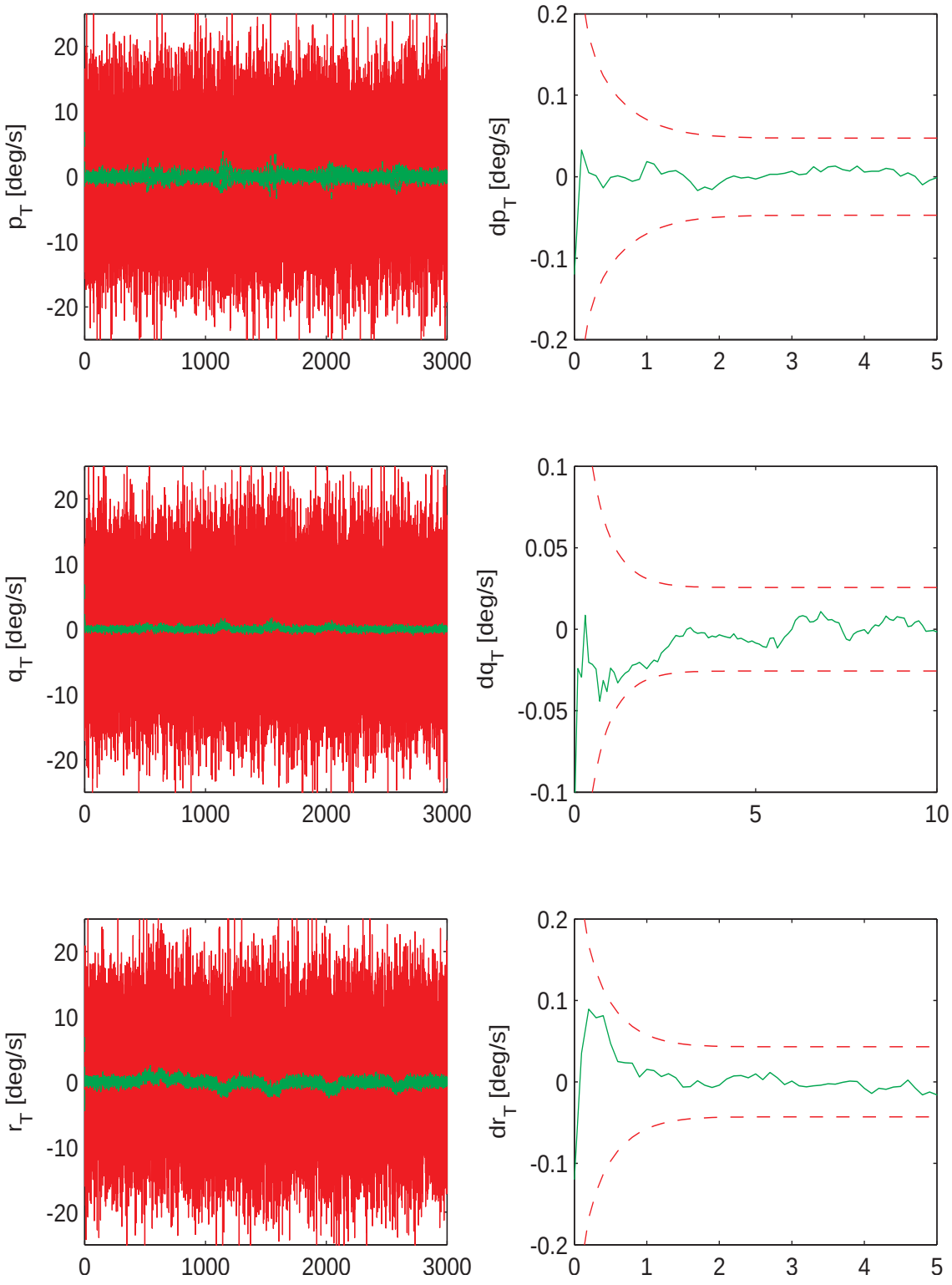

Figure 7.23. Measured and Estimated Angular Velocity Components.

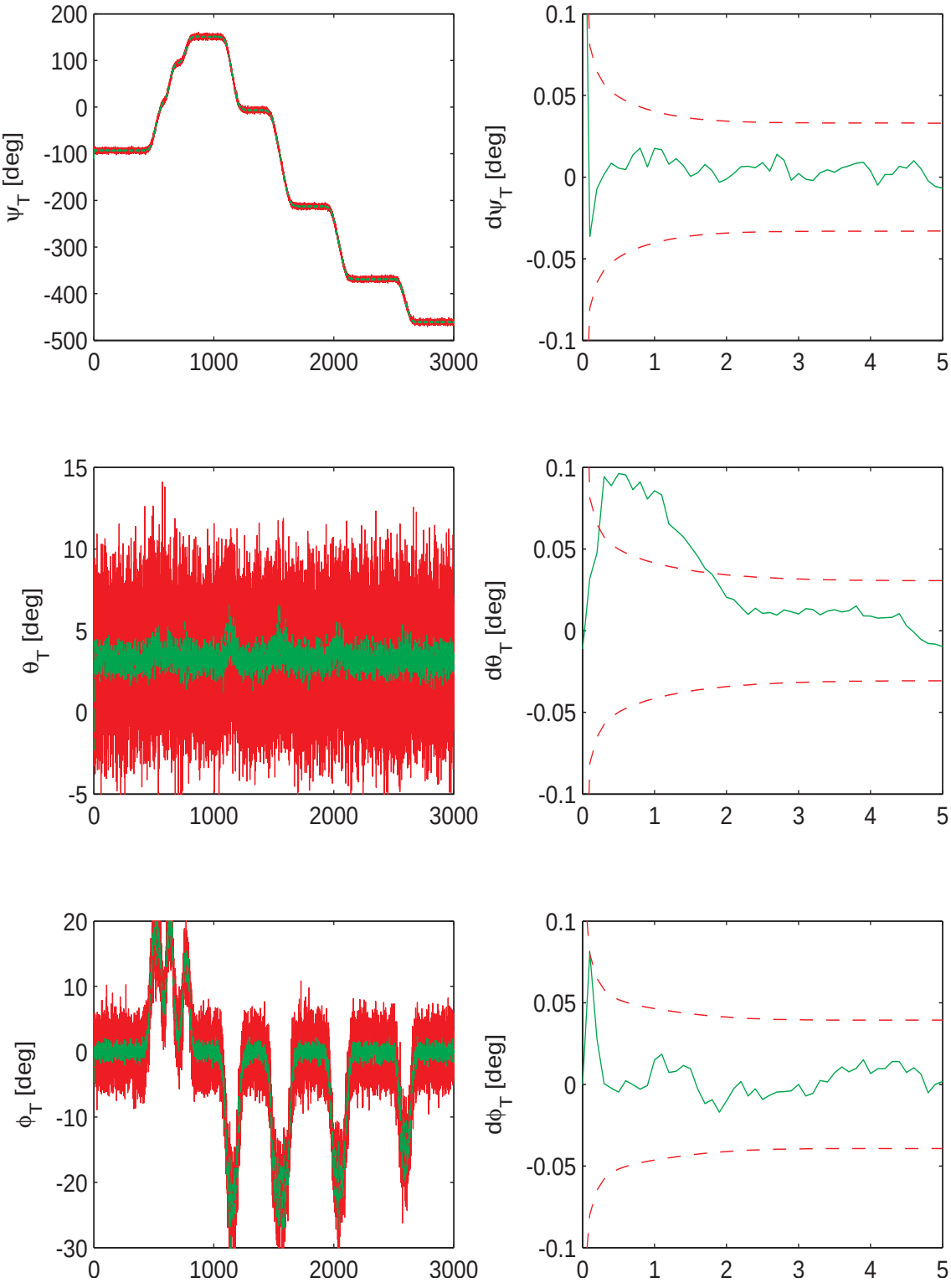

Figure 7.24. Measured and Estimated Euler Angles.

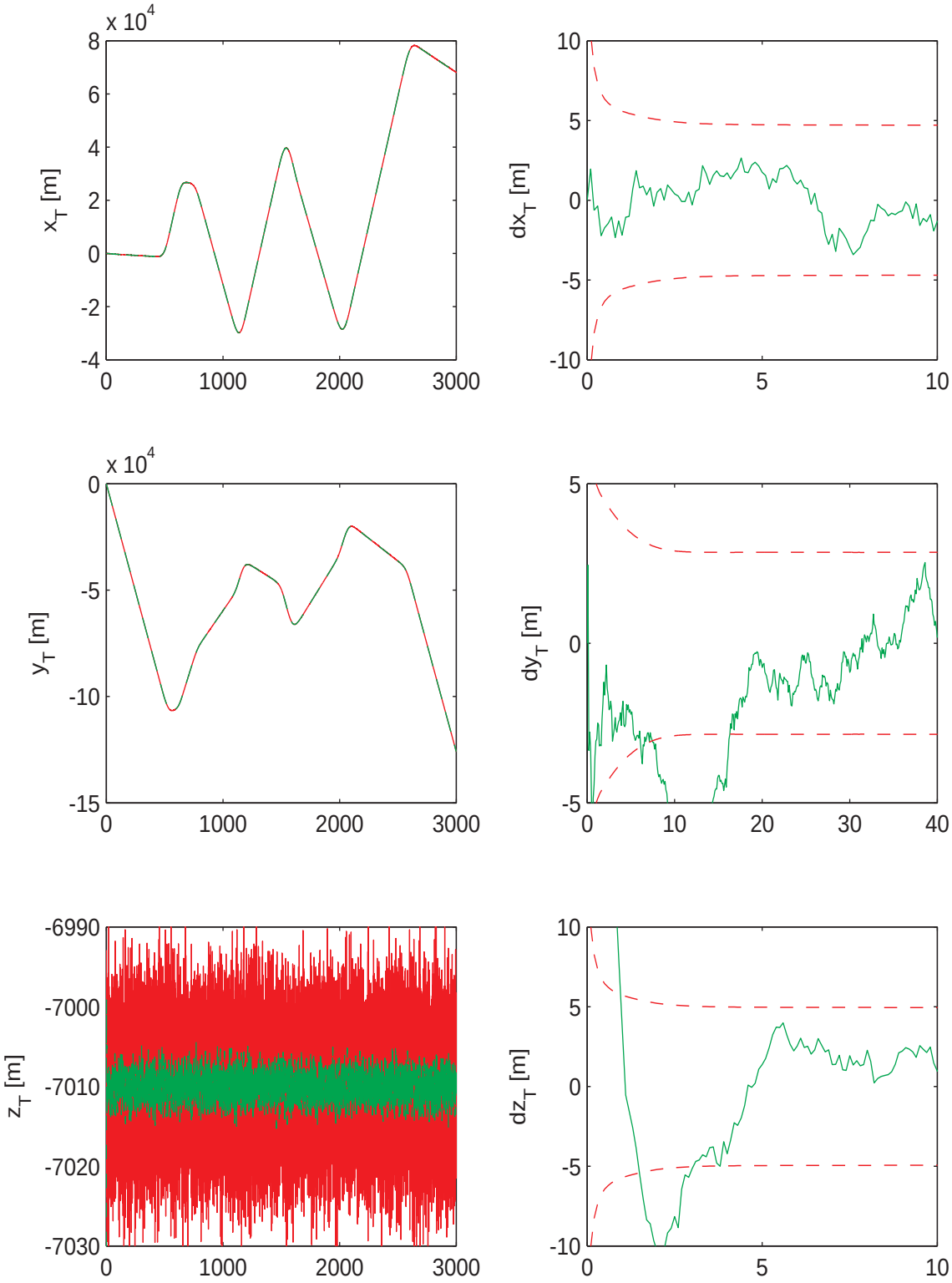

Figure 7.25. Measured and Estimated Position Components.

7.2.2 Case IV: Prevailing Wind from Flight Data and Large Measurement Noise

In this case, the tanker aircraft is exposed to the prevailing wind profile extracted from the test flight data with Dryden turbulence. The measurement has a large level of noise with the characteristics listed in Table 2.3.

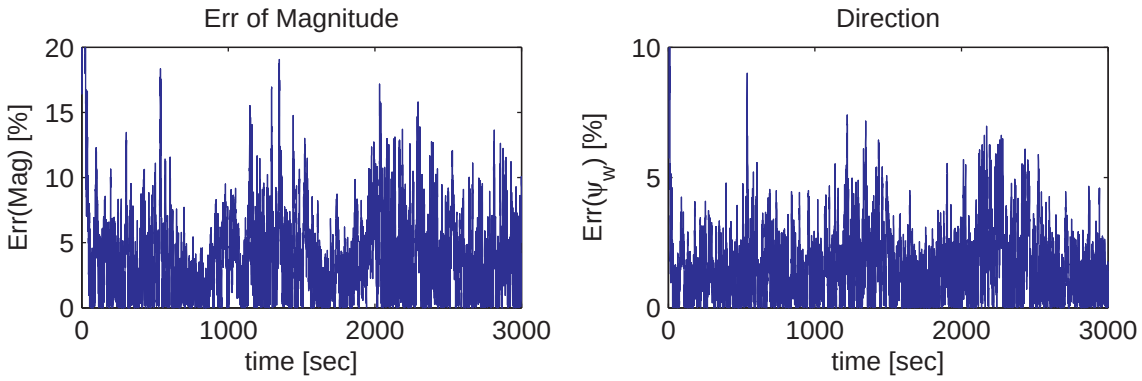

Figure 7.26. Percent Errors of Wind Estimate (Case IV).

The estimated wind vector has the percentage errors as shown in Fig. 7.26 in terms of its magnitude and direction. The magnitude error is usually less than 10% and the direction error in general remains less 5%. The plots on the left hand side of Fig. 7.27 show the components of the reference wind and the estimated wind throughout the whole simulation. The figures show that the estimation is successful in capturing the time variation of the wind obtained from the test flight data. On the right hand side of Fig. 7.27, the estimation errors, in the component form, are shown in the first 200 seconds and compared with the 3σ bounds. The x- & y-component errors converge to the respective 3σ bounds in 40 seconds while the z-component error converges almost immediately.

Figures 7.28 to 7.31 show a comparison of the estimated aircraft states with the measured states. All the states are successfully estimated while the tanker aircraft

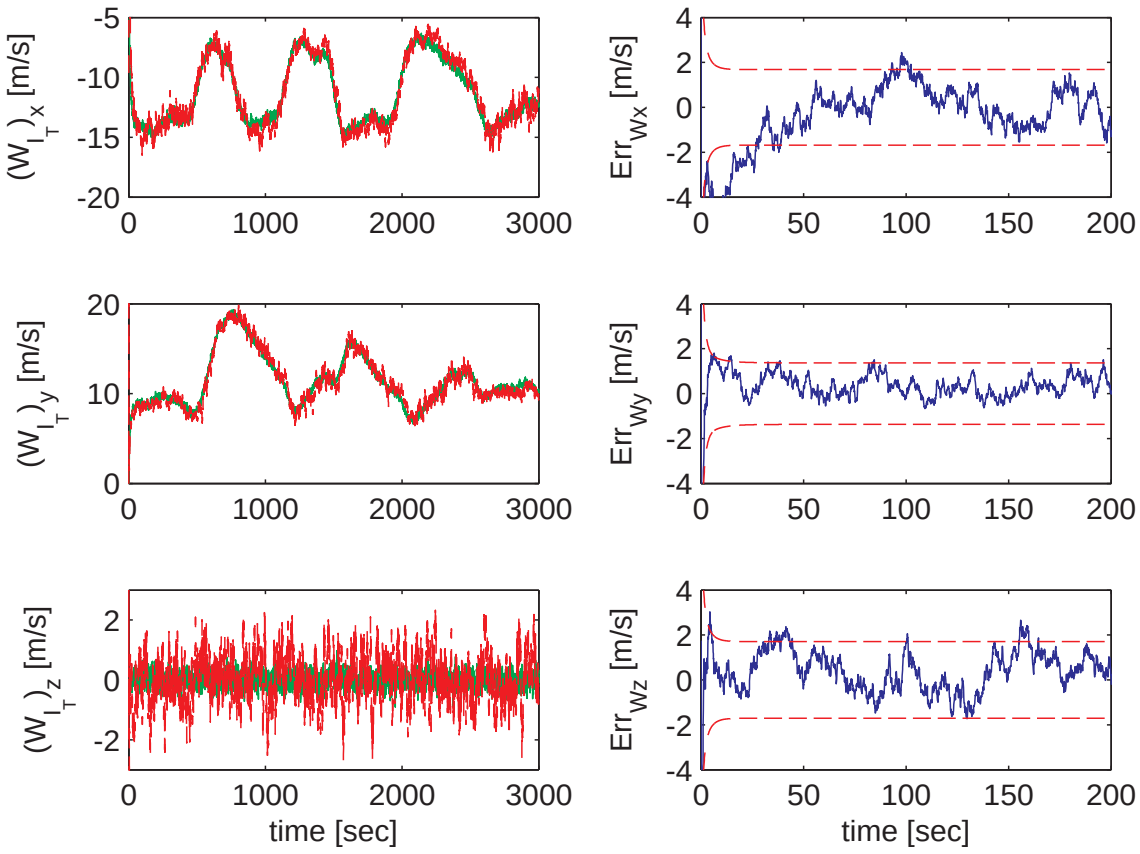

Figure 7.27. Comparison Between Reference and Estimated Wind (Case IV).

goes through various straight-level and turning segments of the commanded trajectory while experiencing time varying prevailing wind and turbulence. Further, the noise levels in all the estimated states are reduced as compared to the respective measured states. The right sides of Figs. 7.28 to 7.31 show the estimation error and the transient of each estimate as compared to their respective 3σ bounds.

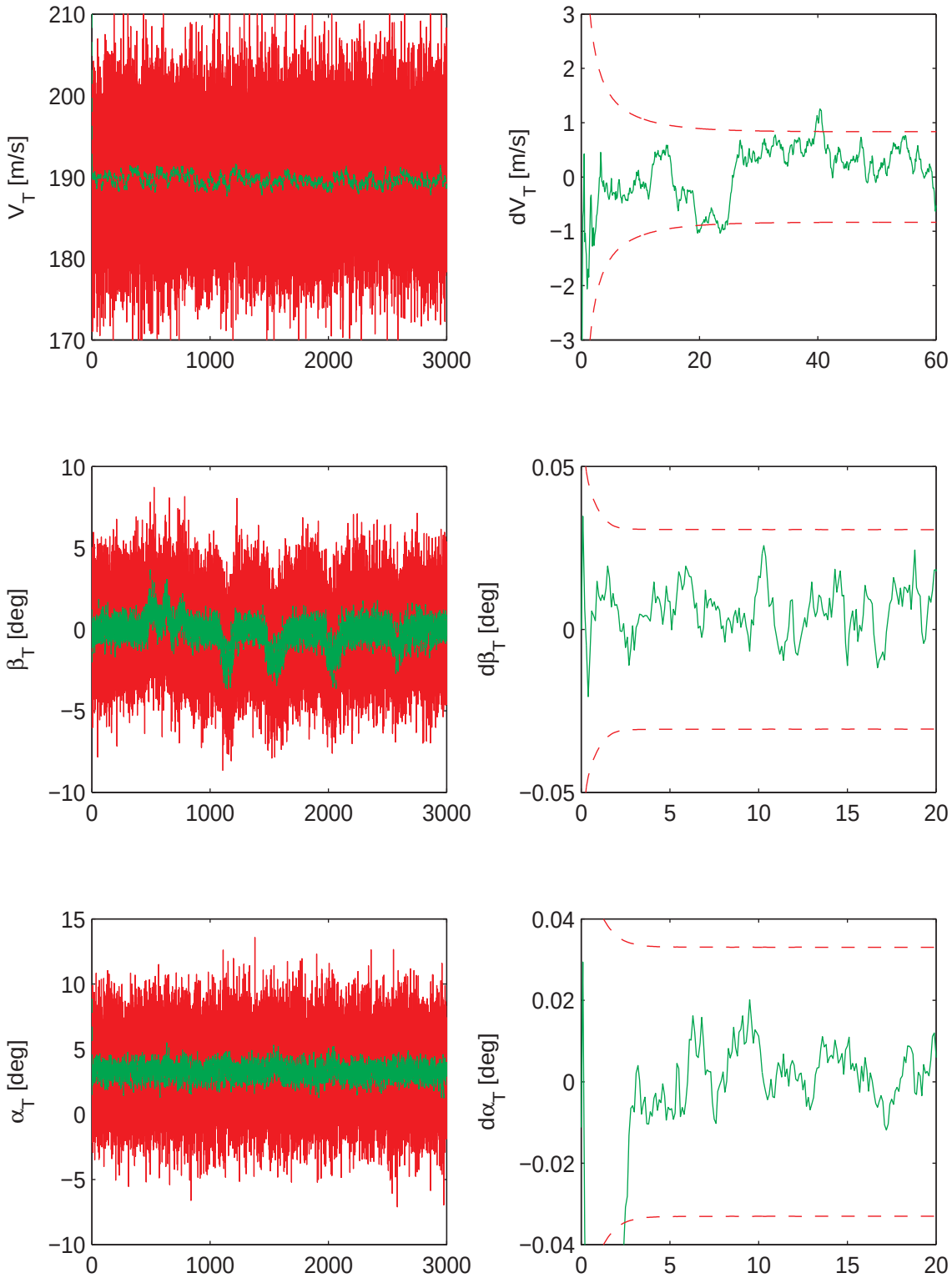

Figure 7.28. Measured and Estimated Airspeed, Sideslip Angle and Angle of Attack.

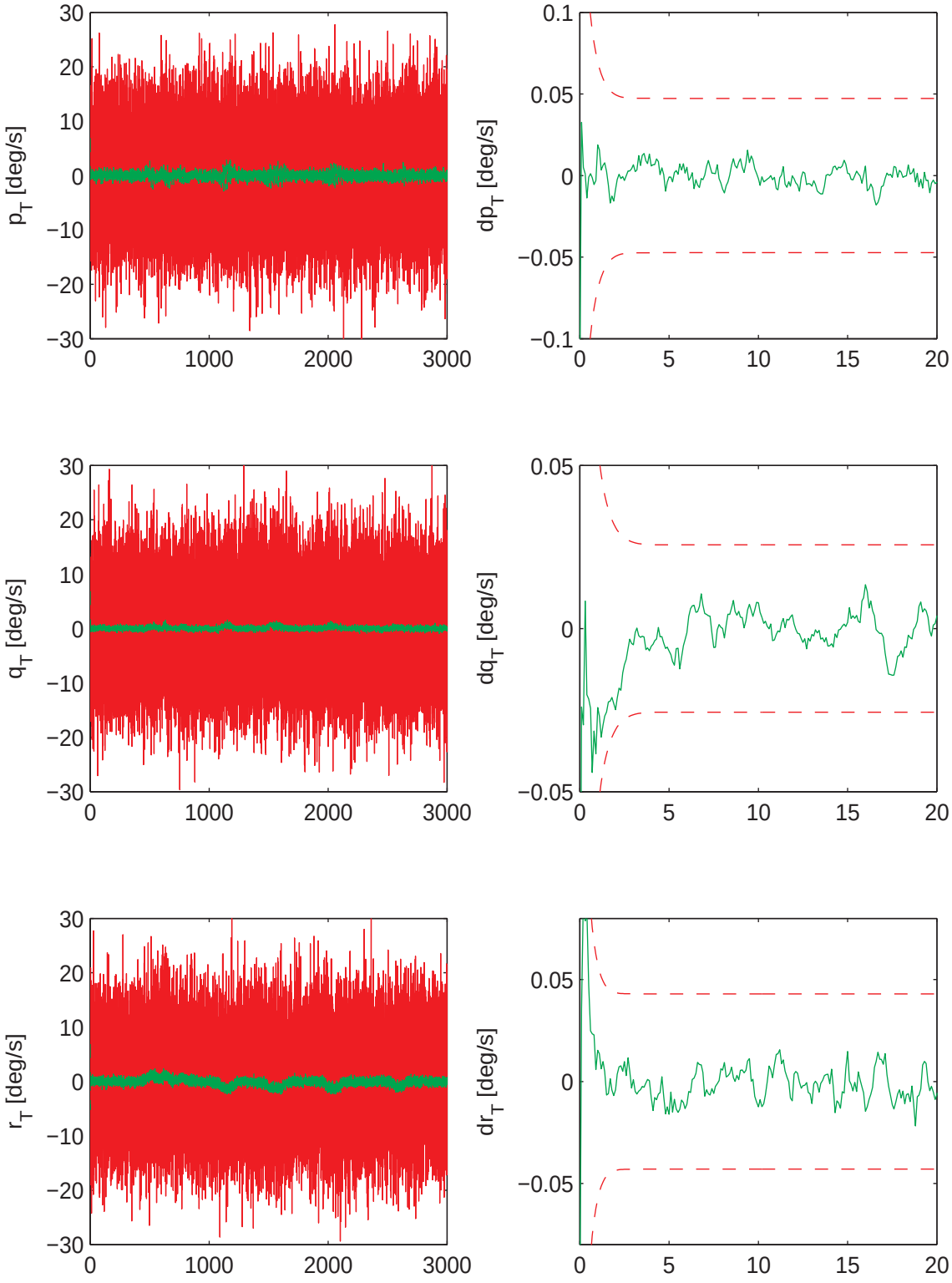

Figure 7.29. Measured and Estimated Angular Velocity Components.

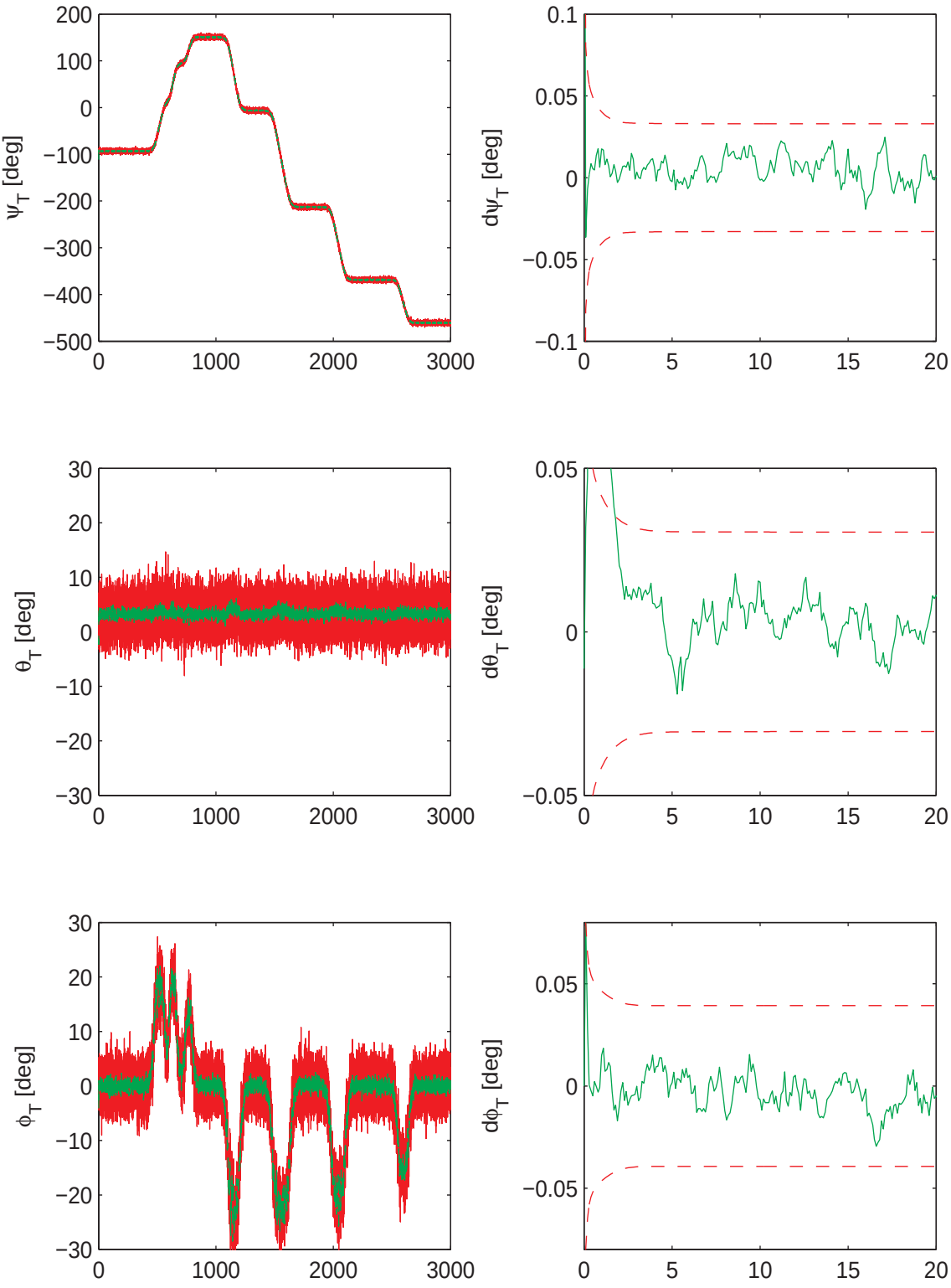

Figure 7.30. Measured and Estimated Euler Angles.

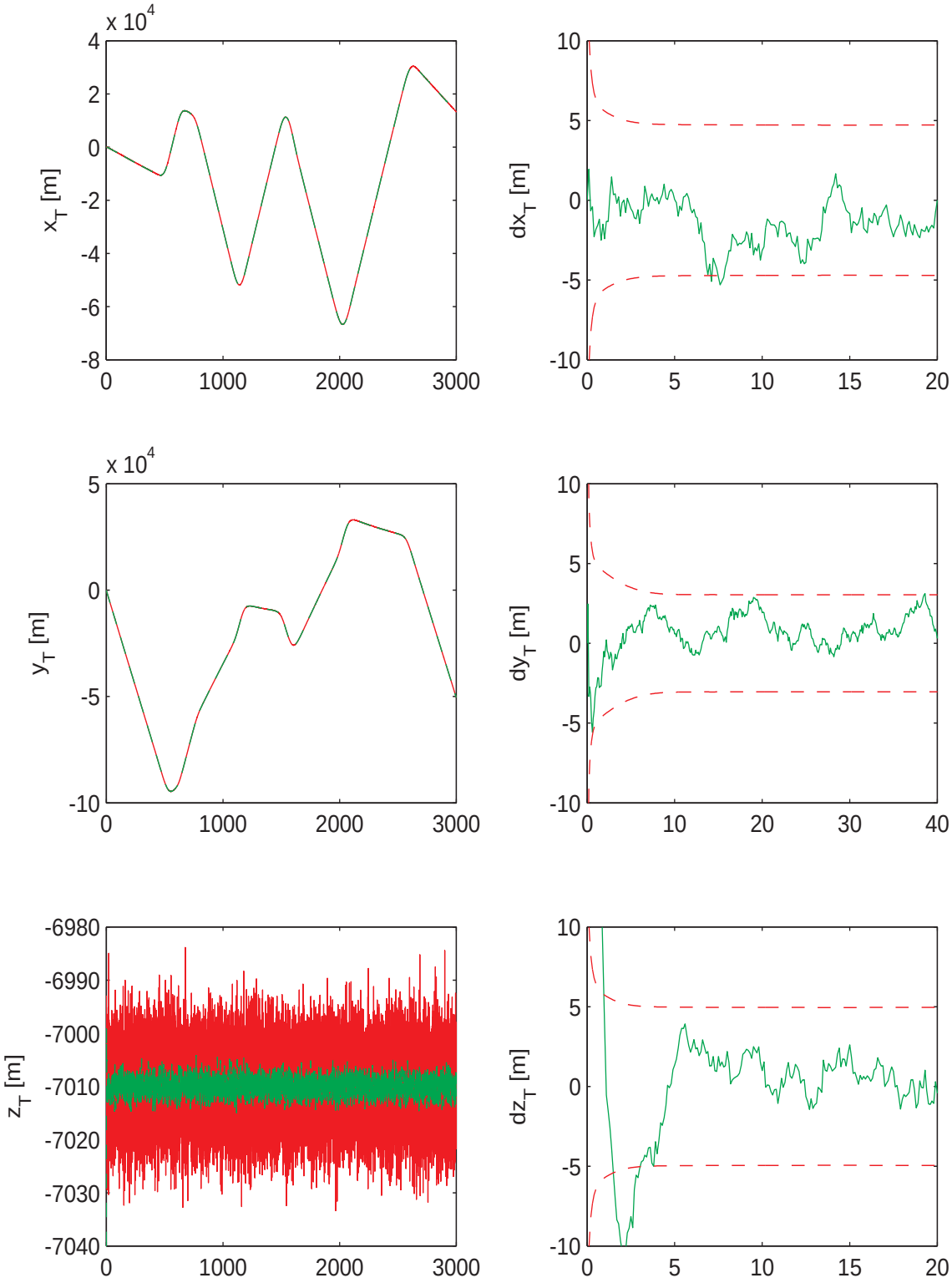

Figure 7.31. Measured and Estimated Position Components.

7.3 Tanker State and Wind Estimation Under Colored Measurement

This section presents the simulation results when the sensors have colored measurement noise with a correlation time constant of 20 seconds. Two cases are studied. In the first case studied, the measurement noise has small variances as described in Table 2.2 and the second case has large variance, listed in Table 2.3. In both cases, the prevailing wind is generated by the ECWM. For the controller of the tanker, the actual states are used in the feedback control.

7.3.1 Case II: ECWM Prevailing Wind and Small Measurement Noise

In this case, the variances of the colored measurement noises during the simulation are characterized in Table 2.2.

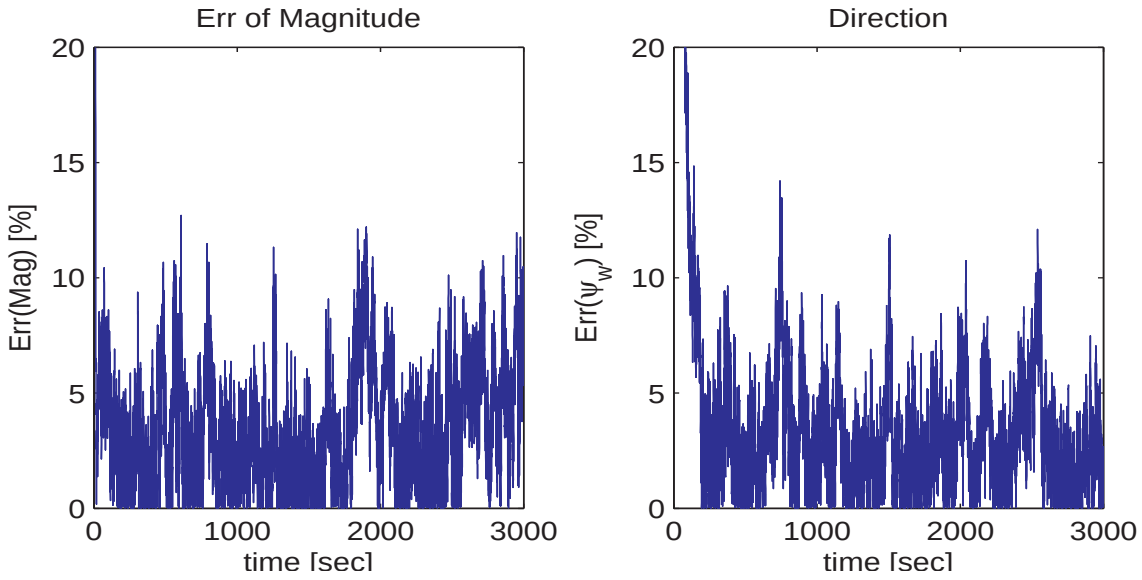

Figure 7.32. Percent Errors of Wind Estimate (Case II).

The percentage errors of the estimated wind in terms of magnitude and direction are shown in Fig. 7.32. The magnitude error is usually less than 10% and the direction

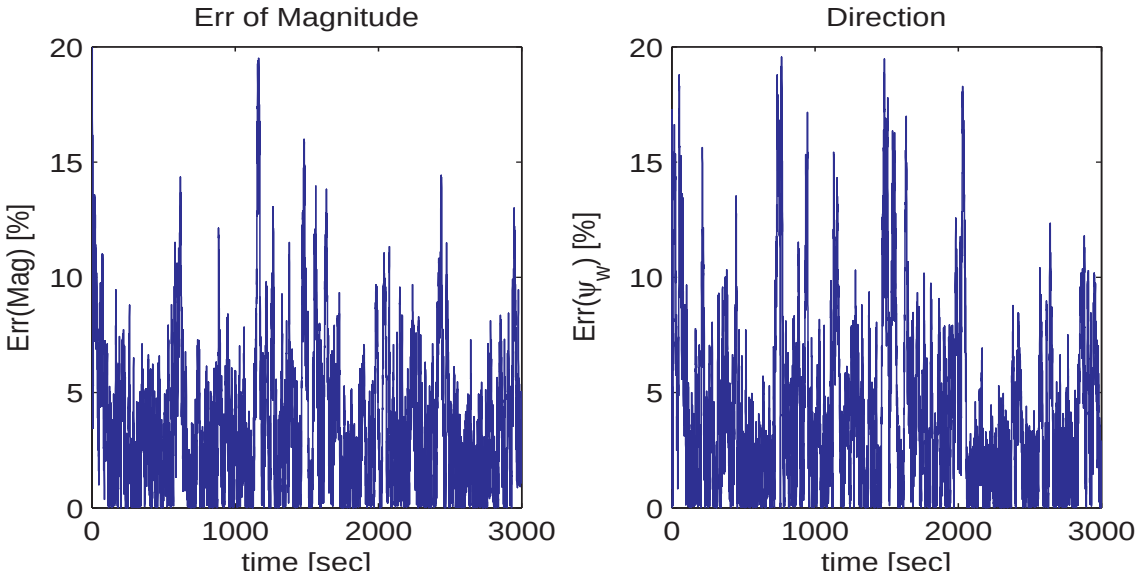

Figure 7.33. Percent Errors of CMW (Case II).

error in general remains less than 10%. Comparison of Figs. 7.32 and 7.33 shows that the error of the estimated wind is only slightly smaller than that of the CMW. This is because the CMW is calculated from the measured states by Eq. (4.6) and Eq. (4.7) and the state measurements have only small errors. When the measurement noises are large, as will be in the next case, the performance of the CMW calculation will worsen, and will not be comparable.

The plots on the left hand side of Fig. 7.34 show the components of the reference wind and the estimated wind throughout the whole simulation. The figures show that the estimation is successful in capturing the time variation of the wind. On the right hand side of Fig. 7.34, the estimation errors, in the component form, are shown in the first 400 seconds and compared with the 3σ bounds. The x- & y-component errors converge to the respective 3σ bounds in 100 seconds while the z-component error converges to the 3σ bound in 80 seconds.

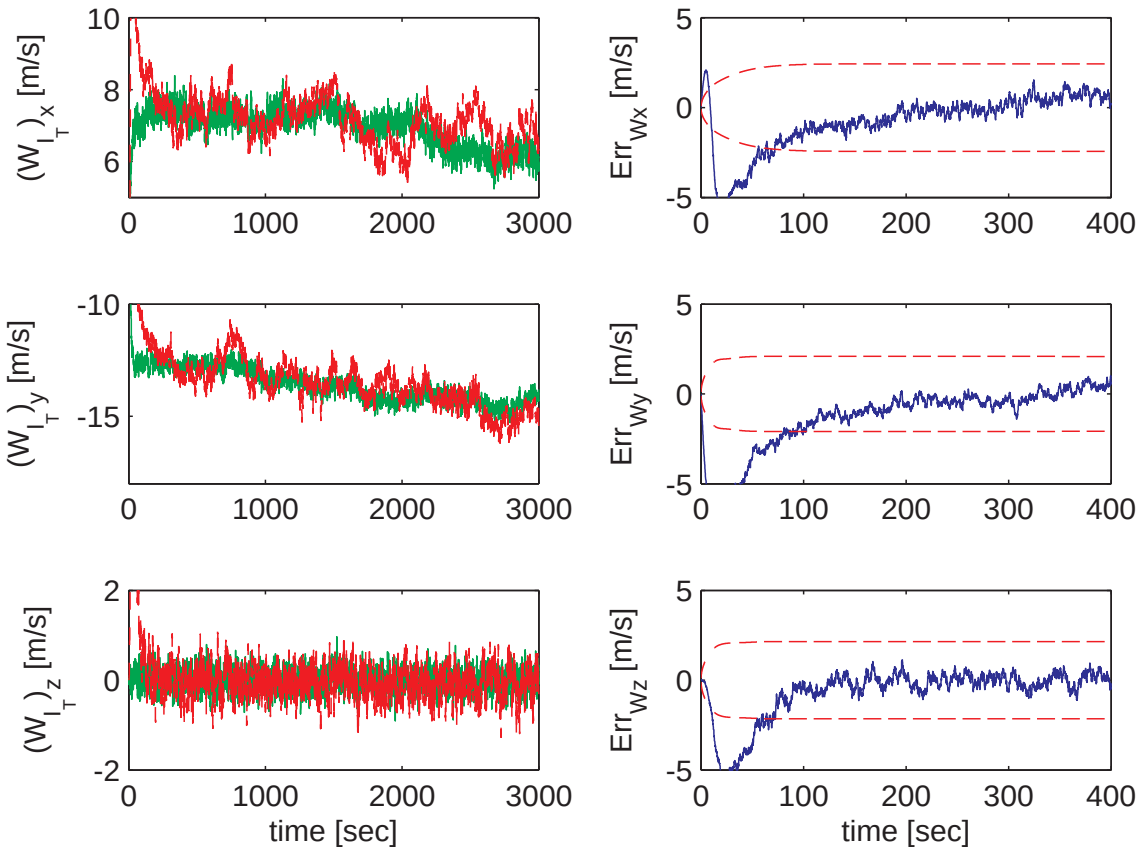

Figure 7.34. Comparison Between Reference and Estimated Wind (Case II).

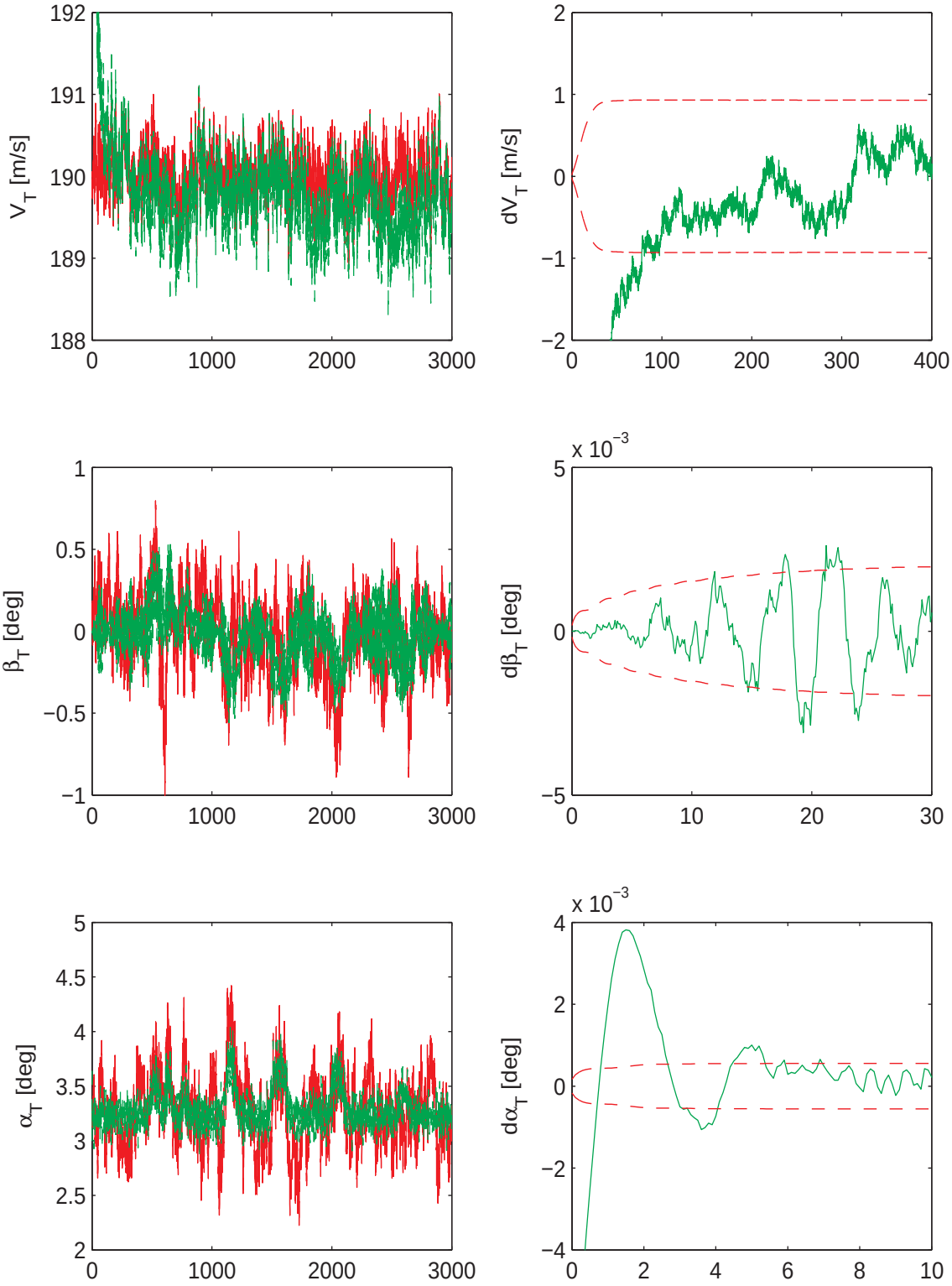

Figure 7.35. Measured and Estimated Airspeed, Sideslip Angle and Angle of Attack.

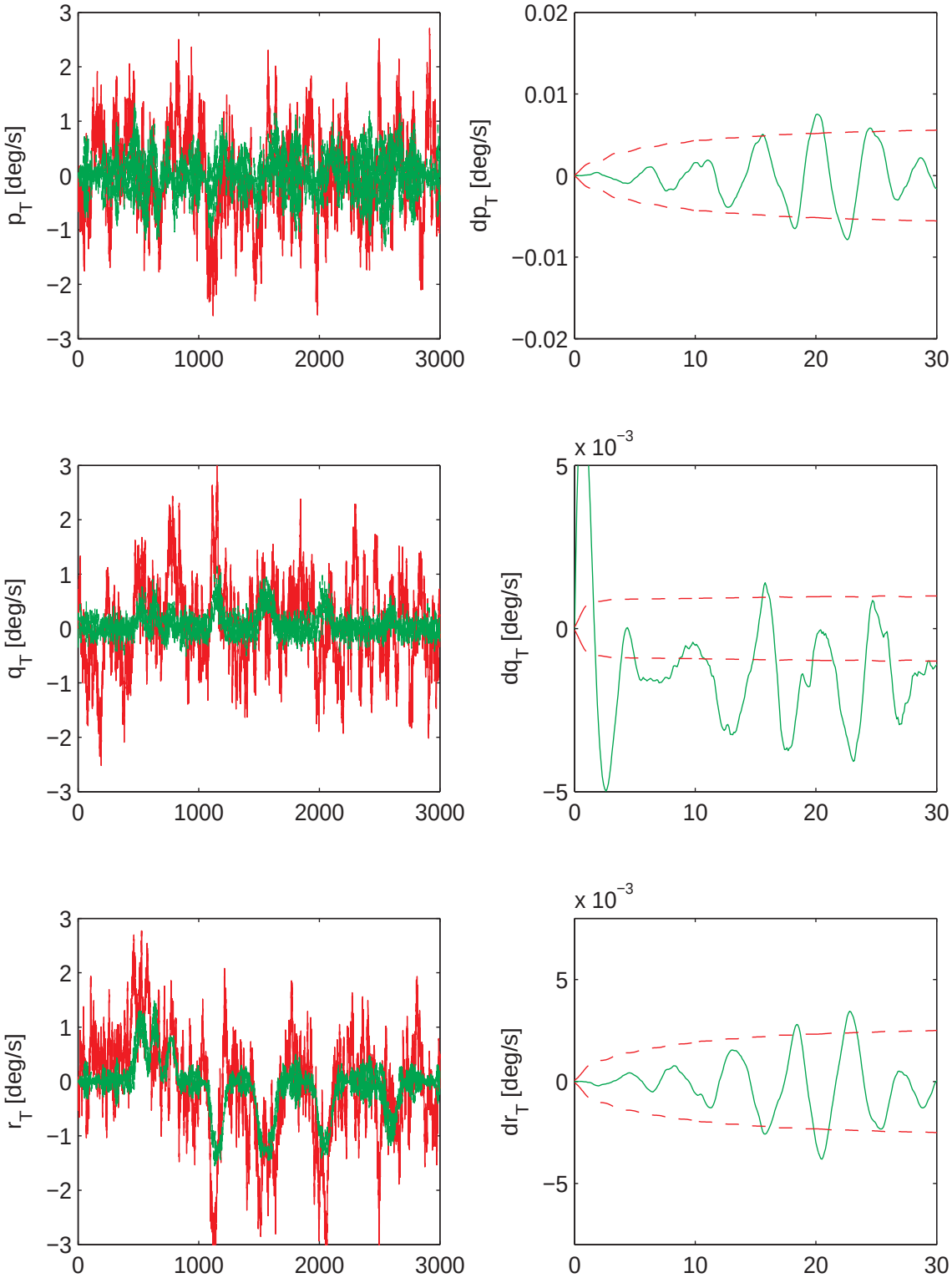

Figure 7.36. Measured and Estimated Angular Velocity Components.

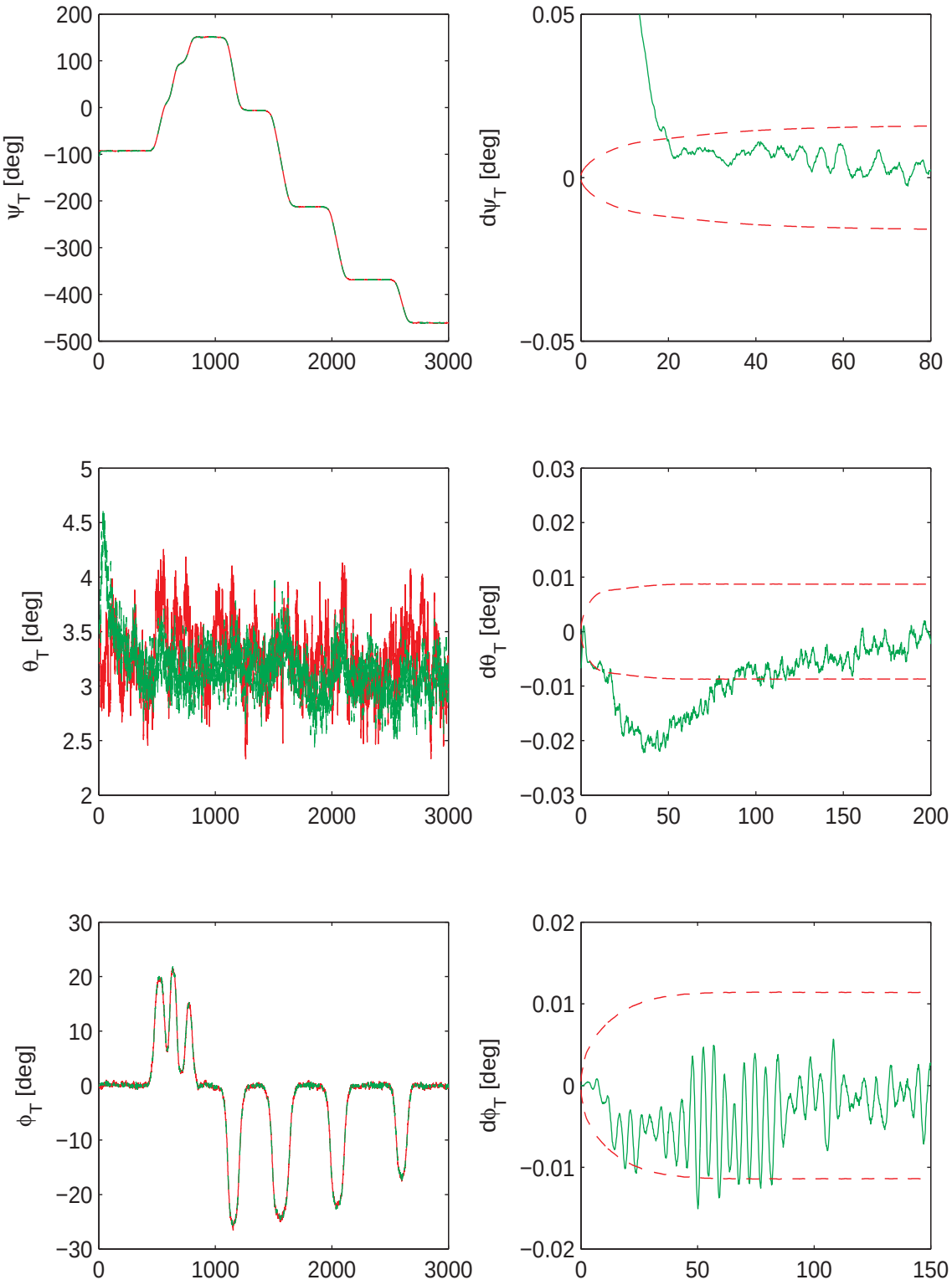

Figure 7.37. Measured and Estimated Euler Angles.

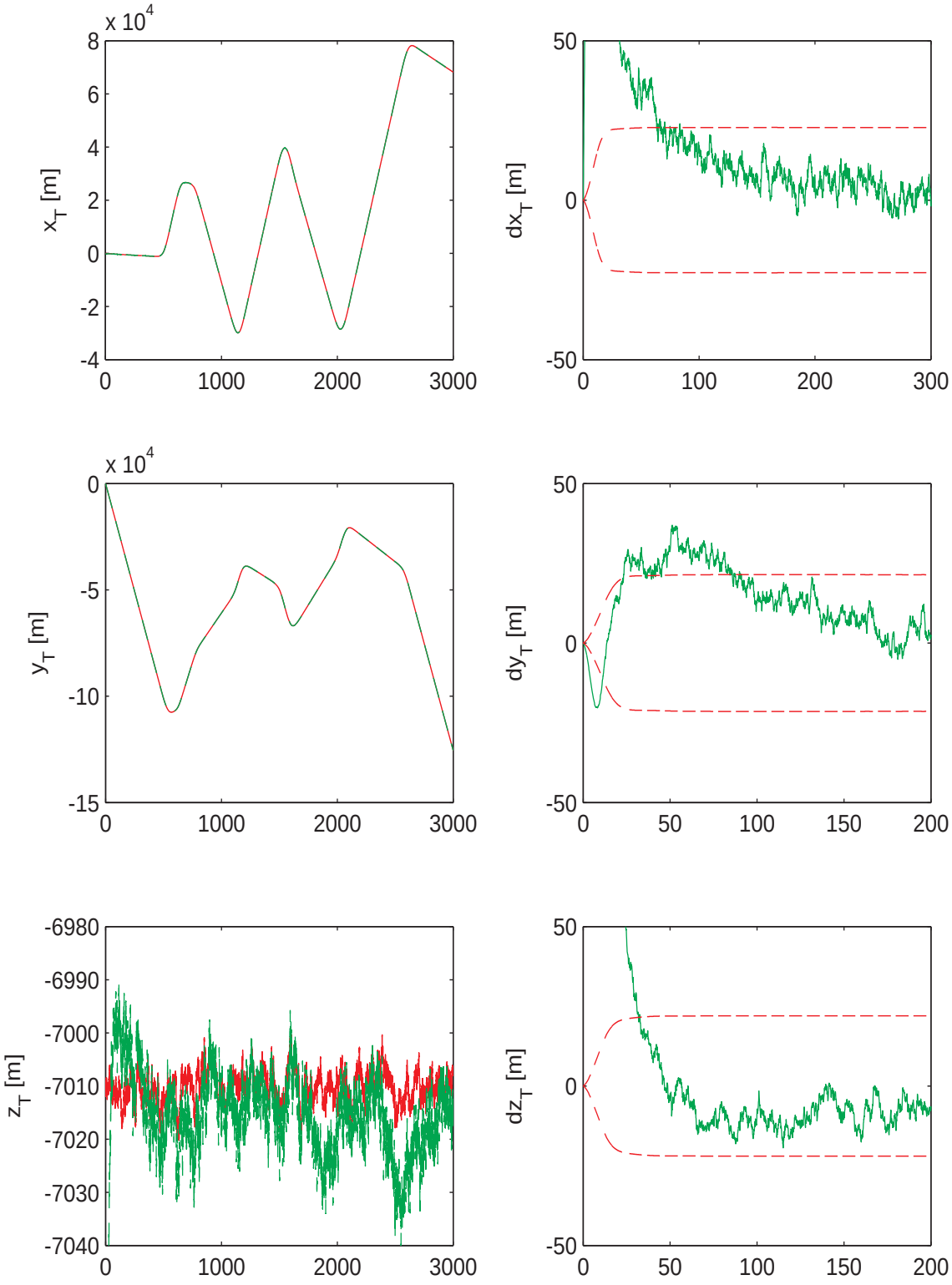

Figure 7.38. Measured and Estimated Position Components.

Figures 7.35 to 7.38 show the comparison of the estimated aircraft states with the measured states. All the states are successfully estimated while the tanker aircraft goes through various straight-level and turning segments of the commanded trajectory while subject to time varying prevailing wind and turbulence. Further, the noise levels in $(\beta_T, \alpha_T, p_T, q_T, r_T, \theta_T)$ are reduced as compared to the respective measured states. For instance, the measurement of the roll angular velocity has a standard deviation of 0.8 degree while estimate of that has a standard deviation of 0.4 degree. The right side of the figures show the estimation error and the transient of each estimate.

7.3.2 Case III: ECWM Prevailing Wind and Large Measurement Noise

The variance of the colored measurement noise during the whole time is based on Table 2.3.

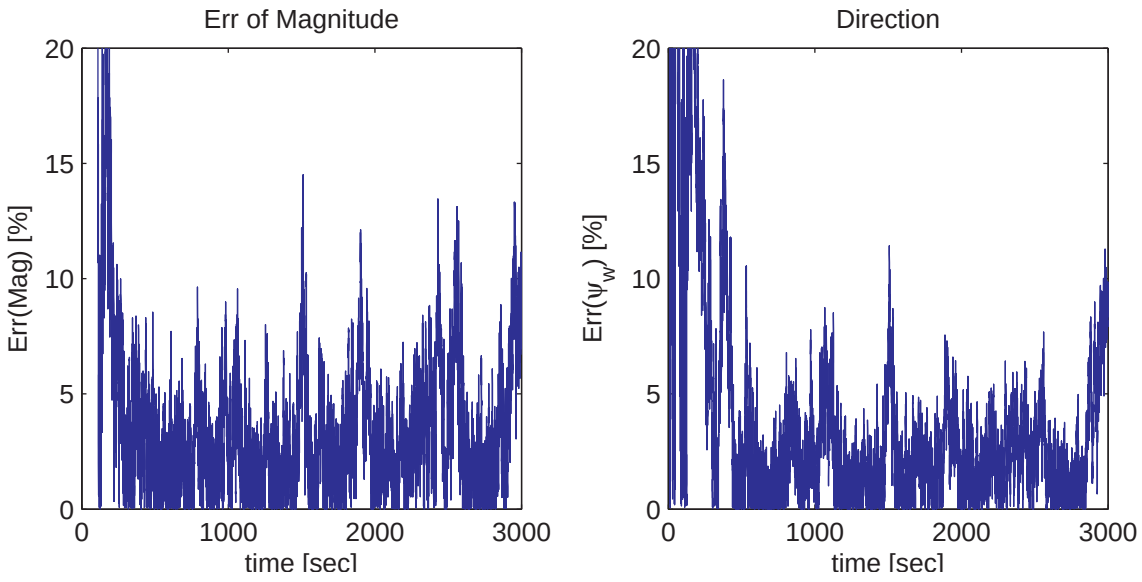

Figure 7.39. Percent Errors of Wind Estimate (Case III).

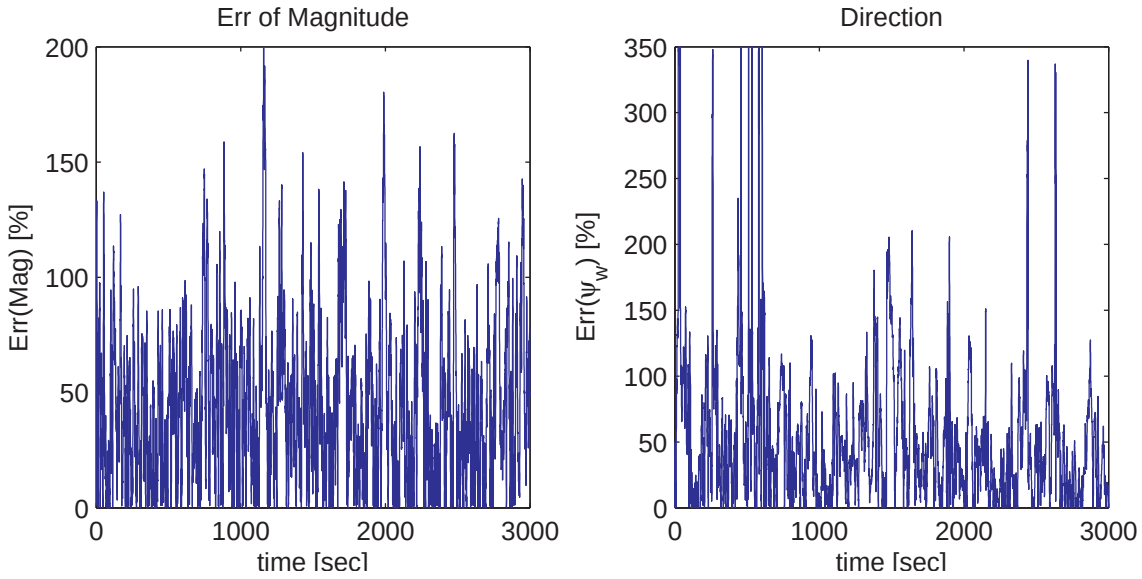

Figure 7.40. Percent Errors of CMW (Case III).

The percentage errors of the estimated wind in terms of magnitude and direction are shown in Fig. 7.39. The magnitude error is usually less than 10% and the direction error in general remains less 10%. Comparison of Figs. 7.39 and 7.40 shows that the error of the estimated wind is significantly smaller than that of the CMW, which is calculated from the available measurements by Eqs. (4.6) and (4.7).

Fig. 7.41 shows that the estimation is successful in capturing the time variation of the wind. On the right hand side of Fig. 7.41, the estimation errors, in the component form, are shown in the first 1000 seconds and compared with the 3σ bounds. The x- & y-component errors converge to the respective 3σ bounds in 200 and 120 seconds respectively while the z-component error converges almost immediately.

Figures 7.42 to 7.45 show the comparison of the estimated aircraft states with the measured states. All the states are successfully estimated while the tanker aircraft goes through various straight-level and turning segments of the commanded trajectory in the presence of time varying prevailing wind and turbulence. Further, the noise

levels in all the estimated states except for the components of position are reduced as compared to the respective measured states. The worse estimation in the position vector appears when correlation time constant of the colored noise is colored. For instance, the measurement of the roll angular velocity has a standard deviation of 7.5 degree while estimate of that has a standard deviation of 0.4 degree after the roll angular velocity estimation has converged. The right side of the figures show the estimation error and the transient of each estimate with 3σ bounds.

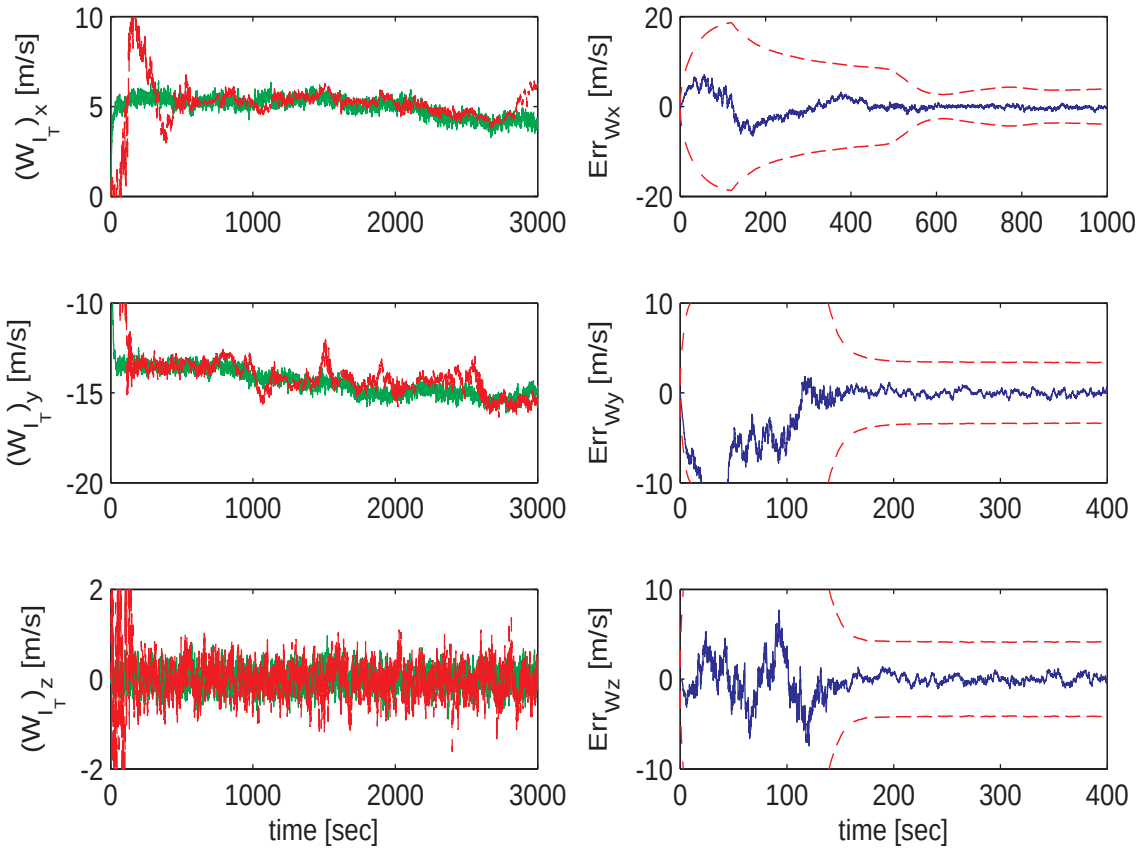

Figure 7.41. Comparison Between Reference and Estimated Wind (Case III).

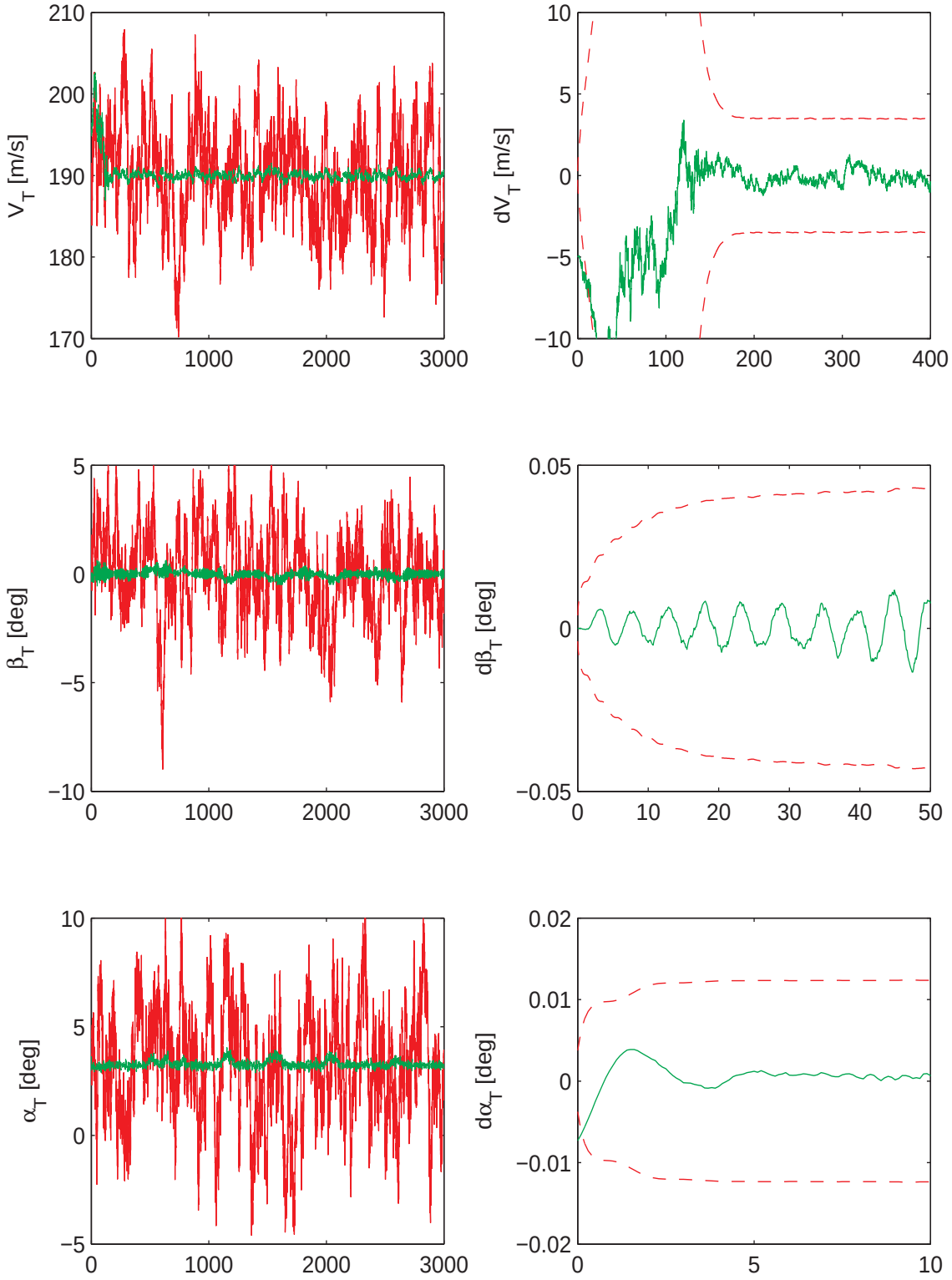

Figure 7.42. Measured and Estimated Airspeed, Sideslip Angle and Angle of Attack.

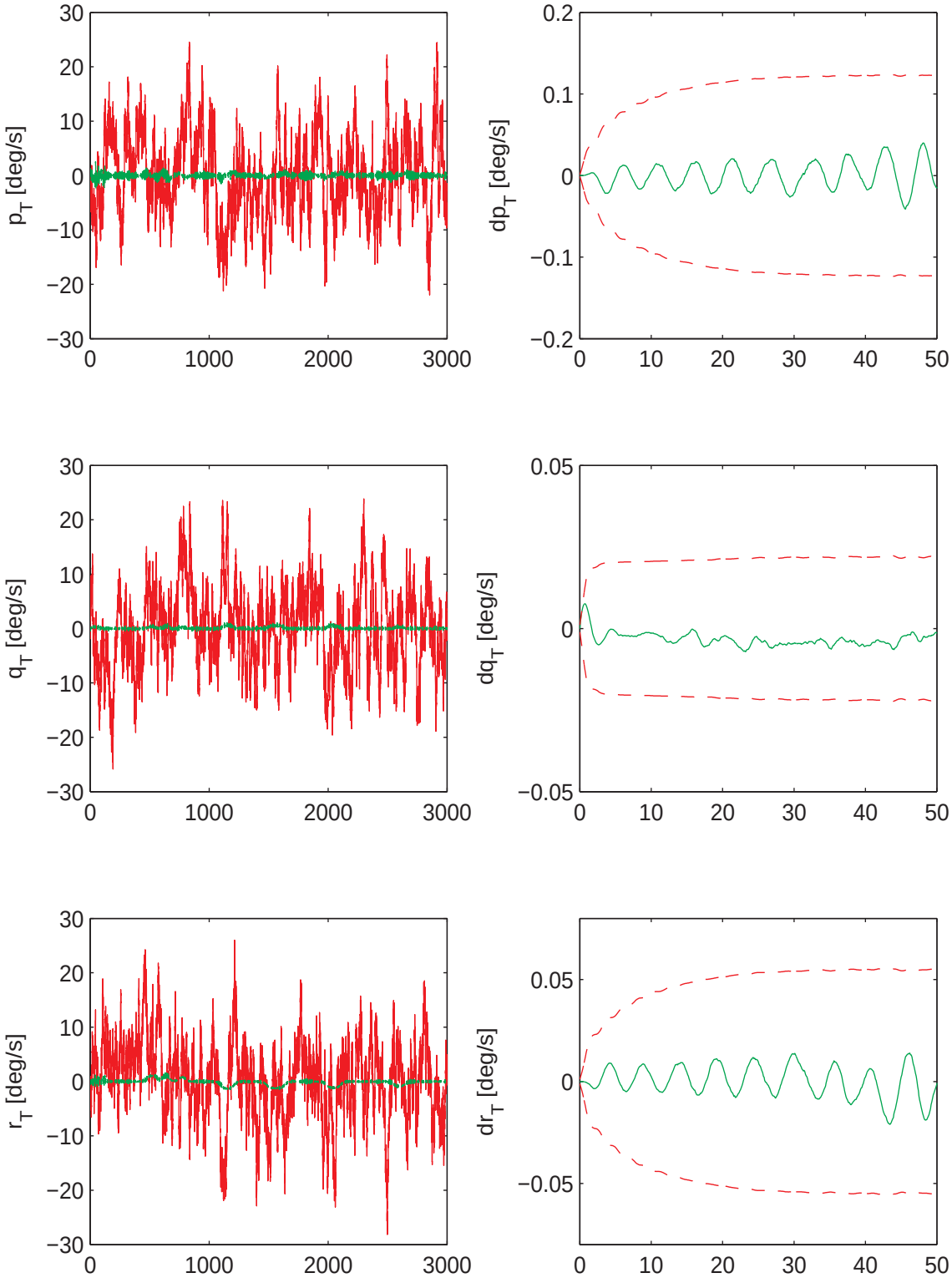

Figure 7.43. Measured and Estimated Angular Velocity Components.

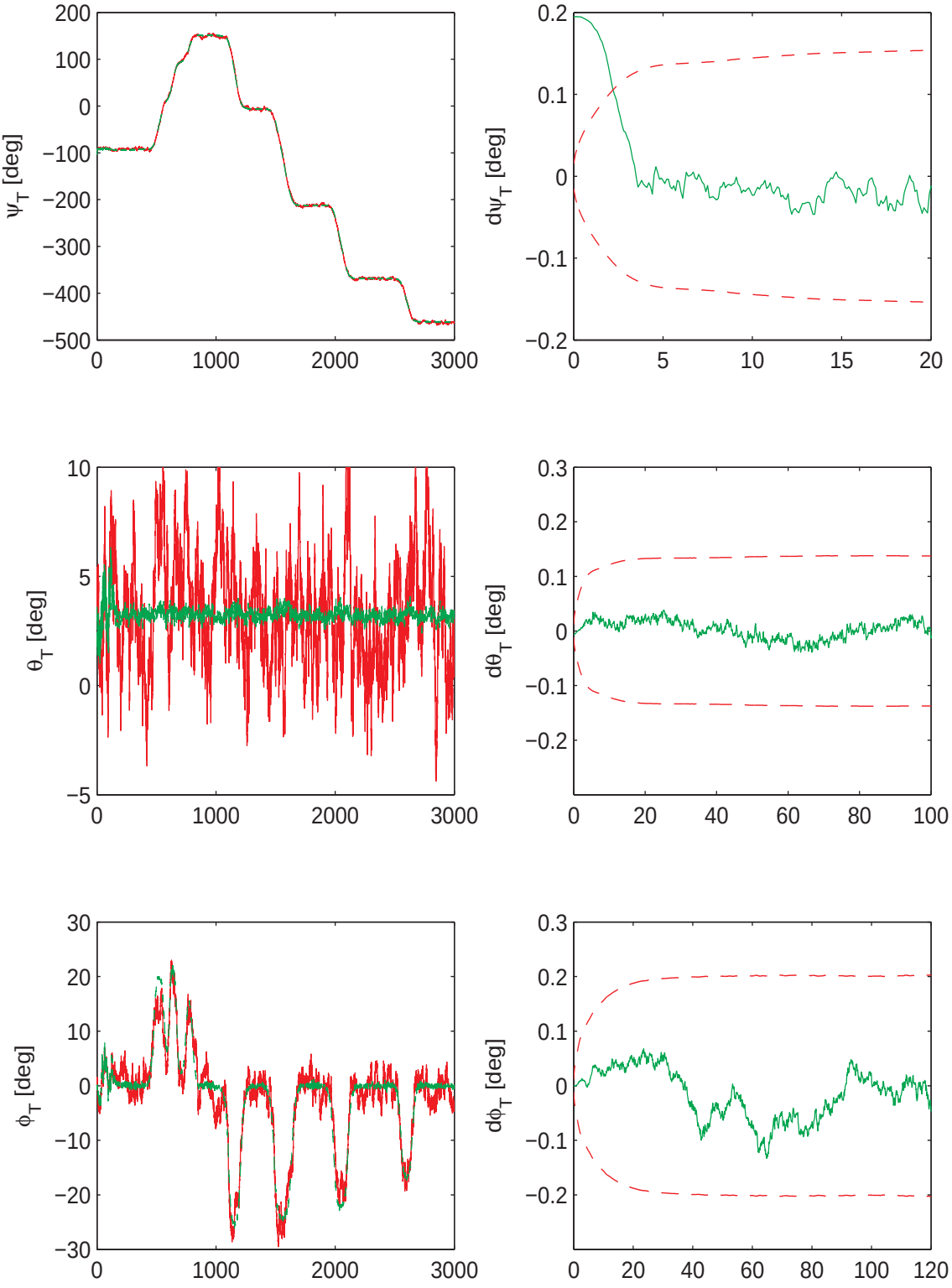

Figure 7.44. Measured and Estimated Euler Angles.

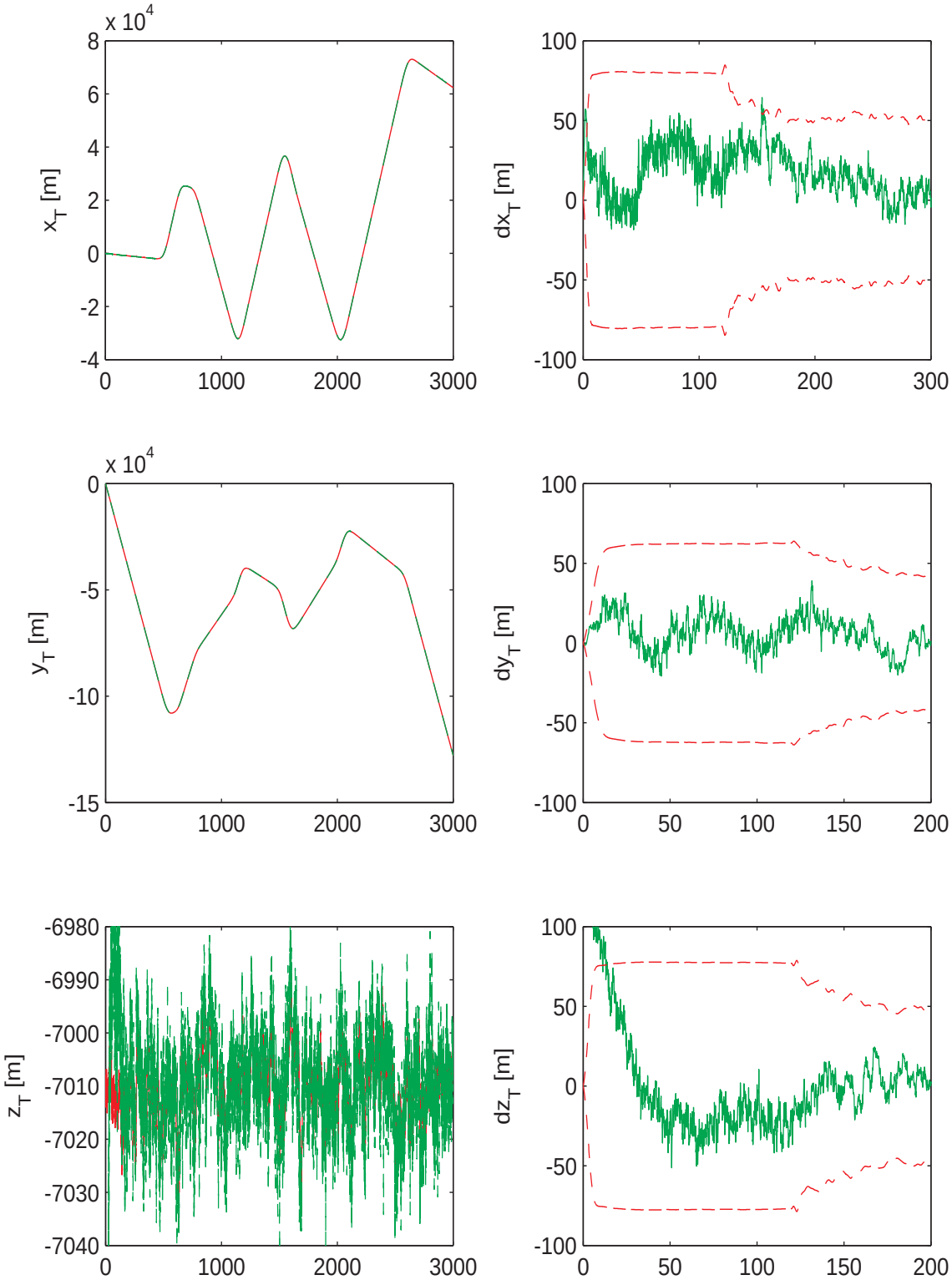

Figure 7.45. Measured and Estimated Position Components.

7.3.3 Parameter Study with Colored Measurement Noise

As stated earlier, the white noise assumption in the KF development is a theoretical abstraction and it is more likely to have colored measurement noise in the physical world. Thus, a method, described in Section 4.4, is used to handle colored measurement noise in the KF framework. Note that for the control of the tanker aircraft, the actual states are used as the feedback signal. The estimated states of the tanker are used in the estimation of the receiver as the receiver system model depends on some of the tanker states. The parameter study presented in this section is carried out to determine the limitations of the SR-UKF estimation as implemented in the tanker aircraft when the measurement error is colored noise. The effects of the variations of two parameters on the estimation performance are investigated. The first parameter, the correlation time constant τ_{v}, defines the "coloredness" of the measurement noise while the second set of parameters, turbulence intensity (σ_u,σ_v,σ_w), quantity the strength of the process noise of the aircraft, turbulence part of the wind. This parameter study is repeated for two different levels of measurement noise, low level from Table 2.2 and high level from Table 2.3. The prevailing wind is generated by the ECWM, described in Section 2.5.1.2. The ECWM randomly generates the initial conditions of the wind components. However, to isolate the effect of the two parameters selected, the initial condition of the wind are set to constants, i.e., $(W_{pre,x0}, W_{pre,y0}, W_{pre,z0})$ are equal to (7,-13,0) m/s for all the simulation runs conducted to generate the results of the parameter study. The effects of the variation of the parameters on the wind estimation are quantified by two characteristics of the wind estimations: (i) the convergence time and (ii) the variance of the estimation error.

7.3.3.1 Parameter Study: Correlation Time Constant

The correlation time constant influences to the extent of the correlation of CMN, which causes the exponentially correlated error to behave like a bias error. If correlation time constant approaches to zero, the signal becomes more like white signal, and if the correlation time constant increases up to 10 or 100 seconds, the signal becomes a colored signal.

The wind estimation of the left side of Fig. 7.46 indicates that the signal when the correlation time constant is 0.05 second has a short convergent time while the signal when the correlation time constant is 10 or 100 seconds has a long convergent time under the measurement characteristics of Table 2.3. The characteristic of the estimation affected by the variance of the correlation time constant is the variance of the estimation error. The variance of the estimation error in x-y components increases when the correlation time constant increases, as shown in the right side of Fig. 7.46. The amount of the change in z direction of the variance error is relatively small compared with the amount in x-y direction.

When the measurement characteristics are of Table 2.2, which are one tenth of the measurement characteristics of Table 2.3 in standard deviation, the left side of Fig. 7.47 shows that the convergent time increases exponentially like 1000 seconds as the correlation time constant increases until 50 seconds. A possible reason for the long convergent time may be the improperly selected process noise matrix. As shown in Fig. 7.47, the variances of the estimated wind errors increase slowly. When the correlation time constant is greater than 50 seconds, the variances of the estimated wind errors increase dramatically. Hence, the feasible range of the correlation time constant is from 0.05 to 50 seconds with the current process noise covariance matrix.

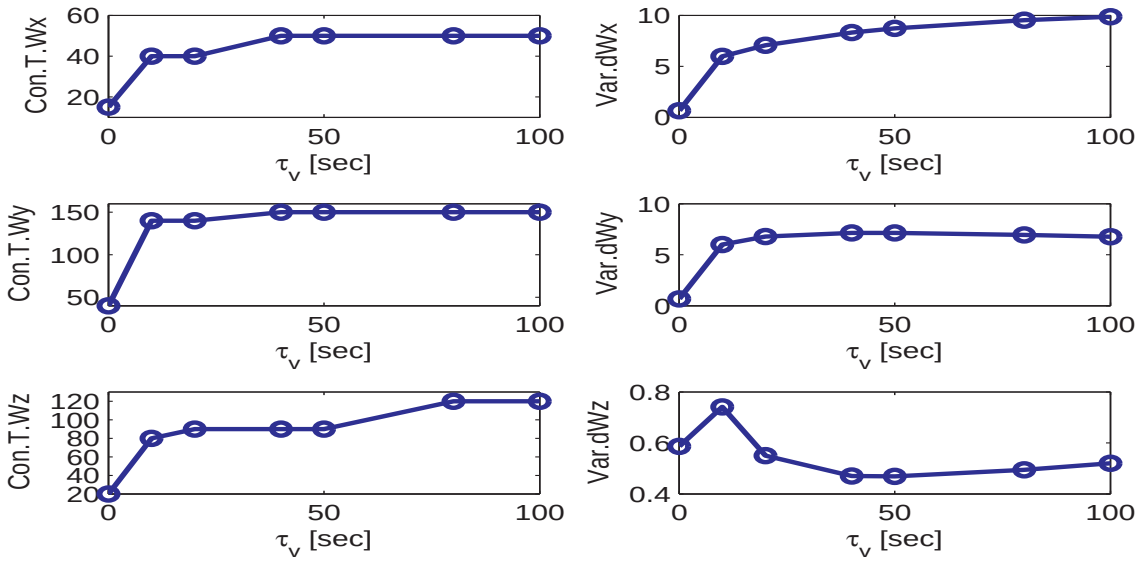

Figure 7.46. Correlation Time Constant Effect on Tanker Aircraft with Table 2.3.

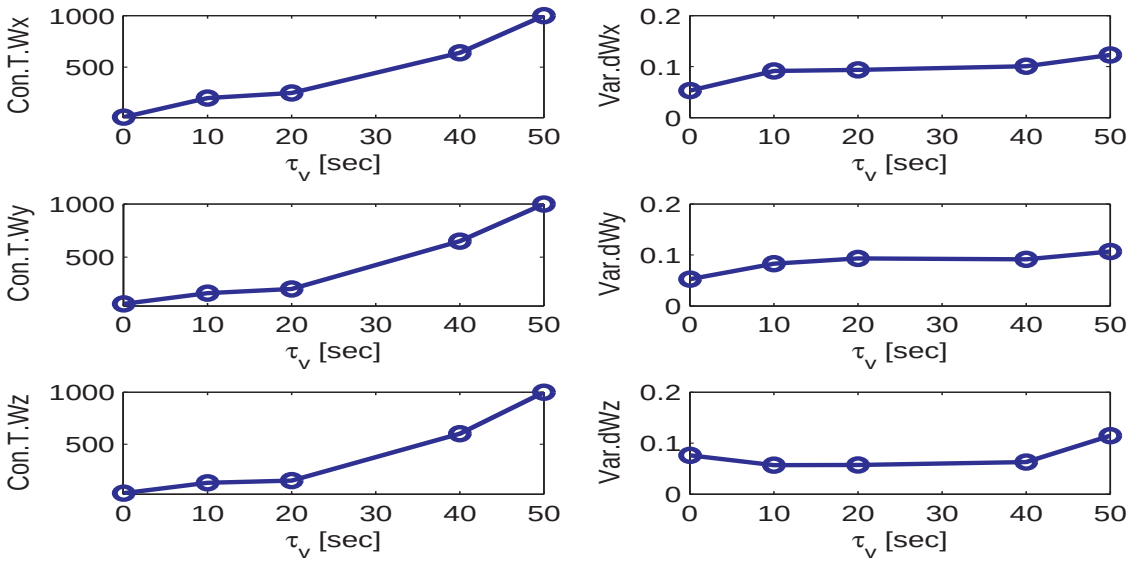

Figure 7.47. Correlation Time Constant Effect on Tanker Aircraft with Table 2.2.

The change of the measurement characteristics from Table 2.3 to Table 2.2 influences the performance of the estimation. Additionally, the process noise covariance matrix that newly selected by changing the variance of the measurement influences the performance of the estimation. The variance of the estimated errors in the right side of Fig. 7.47 is smaller than Fig. 7.46 due to the comparatively small noise level of the measurement.

In summary, the estimation algorithm with the colored measurement works well within a reasonable error range when the correlation time constant is between 0 and 20 seconds due to the convergent time of Fig. 7.47.

7.3.3.2 Parameter Study: Turbulence Intensity

The reference turbulence wind generated by Dryden model is characterized by the intensity and the wave length, whose values given in Chapter 2.5.1 and used in the simulation runs so far, represent a light turbulence. This section investigates the effect of the Dryden turbulence intensity as a parameter study. For this study, the correlation time constant is set to 20 seconds. The left sides of Fig. 7.48 and Fig. 7.49 show that the convergent time for wind estimation may not be influenced by the turbulence intensity. However, as the turbulence intensity increases, the variances of the estimated wind errors in x-y-z components increase. Hence, the working range of the turbulence intensity, highlighted on Fig. 2.5 by the yellow color, is from 0 to 3 m/s. Beyond the maximum intensity of turbulence, the estimation is divergent from the measurement signal.

In summary, an increase in the correlation time constant increases the convergence time and estimation error, and an increase in the turbulence intensity does not influence the convergence time but affects the estimation error. The change of the

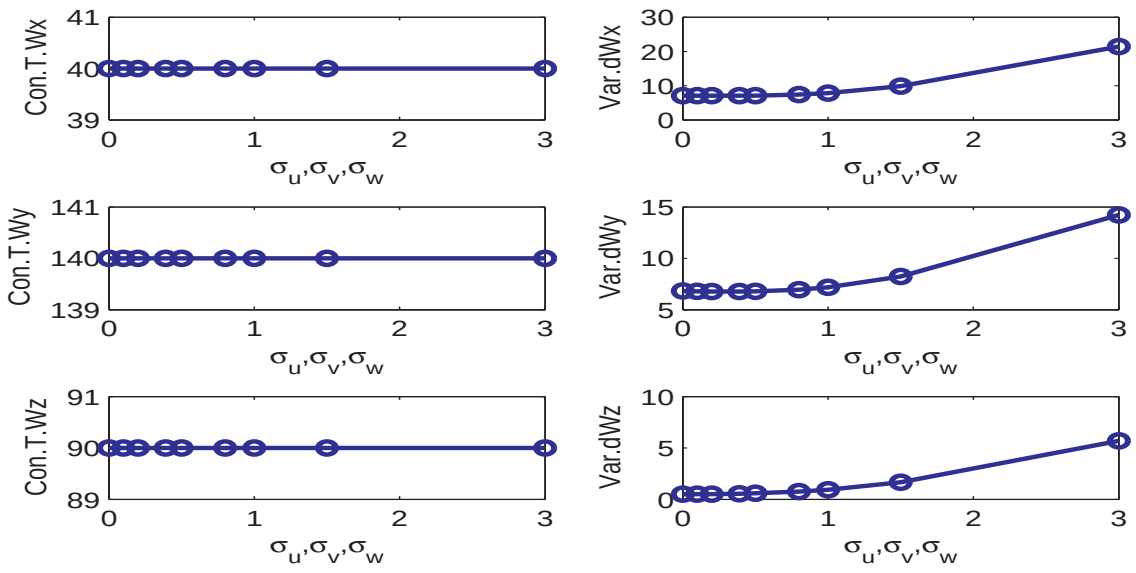

Figure 7.48. Intensity of Turbulence on Tanker Aircraft under Large Noise.

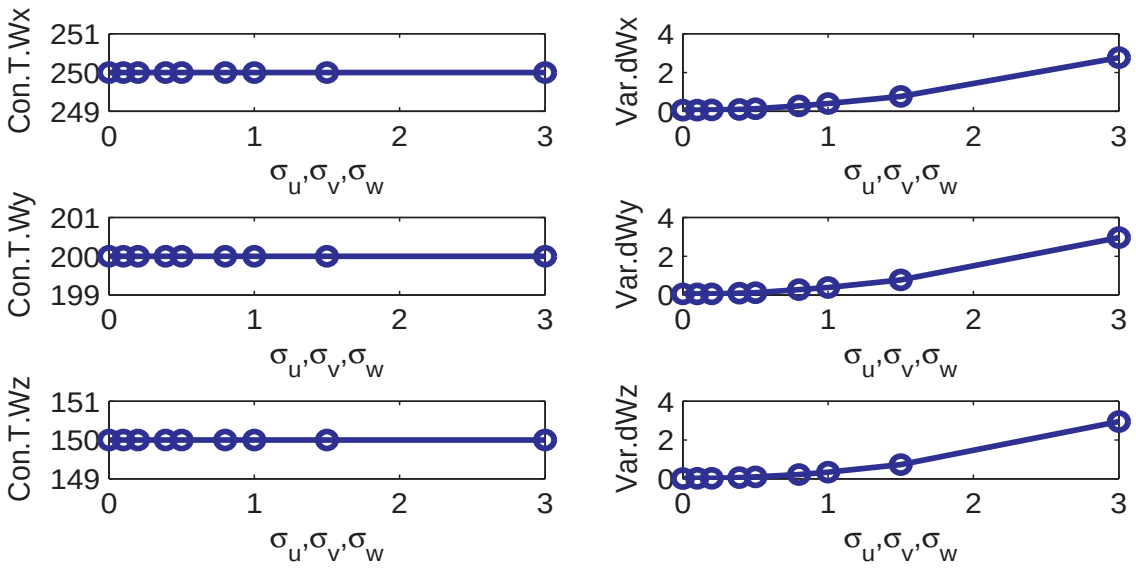

Figure 7.49. Intensity of Turbulence on Tanker Aircraft under Small Noise.

measurement characteristics influences the convergence time and the estimation error with a proper selection of the process noise covariance matrix.

7.4 Relative Position Control of Receiver Aircraft Through Estimated State Feedback and Parameter Study

For an automated aerial refueling capability, the position of the receiver aircraft should be controlled by its flight control system relative to the tanker, which is flying through a specified pattern by its pilot. The trajectory tracking controller of the receiver is briefly described in Section 2.4. Fig. 7.50 shows an example of the commanded and the actual position components of the receiver relative to the tanker aircraft expressed in the tanker's body frame. Note that the receiver aircraft is commanded to stay at and maneuver between the observation and contact position (see Fig. 2.1) as the tanker is flown through its commanded trajectory relative to the inertial frame, as shown in Fig. 7.1 with commanded constant speed and constant altitude. Due to the large noise levels of the measurement, the existing LQR-based controller of the receiver aircraft does not work properly if the measured signals are used for feedback. To minimize the measurement noise level, the proposed estimation algorithm is applied to estimate the full state of the receiver aircraft. This section studies the performance of the closed-loop system of the receiver when the estimated states of the receiver as well as the estimated tanker states are used as feedback signals. This is done in two case of measurement noise: white measurement and colored measurement. The descriptions of the two cases are given in Table 7.2. Specifically, in the colored measurement case, a parameter study is conducted for the correlation time constant, turbulence intensity, and measurement noise level with respect to the relative position error. Fig. 7.51 depicts the relative position error indicating a feasible range of the boom for the fuel transfer. (x_c, y_c, z_c) is the commanded relative position

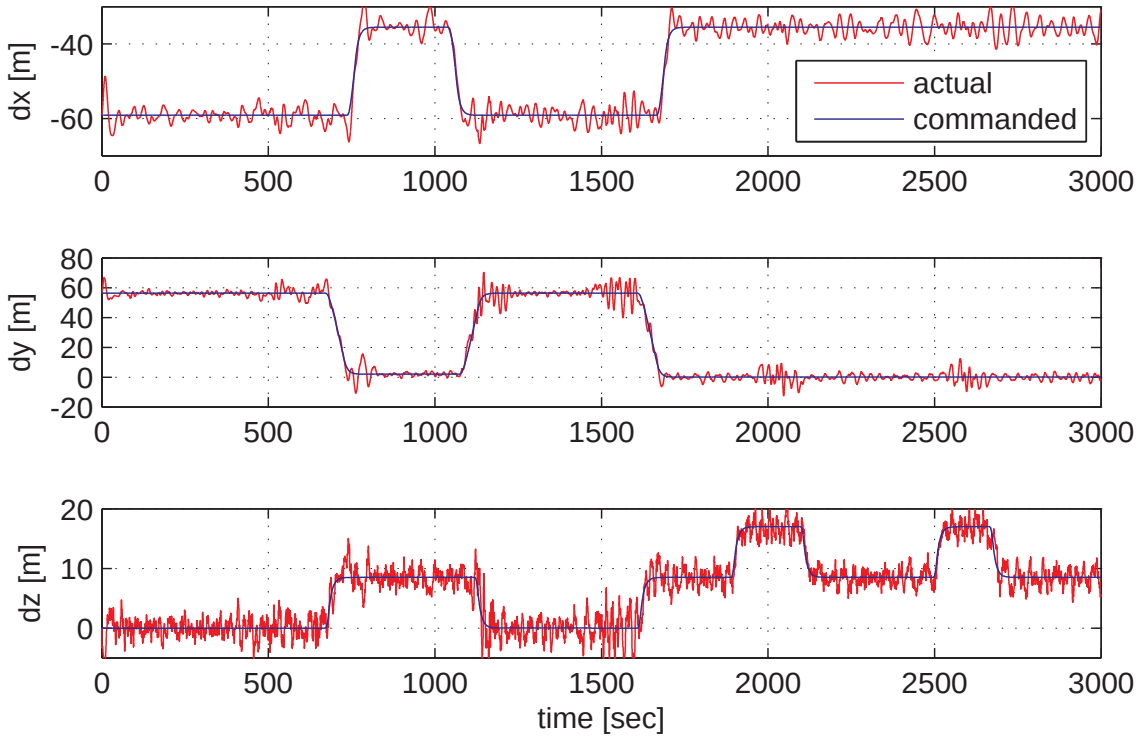

Figure 7.50. Position of Receiver Aircraft.

of the receiver aircraft. (ΔX,ΔY,ΔZ) is the relative position error by the difference between the true signals and the commanded signals. The acceptable relative position error along each direction for the successful fuel transfer without disconnecting the boom in an actual fuel transfer is 2 meter in all three directions. In this research, no attempt is made to reduce the relative position errors down to the acceptable limits. The investigation in this section focuses on identifying the effect of using estimated signals for feedback as opposed to using measured signals on position errors.

Table 7.2. Two Simulation Cases for Relative Position Control

	W_{tur}	W_{pre}	*Measurement Noise*	*Feedback Signal*
Case I	Dryden	Flight Data	White, Small Level	Estimated
Case II	Dryden	ECWM	Colored, Small Level	Estimated

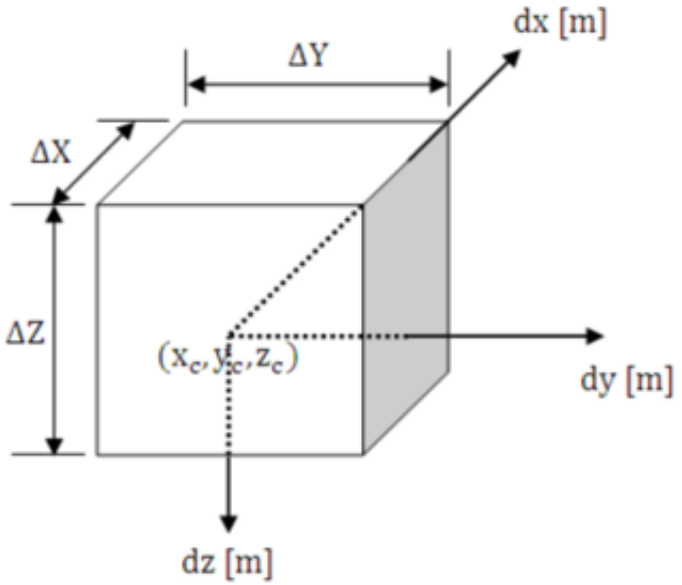

Figure 7.51. Definition of Relative Position Error.

7.4.1 Relative Position Control with White Measurement Noise and Parameter Study

This section deals with the relative position control with estimated state feedback in the case of white measurement noise. In this case, the prevailing wind is used from the flight data as described in Section 2.5.1.1, the Dryden model generates the turbulence as described in Section 2.5.2 for the tanker and the receiver aircraft and the vortex induced wind is generated as described in Section 2.5.3.

The light turbulence is generated by the Dryden model with the intensity of (0.39, 0.39, 0.39) m/s and the wave length of (533.4, 533.4, 533.4) meter in component forms, and the variance of the measurement is as listed in Table 2.2. Under these conditions, the relative position control of the receiver aircraft is successfully accomplished with estimated state feedback. Especially, at the contact position, the relative position error as shown in Fig. 7.52 are smaller than 3, 4 and 3 meters in x, y and z directions, respectively.

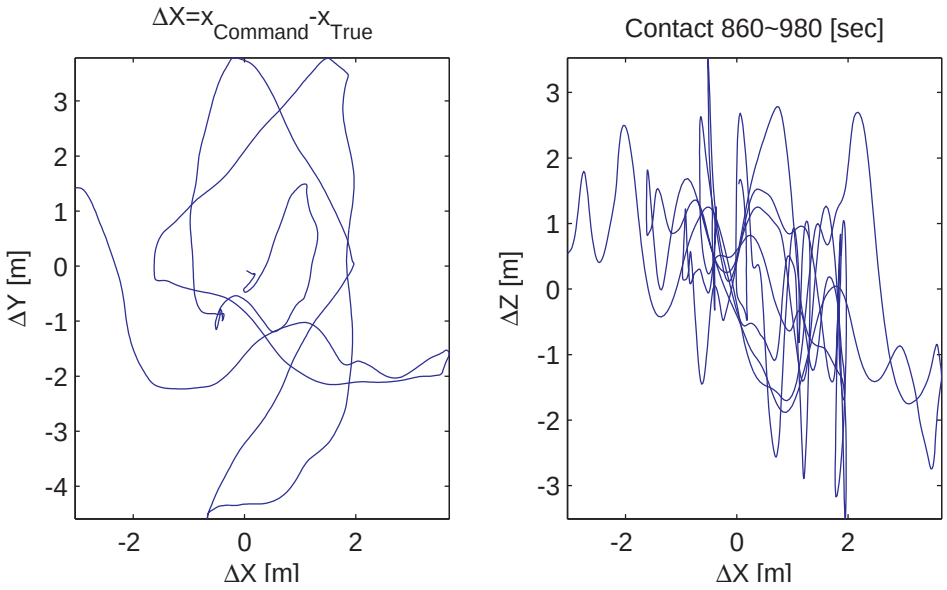

Figure 7.52. Relative Position Error at a Contact Position with White Noise.

In the case of white measurement noise, the estimated wind in the receiver aircraft is shown Figs. 7.53 and 7.54. By the percentage errors in terms of magnitude and direction, the magnitude error is usually less than 8% and the direction error in general remains less than 5%.

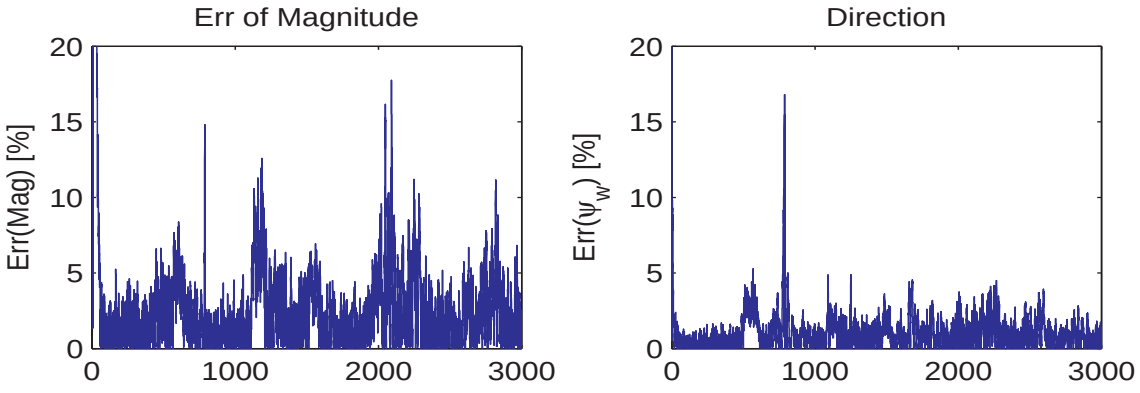

Figure 7.53. Percent Errors of Wind Estimate (Case I).

The plots on the left hand side of Fig. 7.54 show the components of the reference wind and the estimated wind throughout the whole simulation. The figures show that the estimation is successful in capturing the time variation of the wind. On the right hand side of Fig. 7.54, the estimation errors, in the component form, are shown in the first 100 seconds and compared with the 3σ bounds. The x- & y-component errors converge to the respective 3σ bounds in 60 seconds while the z-component error converges to the 3σ bound in 20 seconds. When the receiver moves to the contact position, it is behind the tanker and influenced by the nonuniform wind induced by the tanker's wake vortices. The contact position is in the downwash region of the nonuniform wind field. As shown in the $(W_{I_R})_z$ plot on the left side of Fig. 7.54, the estimated wind precisely captures the downwash exposure whenever the receiver goes to the contact position. The z-component of the wind is zero when the receiver is at the observation position and thus outside the wake of the tanker. Another way to identify the wake vortex induced wind is to compare the estimated wind by the tanker estimator with that by the receiver estimator. For example, the difference between the z-components of the estimated winds of the tanker in Fig. 7.3 and that of the receiver in Fig. 7.54 is clearly the vortex-induced wind as the tanker is not exposed to the nonuniform wind field. Figure 7.55 shows the effect of the measurement noise level on the station-keeping performance of the closed loop system in a comparative way between measured state feedback versus estimated state feedback. The level of measurement noise is quantified by factor G, which multiplies the standard deviations of the state measurements listed in Table 2.2. The larger factor G is, the more noisy the measurements are. Figure. 7.55, simulated between 860 and 980 seconds, shows that the controller using measured state feedback works only when G is less than 0.6. On the other hand, the controller using the estimated state feedback can perform

station-keeping until G is 7. This shows that the estimated state feedback increases the robustness of the closed loop system against the measurement noise.

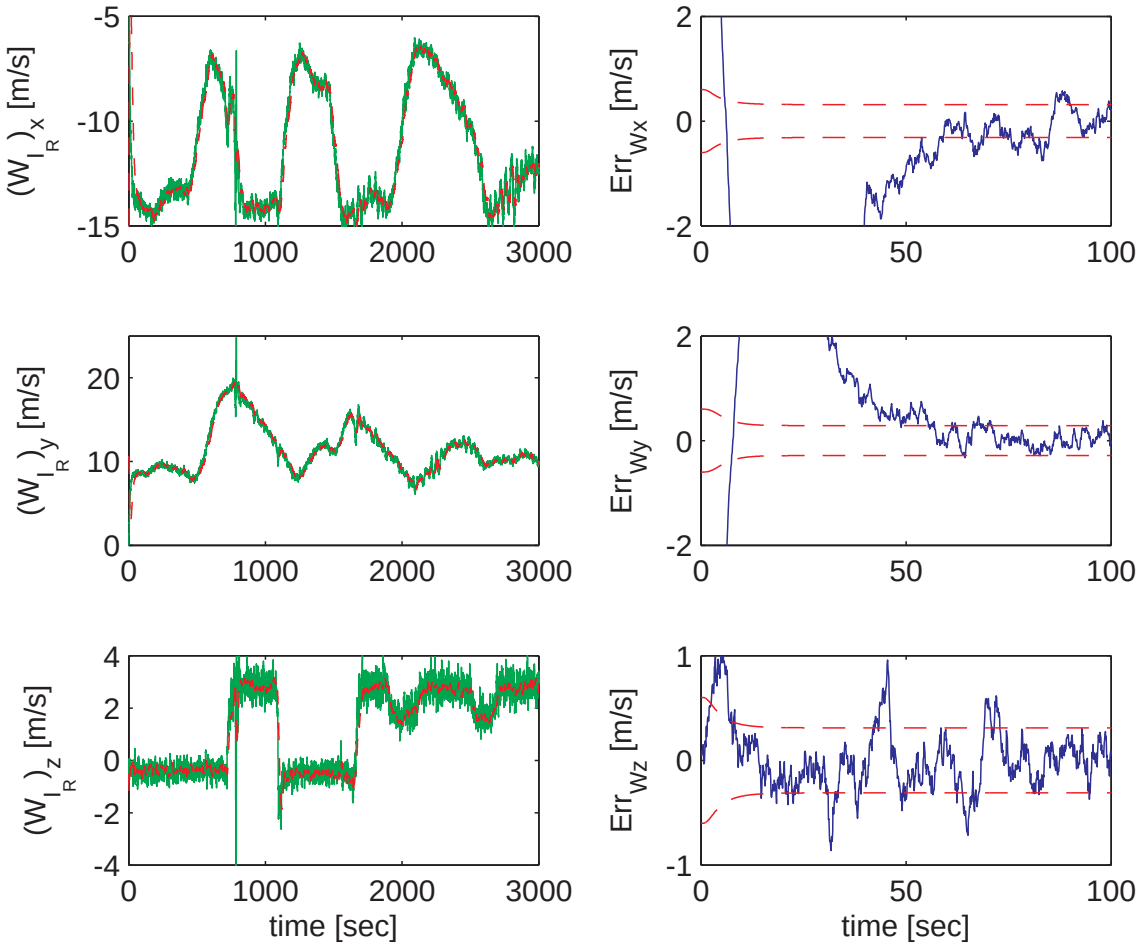

Figure 7.54. Comparison Between Reference and Estimated Wind (Case I).

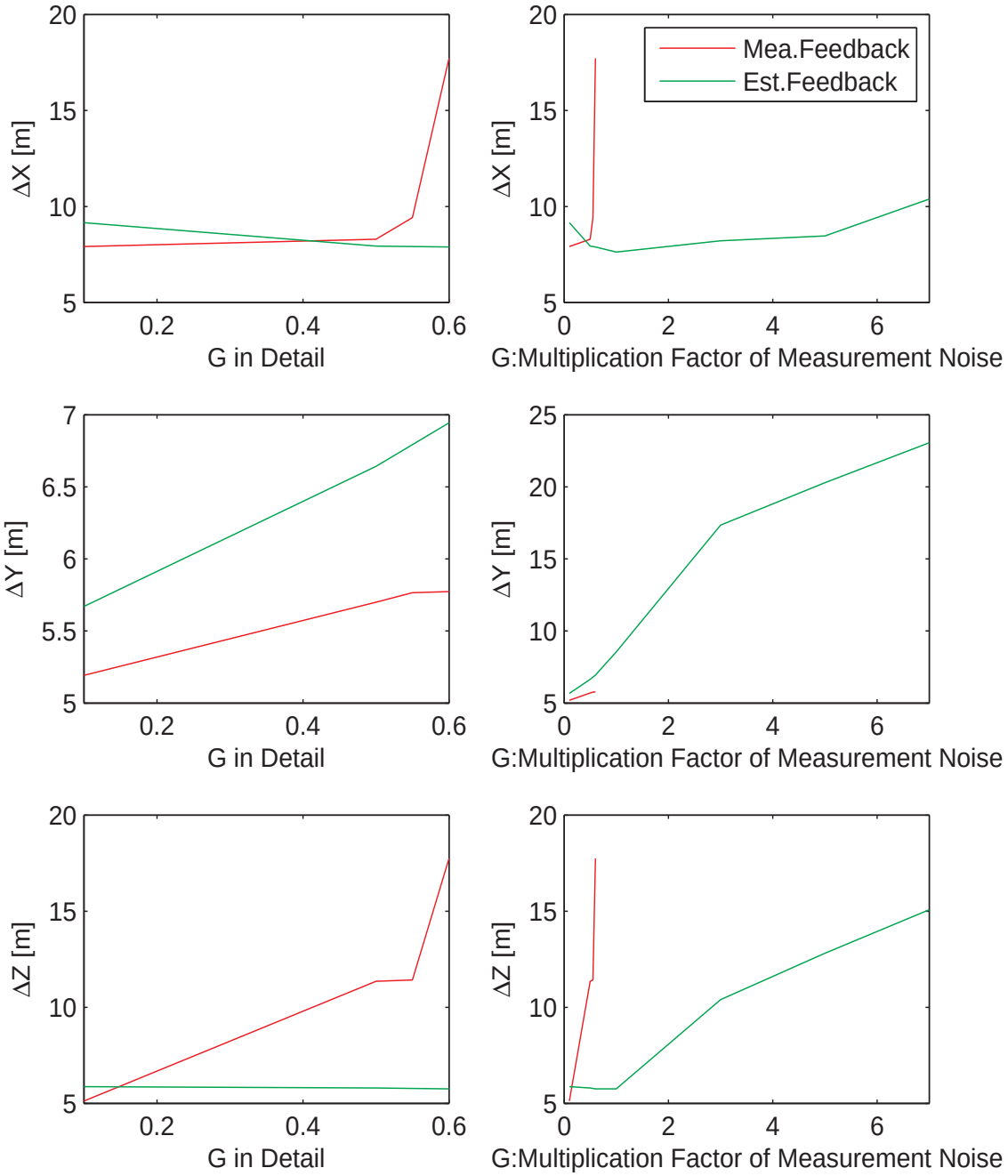

Figure 7.55. Parameter Study of White Measurement Noise Variance by Multiplying G with the Noise Characteristics of Table 2.2. Turbulence Intensity is 0.39 m/s. Simulation Time at the Contact Position is between 860 and 980 Seconds.

7.4.2 Relative Position Control with Colored Measurement Noise and Parameter Study

In this case, the sensors have colored measurement noises, the prevailing wind is generated by ECWM, and the light turbulence is generated by Dryden model with intensity of (0.39, 0.39, 0.39) m/s and a wave length of (533.4, 533.4, 533.4) meter in component forms, the variances of the measurements is of Table 2.2, and correlation time constant (τ_v) is 1 second. Under these conditions, the relative position control of the receiver aircraft is successfully performed. Especially, at the contact position, the relative position error shown in Fig. 7.56 is smaller than about 2 meters in all three directions.

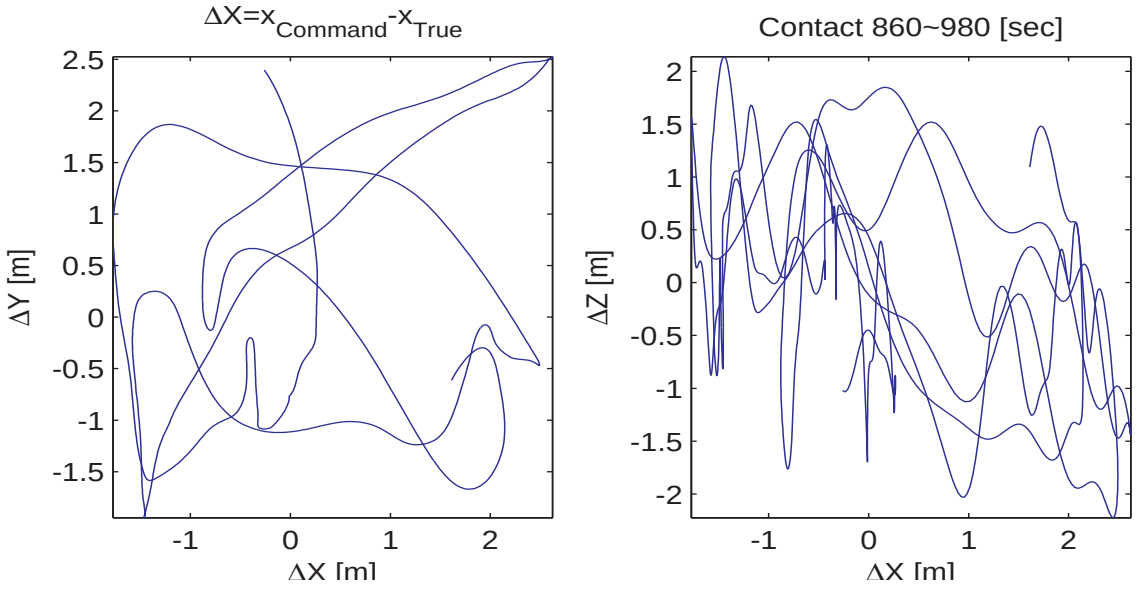

Figure 7.56. Relative Position Error at a Contact Position with Colored Noise.

In this case of the colored measurement noise, the estimated wind in the receiver aircraft is shown in Figs. 7.57 and 7.58. As shown in Fig. 7.57, the magnitude error is usually less than 5% and the direction error in general remains less than 5%.

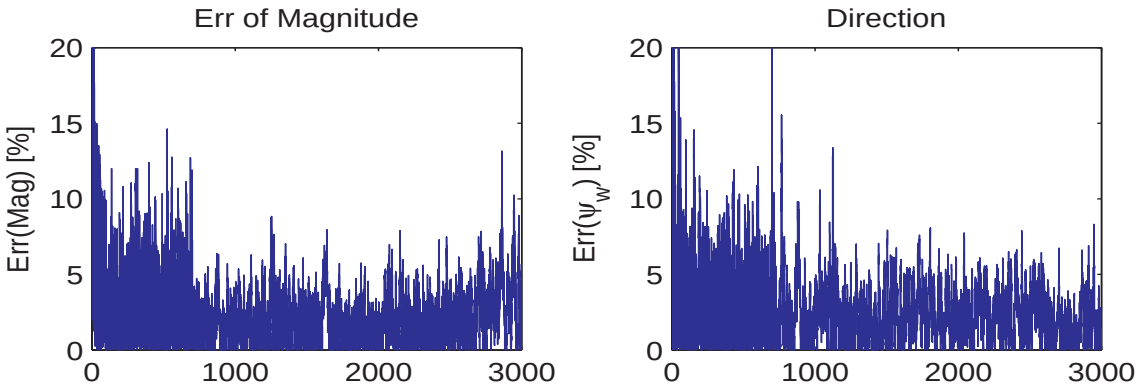

Figure 7.57. Percent Errors of Wind Estimate (Case II).

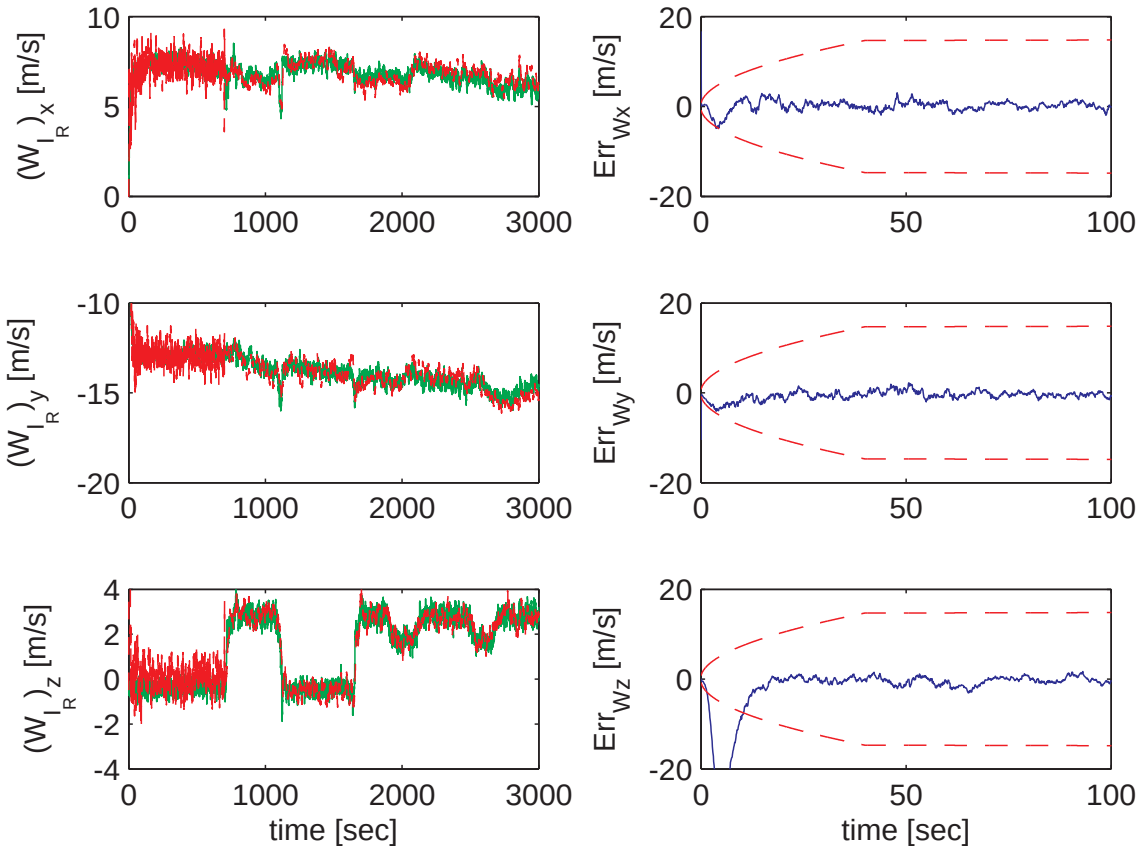

Figure 7.58. Comparison Between Reference and Estimated Wind (Case II).

The plots on the left hand side of Fig. 7.58 show the components of the reference wind and the estimated wind throughout the whole simulation. The figures show that

the estimation is successful in capturing the time variation of the wind. On the right hand side of Fig. 7.58, the estimation errors, in the component form, are shown in the first 100 seconds and compared with the 3σ bounds. The x- & y-component errors converge to the respective 3σ bounds in 10 seconds while the z-component error converges to the 3σ bound in 18 seconds. As previously discussed in Section 7.4.1, when the tanker aircraft moves to the contact position, it is exposed to downwash due to the tanker's wake vortex induced wind field. The z-plot in Fig. 7.58 clearly shows that the downwash is accurately estimated whenever the receiver goes to the contact position. The estimated z-wind (downwash) is due to the tanker's wake vortices because the prevailing wind does not have z-component.

As shown in Fig. 7.59, as the level of noise increases (i.e., multiplication factor G increases), the station-keeping error in all three directions increases as well in both cases: (i) measured state feedback and (ii) estimated state feedback. This analysis is repeated with two different values of correlation time constant: (i) $\tau_{\mathrm{v}} = 0.05$ second on the left side of Fig. 7.59 and (ii) $\tau_{\mathrm{v}} = 1$ second on the right side of Fig. 7.59. For all values of G, the estimated state feedback yields smaller station keeping error as compared to the performance of the direct state measurement feedback in both cases of the correlation time constants. Only exception is in the y-component in the case of $\tau_{\mathrm{v}} = 1$ second. In this case, the y-error is smaller with measurement feedback, but only for very small values of G. Even in this case, when G is greater than about 0.6, the measurement feedback yields much larger error. Another important advantage of using estimated state feedback is shown by the maximum value of G for which the feedback controller can manage to provide station keeping even if with slightly larger errors. Figure 7.59 shows that the measurement feedback works only for very small values of G in both cases of τ_{v}. On the other hand, the state estimate feedback works up to G = 3 when $\tau_{\mathrm{v}} = 0.05$ second up to G = 7 when $\tau_{\mathrm{v}} = 1$

second. This analysis shows that the algorithm developed in this research to handle colored measurement noise is limited mainly by the correlation time constant. The largest correlation time constant the estimation can work is 1 second. Recall that the larger the correlation time constant is, the more "colored" the measurement noise becomes. If the measurement noise is too colored, the estimation cannot converge, probably because the algorithm cannot remove the coloredness of the measurement. This limitation can be eased up by better tuning the process noise covariance in the KF.

Fig. 7.60 shows the effect of the turbulence intensity on the station keeping performance and compares the performances of two cases: (i) estimated state feedback and (ii) measured state feedback. The simulations that generated these results use the same multiplication factor G = 1 and same correlation time constant $\tau_v = 1$ at a contact position simulated between 860 and 980 seconds. The figure shows that the components of the relative position errors increase in both cases as the turbulence intensity increases. The maximum intensity at which the controller still works is higher, 2 m/s (6.56 ft/sec), with estimated state feedback than that, 1.2 m/s (3.94 ft/s), with measured state feedback. Note that Fig. 2.5 shows the range of the turbulence goes up to moderate turbulence with estimated state feedback while it stays close to light turbulence with measured state feedback. Figure 7.60 also shows that the station keeping performance (the range of position error relative to the commanded contact position) of the closed loop system is much better with estimated state feedback throughout the whole feasible turbulence range. Therefore, this analysis clearly shows the benefit of using estimated state feedback over the measurement feedback.

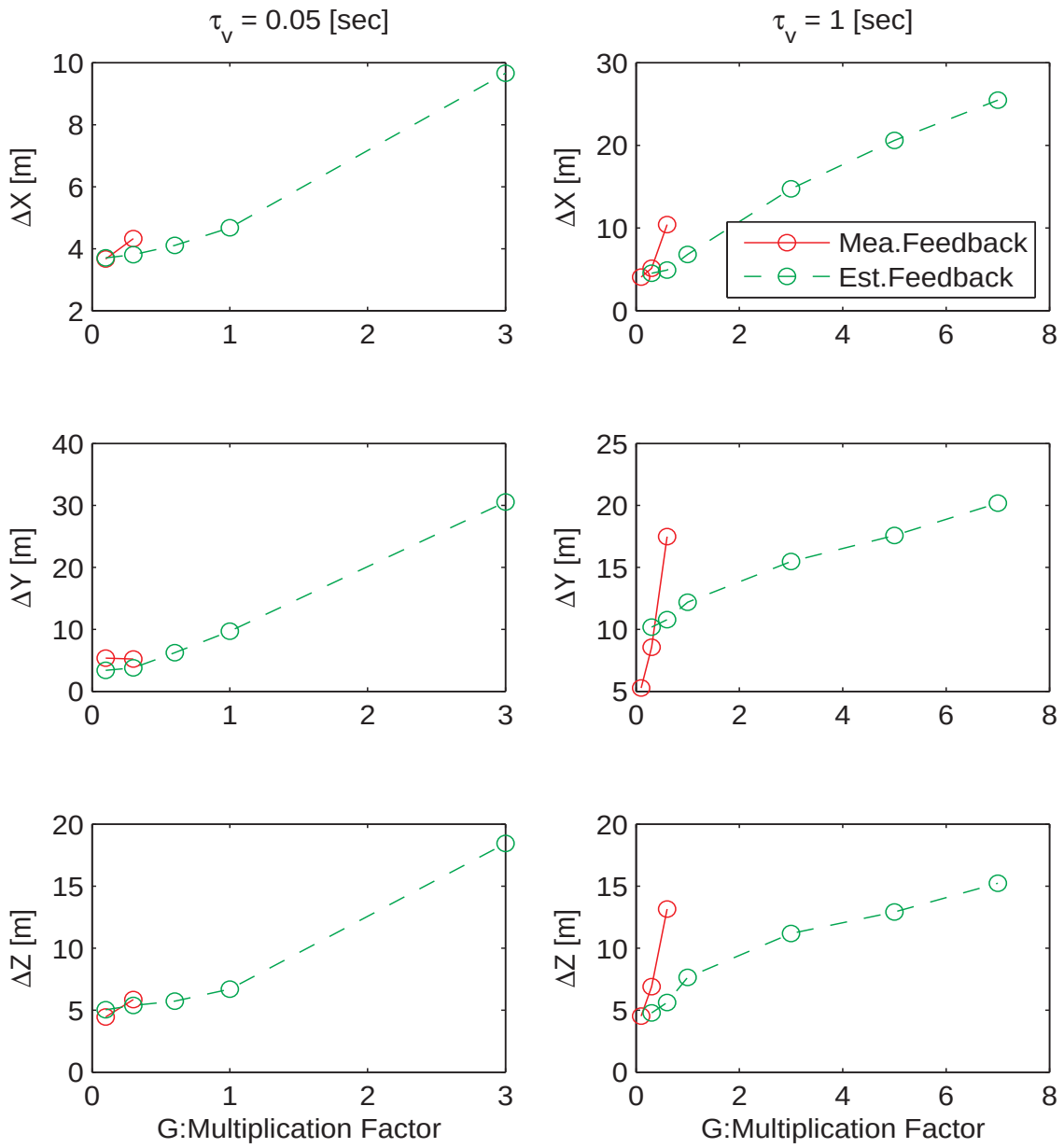

Figure 7.59. Parameter Study of Colored Measurement Noise Variance by Multiplying G with the Noise Characteristics of Table 2.2. Turbulence Intensity is 0.39 m/s.

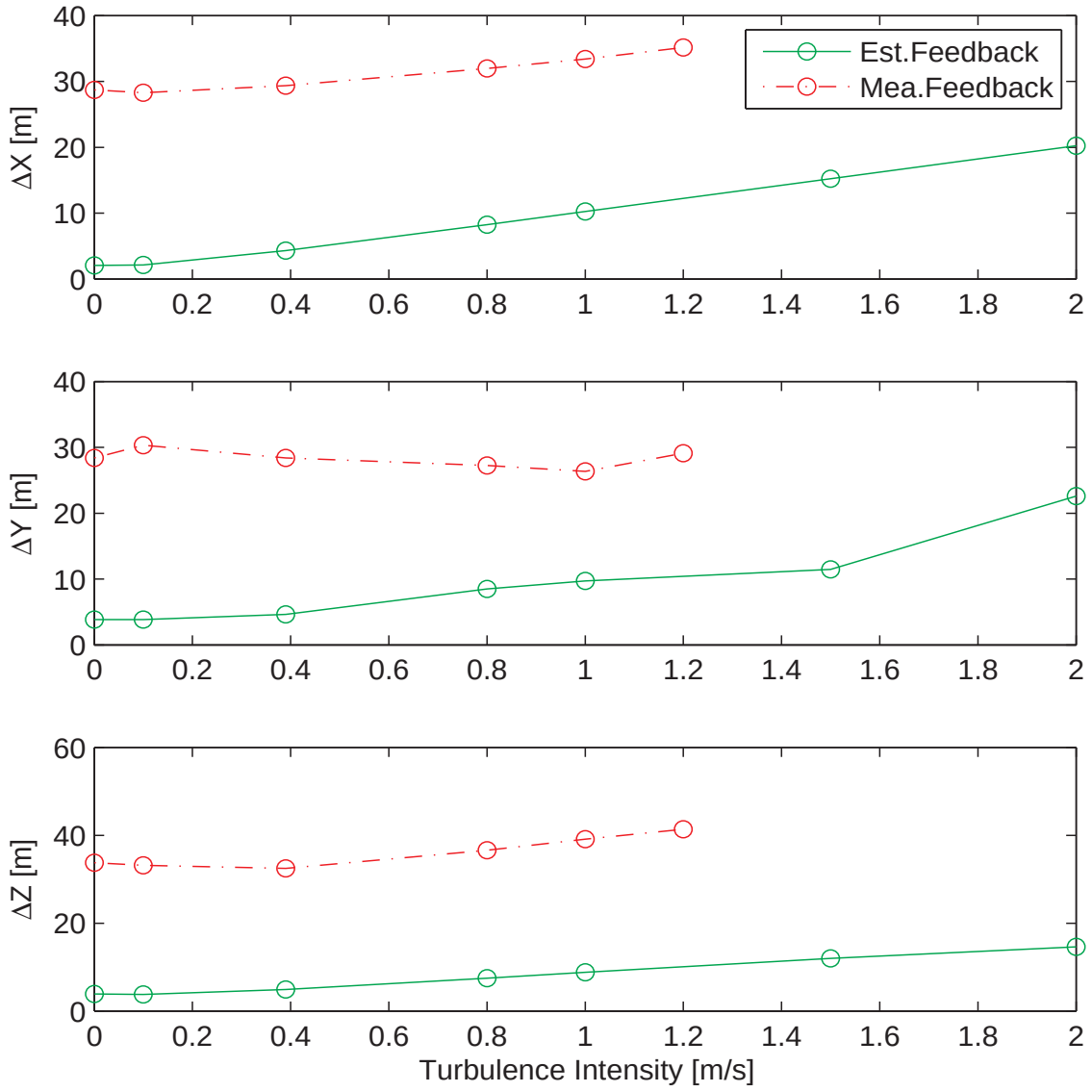

Figure 7.60. Parameter Study of Turbulence Intensity at a Contact Position Simulated between 860 and 980 Seconds When G is 1 and τ_v is 1 Second.

CHAPTER 8

CONCLUSION AND FUTURE WORK

Kalman Filter based estimation algorithms are developed for the estimation of the aircraft states and the wind exposure, separately for the tanker and receiver aircraft flying in formation for an aerial refueling operation. The aircraft states are estimated by a Square-Root Unscented Kalman Filter (SR-UKF) because the mathematical models of tanker and receiver aircraft are highly non-linear, the flight operation covers various trim conditions, and aircraft are exposed to various sources of wind. A main advantage of UKF and SR-UKF in implementation is that they do not require the calculation of complex Jacobian matrices. The scalar forms of the equations need to be used in the UKF or SR-UKF. A wind estimation model for the tanker or receiver aircraft is obtained by rearranging the translational dynamics in terms of wind terms. The wind can also be calculated through a combination of the available measurements without estimation, which is called Calculated Measurement of Wind (CMW) in this work. The CMW has large magnitudes of noise even after the CMW is passed through a moving average filter to reduce its large noise level. If the CMW is used in the estimation of the state of the tanker aircraft or the receiver aircraft, the state estimation will be divergent or have the problem of mathematical singularity. In other words, the covariance of the state of SR-UKF has a large possibility to be divergent. To avoid the divergence of the covariance of the state, the wind estimation is done by augmenting the equations of motion of the tanker or the receiver aircraft with the wind model in the SR-UKF. However, the augmented equations of motion have a singularity problem due to the fact that the wind model

is a modified version of the translational dynamics equations, which is part of the augmented system update in the SR-UKF along with the wind equation. This singularity problem is resolved by tuning the covariance matrix of the process noise in the estimation. Another reason to tune the covariance matrix of the process noise is to represent the effect of turbulence, which is the process noise to the aircraft dynamics.

The SR-UKF estimator developed for the tanker and receiver aircraft are evaluated in an integrated simulation environment. The simulation includes three sources of wind: (i) prevailing wind, (ii) turbulence and (iii) wake vortex induced wind. The tanker is exposed to the superposition of prevailing wind and turbulence while the receiver experiences the superposition of all the three sources. The prevailing wind is generated by two different methods: (i) a wind profile extracted from a test flight data, and (ii) a probabilistic method that is based on filtering a white noise process through a linear filter. The estimation algorithms work equally well in either case of the prevailing wind in both tanker and receiver aircraft. The receiver aircraft is exposed to the vortex-induced wind when it flies in the wake of the tanker in addition to the prevailing wind and turbulence. Since the SR-UKFs estimate the total wind each aircraft experiences, the receiver estimator successfully determines the effect of the vortex-induced wind in the total wind exposure whenever the receiver aircraft moves behind the tanker aircraft. The difference between the winds estimated in the tanker and receiver aircraft reveals the vortex induced wind since the aircraft are exposed to the same prevailing wind and turbulence.

The wind estimation algorithms are developed to work with colored measurement noise as well as zero-mean Gaussian white noise in the SR-UKF. To deal with colored measurement noise in Kalman filter, a new measurement that have the characteristics of a zero-mean Gaussian white noise is defined. By using this new mea-

surement equation for the measurement update of SR-UKF, the SR-UKF becomes a conventional KF based on the white measurement noise.

A parameter study is conducted to determine the verifications of the estimation algorithms in the case of colored measurement noise. The maximum available correlation time constant, which is a key parameter to determine sensor's specifications, is 100 seconds for the tanker without estimation feedback control, and 1 second for the receiver aircraft with estimated state feedback control. An additional parameter study is performed to evaluate the robustness of the estimation algorithm. As turbulence intensity increases, the variance of the estimation error increases in both aircraft. The maximum turbulence intensity is 3 m/s for the tanker and 2 m/s for the receiver aircraft estimators to still yield convergent results. The maximum intensity values represent moderate turbulence while 0.39 intensity which is default in the estimation algorithm represents light turbulence.

The controller for the receiver aircraft to track position commands relative to the tanker aircraft is provided with the estimated states instead of the measured states to determine whether estimated state feedback improves closed loop performance. Another parameter study is conducted to investigate the sensitivity of the station-keeping performance of the receiver against the level of measurement noise. The level of measurement noise is quantified by a multiplication factor for the variations of all the state measurement errors in a baseline case. The parameter study shows that the station-keeping controller is able to perform its task with the multiplication factor increased up to seven when the controller uses the estimated state feedback. On the other hand, when the measured states are fedback, the controller fails if the multiplication factor is greater than 0.6. This indicates that the estimated state feedback improves the robustness of the station keeping performance against the measurement noise.

One of the limitations of the proposed estimation algorithm is that it depends on the process noise covariance, which is not known. The process noise covariance from the Dryden turbulence model cannot be used in estimation because the estimated wind model, calculated from the estimated states, does not reflect the process noise. Thus, the process noise covariance in SR-UKF is not known, and thus needs to be tuned. Since no systematic tuning procedure is suggested, the selection of the process noise covariance matrix, based on simulation experiments, is not necessarily the best one and may yield a degraded performance in actual implementation. An adaptive process noise covariance in non-linear Square-Root Unscented Kalman Filter should be developed for tuning the process noise covariance automatically. This will remain as a future work. If an adaptive procedure is developed, the performance of the estimation method will be enhanced even though a large correlation time constant is applied. Further, this research focuses on the estimation of the translational wind. However, the receiver aircraft is also exposed to rotational wind when flying behind the tanker. Since this effect is not taken into account in the estimation, it is stated as unmodeled disturbance in the system update part of the estimation. If the rotational wind can also be estimated along with the translational wind, the performance of the estimation may improve. Thus, the estimation of the rotational wind should be a topic for future work.

In this research, no attempt is made to tune the controller to improve the station-keeping and trajectory-tracking performance of the receiver controller. This research is focused on improving the closed loop performance by employing estimation techniques for a fixed controller. Another item for future work is to re-tune the current controller or design different controllers using estimated state feedback in order to further improve the relative position tracking performance of the receiver aircraft.

When the receiver aircraft flies behind the tanker, it is exposed to nonuniform wind field. This means that the airdata sensor on the receiver will read different airspeed, side-slip angle and angle-of-attack data, depending on its placement on the aircraft. Namely, the airdata sensor will provide local readings while the aircraft dynamics is affected by the distribution of the wind over the aircraft. In the current research, the receiver estimator uses data from effective airspeed, side-slip angle and angle-of-attack calculations, instead of local readings. The overall effect of this practice in simulation should be investigated and eventually local airdata sensor readings should be used in the estimation.

APPENDIX A

SCALAR FORM OF EQUATIONS OF MOTION FOR TANKER

The equations of motion for tanker aircraft including wind are described in Ref. [31]. The scalar forms of tanker equations are required for development of the family of the unscented Kalman filters.

A.1 Translational Dynamics of Tanker Aircraft

The translational dynamics in scalar form are

$$\begin{aligned}
\dot{V}_{_T} &= g[\cos\alpha_{_T}\cos\beta_{_T}(-\sin\theta_{_T}) + \sin\beta_{_T}(\sin\phi_{_T}\cos\theta_{_T}) \\
&+ \cos\beta_{_T}\sin\alpha_{_T}(\cos\phi_{_T}\cos\theta_{_T})] \\
&+ \frac{1}{m_{_T}}[-D_T + T_{_T}\cos(\alpha_{_T}+\delta_T)\cos\beta_{_T}] \\
&- \left[(\dot{W}_{I_{_T}})_x R_{11} + (\dot{W}_{I_{_T}})_y R_{12} + (\dot{W}_{I_{_T}})_z R_{13}\right]\cos\alpha_{_T}\cos\beta_{_T} \\
&- \left[(\dot{W}_{I_{_T}})_x R_{21} + (\dot{W}_{I_{_T}})_y R_{22} + (\dot{W}_{I_{_T}})_z R_{23}\right]\sin\beta_{_T} \\
&- \left[(\dot{W}_{I_{_T}})_x R_{31} + (\dot{W}_{I_{_T}})_y R_{32} + (\dot{W}_{I_{_T}})_z R_{33}\right]\cos\beta_{_T}\sin\alpha_{_T} \qquad \text{(A.1)}
\end{aligned}$$

where $\left[(\dot{W}_{I_{_T}})_x, (\dot{W}_{I_{_T}})_y, (\dot{W}_{I_{_T}})_z\right]$ are the derivative of the components of the wind expressed in the inertial frame .

$$\begin{aligned}
\dot{\beta}_{_T} &= p_{_T}(\sin\alpha_{_T}) - r_{_T}(\cos\alpha_{_T}) \\
&+ \frac{g}{V_{_T}}[(-\cos\alpha_{_T}\sin\beta_{_T})(-\sin\theta_{_T}) + \cos\beta_{_T}(\sin\phi_{_T}\cos\theta_{_T}) \\
&+ (-\sin\alpha_{_T}\sin\beta_{_T})(\cos\phi_{_T}\cos\theta_{_T})] \\
&- \frac{1}{m_{_T}V_{_T}}[S_T + T_{_T}\cos(\alpha_{_T}+\delta_T)\sin\beta_{_T}] \\
&+ \frac{1}{V_{_T}}\left[(\dot{W}_{I_{_T}})_x R_{11} + (\dot{W}_{I_{_T}})_y R_{12} + (\dot{W}_{I_{_T}})_z R_{13}\right]\cos\alpha_{_T}\sin\beta_{_T} \\
&- \frac{1}{V_{_T}}\left[(\dot{W}_{I_{_T}})_x R_{21} + (\dot{W}_{I_{_T}})_y R_{22} + (\dot{W}_{I_{_T}})_z R_{23}\right]\cos\beta_{_T} \\
&+ \frac{1}{V_{_T}}\left[(\dot{W}_{I_{_T}})_x R_{31} + (\dot{W}_{I_{_T}})_y R_{32} + (\dot{W}_{I_{_T}})_z R_{33}\right]\sin\alpha_{_T}\sin\beta_{_T} \qquad \text{(A.2)}
\end{aligned}$$

$$
\begin{aligned}
\dot{\alpha}_{_T} &= q_{_T} - r_{_T}(\tan\beta_{_T}\sin\alpha_{_T}) - p_{_T}(\tan\beta_{_T}\cos\alpha_{_T}) \\
&+ \frac{g}{V_{_T}}[(-\sec\beta_{_T}\sin\alpha_{_T})(-\sin\theta_{_T}) + (\cos\alpha_{_T}\sec\beta_{_T})(\cos\phi_{_T}\cos\theta_{_T})] \\
&- \frac{\sec\beta_{_T}}{m_{_T}V_{_T}}[L_T + T_{_T}\sin(\alpha_{_T}+\delta_T)] \\
&+ \frac{\sec\beta_{_T}}{V_{_T}}\left[(\dot{W}_{I_T})_x R_{11} + (\dot{W}_{I_T})_y R_{12} + (\dot{W}_{I_T})_z R_{13}\right]\sin\alpha_{_T} \\
&- \frac{\sec\beta_{_T}}{V_{_T}}\left[(\dot{W}_{I_T})_x R_{31} + (\dot{W}_{I_T})_y R_{32} + (\dot{W}_{I_T})_z R_{33}\right]\cos\alpha_{_T}
\end{aligned} \tag{A.3}
$$

In addition to the gravitational force, the external forces are aerodynamics force (D_T, S_T, L_T) and thrust (T_T).

The aerodynamic forces are given by

$$
\begin{aligned}
D_T &= \frac{1}{2}\rho V_{_T}^2 S_{_a} C_{D_T} \\
S_T &= \frac{1}{2}\rho V_{_T}^2 S_{_a} C_{S_T} \\
L_T &= \frac{1}{2}\rho V_{_T}^2 S_{_a} C_{L_T}
\end{aligned} \tag{A.4}
$$

where $S_{_a}$ is the reference area of the tanker aircraft. The aerodynamic coefficients are

$$
\begin{aligned}
C_{D_T} &= C_{D_0} + C_{D_{\alpha^2}}\alpha_{_T}^2 \\
C_{S_T} &= C_{S_0} + C_{S_\beta}\beta_{_T} + C_{S_{\delta_r}}\delta_{r_{_T}} \\
C_{L_T} &= C_{L_0} + C_{L_\alpha}\alpha_{_T} + C_{L_{\alpha^2}}(\alpha_{_T} - \alpha_{ref})^2 + C_{L_q}\frac{c_{_T}}{2V_{_T}}q_{rel} + C_{L_{\delta_e}}\delta_{e_T}
\end{aligned} \tag{A.5}
$$

In scalar form of the relative angular velocity,

$$
\begin{aligned}
p_{rel} &= p_{_T} - p_{eff} \\
q_{rel} &= q_{_T} - q_{eff} \\
r_{rel} &= r_{_T} - r_{eff}
\end{aligned} \tag{A.6}
$$

where $p_{_T}$, $q_{_T}$, and $r_{_T}$ are angular velocity relative to the inertial frame. p_{eff}, q_{eff}, and r_{eff} are rotational wind relative to the inertial frame.

Rotational matrix ($\mathbf{R_{B_TI}}$) from the inertial frame to the tanker body frame is given by

$$\mathbf{R_{B_TI}} = \begin{bmatrix} R_{11} & R_{12} & R_{13} \\ R_{21} & R_{22} & R_{23} \\ R_{31} & R_{32} & R_{33} \end{bmatrix} \tag{A.7}$$

where each element is

$$\begin{aligned}
R_{11} &= \cos\theta_{_T}\cos\psi_{_T} \\
R_{12} &= \cos\theta_{_T}\sin\psi_{_T} \\
R_{13} &= -\sin\theta_{_T} \\
R_{21} &= -\cos\phi_{_T}\sin\psi_{_T} + \sin\phi_{_T}\sin\theta_{_T}\cos\psi_{_T} \\
R_{22} &= \cos\phi_{_T}\cos\psi_{_T} + \sin\phi_{_T}\sin\theta_{_T}\sin\psi_{_T} \\
R_{23} &= \sin\phi_{_T}\cos\theta_{_T} \\
R_{31} &= \sin\phi_{_T}\sin\psi_{_T} + \cos\phi_{_T}\sin\theta_{_T}\cos\psi_{_T} \\
R_{32} &= -\sin\phi_{_T}\cos\psi_{_T} + \cos\phi_{_T}\sin\theta_{_T}\sin\psi_{_T} \\
R_{33} &= \cos\phi_{_T}\cos\theta_{_T}
\end{aligned} \tag{A.8}$$

A.2 Rotational Dynamics of Tanker Aircraft

Rotational dynamics in scalar form are

$$\begin{aligned}
\dot{p}_{_T} &= \frac{1}{I_x I_z - I_{xz}^2}\left[I_z\mathcal{L}_T + I_{xz}\mathcal{N}_T + (I_x - I_y + I_z)I_{xz}p_{_T}q_{_T} + (I_z I_y - I_z^2 - I_{xz}^2)q_{_T}r_{_T}\right] \\
\dot{q}_{_T} &= \frac{1}{I_y}\left[\mathcal{M}_T + (I_z - I_x)r_{_T}p_{_T} + (r_{_T}^2 - p_{_T}^2)I_{xz}\right] \\
\dot{r}_{_T} &= \frac{1}{I_x I_z - I_{xz}^2}\left[I_{xz}\mathcal{L}_T + I_x\mathcal{N}_T + (I_{xz}^2 + I_x^2 - I_x I_y)p_{_T}q_{_T} + (I_y - I_z - I_x)I_{xz}q_{_T}r_{_T}\right]
\end{aligned} \tag{A.9}$$

where I_x, I_y, I_z, and I_{xz} are moments of inertia. The moments are given by

$$\begin{aligned}
\mathcal{L}_T &= \frac{1}{2}\rho V_{_T}^2 S_a b_{_T} C_{\mathcal{L}_T} \\
\mathcal{M}_T &= \frac{1}{2}\rho V_{_T}^2 S_a c_{_T} C_{\mathcal{M}_T} + \triangle_{z_T} T_{_T} \\
\mathcal{N}_T &= \frac{1}{2}\rho V_{_T}^2 S_a b_{_T} C_{\mathcal{N}_T}
\end{aligned} \tag{A.10}$$

The moment coefficients are expressed by

$$\begin{aligned}
C_{\mathcal{L}_T} &= C_{\mathcal{L}_0} + C_{\mathcal{L}_{\delta_a}}\delta_{a_T} + C_{\mathcal{L}_{\delta_r}}\delta_{r_{_T}} + C_{\mathcal{L}_\beta}\beta_{_T} + C_{\mathcal{L}_p}\frac{b_{_T}}{2V_{_T}}p_{rel} + C_{\mathcal{L}_r}\frac{b_{_T}}{2V_{_T}}r_{rel} \\
C_{\mathcal{M}_T} &= C_{\mathcal{M}_\alpha}\alpha_{_T} + C_{\mathcal{M}_{\delta_e}}\delta_{e_T} + C_{\mathcal{M}_q}\frac{c_{_T}}{2V_{_T}}q_{rel} \\
C_{\mathcal{N}_T} &= C_{\mathcal{N}_0} + C_{\mathcal{N}_{\delta_a}}\delta_{a_T} + C_{\mathcal{N}_{\delta_r}}\delta_{r_{_T}} + C_{\mathcal{N}_\beta}\beta_{_T} + C_{\mathcal{N}_p}\frac{b_{_T}}{2V_{_T}}p_{rel} + C_{\mathcal{N}_r}\frac{b_{_T}}{2V_{_T}}r_{rel}
\end{aligned} \tag{A.11}$$

A.3 Rotational Kinematics of Tanker Aircraft

Rotational kinematics in scalar form are

$$\begin{aligned}
\dot{\psi}_{_T} &= (q_{_T}\sin\phi_{_T} + r_{_T}\cos\phi_{_T})\sec\theta_{_T} \\
\dot{\theta}_{_T} &= (q_{_T}\cos\phi_{_T} - r_{_T}\sin\phi_{_T}) \\
\dot{\phi}_{_T} &= p_{_T} + (q_{_T}\sin\phi_{_T} + r_{_T}\cos\phi_{_T})\tan\theta_{_T}
\end{aligned} \tag{A.12}$$

where $(\psi_{_T}, \theta_{_T}, \phi_{_T})$ are the Euler angles relative to the inertial frame.

A.4 Translational Kinematics of Tanker Aircraft

Translational kinematics in scalar form are

$$\begin{aligned}
\dot{x}_{_T} &= (V_{_T}\cos\beta_{_T}\cos\alpha_{_T})R_{11} + (V_{_T}\sin\beta_{_T})R_{21} + (V_{_T}\sin\alpha_{_T}\cos\beta_{_T})R_{31} + (W_{I_T})_x \\
\dot{y}_{_T} &= (V_{_T}\cos\beta_{_T}\cos\alpha_{_T})R_{12} + (V_{_T}\sin\beta_{_T})R_{22} + (V_{_T}\sin\alpha_{_T}\cos\beta_{_T})R_{32} + (W_{I_T})_y \\
\dot{z}_{_T} &= (V_{_T}\cos\beta_{_T}\cos\alpha_{_T})R_{13} + (V_{_T}\sin\beta_{_T})R_{23} + (V_{_T}\sin\alpha_{_T}\cos\beta_{_T})R_{33} + (W_{I_T})_z
\end{aligned} \tag{A.13}$$

where $[(W_{I_T})_x, (W_{I_T})_y, (W_{I_T})_z]$ are components of wind velocity expressed in the inertial frame.

A.5 Model of the Wind Experienced by Tanker

Wind components expressed in the inertial frame are

$$\begin{aligned}
(\dot{W}_{I_T})_x &= R_{11}(\dot{W}_{Bt})_x + R_{21}(\dot{W}_{Bt})_y + R_{31}(\dot{W}_{Bt})_z \\
(\dot{W}_{I_T})_y &= R_{12}(\dot{W}_{Bt})_x + R_{22}(\dot{W}_{Bt})_y + R_{32}(\dot{W}_{Bt})_z \\
(\dot{W}_{I_T})_z &= R_{13}(\dot{W}_{Bt})_x + R_{23}(\dot{W}_{Bt})_y + R_{33}(\dot{W}_{Bt})_z
\end{aligned} \tag{A.14}$$

where

$$
\begin{aligned}
(\dot{W}_{Bt})_x &= r_{_T} V_{_T} \sin\beta_{_T} - q_{_T} V_{_T} \sin\alpha_{_T} \cos\beta_{_T} \\
&\quad + \frac{1}{m_{_T}} \left(-m_{_T} g \sin\theta_{_T} - D_{_T} \cos\beta_{_T} \cos\alpha_{_T} + S_{_T} \cos\alpha_{_T} \sin\beta_{_T} + L_{_T} \sin\alpha_{_T} + T_x\right) \\
&\quad - \left(\dot{V}_{_T} \cos\beta_{_T} \cos\alpha_{_T} - \dot{\beta}_{_T} V_{_T} \sin\beta_{_T} \cos\alpha_{_T} - \dot{\alpha}_{_T} V_{_T} \cos\beta_{_T} \sin\alpha_{_T}\right) \\
(\dot{W}_{Bt})_y &= -r_{_T} V_{_T} \cos\beta_{_T} \cos\alpha_{_T} + p_{_T} V_{_T} \sin\alpha_{_T} \cos\beta_{_T} \\
&\quad + \frac{1}{m_{_T}} \left(m_{_T} g \sin\phi_{_T} \cos\theta_{_T} - D_{_T} \sin\beta_{_T} - S_{_T} \cos\beta_{_T} + T_y\right) \\
&\quad - \left(\dot{V}_{_T} \sin\beta_{_T} + \dot{\beta}_{_T} V_{_T} \cos\beta_{_T}\right) \\
(\dot{W}_{Bt})_z &= q_{_T} V_{_T} \cos\beta_{_T} \cos\alpha_{_T} - p_{_T} V_{_T} \sin\beta_{_T} \\
&\quad + \frac{1}{m_{_T}} \left(m_{_T} g \cos\phi_{_T} \cos\theta_{_T} - D_{_T} \sin\alpha_{_T} \cos\beta_{_T} + S_{_T} \sin\alpha_{_T} \sin\beta_{_T} - L_{_T} \cos\alpha_{_T} + T_z\right) \\
&\quad - \left(\dot{V}_{_T} \cos\beta_{_T} \sin\alpha_{_T} - \dot{\beta}_{_T} V_{_T} \sin\beta_{_T} \sin\alpha_{_T} + \dot{\alpha}_{_T} V_{_T} \cos\beta_{_T} \cos\alpha_{_T}\right)
\end{aligned}
\tag{A.15}
$$

APPENDIX B

SCALAR FORM OF EQUATIONS OF MOTION FOR RECEIVER

The equations of motion for receiver aircraft including wind effect are described in Ref. [31]. The scalar forms of tanker equations are required for the development of the family of the unscented Kalman filters.

B.1 Translational Dynamics of Receiver Aircraft

The translational dynamics in scalar form are

$$\begin{aligned}
\dot{V} &= g[\cos\alpha\cos\beta(-\sin\theta_{_T}R_{11} + \sin\phi_{_T}\cos\theta_{_T}R_{12} + \cos\phi_{_T}\cos\theta_{_T}R_{13}) \\
&+ \sin\beta(-\sin\theta_{_T}R_{21} + \sin\phi_{_T}\cos\theta_{_T}R_{22} + \cos\phi_{_T}\cos\theta_{_T}R_{23}) \\
&+ \cos\beta\sin\alpha(-\sin\theta_{_T}R_{31} + \sin\phi_{_T}\cos\theta_{_T}R_{32} + \cos\phi_{_T}\cos\theta_{_T}R_{33})] \\
&+ \frac{1}{m}(-D + T_x\cos\alpha\cos\beta + T_y\sin\beta + T_z\cos\beta\sin\alpha) \\
&+ (p + p_{_T}R_{11} + q_{_T}R_{12} + r_{_T}R_{13})(W_z\sin\beta - W_y\cos\beta\sin\alpha) \\
&+ (q + p_{_T}R_{21} + q_{_T}R_{22} + r_{_T}R_{23})(-W_z\cos\alpha\cos\beta + W_x\cos\beta\sin\alpha) \\
&+ (r + p_{_T}R_{31} + q_{_T}R_{32} + r_{_T}R_{33})(W_y\cos\alpha\cos\beta - W_x\sin\beta) \\
&- (\dot{W}_x\cos\alpha\cos\beta + \dot{W}_y\sin\beta + \dot{W}_z\cos\beta\sin\alpha) \qquad \text{(B.1)}
\end{aligned}$$

$$
\begin{aligned}
\dot{\beta} &= (p + p_{_T} R_{11} + q_{_T} R_{12} + r_{_T} R_{13}) \sin\alpha \\
&- (r + p_{_T} R_{31} + q_{_T} R_{32} + r_{_T} R_{33}) \cos\alpha \\
&+ \frac{g}{V}[-\cos\alpha \sin\beta(-\sin\theta_{_T} R_{11} + \sin\phi_{_T} \cos\theta_{_T} R_{12} + \cos\phi_{_T} \cos\theta_{_T} R_{13}) \\
&+ \cos\beta(-\sin\theta_{_T} R_{21} + \sin\phi_{_T} \cos\theta_{_T} R_{22} + \cos\phi_{_T} \cos\theta_{_T} R_{23}) \\
&- \sin\alpha \sin\beta(-\sin\theta_{_T} R_{31} + \sin\phi_{_T} \cos\theta_{_T} R_{32} + \cos\phi_{_T} \cos\theta_{_T} R_{33})] \\
&- \frac{1}{mV}(S + T_x \cos\alpha \sin\beta - T_y \cos\beta + T_z \sin\alpha \sin\beta) \\
&+ \frac{1}{V}[(p + p_{_T} R_{11} + q_{_T} R_{12} + r_{_T} R_{13})(W_z \cos\beta + W_y \sin\alpha \sin\beta) \\
&+ (q + p_{_T} R_{21} + q_{_T} R_{22} + r_{_T} R_{23})(W_z \cos\alpha \sin\beta - W_x \sin\alpha \sin\beta) \\
&+ (r + p_{_T} R_{31} + q_{_T} R_{32} + r_{_T} R_{33})(-W_y \cos\alpha \sin\beta - W_x \cos\beta) \\
&- (-\dot{W}_x \cos\alpha \sin\beta + \dot{W}_y \cos\beta - \dot{W}_z \sin\alpha \sin\beta)] \qquad \text{(B.2)}
\end{aligned}
$$

$$
\begin{aligned}
\dot{\alpha} &= (p + p_{_T} R_{11} + q_{_T} R_{12} + r_{_T} R_{13})(-\sin\beta \cos\alpha \sec\beta) \\
&+ (q + p_{_T} R_{21} + q_{_T} R_{22} + r_{_T} R_{23}) \\
&+ (r + p_{_T} R_{31} + q_{_T} R_{32} + r_{_T} R_{33})(-\sin\beta \sin\alpha \sec\beta) \\
&+ \frac{g}{V}[-\sec\beta \sin\alpha(-\sin\theta_{_T} R_{11} + \sin\phi_{_T} \cos\theta_{_T} R_{12} + \cos\phi_{_T} \cos\theta_{_T} R_{13}) \\
&+ \cos\alpha \sec\beta(-\sin\theta_{_T} R_{31} + \sin\phi_{_T} \cos\theta_{_T} R_{32} + \cos\phi_{_T} \cos\theta_{_T} R_{33})] \\
&- \frac{1}{mV}(L \sec\beta + T_x \sec\beta \sin\alpha - T_z \cos\alpha \sec\beta) \\
&+ \frac{1}{V}[(p + p_{_T} R_{11} + q_{_T} R_{12} + r_{_T} R_{13})(-W_y \cos\alpha \sec\beta) \\
&+ (q + p_{_T} R_{21} + q_{_T} R_{22} + r_{_T} R_{23})(W_z \sin\alpha \sec\beta + W_x \cos\alpha \sec\beta) \\
&+ (r + p_{_T} R_{31} + q_{_T} R_{32} + r_{_T} R_{33})(-W_y \sin\alpha \sec\beta) \\
&- (-\dot{W}_x \sec\beta \sin\alpha + \dot{W}_z \cos\alpha \sec\beta)] \qquad \text{(B.3)}
\end{aligned}
$$

where (W_x, W_y, W_z) are the components of the wind velocity expressed in the body frame, and ($\dot{W}_x$, $\dot{W}_y$, $\dot{W}_z$) are the derivatives of the wind body components relative to the receiver body frame.

In addition to graviational force, the external forces are aerodynamics forces (D, S, L), and thrust (T_x,T_y, T_z). The components of aerodynamics force are

$$\begin{aligned} D &= \frac{1}{2}\rho V^2 S_a C_D \\ S &= \frac{1}{2}\rho V^2 S_a C_S \\ L &= \frac{1}{2}\rho V^2 S_a C_L \end{aligned} \tag{B.4}$$

where S_a is the reference area of the receiver aircraft. The aerodynamic coefficients are

$$\begin{aligned} C_D &= C_{D_0} + C_{D_\alpha}\alpha + C_{D_{\alpha 2}}\alpha^2 + C_{D_{\delta_e}}\delta_e + C_{D_{\delta_e 2}}\delta_e^2 + C_{D_{\delta_s}}\delta_s + C_{D_{\delta_s 2}}\delta_s^2 \\ C_S &= C_{S_0} + C_{S_\beta}\beta + C_{S_{\delta_a}}\delta_a + C_{S_{\delta_r}}\delta_r \\ C_L &= C_{L_0} + C_{L_\alpha}\alpha + C_{L_\alpha 2}(\alpha - \alpha_{ref})^2 + C_{L_q}\frac{c}{2V_R}q_{rel} + C_{L_{\delta_e}}\delta_e + C_{L_{\delta_s}}\delta_s \end{aligned} \tag{B.5}$$

The relative angular velocity vector is given by

$$\bar{\omega}_{rel} = \bar{\omega}_{B_R} - \bar{\omega}_{eff} \tag{B.6}$$

where

$$\bar{\omega}_{B_R} = \bar{\omega}_{B_R B_T} + \bar{\omega}_{B_T} \tag{B.7}$$

In matrix form, the relative angular velocity of the receiver is expressed at the receiver body frame.

$$\omega_{rel} = \omega_{B_R B_T} + \mathbf{R_{B_R B_T}}\omega_{B_T} - \omega_{eff} \tag{B.8}$$

In scalar form of the relative angular velocity,

$$\begin{aligned} p_{rel} &= p + p_{_T} R_{11} + q_{_T} R_{12} + r_{_T} R_{13} - p_{eff} \\ q_{rel} &= q + p_{_T} R_{21} + q_{_T} R_{22} + r_{_T} R_{23} - q_{eff} \\ r_{rel} &= r + p_{_T} R_{31} + q_{_T} R_{32} + r_{_T} R_{33} - r_{eff} \end{aligned} \tag{B.9}$$

where

$$\begin{aligned} R_{11} &= \cos\theta\cos\psi \\ R_{12} &= \cos\theta\sin\psi \\ R_{13} &= -\sin\theta \\ R_{21} &= -\cos\phi\sin\psi + \sin\phi\sin\theta\cos\psi \\ R_{22} &= \cos\phi\cos\psi + \sin\phi\sin\theta\sin\psi \\ R_{23} &= \sin\phi\cos\theta \\ R_{31} &= \sin\phi\sin\psi + \cos\phi\sin\theta\cos\psi \\ R_{32} &= -\sin\phi\cos\psi + \cos\phi\sin\theta\sin\psi \\ R_{33} &= \cos\phi\cos\theta \end{aligned} \tag{B.10}$$

$$
\begin{aligned}
\dot{p} &= \left(\frac{I_z\mathcal{L} + I_{xz}\mathcal{N}}{I_xI_z - I_{xz}^2}\right) \\
&+ \left(\frac{I_yI_z - I_z^2 - I_{xz}^2}{I_xI_z - I_{xz}^2}\right) \\
&\quad (q + p_{_T}R_{21} + q_{_T}R_{22} + r_{_T}R_{23})(r + p_{_T}R_{31} + q_{_T}R_{32} + r_{_T}R_{33}) \\
&+ \left(\frac{I_zI_{xz} + I_{xz}I_x - I_{xz}I_y}{I_xI_z - I_{xz}^2}\right) \\
&\quad (p + p_{_T}R_{11} + q_{_T}R_{12} + r_{_T}R_{13})(q + p_{_T}R_{21} + q_{_T}R_{22} + r_{_T}R_{23}) \\
&- [r(p_{_T}R_{21} + q_{_T}R_{22} + r_{_T}R_{23}) - q(p_{_T}R_{31} + q_{_T}R_{32} + r_{_T}R_{33})] \\
&- (\dot{p}_{_T}R_{11} + \dot{q}_{_T}R_{12} + \dot{r}_{_T}R_{13}) \qquad \text{(B.11)} \\
\dot{q} &= \frac{\mathcal{M}}{I_y} \\
&+ \frac{I_{xz}}{I_y} \\
&\quad [(r + p_{_T}R_{31} + q_{_T}R_{32} + r_{_T}R_{33})^2 - (p + p_{_T}R_{11} + q_{_T}R_{12} + r_{_T}R_{13})^2] \\
&+ \frac{I_z - I_x}{I_y}(p + p_{_T}R_{11} + q_{_T}R_{12} + r_{_T}R_{13})(r + p_{_T}R_{31} + q_{_T}R_{32} + r_{_T}R_{33}) \\
&- [p(p_{_T}R_{31} + q_{_T}R_{32} + r_{_T}R_{33}) - r(p_{_T}R_{11} + q_{_T}R_{12} + r_{_T}R_{13})] \\
&- (\dot{p}_{_T}R_{21} + \dot{q}_{_T}R_{22} + \dot{r}_{_T}R_{23}) \qquad \text{(B.12)} \\
\dot{r} &= \left(\frac{I_{xz}\mathcal{L} + I_x\mathcal{N}}{I_xI_z - I_{xz}^2}\right) \\
&+ \left(\frac{I_{xz}I_y - I_{xz}I_z - I_{xz}I_x}{I_xI_z - I_{xz}^2}\right) \\
&\quad (q + p_{_T}R_{21} + q_{_T}R_{22} + r_{_T}R_{23})(r + p_{_T}R_{31} + q_{_T}R_{32} + r_{_T}R_{33}) \\
&+ \left(\frac{I_{xz}^2 + I_x^2 - I_xI_y}{I_xI_z - I_{xz}^2}\right) \\
&\quad (p + p_{_T}R_{11} + q_{_T}R_{12} + r_{_T}R_{13})(q + p_{_T}R_{21} + q_{_T}R_{22} + r_{_T}R_{23}) \\
&- [q(p_{_T}R_{11} + q_{_T}R_{12} + r_{_T}R_{13}) - p(p_{_T}R_{21} + q_{_T}R_{22} + r_{_T}R_{23})] \\
&- (\dot{p}_{_T}R_{31} + \dot{q}_{_T}R_{32} + \dot{r}_{_T}R_{33}) \qquad \text{(B.13)}
\end{aligned}
$$

The moments are given by

$$\begin{aligned}
\mathcal{L} &= \frac{1}{2}\rho V^2 S_{_R} b C_{\mathcal{L}} - \triangle_z T_y + \triangle_y T_z \\
\mathcal{M} &= \frac{1}{2}\rho V^2 S_{_R} c C_{\mathcal{M}} + \triangle_z T_x + \triangle_x T_z \\
\mathcal{N} &= \frac{1}{2}\rho V^2 S_{_R} b C_{\mathcal{N}} - \triangle_y T_x - \triangle_x T_y
\end{aligned} \tag{B.14}$$

where b is the wingspan, c is the chord length of the receiver aircraft, and ($\triangle_x$, $\triangle_y$, $\triangle_z$) are the moment arms of the thrust in the body frame of the receiver. The moment coefficients are

$$\begin{aligned}
C_{\mathcal{L}} &= C_{L_0} + C_{L_{\delta_a}}\delta_a + C_{L_{\delta_r}}\delta_r + C_{L_\beta}\beta + C_{L_p}\frac{b}{2V}p_{rel} + C_{L_{r_{rel}}}\frac{b}{2V}r_{rel} \\
C_{\mathcal{M}} &= C_{M_0} + C_{M_\alpha}\alpha + C_{M_{\delta_e}}\delta_e + C_{M_q}\frac{c}{2V}q_{rel} + C_{M_{\delta_s}}\delta_s \\
C_{\mathcal{N}} &= C_{N_0} + C_{N_{\delta_a}}\delta_a + C_{N_{\delta_r}}\delta_r + C_{N_\beta}\beta + C_{N_p}\frac{b}{2V}p_{rel} + C_{N_{r_{rel}}}\frac{b}{2V}r_{rel}
\end{aligned} \tag{B.15}$$

B.3 Rotational Kinematics of Receiver Aircraft

Rotational kinematics is

$$\dot{\psi} = (q\sin\phi + r\cos\phi)\sec\theta \tag{B.16}$$

$$\dot{\theta} = (q\cos\phi - r\sin\phi) \tag{B.17}$$

$$\dot{\phi} = p + (q\sin\phi + r\cos\phi)\tan\theta \tag{B.18}$$

where the orientation (ψ, θ, ϕ), and the angular velocity *(p,q,r)* are relative to the tanker expressed in the receiver body frame.

B.4 Translational Kinematics of Receiver Aircraft

The scalar form of the relative motion of the translational kinematics of the receiver including wind effect are given by

$$\begin{aligned}
\dot{x} &= (V\cos\beta\cos\alpha + W_x)R_{11} + (V\sin\beta + W_y)R_{21} + (V\sin\alpha\cos\beta + W_z)R_{31} \\
&- [V_{xT}(\cos\theta_{_T}\cos\psi_{_T}) + V_{yT}(\cos\theta_{_T}\sin\psi_{_T}) - V_{zT}\sin\theta_{_T}] \\
&+ (r_{_T}y - q_{_T}z) \qquad \text{(B.19)}
\end{aligned}$$

$$\begin{aligned}
\dot{y} &= (V\cos\beta\cos\alpha + W_x)R_{12} + (V\sin\beta + W_y)R_{22} + (V\sin\alpha\cos\beta + W_z)R_{32} \\
&- [V_{xT}(-\cos\phi_{_T}\sin\psi_{_T} + \sin\phi_{_T}\sin\theta_{_T}\cos\psi_{_T}) \\
&+ V_{yT}(\cos\phi_{_T}\cos\psi_T + \sin\phi_{_T}\sin\theta_{_T}\sin\psi_{_T}) + V_{zT}(\sin\phi_{_T}\cos\theta_{_T})] \\
&+ (p_{_T}z - r_{_T}x) \qquad \text{(B.20)}
\end{aligned}$$

$$\begin{aligned}
\dot{z} &= (V\cos\beta\cos\alpha + W_x)R_{13} + (V\sin\beta + W_y)R_{23} + (V\sin\alpha\cos\beta + W_z)R_{33} \\
&- [V_{xT}(\sin\phi_{_T}\sin\psi_{_T} + \cos\phi_{_T}\sin\theta_{_T}\cos\psi_{_T}) \\
&+ V_{yT}(-\sin\phi_{_T}\cos\psi_T + \cos\phi_{_T}\sin\theta_{_T}\sin\psi_{_T}) + V_{zT}(\cos\phi_{_T}\cos\theta_{_T})] \\
&+ (q_{_T}x - p_{_T}y) \qquad \text{(B.21)}
\end{aligned}$$

where (W_x, W_y, W_z) are relative to the inertial frame expressed in the receiver body frame.

B.5 Wind Components of Receiver Aircraft

$$(\dot{W}_{I_R})_x = R_{11}(\dot{W}_{tmp})_x + R_{21}(\dot{W}_{tmp})_y + R_{31}(\dot{W}_{tmp})_z \tag{B.22}$$

$$(\dot{W}_{I_R})_y = R_{12}(\dot{W}_{tmp})_x + R_{22}(\dot{W}_{tmp})_y + R_{32}(\dot{W}_{tmp})_z \tag{B.23}$$

$$(\dot{W}_{I_R})_z = R_{13}(\dot{W}_{tmp})_x + R_{23}(\dot{W}_{tmp})_y + R_{33}(\dot{W}_{tmp})_z \tag{B.24}$$

where

$$\begin{aligned}(\dot{W}_{tmp})_x &= (V\sin\beta)\,(r+T_3) - (V\sin\alpha\cos\beta)\,(q+T_2) \\ &+ g\,(-\sin\theta_T R_{11} + \sin\phi_T\cos\theta_T R_{12} + \cos\phi_T\cos\theta_T R_{13}) \\ &+ \frac{1}{m_{_R}}\,(-D\cos\beta\cos\alpha + S\cos\alpha\sin\beta + L\sin\alpha + T_x) \\ &- \left(\dot{V}\cos\beta\cos\alpha - \dot{\beta}V\sin\beta\cos\alpha - \dot{\alpha}V\cos\beta\sin\alpha\right)\end{aligned} \tag{B.25}$$

$$\begin{aligned}(\dot{W}_{tmp})_y &= -(V\cos\beta\cos\alpha)(r+T_3) + (V\sin\alpha\cos\beta)(p+T_1) \\ &+ g\,(-\sin\theta_T R_{21} + \sin\phi_T\cos\theta_T R_{22} + \cos\phi_T\cos\theta_T R_{23}) \\ &+ \frac{1}{m_{_R}}\,(-D\sin\beta - S\cos\beta + T_y) \\ &- \left(\dot{V}\sin\beta + \dot{\beta}V\cos\beta\right)\end{aligned} \tag{B.26}$$

$$
\begin{aligned}
(\dot{W}_{tmp})_z &= (V\cos\beta\cos\alpha)(q+T_2) - (V\sin\beta)(p+T_1) \\
&+ g\left(-\sin\theta_T R_{31} + \sin\phi_T\cos\theta_T R_{32} + \cos\phi_T\cos\theta_T R_{33}\right) \\
&+ \frac{1}{m_{_R}}\left(-D\sin\alpha\cos\beta + S\sin\alpha\sin\beta - L\cos\alpha + T_z\right) \\
&- \left(\dot{V}\cos\beta\sin\alpha - \dot{\beta}V\sin\beta\sin\alpha + \dot{\alpha}V\cos\beta\cos\alpha\right)
\end{aligned} \tag{B.27}
$$

where

$$
\begin{aligned}
T_1 &= p_{_T}R_{11} + q_{_T}R_{12} + r_{_T}R_{13} \\
T_2 &= p_{_T}R_{21} + q_{_T}R_{22} + r_{_T}R_{23} \\
T_3 &= p_{_T}R_{31} + q_{_T}R_{32} + r_{_T}R_{33}
\end{aligned} \tag{B.28}
$$

$\dot{W}_{I_R}$ is the wind derivative relative to the inertial frame.

The relation between wind derivative relative to the receiver body frame and wind derivative relative to the inertial frame is

$$
[B_R]^T\dot{W}_{B_R} = [B_R]^T\left[R_{B_RI}\dot{W}_{I_R} + S(\omega_{B_R})W_{B_R}\right] \tag{B.29}
$$

where W_{B_R} is the wind velocity components relative to the inertial frame expressed in the receiver body frame.

$$
\dot{W}_{B_R} = \begin{bmatrix}\dot{W}_x \\ \dot{W}_y \\ \dot{W}_z\end{bmatrix}, \quad \dot{W}_{I_R} = \begin{bmatrix}(\dot{W}_{I_R})_x \\ (\dot{W}_{I_R})_y \\ (\dot{W}_{I_R})_z\end{bmatrix}, \quad W_{B_R} = \begin{bmatrix}W_x \\ W_y \\ W_z\end{bmatrix} \tag{B.30}
$$

REFERENCES

[1] W.M.Hollister, E.R.Bradford, and J.D.Welch, "Using Aircraft Radar Tracks to Estimate Winds Aloft," *The Lincoln Laboratory Journal*, vol. 2, no. 3, 1989.

[2] R.E.Cole, S.Green, M.Jardin, B.E.Schwartz, and S.G.Benjamin, "Wind Prediction Accuracy for Air Traffic Management Decision support Tools," *3rd USA/Europe Air Traffic Management R&D Seminar*, June 2000.

[3] N.Ceccarelli, J.J.Enright, E.Frazzoli, S.J.Rasmussen, and C.J.Schumacher, "Micro UAV Path Planning for Reconnaissance in Wind," *Proceedings of the 2007 American Control Conference*, 2007.

[4] D.Delahaye, S.Puechmorel, and P.Vacher, "Windfield Estimation by Radar Track Kalman Filtering and Vector Spline Extrapolation," *IEEE*, 2003.

[5] J.Osborne and R.Rysdyk, "Waypoint Guidance for Small UAVs in Wind," *AIAA Infotech@Aerospace*, 2005.

[6] A.L.Jennings, R.Ordonez, and N.Ceccarelli, "Waypoint Navigation Heuristic for a Small UAV with Non-uniform Settling Lengths," *AIAA Guidance, Navigation, and Control Conference*, August. 2010.

[7] T.A.Lewis, *Flight Data Analysis and Simulation of Wind Effects During Aerial Refueling*. M.S. thesis, The University of Texas at Arlington, Arlington, TX, May 2008.

[8] A.Dogan, T.A.Lewis, and W.Blake, "Wake-Vortex Induced Wind with Turbulence in Aerial Refueling - Part A: Flight Data Analysis," *AIAA Atmospheric Flight Mechanics Conference and Exhibit*, August. 2008.

[9] A.Dogan, T.A.Lewis, and W. Blake, "Wake-Vortex Induced Wind with Turbulence in Aerial Refueling - Part B: Model and Simulation Validation," *AIAA Atmospheric Flight Mechanics Conference and Exhibit*, August. 2008.

[10] C.G.Wagner, L.D.Jacques, B.Blake, and M.Pachter, "An Analytical Study of Drag Reduction in Tight Formation Flight," *AIAA Atmospheric Flight Mechanics Conference and Exhibit*, August. 2001.

[11] W.Blake and D.Multhopp, "Design, Performance and Modeling Considerations for Close Formation Flight," *Proceedings of the 1999 AIAA Guidance, Navigation and Control Conference*, August. 1999.

[12] J.K.Hall and M.Pachter, "Formation Maneuvers in Three Dimensions," *AIAA Paper 2000-4372*, August. 2000.

[13] D.Daban and J.F.Whidborne, "Modeling of Wake Vortex Effects for Unmanned Air Vehicle Simulations," *AIAA Modeling and Simulation Technologies Conference*, August. 2009.

[14] A.Cho, J.Kim, S.Lee, and C.Kee, "Wind Estimation and Airspeed Calibration Using a UAV with a Single-Antenna GPS Receiver and Pitot Tube," *IEEE Transactions on Aerospace and Electronic Systems*, vol. 47, no. 1, January. 2011.

[15] H.J.Palanthandalam-Madapusi, A.Girard, and D.S.Bernstein, "Wind-field Reconstruction Using Flight Data," *American Control Conference*, June. 2008.

[16] M.Pachter, N.Ceccarelli, and P.R.Chandler, "Estimating MAV's Heading and the Wind Speed and Direction Using GPS, Inertial, and Air Speed Measurements," *AIAA Guidance, Navigation, and Control Conference and Exhibit*, August. 2008.

[17] J.W.Langelaan, N.Alley, and J.Neidhoefer, "Wind Field Estimation for Small Unmanned Aerial Vehicles," *AIAA Guidance, Navigation, and Control Conference*, Aug, 2010.

[18] B.Sadeghi and B.Moshiri, "Second-order EKF and Unscented Kalman Filter Fusion for Tracking Maneuvering Targets," *IEEE*, 2007.

[19] S.A.Banani and M.A.Masnadi-Shirazi, "A New Version of Unscented Kalman Filter," *Proceedings of World Academy of Science, Engineering and Technology*, vol. 20, 2007.

[20] F.Gustafsson, F.Gunnarsson, N.Bergman, U.Forssell, J.Jansson, R.Karlsson, and P.Nordlund, "Particle Filters for Positioning, Navigation and Tracking," *IEEE Transactions on Signal Processing*, vol. 50, no. 2, pp. 425–437, 2002.

[21] Y.Cheng and J.L.Crassidis, "Particle Filtering for Sequential Spacecraft Attitude Estimation," *AIAA Guidance, Navigation, and Control Conference and Exhibit*, August 2004.

[22] S. J. Julier and J. K. Uhlmann, "Reduced Sigma Point Filters for the Propagation of Means and Covariances through Nonlinear Transformations," *Proceeding American Control Conference*, 2002.

[23] S.J.Julier and J.K.Uhlmann, "A New Extension of the Kalman Filter to Nonlinear Systems," *In the Proceedings of Aerosense: The 11th International Symposium on Aerospace/Defense Sensing, Simulation, and Controls*, 1997.

[24] S.J.Julier, J.K.Uhlmann, and H.F.Durrant-Whyte, "A New Approach for Filtering Nonlinear Systems," *Proceeding of the American Control Conference*, Jun, 1995.

[25] J.L.Crassidis and J.L.Junkins, *Optimal Estimation of Dynamics System*. Chapman Hall/CRC, 2004.

[26] D.Simon, *Optimal State Estimation*. John Wiley Sons, 2006.

[27] R.v.d.Merwe, *Sigma-point Kalman Filters for Probabilistic Inference in Dynamic State-space Models*. Ph.D. thesis, OGI School of Science & Engineering, Oregon Health & Science University, April 2004.

[28] R.v.d.Merwe and E.A.Wan, "The Square-Root Unscented Kalman Filter for State and Parameter-Estimation," *2001 IEEE International Conference*, vol. 6, 2001.

[29] H.G.Asl and S.H.Pourtakdoust, "UD Covariance Factorization for Unscented Kalman Filter Using Sequential Measurements Update," *World Academy of Science, Engineering and Technology*, vol. 34, Aug, 2007.

[30] S.Haykin, *Kalman Filtering and Neural Networks*. John Wiley & Sons, 2001.

[31] E.Kim, *Control and Simulation of Relative Motion for Aerial Refueling in Racetrack Maneuver*. M.S. thesis, The University of Texas at Arlington, Arlington, TX, May 2007.

[32] A.Dogan, S.Venkataramanan, and W.Blake, "Modeling of Aerodynamic Coupling Between Aircraft in Close Proximity," *Journal of Aircraft*, vol. 42, 2005.

[33] S.Venkataramanan, A.Dogan, and W.Blake, "Vortex Effect Modeling in Aircraft Formation Flight," *AIAA Atmospheric Flight Mechanics Conference and Exhibit*, August 2003.

[34] "Flying Qualitied of Piloted Airplanes," Tech. Rep. U.S. Military Specification MIL-F-8785C, 5 November 1980.

[35] Northrop Group. (2011) LN-251 Advanced Airbone INS/GPS System@ONLINE. [Online]. Available: http://www.es.northropgrumman.com/solutions/ln251-digital-ins-gps/

[36] R.L.Farrenkopf, "Analytic Steady-State Accuracy Solutions for Two Common Spacecraft Attitude Estimators," *Journal of Guidance and Control*, July-August 1978.

[37] J.Wendel, A.Maier, J.Metzger, and G.F.Trommer, "Comparison of Extended and Sigma-Point Kalman Filters for Tightly Coupled GPS/INS Integration," *AIAA Guidance, Navigation, and Control Conference and Exhibit*, August 2005.

[38] F.D.Busse, J.P.How, and J.Simpson, "Demonstration of Adaptive Extended Kalman Filter for Low Earth Orbit Formation Estimation Using CDGPS," *Institute of Navigation GPS Meeting*, 2002.

[39] F.L.Lewis, *Optimal Estimation with an Introduction to Stochastic Control Theory*. John Wiley Sons, 1986.

[40] F.L.Lewis and V.L.Syrmos, *Optimal Control*. John Wiley Sons, 1995.

BIOGRAPHICAL STATEMENT

Je Hyeon Lee was born in South Korea. He has a bachelor's degree in the field of mechanical engineering from Ajou University in South Korea. He graduated from Sejong University as a master degree in South Korea in the field of aerospace engineering in 2004. He got interested in aircraft design, flight dynamics, and stability of aircraft during his graduate program in South Korea. In 2007, he joined the aerospace engineering Ph.D. program at the University of Texas at Arlington (UTA). At UTA, he met Dr. Atilla Dogan, who is a specialist in the aerial refueling and formation flight. With Dr. Dogan, Je Hyeon Lee developed an estimation technique for wind that is essential in aerial refueling. The partial result is published with the title of "Estimation of Aircraft State and Wind Exposure" in an American Institute of Aeronautics and Astronautics (AIAA) conference in August 2011. Je Hyeon Lee will pursue a fulltime researcher or faculty position in the field of flight dynamics, estimation and control.